Universitat de les
Illes Balears

Quantification of the different contributions to long-term sea-level variability in the Mediterranean Sea

Francisco J. Mir Calafat

Mallorca, 7 de Maig de 2010

Damià Gomis Bosch, Professor Titular del Departament de Física de la Universitat de les Illes Balears,

CERTIFICA

Que aquesta tesi ha estat realitzada pel Sr. *Francisco J. Mir Calafat* sota la seva direcció. I per a que així consti, firma la present,

a Palma de Mallorca, a dia 7 de maig de 2010

Damià Gomis Bosch

To my wife, Maki, for being my inspiration

To my parents, Aina i Pep

Agraïments

En primer lloc vull agrair al meu director de tesi, en Damià Gomis, el suport, la confiança i l'amistat que m'ha dispensat al llarg d'aquests quasi quatre anys. En Damià ha estat sempre allà per escoltar el que tenia que dir-li i per donar-me consell sempre que ha fet falta. La seva direcció de la tesis ha estat impecable i en tot moment ha sabut generar un clima que ha afavorit la discussió de problemes científics no només entre ell i jo, sinó també entre tots els membres del grup. També li vull donar les gràcies per la qualitat de les idees que m'ha transmès, moltes de les quals estan plasmades en aquesta tesi, i per la paciència que ha tingut a l'hora de revisar els meus articles. Sens dubte, si aquest treball ha arribat a bon port és, en bona mesura, gràcies a ell.

A na Marta Marcos probablement li dec, entre moltes altres coses, el fet de que aquesta tesi tingui un capítol sobre gravimetria i component de massa. Ella em va animar a processar les dades GRACE i va confiar en jo quan jo dubtava de mi mateix. Són incomptables les hores que hem passat discutint sobre el famós GIA, els harmònics esfèrics (i jo que pensava que només eren cosa de la Física Quàntica!) i els polinomis de Legendre (i la seva constant de normalització...). Són també nombrosos els viatges i congressos que hem compartit per tota Europa (Viena, Rhodes, Toulouse, Madrid, etc.). Per tot això i per estar sempre oberta a escoltar i debatre sobre qualsevol qüestió amb la que vagis a molestar-la al seu despatx, moltes GRÀCIES!

A en Biel Jordà li vull donar les gràcies per guiar-me en el procés d'aprenentatge dels models numèrics així com també per plantejar-me preguntes molt interessants amb la intenció d'ajudar-me a donar resposta als meus problemes (tant científics com computacionals) i aprofundir en el coneixement del tema en qüestió. També, gràcies a ell, he descobert funcions Matlab que no sabia ni que existien i que m'han facilitat la vida i han escurçat sensiblement el temps de càlcul que he dedicat al tractament i anàlisi de les dades.

M'agradaria també esmentar a en Sebastià Montserrat per ensenyar-me a calcular i analitzar espectres durant els cursos del Màster en Física i per lo bé que ens ho hem passat en els sopars i en el viatge a Rhodes. La seva generositat a l'hora d'aportar diners al pot comú no té límits. A n'Ananda Pascual i en Simón Ruiz els vull agrair l'ajuda de tot tipus que m'han dispensat des de que vaig començar la meva tesi allà per l'any 2006. No em vull oblidar tampoc del darrer fitxatge del nostre grup, na Marga Palmer, per haver compartit els nostres doctorats i amb qui he passat incomptables hores discutint

sobre temes científics (i no tant científics) relacionats tant amb el seu camp d'estudi com amb el meu. Esment especial per una de les al·lotes més simpàtiques i treballadores de l'IMEDEA, na Mar Flexas, amb qui he tingut la sort de compartir grup i passadís i de qui espero se m'hagi aferrat un poc de la seva tenacitat, valentia i optimisme. També donar les gràcies a la gent de Puertos del Estado n'Enrique, na Begoña, na Macu, en Roland...per la seva fructífera col·laboració amb el nostre grup.

Gràcies també a tot el personal de l'IMEDEA i del Departament de Física de la UIB amb qui sempre m'he sentit com a casa. A tots els meus companys de despatx, tant a la EFE com a l'IMEDEA, els vull agrair el bon ambient de treball que han sabut crear i els desitjo el millor en el seu futur. Als meus companys de dinar a l'IMEDEA; en José, en Joan, n'Alex, na Regina (que ja no hi és), etc; els vull donar les gràcies per fer dels dinars autèntiques tertúlies científiques de les quals vaig aprendre moltíssim, sobretot de biologia.

També vull donar-li les gràcies al Dr. Mikis Tsimplis per donar-me l'oportunitat de visitar el NOC i viure durant un parell de mesos a Southampton (la ciutat amb més encant del mon, a pesar de la cervesa calenta i de la pluja, a que sí Maki?). En Mikis em va ensenyar com formular preguntes científiques i em va mostrar les diferents maneres d'afrontar un problema científic. Ell és una espècie de mag de la ciència capaç de fer aflorar les idees més brillants que hi ha dintre d'un mateix i crear del no-res un article en un parell de dies. Andrew Shaw és un altre investigador amb qui vaig compartir despatx al NOC durant 2 mesos i de qui vaig aprendre moltes coses. Gràcies per la teva amabilitat i afecte durant aquells mesos en els quals vaig estar lluny de casa.

Com em podria oblidar dels meus companys del Màster de Física i del CAP: Carles Bona, Sara Guijarro, Miquel Tries, Llúcia Sancho, Roberto Soler, Lorena Garcies, i molts altres que segur que em deixo. Cap a ells només tinc paraules d'admiració i els desitjo tota la sort del món (tot i que sort no els fa falta ja que tots ells són persones super brillants).

En definitiva, vull donar les gràcies a totes les persones que d'una manera o una altre m'han donat suport, m'han ensenyat alguna cosa o simplement han confiat en mi durant aquests darrers quasi 4 anys.

Als meus pares els vull donar les gràcies per haver-me donat la vida. A la meva mare especialment dir-li que sempre li estaré eternament agraït per tots els esforços que ha fet per donar-nos a la meva germana Aina i a mi la millor de les educacions i els coneixements necessaris per poder pensar i decidir en tot moment per nosaltres mateixos. Gràcies també per recordar-me tantes vegades que déu estreny però no ofega. A la meva germana Aina, al meu fillol Joan, a la meva família i a tots els meus amics (vosaltres sabeu qui sou) dir-vos que sense vosaltres res valdria la pena.

Finalment, però no menys important, a la meva estimada dona, na Maki, vull dir-li que sense ella no sóc res. Gràcies per ensenyar-me que estimar no consisteix en mirar-se l'un a l'altre sinó en mirar tots dos junts en la mateixa direcció. Gràcies també per haver-me demostrat que ni 10,000 km ni deixar el teu país, Japó, (i la comoditat i prosperitat que suposen viure en el país tecnològicament més avançat del món) no són obstacles quan l'amor es vertader. Són moltes les hores que he passat a casa davant l'ordinador preparant aquesta tesi i mai t'has queixat ni m'has tirat en cara que no et dedicava el temps necessari, tot el contrari, sempre m'has donat suport i m'has mostrat comprensió. Això va per tu!

Acknowledgments

First of all I want to thank my thesis' supervisor, Damià Gomis, for the support, the confidence and the friendship that he has offered to me during those nearly four years. Damià was always there to listen and to give advice. His supervision of the thesis has been perfect and he has always created a proper environment that has favored the discussion of research problems not only between him and me but also with the others members of the research team. I am also grateful to him for the quality of the ideas that he has transmited to me, many of which are captured in this thesis, and for his patience when reviewing my papers. With no doubt, if this work has had a successful ending it is thanks to him.

To Marta Marcos I probably owe her the fact that this thesis has a chapter on gravimetry and the mass component of sea level. She encouraged me to process GRACE data and she trusted me when I doubted on myself. We have spent countless hours discussing about the famous GIA, the spherical harmonics (I thought those were only a Quantum Physics matter!) and the Legendre polynomials (and their normalization constant…). Many are also the trips and conferences that we have attended together all around Europe (Vienna, Rhodos, Toulouse, Madrid, etc). For all these things and for being always open to listen and debate about any topic with which one goes to bother her to her office, many THANKS!

I want to thank Biel Jordà for guiding me in the learning process of numerical models, as well as for asking me questions aimed to solve my problems (whether scientific or computational). Also, thanks to him I have discovered Matlab functions that I did not know that they existed and that have made my life easier and have saved me a lot of computation time.

I would like to mention Sebastià Montserrat for teaching me how to compute and analyze spectra during the lessons of the Master in Physics. Also for the good time we spent together in various dinners and in Rhodes. His generosity when it comes to contribute to a collective pool of money is endless. I am grateful to Ananda Pascual and Simón Ruiz for all the help they have given me since I began my Ph.D back in 2006. I also want to remember here the last incorporation of our team, Marga Palmer, for having shared our Ph.D's and with whom I have spent countless hours discussing about

research topics related to both her field and my field. Mar Flexas deserves special mention for being one of the most friendly and hard-working girls at IMEDEA. I have been so fortunate to be in the same team and corridor then her at IMEDEA. I hope she has transmitted some of her tenacity, courage and optimism to me. I also want to thank the people from Puertos del Estado: Enrique, Begoña, Macu, Roland...for their fruitful colaboration with our team.

Thanks also to everybody from IMEDEA and from the UIB Physics Department with whom I have always felt like at home. I want to thank all the colleagues of my office, whether at the EFE room or at IMEDEA, for the good environment that they have created; I wish them the best in their future. I want to thank my colleagues with whom I take lunch everyday at IMEDEA; en José, en Joan, n'Alex, na Regina (who is already gone), etc; for making the lunch to become a trully scientific gathering from which I have learnt a lot, specially about biology.

Also I want to thank Mikis Tsimplis for giving me the opportunity of visiting the NOC and to live in Southampton for a couple of months. Mikis taught me how to ask scientific questions and showed me the different ways to confront a research problem. He is a sort of wizard of science, able of bringing out the good ideas in anyone and making a paper out of nothing in a couple of days. Andrew Shaw is another researcher with whom I shared office at NOC for 2 months and from whom I learnt many things. Thank you for your kindness and affection during those months in wich I was far away from home.

How could I forget my mates from the Master in Physics and the CAP: Carles Bona, Sara Guijarro, Miquel Tries, Llúcia Sancho, Roberto Soler, Lorena Garcies and many more. I only have words of admiration for them and I wish them all the luck in the world (thouth they really do not need it, since they are all very brilliant).

In summary, thanks to everybody who, in one way or another, has supported me, taught me something or simply has had confidence in me during the last 4 years.

I want to thank my parents for giving birth to me. I want to tell my mum specially that I will always be in debt with her for all the efforst she has made in order to provide my sister Aina and I with the best education and the necessary knowledge to think and decide by ourselves. Thank you for reminding me so many times that God may press your throat but never too hard to strangle you. To my sister Aina, my godson Joan, my family and all my friends (you know who you are) I want you to know that life would be worthless without you.

Last, but not least, I want my lovely wife, Maki, to know that I am nothing without her. Thank you for teaching me that love is not just looking at each other but it is looking together in the same direction. Thank you too for having shown me that neither 10,000 km nor leaving your country, Japan (and the comfort and prosperity that the most technologically advanced country is supposed to provide you with), are obstacles when love is pure. Countless are the hours that I have spent at home in order to finish this thesis and you have never complained nor have thrown in my face that I did not devote enough time to you. Instead, you have always supported me and have understood me. This goes for you!

Table of contents

Resum

Els estudis de nivell del mar són de gran importància per els ports, l'erosió de les costes o el disseny de defenses costaneres contra les inundacions. Tradicionalment el que interessava eren les fluctuacions més o menys sobtades de nivell, car es considerava que el nivell mitjà era essencialment constant. El recent interès en el nivell del mar mitjà es deu a la possibilitat de pujades significatives durant aquest segle com a resultat de l'escalfament global. I és que més de 100 milions de persones viuen a llocs situats no més d'1 m per sobre del nivell del mar actual.

La pujada del nivell mitjà pot afectar les zones costaneres de diferents maneres. La inundació permanent pot afectar una zona més o menys extensa depenent del gradient local de la costa. Les configuracions geogràfiques amb gradients costaners petits més susceptibles de ser inundades són les platges, els deltes, les maresmes, els estuaris, les llacunes i les badies. Això inclou per exemple bona part dels Països Baixos, la zona sud del Bàltic, els estuaris de la zona est del Regne Unit, i els deltes dels grans rius. A la Mediterrània, inclou deltes de rius com l'Ebre o el Nil. També moltes illes de corall tenen una elevació mitjana de només 1.5-2 m sobre el nivell del mar, i per tant tenen un alt risc d'inundació. La freqüència d'episodis puntuals d'inundació també augmentarà, ja que una pujada del nivell del mar implica un augment de la cota d'inundació derivada d'ones de tempesta d'una determinada altura. Igualment, una pujada del nivell del mar pot provocar un augment de la intrusió d'aigua salada en els aqüífers costaners.

Queda clara doncs la importància d'estudiar i entendre els distints processos físics que tenen un efecte sobre el nivell del mar. Aquest coneixement és essencial per tal de poder fer prediccions fiables de la seva evolució, amb l'objectiu final d'adoptar mesures de prevenció. A més, l'augment del nivell del mar causat per l'escalfament global no serà uniforme a tot el planeta. Per tant és també prioritari estudiar i entendre la variabilitat del nivell del mar a escala regional. Això és precisament el que s'intenta fer en aquesta tesis, que té com a marc geogràfic la Mediterrània.

La tesis s'ha duit a terme com a part del projecte VANIMEDAT (CTM2005-05694-C03/MAR), finançat pel Ministeri Espanyol de Ciència i Tecnologia i el programa FEDER de la Unió Europea. L'objectiu general del projecte era estudiar la variabilitat decadal i interdecadal del nivell del mar, posant especial atenció en les tendències a llarg termini i en els fenòmens extrems. Tot dintre del context geogràfic de l'oceà i els mars que envolten la Península Ibèrica.

El projecte tenia tres objectius específics. El primer era determinar la variabilitat espacial i temporal del nivell del mar, posant una atenció especial en la consistència entre les observacions costaneres i les de mar obert. El segon objectiu era quantificar la contribució, a nivell regional, del diferents mecanismes responsable de la variabilitat del nivell del mar. A saber: i) quantificar l'efecte de la pressió atmosfèrica i el forçament del vent sobre el nivell del mar a partir de l'anàlisi de residus del nivell del mar produïts per un model barotròpic; ii) quantificar la contribució de la component estèrica (i els patrons de circulació associats) a partir d'observacions hidrogràfiques y dels resultats de models baroclins; iii) calcular l'increment de massa com la diferència entre el nivell del

mar total i les altres dues components determinades abans. El tercer objectiu era estudiar els fenòmens extrems.

En aquesta tesi ens centrem només en els dos primers objectius del projecte VANIMEDAT. Concretament, el tipus de qüestions que intentem respondre són: ha pujat el nivell del mar mitjà a la Mediterrània durant la segona meitat del segle XX ? En cas de que així sigui, quant ha pujat ? Ha estat una pujada uniforme a tota la regió ? Quina component del nivell del mar ha contribuït més a les tendències observades ? Poden els models numèrics baroclins reproduir de manera fiable la variabilitat observada ? Es pot tancar el balanç del nivell del mar a la Mediterrània ?

Per tal de respondre a les preguntes anteriors la tesis s'ha dividit en dues parts ben diferenciades. A la primera part de la tesi, es defineixen clarament cadascuna de les contribucions de la variabilitat del nivell del mar y les diferents tècniques que s'utilitzen per mesurar-les. Els diferents conjunts de dades utilitzats per caracteritzar la variabilitat del nivell del mar i quantificar els diferents processos físics són també introduïts en aquest primera part. Finalment, es fa una descripció general dels models numèrics i es presenten els models concrets que s'utilitzen a la tesi.

La segona part de la tesis és el seu nucli, car és on es mostren els resultats obtinguts en aquest treball. En primer lloc es presenta una anàlisi en components principals (PCA) de la variabilitat del nivell del mar a la Mediterrània a partir de dades de satèl·lits altimètrics. Aquesta anàlisi es compara amb els resultats obtinguts utilitzant un PCA no lineal. Seguidament es reconstrueix el nivell del mar per a tota la conca durant els darrers 50 anys, combinant dades de mareògrafs i de satèl·lits altimètrics i emprant una metodologia basada en una anàlisi de PCA. Els resultats obtinguts, millors en el cas de l'anàlisi lineal que en el del no lineal, indiquen que per a l'anàlisi del nivell del mar a la Mediterrània és suficient (i preferible) la utilització de tècniques lineals. Així i tot els resultats obtinguts a partir de les reconstruccions anteriors no són del tot satisfactoris i, per tant, el següent pas es reconstruir el nivell del mar utilitzant una tècnica més sofisticada. La tècnica utilitzada és un interpolació òptima amb reducció dimensional mitjançant un PCA. Els resultats obtinguts a partir d'aquesta reconstrucció sí són molt satisfactoris i ens permeten obtenir per primera vegada la distribució espacial de tendències del nivell del mar a tota la conca durant la segona meitat del segle XX. A partir de la reconstrucció també es calcula el ritme de pujada del nivell del mar (promitjat sobre tota la conca) durant les darreres dècades i s'estudia també la seva variabilitat interanual.

Una vegada s'ha reconstruït el nivell del mar total, es passa a la quantificació de les diferents contribucions a la variabilitat del nivell del mar. La component atmosfèrica del nivell del mar està ja calculada a treballs anteriors, a partir de dades de models baròtrops; aquí només es resumeixen els resultats principals. La component estèrica es calcula a partir de dades de temperatura i salinitat de models numèrics baroclins i també a partir de dades hidrogràfiques. En el cas dels models, s'utilitzen dos models numèrics regionals i un de global. La component de massa es calcula a partir de les dades proporcionades pel satèl·lit gravimètric de la missió GRACE (pel període 2002-2008) i a partir del nivell del mar total corregit per les components estèrica i atmosfèrica (pel període 1948-2000).

Tot plegat, s'aconsegueix respondre a les preguntes plantejades anteriorment i es dona, com a resum del treball, una sèrie de taules amb les millors estimes a dia d'avui de les tendències de nivell del mar total i de cadascun dels seus components. Com a resum executiu dels resultats es pot dir que durant la segona meitat del segle XX, el

nivell mitjà de la mar Mediterrània ha pujat a un ritme sensiblement inferior a la mitjana global. La raó principal ha estat l'efecte negatiu de l'increment de pressió atmosfèrica observat entre els anys 60 i els anys 90 sobre la regió, tot i que la component estèrica també ha estat sensiblement inferior a la global durant aquest període. Contràriament, la millor estima de que disposem per a la component de massa indica que a la Mediterrània seria del mateix ordre que la mitjana global.

Chapter 1

Preface

SINCE ancient times oceans have a special fascination, and the mechanisms responsible for phenomena such as tides and catastrophic floods due to storms and tsunamis have challenged human imagination. Indeed, ocean observers from ancient times were already able to link the tides to the movements of the moon and sun, although for them they had a religious significance; they considered tides as a manifestation of the power of Gods. The earliest reference that relates the tides to the moon and sun is in the Samaveda of the Indian Vedic period (2000 to 1400 BC), although Pytheas of Massilia (4th century BC) was the first to associate the tides to the phases of the moon. Many were the physicists, mathematicians and astronomers who tried to explain the connection between the moon and the tides in the following centuries, though their theories were rather invalid. It was in 1595 when Galielo Galileli came up with his explanation for the tides. The idea occurred to him while travelling on a barge that was ferrying freshwater to Venice. He noticed that whenever the barge's speed or direction were altered, the freshwater inside sloshed around accordingly. If the vessel suddenly ground to a halt on a sandbar, for example, the water pushed up towards the bow then bounced back toward the stern, doing this several times with ever decreasing agitation until it returned to a level state. Galileo thought that the Earth's dual motion might have the same effect on oceans as the vessel had on its freshwater cargo. Galileo thought that he had discovered the correct explanation for the tides; however, in 1609, the German mathematician Johannes Kepler wrote

> ... The sphere of influence of the attraction which is in the moon extends as far as the Earth, and incites the waters up from the torrid zone...

suggesting that the tides were caused by the moon's gravity acting on the Earth's oceans. Galielo dismissed Kepler's idea as a "useless fiction", and it was not until Sir Isaac Newton published his law of universal gravitation in 1687 that Kepler's theory was proven right. This quick run through history of one of the oldest branches of physical oceanography (tides) simply shows how fascinating oceans have been since many centuries ago.

Today, sea level studies are concerned with problems such as marine transport, coastal erosion or the design of coastal defences against flooding. Interest in mean sea level (MSL) changes has recently focused attention on the possibility of significant increases over this century as a result of global warming. Indeed, global MSL is of immense importance. More than 100 million people live within 1 m of the MSL. A rise in global MSL will affect coastal zones through several processes. Permanent inundation will affect many areas depending on the local gradient of the coast. Low gradient coastal landforms most susceptible to inundation include beach ridge, deltas, mudflats, estuaries, lagoons, bays, etc. This includes the European Low Countries, the southern Baltic, the estuaries of eastern UK, and major river deltas. In the Mediterranean Sea it includes river deltas such as those of the Ebro and the Nile. Coastal wetlands will be among the most severely affected ecosystems, since these form largely in the intertidal zone. Many coral islands have an average elevation of only 1.5-2 m above sea level, and are therefore at risk to inundation. Potentially vulnerable islands include Indian Ocean Islands such as the Maldives, many Pacific and Caribbean Islands and also Australian's Great Barrier Reef. Episodic inundation frequency will also increase because a rise in MSL will result in a greater frequency of occurrence of a storm surge at a given height. Also the rate and extent of coastal erosion is expected to intensify as a result of increased sea level rise. Finally, sea level rise will promote saltwater intrusion into coastal aquifers. For instance, a large part of Holland presently lies below MSL, so that saltwater seeps upward into the subsoil, via groundwater flow.

Those are some of the threats derived from sea level rise. A brief glance to the most recent estimates of past and future sea level rise rates must start from the Intergovernmental Panel on Climate Change (IPCC) Fourth Assessment Report (IPCC AR4, 2007). The IPCC report states that global MSL has been rising during the 20th century at an average rate of 1.7±0.5 mm/yr (Church and White, 2006; Bindoff et al., 2007), an estimate obtained from reconstructions based on altimetry and tide gauge records. More recently, Domingues et al. (2008) have given an updated value of 1.6 mm/yr for the period 1961-2003. By the end of the 21st century, global climate models have predicted a global MSL rise of between 0.18 m and 0.59 m (Meehl et al., 2007), although more recent approaches estimated rises of about 0.8 m (Pfeffer et al., 2008) and 0.5-1.4 m (Rahmstorf, 2007). However, both past and future sea level changes are regionally variable. In the Mediterranean Sea, all long-term sea level trends reported up to date have been estimated from individual tide gauge records, not from basin-wide sea level fields. As an example, Tsimplis et al. (2005) evaluated sea level trends of between 0.4 and 0.8 mm/yr for the period 1958-2001. They identified two periods with marked positive trends (before 1960 and after 1994) and an intermediate period for which most tide gauges show clearly negative trends. It then follows that Mediterranean sea level would have been rising at a much lower rate than global sea level, which explains why regional studies are one of the priorities of present research.

Another priority of sea level research is the quantification of the different processes underlying sea level rise: the ocean mass increase derived from the melting ice sheets (a global scale phenomena), the volume increment derived from the warming of the oceans, referred to as the steric component of sea level, and the meteorological regional contribution. It is also important to determine the extent to which open ocean estimates (given by satellite altimetry or models) are representative of coastal sea level (measured by tide gauges).

This thesis has been carried out in the framework of the VANIMEDAT project (CTM2005-05694-C03/MAR) funded by the Spanish Marine Science and Technology

Program and by the FEDER program of the European Union. The general objective of the project was to study the decadal and interdecadal sea level variability, with particular attention to sea level trends and extreme events. All it in the geographical context of the ocean and seas surrounding the Iberian Peninsula.

The project had several specific objectives. The first one was to determine the spatial and temporal sea level variability, devoting special attention to the consistency between coastal and open sea observations. The second objective was to quantify the contribution, at a regional level, of the different mechanisms that drive sea-level variability. Namely: i) to quantify the effect of atmospheric pressure and wind forcing on sea level from the analysis of sea level residuals produced by a barotropic model; ii) to quantify the contribution of the steric component (and the associated circulation patterns) from hydrographic observations and from the results of a 3D baroclinic model; iii) to estimate the ocean mass increase as the difference between total sea level and the two contributions previously determined. The third objective was the study of extreme events. Tide gauge observations and models allow to examine sea level extremes from a double standpoint: first, by comparing observations and numerical hindcasts, in order to assess the prediction capabilities of the numerical model; and second, by investigating trends in the frequency and amplitude of extremes occurrence (which can take place simultaneously to the other trends referred above) in order to assess future coastal risks.

In this thesis we will focus only on the first two objectives of the VANIMEDAT project. In particular, the type of questions we intend to reply are: has MSL been rising in the Mediterranean Sea during the second half of the 20th century?. If so, how much?. Has sea level rise been uniform in the Mediterranean?. Which component of sea level has contributed the most to the observed Mediterranean sea level trends?. Can baroclinic numerical models accurately reproduce Mediterranean sea level variability?. Can the Mediterranean sea level budget be closed?.

To successfully accomplish this goal, it is first necessary to describe the different contributions to sea level variability and the various techniques that are currently used for their measurement. Consequently, in the first part of this thesis, the necessary concepts are introduced and the different data sets used to obtain the results are described. We start by defining sea level variability and its different contributions: the steric, atmospheric and mass components. Then we present the different techniques used to measure sea level, remarking their main advantages and disadvantages (Chapter 2). The third chapter is dedicated to introduce the data sets used to characterize sea level variability and to quantify the different physical processes. In the fourth chapter we present a summary of the basics of ocean modelling and dynamics. The specific models that are used in this work are also presented in Chapter 4.

The results, which constitute the nucleus of this thesis, are presented in a second group of chapters as follows:

- Chapter 5. This chapter and the next one investigate the Mediterranean long-term sea level variability as reconstructed from available observations. First, a detailed description of the main techniques that are used to analyse climatic data sets is needed. These data sets usually involve phase spaces with thousands of dimensions, making it really difficult to interpret or understand the physical phenomena that they contain. Thus, it is important to use techniques suitable to analyse massive multivariate datasets. One of the most common techniques used in oceanography and meteorology is Principal Component Analysis (PCA), also known as Empirical Orthogonal Function (EOF) analysis. PCA is

an objective technique that attempts to characterise lower-dimensional structures in large multivariate datasets. If the physical processes described by the data are linear, then PCA is an optimal technique; however, if some of those processes are nonlinear, other techniques, such as nonlinear PCA, may be more effective in detecting such structures. Therefore, we start by describing both types of techniques and then we apply them to the analysis of Mediterranean sea level variability for the last decades. The aim of such a comparison is to determine the degree of nonlinearity of the Mediterranean sea level variability at decadal and interdecadal scales, and whether it is worth using nonlinear techniques in spite of its complexity. In this chapter we also obtain a first reconstruction of sea level fields. As stated above, all long-term sea level trends reported up to date have been estimated from individual tide gauge records, so that obtaining basin-wide sea level fields is crucial to revise those estimates. In this first attempt we used a simple technique that, however, did not yield satisfactory results.

- Chapter 6. In this second part we present a more sophisticated methodology to reconstruct sea level variability in the Mediterranean Sea: a reduced space optimal interpolation analysis. This technique intends to combine in an optimal way the benefits of the available long tide gauge series with the complete spatial coverage offered by satellite altimetry; moreover, it gives a theoretical estimate of the errors associated to the reconstructed field. The robustness of the reconstruction is studied by means of several sensitivity tests. Results are presented for two different periods: 1993-2000 and 1945-2000. For the period 1993-2000 the results are compared with observations from satellite altimetry, which allows testing them over the whole domain, whereas for the period 1945-2000 the reconstruction can be validated only against tide gauges. Key results obtained from the reconstruction are the time evolution of Mediterranean MSL and the spatial distribution of sea level trends for the period 1945-2000.

- Chapter 7. The information derived from the reconstruction concerns total sea level variability. In this chapter we set our next target: to identify and quantify the different contributions of that variability: the steric, mass and atmospheric components. Changes in global MSL are driven by the steric variations that result from the expansion/contraction of the water column (due to changes in temperature and salinity) and by water mass changes that essentially derive from changes in the terrestrial storage of freshwater (i.e., melting rate of continental glaciers and ice-sheets and river run-off; the precipitation-evaporation rates are assumed to keep constant at global scale). At regional scale, the mass content of a basin is also affected by the atmospheric pressure, which drives water exchanges between adjacent basins. It can be argued that the atmospheric component could be included within the mass component, since it is in fact a mass displacement, but the distinct nature of the forcing and the fact that it averages to zero at global scale suggests to deal with it as a separate contribution. The atmospheric component has already been studied by several authors; a brief summary of those results is presented within this chapter..

- Chapter 8. The study of the steric contribution to long-term sea level variability is usually undertaken either from available hydrographic data bases or from hindcasts of the last decades (changes in the volume of the water column can be

computed from temperature and salinity distributions). Observations are obviously more accurate than models, but they are handicapped by their spatial and temporal distribution. A further advantage of the hindcasts over observations is that they give a more complete information on the physical processes driving sea level variability. In this chapter we first compare the 1945-2000 reconstruction of Mediterranean sea level carried out in Chapter 6 with a 1961-2000 3D hindcast simulation carried out with OPAMED8 by Somot et al. (2006), in order to assess the reliability of the latter. The two representations are fully independent and based on different hypotheses. The comparison between the reconstruction and the hindcast is performed for two different periods: 1993-2000 (for which altimetry data are available) and 1961-2000 (the longest period common to both distributions). It is of great interest to compare both sea level representations and to determine their strengths and weaknesses for the pre-altimetric period. Once the reconstruction and the model have been compared in terms of total sea level, the steric component is evaluated from the model.

- Chapter 9. In order to understand and explain some of the discrepancies found in Chapter 8 between the model and observations, a more in-depth analysis of numerical models in the Mediterranean Sea is necessary. In the Mediterranean Sea, global models are handicapped by their low resolution, which usually prevents an accurate representation of key processes such as deep water formation or the water exchange through Gibraltar. On the other hand, regional hindcasts such as the one analyzed in Chapter 8 (Somot et al., 2006) or the one carried out by Sannino et al. (2009) have enough resolution, but it must be emphasized that sea level variations inside the Mediterranean basin will depend on the boundary conditions imposed at the Atlantic boundary of the domain, which are usually obtained from global models. In this chapter we carry out an intercomparison between two regional models (Somot et al., 2006; Sannino et al., 2009) and a global model (Barnier et al., 2006). The intercomparison pays particular attention to the Eastern Mediterranean Transient (EMT) as a case study in which spatial resolution is crucial. The EMT defines a period (1987-1995) characterized by a change in the location of dense water formation in the Eastern Mediterranean. The Mediterranean Sea is believed to have the Adriatic Sea as the major source of deep waters during most of the last century; however, between 1987 and 1995 the Aegean Sea became the major source of deep water formation in the Eastern Mediterranean; after 1995 the situation returned back to normal. These changes in the thermohaline circulation of the Eastern basin had its reflection in the sea level variability of the region, which was captured by satellite altimeters. The objective of the intercomparison is not only to study the EMT and the sea level changes associated with it, but also to throw some light on the reasons why some models reproduce such an event better than others, which hopefully will give modelers some clues about what can be done to improve the performance of future simulations. We first carry out a comparison of water properties, such as temperature, salinity and potential density, between the models and hydrographic observations. Second, we assess the performance of the models in reproducing the dense water formation processes that took place during the years of the EMT in the Aegean and Ionian Seas. Then we analyze the total and steric sea level derived from the models. Again, results are presented for two different periods: 1993-2000 and 1961-

2000. For the first period, total sea level from the models is compared with altimetry data, while for the second period the comparison is with the reconstructed sea level. For both periods the steric sea level derived from the models is compared with the steric sea level derived from hydrographic observations.

- Chapter 10. In this chapter we estimate the third and last component of Mediterranean sea level variability: the changes in the water mass of the basin. We first use altimetry, gravimetry (from the GRACE mission) and hydrographic observations spanning the period 2002-2006 to assess the consistency between total sea level and its components in the Mediterranean Sea. The good agreement found between GRACE observations and steric- (and atmospheric-) corrected altimetry supports the quantification of the mass contribution in terms of the non-steric sea level in the Mediterranean. We do it for the period 1948-2000, using total sea level fields from the reconstruction obtained in Chapter 6 and steric sea level fields estimated from historical hydrographic measurements.

- Chapter 11. Each chapter has its own conclusions section; here we only summarize the main contributions of this thesis to the knowledge of long-term Mediterranean sea level variability. The natural continuation of this work is also presented: once we have characterized the sea level variability of the last decades of the 20th century, it is time to predict the sea level variations expected for the 21th century under different greenhouse gases scenarios This work will be carried out in the framework of the VANIMEDAT-2 project (CTM2009-10163-C02-01, funded by the Spanish Marine Science and Technology Program and by the Plan-E of the Spanish Government) and of a contract sponsored by the Spanish Met Office (AEMET), again in the geographical context of the ocean and seas surrounding the Iberian Peninsula.

Part I

Introduction

Chapter 2

An overview of sea level variability

SEA level is the universal datum to which heights on land and depths in the sea are referred. Where considerable heights or depths are involved, an approximate determination of sea level is frequently all that is required. However, if a more accurate determination is needed it can become a complex determination since sea level is continuously disturbed by many factors. Variations in sea level include contributions from different physical processes that can be separated in terms of their time scale. These processes range from surface gravity waves, with periods of 1 to 20 seconds; seiches and tsunamis, with periods of minutes to over an hour; tides, centred around 1/2 and 1 day; meteorological effects of several days to a few months; a seasonal cycle, mainly due to steric effects, but also to atmospheric pressure and winds; long-term variability (inter-annual and inter-decadal), also due to steric and pressure changes; and longer term trends in the MSL caused by climatological and geological effects. Also the amplitude of these components varies enormously. Surface gravity waves have amplitudes of up to 30 m. A tsunami in the deep ocean has a typical amplitude of about 1 m, but as the tsunami approaches the coast and the waters become shallower its amplitude grows enormously reaching amplitudes of over 10 m. Storm surges may be of the order of a few metres in shallow seas. Tides have amplitudes from a few centimeters to a few meters. Intraseasonal meteorological effects and the seasonal cycle are of the order of a few tens of centimeters.

As stated above, this work focuses on the interannual and interdecadal variability and trends. At global scale these long-term variations are due to changes in the water content of the oceans (mostly due to the melting or accumulation of land-based ice in Greenland, Antarctica, and mountain glaciers) and to changes in the volume of the oceans resulting from an expansion or a contraction of the water body (without changing its mass). The former is what we refer to as the mass component. The latter is referred to as the *steric* contribution and it is mostly due to temperature changes (thermosteric variations), although salinity changes (halosteric variations) can also be important. The impact of long-term atmospheric pressure variations and changes in the ocean circulation over sea level cancel out at global scale, but can be very relevant at regional scale. The amplitude of interannual and interdecadal variability is of the order of a few tens of centimetres, while secular trends may be of the order of 1 mm/yr.

Attending to the physical forcing and in absence of very specific events such as a tsunami, any instantaneous measurement of sea level can be considered the sum of three components:

$$\text{sea level} \approx \text{MSL(t)} + \text{tides} + \text{meteorological residuals} \qquad (2.1)$$

Each of these components is controlled by separate physical processes and the variations of each part are essentially independent of the variations in the other parts. The next section is devoted to a more detailed explanation of the terms of Eq. (2.1).

2.1 The different contributions to sea level

2.1.1 Tides

Tides can be defined as periodic variations of sea level which are directly related in amplitude and phase to some periodic geophysical force. The dominant geophysical forcing function is the variation of the gravitational field on the surface of the earth, caused by the regular movements of the moon-earth and earth-sun systems. Tides propagate as long waves on a rotating earth. Reflection of progressive waves leads to standing waves, which on a rotating earth become amphridromic systems. Amphridromic systems are locations where there is zero tidal amplitude and around which the tidal waves progress in a clockwise sense in the southern hemisphere and an anti-clockwise sense in the northern hemisphere. Where the natural dimensions of a basin are close to a quarter wave-length of the progressive tidal wave, resonance occurs and the resulting amplitudes at the head of the basin may become very large.

The observed tides in the main oceans have ranges of about 1 m, but in some local areas of the continental shelves, ranges may exceed 10 m. An extreme example is found in the Bay of Fundy, where ranges of 15 m may sometimes occur. In the Mediterranean Sea tides are small, however this is not to say that there are no tides at all. Indeed, they generate a mean variation of about 40 cm, but atmospheric conditions often hide the rise and fall in sea level. The highest amplitudes are observed in the Gulf of Gabes, off the coast of Tunisia, where they have a range of nearly 2 m. Amphidromic points are located in the Adriatic Sea and south of Sicily, but both the Western and Eastern basins have also nodal lines where the tidal range is zero (Fig. 2.1).

In most places the tides are dominated by semidiurnal patterns, but there are places where diurnal tides dominate. Elsewhere, there are mixed tidal regimes where the pattern may vary between semidiurnal and diurnal in its characteristics.

2.1.2 Meteorogical residuals

Meteorological residuals are the dominant component of the intraseasonal variability once the tidal signal is removed (e.g. via spectral filtering) from sea level measurements. They are irregular, as are the variations in the weather. Sometimes the term *surge residual* is used, but more commonly *surge* is used to describe a particular event during which a very large non-tidal component is generated.
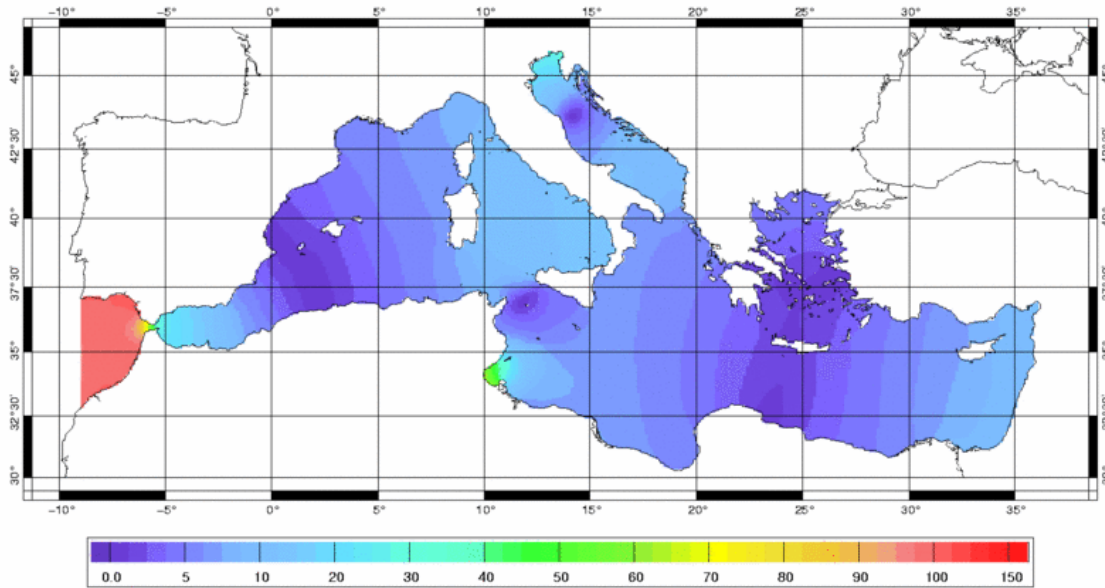
Figure 2.1. Amplitude (in cm) of the principal (M2) lunar tide in the Mediterranean predicted by the CEFMO model.

It must be stated that in this work, the meteorological residuals will refer only to the intraseasonal mechanical forcing of the atmosphere onto the ocean. This forcing acts in two different ways: changes in atmospheric pressure act vertically on the sea surface and result in water mass displacements. When a new equilibrium situation is reached, a millibar increase/decrease of atmospheric pressure will have decreased/increased sea level by 1 cm (actually 0.993 cm). This is called the inverted barometer effect. The second way in which the atmosphere acts mechanically on sea level is through the drag exerted by the wind, which increases as the square of the wind speed to a first approximation. This drag sets the water in motion and when the water transport is impeded by land boundaries there is an increase in coastal sea level: the storm surge. Conversely, the effect of the wind is usually negligible at open sea.

The mechanical atmospheric forcing is also relevant at seasonal and longer time scales, but these effects will be included within the MSL(t) term of eq. (2.1) and referred to as the atmospheric contribution to MSL(t). Finally, it is also worth noting that the atmosphere also acts on sea level through heat and freshwater fluxes. These effects are more relevant at seasonal and longer time scales and will not be considered as part of the meteorological residuals, but as part of MSL(t).

2.1.3 Mean sea level

If an operator of a tide gauge was asked what MSL is, he would probably say that it is the arithmetic mean of the heights observed over some specified period of time such that periodic changes in sea level are averaged out. MSL to a geodesist usually means the local height of the global Mean Sea Surface (MSS) above a level reference surface called geoid.

We can think of a level surface as a surface in which you do not have to do any work to move along. As a first approximation the level reference is an oblate ellipsoid: an ellipse with a smallest radius of 6356.76 km at the poles, and a largest radius of 6378.14 km at the equator, rotated around the Earth's rotation axis. However, this ellipsoid is not exactly a level surface. Concentrations of mass in different parts of the earth's interior, and topography all result in a gravitational attraction which deforms the level surfaces. The geoid is the closest level surface to the MSS. It departs from an ellipsoid by about 100 m in each direction, depending on position on the Earth. If there were no tidal forcing, no differences in water density, no currents and no atmospheric forcing, then MSS and geoid would be the same surfaces. However, while the effects of the tide on sea level balance out if the observations are continued over a long period of time, the effects of wind and variations in the atmospheric pressure do not balance out, but leave a resultant effect. Therefore, the MSS is not a level surface, and it departs from the geoid by about 1-2 m, even after averaging out the effects of tides. For instance, the Atlantic Ocean as a whole is about 40 cm lower than the Pacific.

In Eq. (2.1) sea level at any instant was defined as the MSL plus the tide and the meteorological residual components. The MSL term was deliberately written as a function of time, since there are pronounced annual and semi-annual variations of MSL due to seasonal changes in atmospheric pressure, water density and ocean circulation. Also geological and climatological effects cause variations of MSL. Long-term changes of MSL are called *secular* changes. Global changes in the MSL are called *eustatic* changes. Vertical land movements of regional extent are called *eperiogenic* movements.

There are many global and regional analyses of MSL trends. At global scale, MSL trends have been estimated by different authors. Widely accepted values are the 1.8 mm/yr given by Church et al. (2004) for the period 1950-2000, and the 1.7 mm/yr given by Church and White (2006) for the whole 20th century, both obtained from reconstructions based on altimetry and tide gauge records. More recently, Domingues et al. (2008) have considered the bias affecting part of the historical observations and have given an updated value of 1.6 mm/yr for the period 1961-2003. In the Mediterranean Sea all long-term sea level trends reported have been estimated from individual tide gauge records, not from a basin-wide sea level reconstruction. As an example, Tsimplis et al. (2005) evaluated sea level trends of between 0.4 and 0.8 mm/yr for the period 1958-2001. They identified two periods with marked positive trends (before 1960 and after 1994) and an intermediate period for which most tide gauges show clearly negative trends. Tsimplis et al. (2005) and Gomis et al. (2008) pointed to the atmospheric pressure as responsible for the negative trends: its contribution has been evaluated as -0.6 mm/yr for 1958-2001 and -1.0 mm/yr for 1960-1994.

These changes are very small when compared with the daily tidal and surge changes of sea level. However, over geological periods there have been considerable changes in MSL. For instance, Aloisi et al. (1978) carried out a detailed study on the Gulf of Lions (in the Mediterranean Sea) based on a set of some 80 radiocarbon dates and obtained a Holocene sea level rise of over 50 m as a result of the deglaciation that followed the last glacial maximum of 21 000 years ago. Most of that sea level rise occurred in the early-Holocene, while it gradually slowed down 8000 years ago, when sea level was some 15 m below that of today. The increase then proceeded more gradually until present levels were reached some 4000 years ago. Since that time the changes have consisted of oscillations of small amplitude. Indeed, several data from tectonic and non-tectonic areas in the Mediterranean Sea are consistent with a global eustatic near stability during the last 6000 years (Pirazzoli, 2004).

It is important to remark that the change of MSL relative to a fixed point on land is a measure only of the difference between the vertical movements of the MSL and of the land itself. During periods of glaciation sea level falls because water is locked into the polar ice-caps; as the glaciers recede, global sea level increases, but this general increase in level may not be apparent along coasts which have only recently been relieved of their ice burden. Along these coasts there is an isostatic land uplift, which is measured as a decrease in local sea level. Moreover, when land ice melts the distribution of the mass of water around the global ocean is by no means uniform. A large melting would result in a modification in the Earth's gravity field which would result in sea level changes being higher in some places than in others. One of the major problems when interpreting MSL is the identification of separate eustatic changes and vertical land movements when only secular changes are directly measurable at a particular location.

2.1.4 The different contributions to long-term sea level variability

This thesis focuses on long-term sea level variations (the seasonal cycle and longer); that is, on the MSL(t) term or eq. (2.1). As it was mentioned earlier in this Chapter, these long-term variations are mainly caused by steric and mass changes, and long-term atmospheric pressure variations. The sum of these three contributions results in the total sea level. Therefore, it is now appropriate to characterize more extensively what we really mean by the steric, mass and atmospheric components.

The steric component

The changes in the volume of the oceans resulting from an expansion or a contraction of the water body (without changing its mass) due to temperature and salinity changes are referred to as the steric contribution.

The rate of the thermosteric (i.e., due to temperature only) component of global sea level rise has usually been evaluated from gridded ocean temperature data sets (Levitus et al., 2000; Ishii et al., 2003; Levitus et al., 2005). Antonov et al. (2005) estimated the thermosteric trend to be 0.33 mm/yr for the period 1955-2003. For the same period, Ishii et al. (2006) give values of 0.31±0.07 and 0.04±0.01 mm/yr for the thermosteric and the halosteric sea level, respectively. However, a recent result obtained by Domingues et al. (2008) from in-situ hydrographic measurements spanning the period 1961-2003 increases the thermosteric sea level trend up to 0.52±0.08 mm/yr. All these estimates correspond to the thermosteric contribution of the upper 700 m. Estimates of the thermal expansion of the ocean below 700 m are much more uncertain and they vary from the 0.07 mm/yr computed from observations spanning the period 1961-2003 given by Domingues et al. (2008) to the 0.3 mm/yr given by the German Consortium for Estimating the Circulation and Climate of the Ocean Model for the period 1962-2001. At regional scale, the estimates of the trends of the thermosteric component vary significantly. For instance, Antonov et al. (2005) give values of 0.60, 0.25 and 0.22 mm/yr for the Atlantic, Indian and Pacific Oceans, respectively, for the period 1955-2003. In the Mediterranean Sea, Tsimplis et al. (2008) found steric sea level trends of -0.16±0.06 and -0.26±0.06 mm/yr in the Western Mediterranean and in the Adriatic, respectively, for the period 1960-2000.

The mass component

Water mass changes of the global ocean essentially derive from changes in the terrestrial storage of freshwater (i.e., melting rate of continental glaciers and ice-sheets and river run-off), since the precipitation-evaporation rates are assumed to keep constant at global scale. At regional scale, the mass content of a basin is also affected by the atmospheric pressure, which drives water exchanges between adjacent basins, but this effect will be included within the atmospheric component described later on.

Few estimates have been published for the mass contribution to sea level. Due to the lack of direct, independent observations, the mass component has been estimated in two different ways: i) from estimations of the components of the hydrological budget; ii) computing the non-steric (total minus steric) sea level. The first method has the problem that the components of the hydrological budget are subjected to large uncertainties. The second method has the problem that, on a long term basis, total sea level has only been recorded by tide gauges located at coastal sites which may not be representative of the basin average sea level. In order to overcome this problem, Domingues et al. (2008) estimated the mass component from global reconstructions of total sea level (from tide gauges and altimetry) and of the steric component (from hydrographic observations); they found that the contribution of the mass component to global sea level rise would range between 0.8 and 1.1 mm/yr for the period 1961-2003.

Since 2002, the Gravity Recovery and Climate Experiment (GRACE) Mission measures the variations in the gravity field caused by changes in the water mass of the Earth, then providing the first direct and independent measure of the mass contribution to sea level change. Total sea level measurements and hydrographic data (to estimate the steric component) can then be used to validate the estimation of the mass component as measured by GRACE. Willis et al. (2008) presented an analysis of altimetry, steric sea level and GRACE observations for the period July 2003 to June 2007 and concluded that the 4-year trends of the three signals were not consistent. Conversely, Leuliette and Miller (2009) carried out a similar analysis for the period January 2004 to December 2007 and stated that the total sea level trend (2.4±1.1 mm/yr) is not statistically different from the sum of the steric and mass trends (1.5±1.0 mm/yr). More recently, Cazenave et al. (2009) found that the total sea level trend (2.5±0.4 mm/yr) is in good agreement with the sum of the mass and steric trends (2.3±0.2 mm/yr) for the period 2003-2008. All these analysis refer to global sea level.

The atmospheric component

Global sea level rise is significantly modulated at regional scale by changes in the atmospheric pressure and wind forcing and by the oceanic circulation. The mechanical atmospheric forcing not only contributes to long-term sea level trends, but also to the inter-annual and inter-decadal variability. At these scales the Mediterranean Sea is submitted to the influence of atmospheric modes such as the North Atlantic Oscillation (NAO). A clear correlation has been found between the NAO index and sea level in the NE Atlantic (Wakelin et al., 2003; Woolf et al., 2003; Yan et al., 2004). In the Mediterranean, sea level variability has also been related to the NAO through the combined effects of atmospheric pressure anomalies and changes in the evaporation-precipitation budget (Tsimplis and Josey, 2001; Gomis et al., 2008; Ruiz et al., 2008).

In the absence of wind and tidal forcing, and frictional influences, the sea surface elevation follows very closely the atmospheric pressure forcing. This is nothing but a statement of hydrostatic balance in which sea level adjusts instantaneously to changes in atmospheric pressure at its surface (the barometer response mentioned above). This is not exact at high frequencies and on broad shelves and semienclosed seas, but on seasonal and longer time scales the inverse barometer response is quite accurate.

The impact of long-term atmospheric pressure variations and changes in the ocean circulation over sea level cancel out at global scale, but at regional scale they can also play a key role. For instance, the contribution of the atmospheric pressure and wind to Mediterranean sea level variability for the period 1958-2001 has been estimated in -0.60±0.04 mm/yr (Gomis et al., 2008).

Finally, it has been mentioned that changes in the circulation can also modulate global sea level. It must be noted, however, that geostrophic changes in response to changes in the density distribution are already accounted for by the steric component. That is, only changes in the barotropic mode of the circulation and changes in the ageostrophic motion should be considered. These changes are usually small and average out at basin scale; hence, although they can be relevant at local scale, they are often neglected when dealing with a domain such as the Mediterranean Sea.

2.2 Sea level measurement

Now that we have defined the different contributions to sea level variability, it is appropriate to describe the type of instruments that are presently available for the measurement of sea level. Sea level from the past can be derived from geological and archaeological sources, while relatively recent values have been obtained from tide gauge measurements and, in the last two decades, from space by satellite altimetry. Archaeological and geological data are important in providing a view of underlying sea level change on timescales of several centuries or thousands of years. However, tide gauges have been the major source of sea level information over the past two centuries (the oldest tide gauge is the one in Amsterdam and dates from 1682). The reference frame used by tide gauges and altimetric satellites for the measurement of sea level are different: while tide gauges measure sea level changes relative to the land upon which the measuring instrument is located, altimetric satellites determine the absolute sea level, because they make measurements with respect to the Earth's centre of mass. Hence, when comparing both types of measurements, land movements such as the Glacial Isostatic Adjustment (GIA, sea section 2.2.4) and local techtonics must be taken into account.

In addition to tide gauges and satellite altimeters, also gravimetric measurements deserve some comments. Local gravimetric observations date back to a few decades, but the first systematic measures started with the launching of satellite missions. The first one was the GRACE mission; lunched in 2002, it is based on a paired satellite-satellite tracking system that measures the time dependence of the Earth's gravitational field. Although it does not measure sea level directly, it can be used to infer mass variations in sea level with a spatial resolution of several hundred km. The newest satellite mission is the Gravity field and steady-state Ocean Circulation Explorer (GOCE), launched on March 2009. GOCE also measures the Earth's gravity field, but with a spatial resolution better than 100 km.

2.2.1 Tide gauges

Tide gauges can measure relative sea level with a high accuracy. However, the measurements obtained from the global tide gauge network are handicapped by the uneven geographical distribution of the instruments and by the complication of land movements in the records. Because most tide gauges were originally installed for local purposes, such as harbour navigation or storm surge flood protection, the global network of sea level monitoring stations has not evolved in a geographically uniform way; in fact, sea level is still monitored poorly in many remote parts of the world.

The choice of the tide gauge site is very important and many considerations must be taken into account. The installation must be capable of withstanding bad environmental conditions; River estuaries should be avoided, for instance, since during a tidal cycle the water density could fluctuate affecting float gauge measurements; The ground on which the installation is set should be as stable as possible; Risk collision with boats should be avoided; The gauge site should have continuous mains electrical power and telephone or satellite for transmission of data; The access to the gauge site must be adequate for installation and maintenance; The area around the site must be capable of hosting the benchmarks required for the geodetic control of sea level data; and many more. An important consequence of those constrains is that tide gauges are installed only at coastal stations and, therefore, they can only measure coastal and island sea level.

There are mainly four types of tide gauges:

- The stilling well gauge. Most of the first tide gauges were of this type. The well is connected to open sea by a hole located well below the sea surface and its function is to filter out the surface gravity waves so that the tides and longer-term processes can be recorded accurately. The instrument consists of a float gauge following the oscillations of the sea surface within the well and connected by a chain to a pen and chart recorder; more recently, the float is connected to a shaft encoder such that the readings of sea level can be digitized automatically.

- Pressure gauges. The principle of this type of gauges is the measurement of the hydrostatic pressure of the water column above a fixed, leveled point and the conversion of that hydrostatic pressure into a sea level equivalent. For an accurate conversion of pressure to sea level, the density of the water column must be known. The density can be computed from temperature and salinity measurements, usually obtained by independent sensors attached to the tide gauge. A common assumption is that the density measured by the tide gauge is representative of the whole water column above the instrument. In estuarine locations, however, the density can have marked differences with depth, so that some density corrections will have to be included in the data processing. The most commonly used types of pressure gauges are the pneumatic bubbler gauges and gauges in which the pressure sensor is mounted directly in the water.

- Acoustic tide gauges. The functioning of acoustic gauges is based on the measurement of the travel time of acoustic pulses reflected vertically from the air-sea interface. The main problem related to the use of acoustic tide gauges arises from the dependence of the speed of sound on air temperature. That problem can be partially compensated by constraining the acoustic signal to travel within a narrow vertical sounding tube. The air temperature can then be

measured continuously at a point in the air column and used to calculate the sound velocity. A more accurate way of compensation is by using an acoustic reflector at a fixed level in the air column. By relating the reflection from the sea surface to that from the fixed reflector, direct compensation for variation in sound velocity between the acoustic transducer and the fixed reflector can be achieved. Another kind of acoustic gauge makes the measurements in the open air, with the acoustic transducer mounted vertically above the sea surface, but in certain conditions the reflected signal may be lost.

- Radar gauges. They have become available during the last few years. They are very easy to operate and maintain, as acoustic gauges, and do not share the disadvantage of the dependence on the air temperature. The active part of the gauge is located above the water surface and measures the distance between this point and the air-sea interface. Key advantages over traditional tide gauges are that it makes a direct measurement of sea level and that the effects of density and temperature variations in the atmosphere are unimportant. The main constraint is that the power consumption may be relatively large in radar systems if they are used on a continuous basis in a rapid sampling mode.

The accuracy of tide gauges depends on the measurement system, but it is usually better than 1 cm (i.e., more than enough for most applications).

Datum control

It is important to recall that tide gauges provide a measure of sea level relative to a land benchmark, and that land is not quiet over long periods of time. The vertical movements of the land are associated with a range of natural processes such as co-seismic activity, glacial isostatic adjustment and plate tectonics, but also with a range of human activities. It is obvious then that for long-term sea level studies, tide gauge measurements must be corrected for land movements in order to obtain the real sea level changes. This is achieved by careful definition of tide gauge datums, by local levelling procedures, and by making independent measurements of land movements using modern geodetic techniques that derive from the use of very high resolution Global Positioning System (GPS) receivers and absolute gravimeters.

For sea level observations, a land benchmark is used as the primary reference point. The benchmark is a clearly marked point located on a stable surface. The tide gauge benchmark (TGBM) is chosen as the main bench mark for the tide gauge and it serves as the datum to which the values of sea level are referred. Another important benchmark is the GPS benchmark (GPSBM), which is another mark of the available set that is used for GPS measurements near the gauge.

Over the past decade, advances in modern geodetic techniques, such as the GPS and the Radiopositioning Integrated by Satellite (DORIS) system, have provided new methods for fixing tide gauge bench marks. The space geodesy measurements can be used to fix into a geocentric reference frame the GPSBM, which should be connected to the TGBM by levelling. In this way, the MSL at the tide gauge can be defined in a global geocentric reference frame, which provides an absolute measure of MSL, rather than MSL relative to each local TGBM. Figure 2.2 shows a diagram of a tide gauge installation to measure absolute sea level.

Ideally, all tide gauge sites should be equipped with a permanent continuous GPS receiver. However, in practice, the financial resources required are large and, therefore,

permanent GPS receivers are only installed at strategic tide gauges. This makes that tide gauge data are usually corrected for vertical land movements (mainly due to GIA) using numerical models(see section 2.2.4).
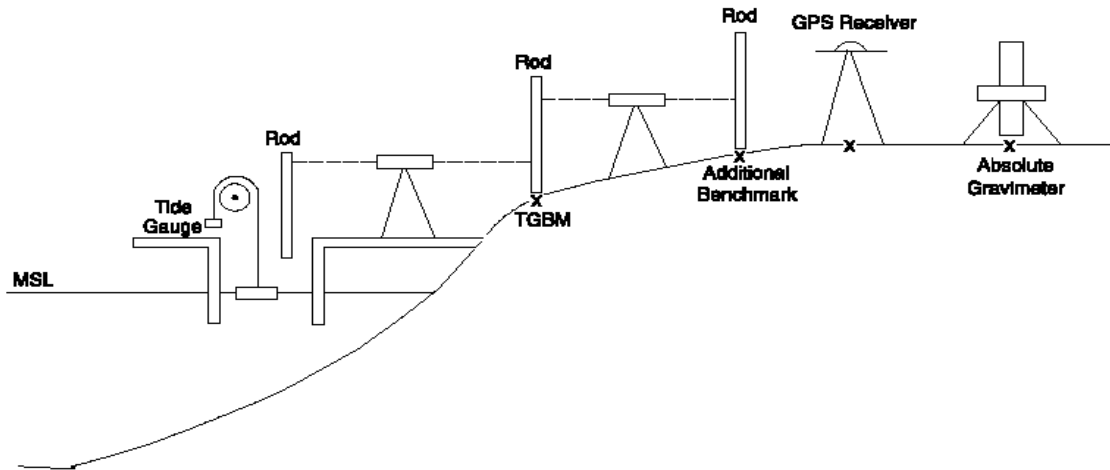

Figure 2.2. Diagram of a tide gauge installation to measure absolute sea level.

2.2.2 Satellite altimetry

Satellite altimetry was initially designed to measure sea level by a combination of radar technique, which measures the distance from the satellite to a reflecting surface, and a positioning technique, which allows a very precise location of the satellite on its orbit. The seventies saw the development of accurate satellite altimeter systems such as *Skylab*, *Geos-3* and *Seasat*, although their orbit error (over 50 cm) was still too large to observe sea surface height variations accurately enough. The first altimeter with an orbit error lower then 40 cm, *Geosat*, was launched in 1985 by the U.S. Navy with the purpose of mapping the mean surface of the Earth for defence applications. However, after the successful 18-month geodetic mission, the satellite was set into a 17.4-day exact repeat orbit along the same tracks as *Seasat* and provided 2-1/2 years of data on ocean circulation. The next satellite altimeter was the European Remote Sensing (ERS)-1, launched on July 1991 and switched off in June 1996 (retired in March 2000).

The first of a new generation of altimeters was launched in August 1992: the *Topex/Poseidon*, with a precise orbitography and location system like DORIS, became the first satellite altimeter to provide useful data of sea surface height variations due to low-amplitude ocean dynamical processes. The next one, ERS-2, was launched in April 1995 as the follow-on from ERS-1, with which it was used in tandem from August 1995-1996 (they had identical orbits of 35 days repeating period with a one-day shift between them). On June 2003, ERS-2's onboard tape recorder used for the altimeter data experienced a number of failures. Since then, ERS-2 data are unavailable except for when the satellite is within visibility of ESA's ground stations over Europe, North Atlantic, the Artic and Western North-America.

The last generation of altimeters started with the launch, in December 2001, of *Jason-1*, the follow-on of Topex/Poseidon. In March 2002 it was the time of the *Envisat*

satellite, the follow-on to ERS-1 and ERS-2. Both satellites have an accuracy of the order of a few centimetres. Finally, in the framework of a cooperation between CNES, Eumetsat, NASA and NOAA, the Jason-2/OSTM altimetry satellite was launched on the 20th of June of 2008.

For the medium term, consideration is now being given to altimetry missions capable of scanning the ocean surface at spatial scales of a few tens of kilometres and passing over the same spots every few days. Altimeter-interferometers are also under study. In 2010 there are several missions to be launched: Cryosat-2, Saral and HY-2. Several options are being considered for 2011 and beyond: Sentinel-3 (2012), Jason-3 (2013-2014), Swot (2016-2018).

The general principle of satellite altimetry (Figure 2.3) is simple: the satellite sends out radar pulses and measures the time of the return reflection from the ocean surface; by knowing the orbit of the satellite we can determine the actual ocean height with respect to some land based geodetic network or to some mathematical surface (e.g., a reference ellipsoid). It's worth stressing that, due to atmospheric effects on the speed of electromagnetic waves, orbit fluctuations and other minor perturbations, satellite altimetry data must be submitted to a whole set of geophysical corrections. Even after the corrections, the accuracy of the measurements is of order of 1-2cm.

Another significant handicap of altimetry is that ocean surface is by no means an ellipsoid; the geometry of the ocean at rest (the geoid) is much more complex due to the spatial variations of the gravity field. The departures of the geoid with respect to the ellipsoid are much larger (up to a hundred of meters) than the departures of sea level from the geoid due to ocean dynamics (up to a few tens of cm, or a few meters if tides are considered). Therefore, the geoid must be subtracted from the measurements in order to isolate the dynamical signal. The problem is that the geoid is not know with enough accuracy…The only option to remove the geoid from the measurements is to average as many years as possible of data, assuming that, on average, the ocean surface will have the same geometry of the ocean at rest. However, that is not entirely true, since there are almost stationary currents that create quasi-permanent sea level structures. Hence, when the mean altimetric field is subtracted from the measurements, these permanent features are also subtracted, the remaining signal reflecting not only the departures from geoid, but also from the permanent sea-level structures. The remaining signal (the one distributed by the agencies that routinely process altimetry data) is referred to as sea level anomaly (SLA).

The repeating cycle of altimetric satellites depends on the satellite: *Topex/Poseidon* and its successors *Jason-1* and *Jason-2* have a repeating cycle of 10 days, while ERS satellites and their successor *Envisat* have a repeating cycle of 35 days. Because altimetric maps are interpolated from track data that have been obtained at spread time instants within the repeating cycle period, there is a danger of aliasing due to rapid sea level fluctuations that are mostly caused by tides and the mechanical atmospheric forcing. This is why both, tides and the sea-level response to atmospheric pressure and wind are usually subtracted from track data prior to their interpolations onto grid points.

Finally, it is worth mentioning that some Agencies are presently supplying multimission altimetric data, taking advantage of the coexistence of several satellite altimeters. This implies a complex intercalibration of the different data sets prior to mergin, but it results in a product with an increased effective spatial and temporal resolution.
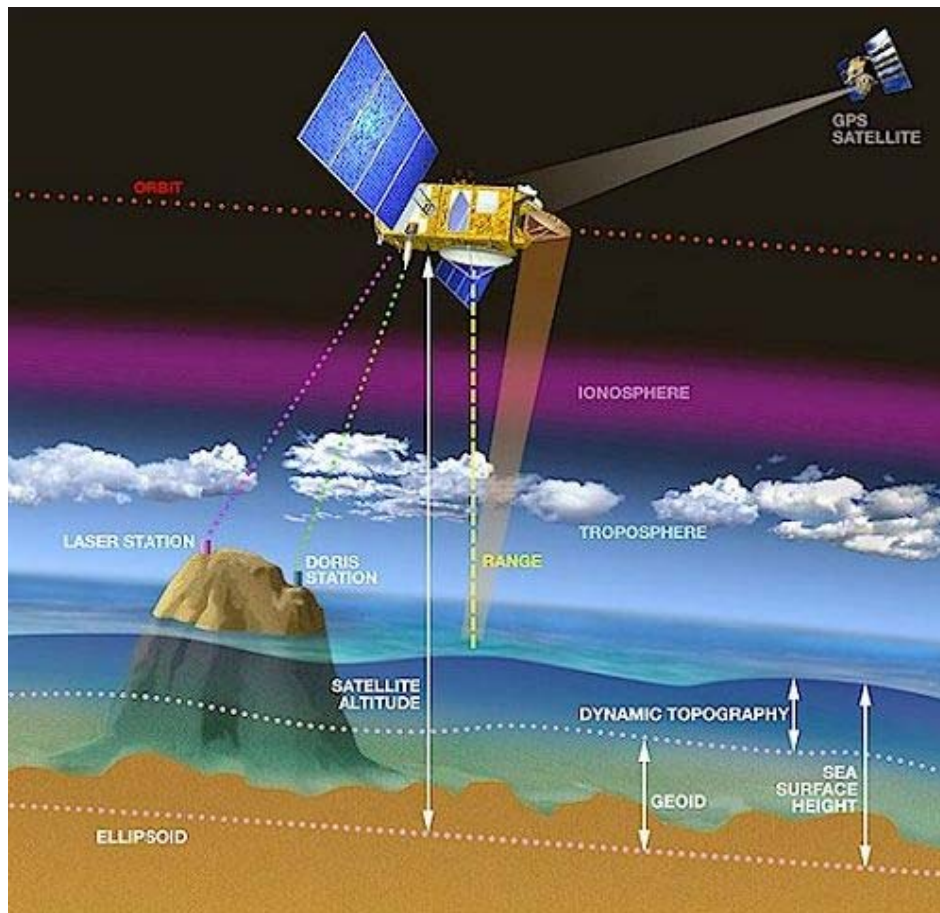
Figure 2.3. Satellite altimetry principle.

2.2.3 The GRACE mission

The primary goal of the GRACE project is to determine variations in the Earth's gravity field at monthly intervals and at a spatial resolution of several hundred km. This objective is achieved by making continuous measurements of the change in the distance between twin spacecraft co-orbiting in ~500 km altitude, near circular, polar orbits spaced ~220 km apart, using a microwave ranging system. The satellite orientation and position are precisely measured using twin star cameras and a GPS receiver, respectively.

Spatial and temporal variations in the Earth's gravity field affect the orbits of the twin spacecrafts differently. These differences are manifested as changes in the distance between the spacecrafts, as they orbit the Earth. This change in distance is reflected in the time-of-flight of microwave signals transmitted and received nearly simultaneously between the two spacecraft. The change in this time of flight is continuously measured by tracking the phase of the microwave carrier signals. The so-called dual-one way range change measurements can be reconstructed from these phase measurements. This range change, along with other mission and ancillary data, is subsequently analyzed to extract the parameters of an Earth gravity field model.

The Earth's gravity field (*V*) at any point *P*, exterior to the Earth, is typically represented using an infinite spherical harmonic series. The field point *P* is specified by its geocentric radius *r*, geographic latitude φ, and longitude λ. If μ represents the gravitational constant of the Earth, and a_E represents its mean equatorial radius, then *V* can be represented as (Heiskanen and Moritz, 1967)

$$V(r,\varphi,\lambda,t) = \frac{\mu}{r} + \frac{\mu}{r} \sum_{l=2}^{N_{max}} \left(\frac{a_E}{r}\right)^l \sum_{m=0}^{l} P_{lm}(\sin\varphi)\left[C_{lm}(t)\cos m\lambda + S_{lm}(t)\sin m\lambda\right] \quad (2.2)$$

where $P_{lm}(\sin\varphi)$ are the fully normalized Associated Legendre Polynomials of degree *l* and order *m*. C_{lm} and S_{lm} are the fully normalized spherical harmonic geopotential coefficients. Although the spherical harmonic series (2.2) is exact only if the summation is carried out to an infinite degree, in practice it is truncated at some value N_{max}.

The values of the gravitational coefficients along with other dynamical orbit parameters are estimated by the GRACE project from the observed variations in the range rate between the two satellites and other tracking data by means of least squares estimation in order to minimize the misfit between a modeled orbit and the observations (Bettadpur, 2004). Estimations of the gravity field coefficients are made approximately every month to degree/order 120, which corresponds to wavelengths of about 300 km and longer.

2.2.4 The GIA and relative sea level

During the late Quaternary epoch of Earth history, Earth's climate has been very sensitive to the small changes in effective solar insolation caused by the changing geometry of Earth's orbit around the Sun. Although small, such changes have been responsible for the ice-ages that have dominated climate system variability in the latter half of the Pleistocene period (Hays et al., 1976). The Pleistocene has been marked by a number of glaciation and deglaciation events, each cycle having a characteristic duration of about 100,000 years. During each glaciation phase of the cycle, sea level has fallen on average by approximately 120 m as freshwater produced by evaporation from the oceans has been deposited as snow at high northern latitudes. The snow then transforms into ice by means of a complex sequence of compression, partial melting and re-freezing resulting in a thickening of the ice sheets, which reached thicknesses of about 4 km at the end of the glaciation phase. During the last deglaciation phase, which began 21,000 years ago, sea level rose on average by about 120 m due to the melting of the ice sheets that formed during the glaciation.

Although the last deglaciation was essentially over about 6000 years ago, relative sea level has continued changing beyond that date. Sea level changes occurring after the deglaciation was complete are the result of the Earth's delayed viscoelastic response to the redistribution of mass on its surface that accompanied deglaciation. These sea level changes are larger in regions that were previously glaciated, such as Northern Europe and Canada, where relative sea level is still falling in some areas at rates larger than 10 mm/yr due to the ongoing postglacial rebound (PGR) of the crust. However, even at sites far away from those glaciated regions, the rates of sea level change due to GIA are

not negligible. In these regions sea level is falling mainly due to the redistribution of water over the ocean basins that accompanies the changing shape of the Earth. A more detailed explanation of the GIA process can be found in the literature (Peltier, 2002; Paulson et al., 2007; Peltier, 2007).

As it was mentioned earlier in this chapter, tide gauges measure sea level relative to land marks, and therefore significant land movements can contaminate the trends. Without independent estimates of these vertical land movements, tide gauges can not determine whether sea level is raising/falling, the land is sinking/rising, or both. Therefore, such contamination needs to be removed from tide gauge data in order to obtain an accurate measurement of sea level trends. With respect to satellites, they also require a correction for GIA, although this correction is different from the one used for tide gauges because satellites measure sea level with respect to the Earth's centre of mass, as opposed to the surface of the solid Earth in the case of tide gauges (Peltier, 2002). Correcting satellite observations (altimetry and GRACE) for the effect of GIA involves the prediction of the rate at which the geoid changes height, which in turn is the sum of two terms: the present-day rate of relative sea level rise due to GIA and the rate of increase of the local radius of the solid Earth relative to the centre of mass of the Earth. Subtracting this sum from satellite observations yields the actual sea level change.

It has been shown in different studies that the GIA contamination affecting tide gauges is significant (Peltier, 1986, Peltier 2002). For instance, when the GIA signal was removed from long tide gauge records from the Permanent Service for Mean Sea Level (PSMSL), the trend of global sea level rise obtained for the second half of the last century was 1.84 mm/yr (Peltier, 2002), which is in good agreement with the global trend of 1.8 mm/yr obtained by Church et al. (2004) from global sea level reconstruction for the period 1950-2000. Peltier (2002) also estimated the GIA correction to be applied to satellite measurements: using the ICE-4G VM2 model (Peltier 1994, 1996), he found that satellite observations are biased down by approximately 0.3 mm/yr at global scale. At regional scale, the trends computed from both, recent GPS series (Wöppelmann et al., 2007) and altimetry and tide gauge series (García et al., 2007) suggest that most Mediterranean shores would be slightly subducting; however, GPS series are too noisy to be reliable over the short periods collected at present and do not cover all tide gauges sites. GPS measurements require a decade or more to determine solid Earth uplift or subsidence rates of less than 1 mm/year. Other methods have therefore been used to correct historical sea level data for the effect of GIA. Theoretical models of global GIA are the preferred choice nowadays.

In this thesis the ICE-5G VM2 model developed by Peltier (2004) will be used to correct all tide gauges and satellite observations. Figure 2.4 shows the values of present-day rate relative sea level rise (or equivalently, the rate of land subduction, with negative values then implying land uplift) at all PSMSL tide gauge sites as predicted by the ICE-5G VM2 model. At global scale, the largest negative trends are found in Fennoscandia and Canada, with values that reach -10 mm/yr at some locations. Positive trends are found in both the Atlantic and Pacific coast in North America (up to 3 mm/yr). In the Mediterranean Sea the model predicts slightly negative values almost everywhere, with a maximum falling relative sea level of -0.3 mm/yr in the Adriatic shores. Given the sign convention, the values of Figure 2.4 must be subtracted to the trends computed from tide gauge records in order to obtain absolute sea level trends.
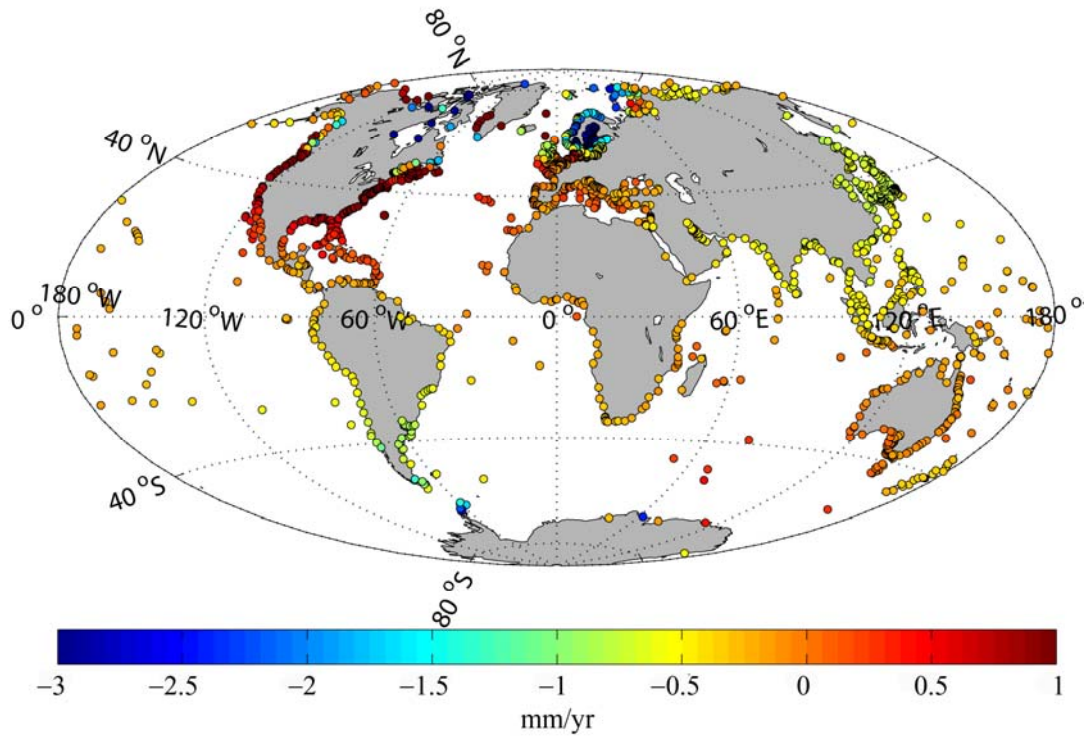
Figure 2.4. Present-day rate of relative sea level rise derived from the GIA (or equivalently, the rate of land subduction, with negative values then implying land uplift) at the PSMSL tide gauge sites as predicted by the ICE-5G VM2 model developed by Peltier et al. (2004).

Chapter 3

Data sets

IN Chapter 2 we have given an introductory run through sea level variability, its
different contributions and the different techniques that are currently used to obtain a
measure of sea level. In this chapter we present the data sets that are used in this work
for the analysis of the sea level variability in the Mediterranean sea. Since many of the
results presented in the second part of this thesis base on the estimation of linear trends,
the methodology followed to obtain this estimations and their associated uncertainty is
also presented (see section 3.5).

3.1 Tide gauge records

The tide gauge data set used in this thesis consists of monthly MSL series obtained from
the data archive of the PSMSL (Woodworth and Player, 2003). All data used in this
work are Revised Local Reference (RLR) data. The RLR datum at a tide gauge site is a
datum defined as a simple offset from the TGBM, such that values of sea level
expressed relative to the RLR datum have numerical values around 7000 mm. The
concept of the RLR datum was invented by the PSMSL so that long time series of sea
level change at a site could be constructed, even if parts of the time series had been
collected using different gauges and different, but geodetically connected, TGBMs. The
approximate value of 7000 mm was chosen to avoid that contemporary computers (the
value was set in the late 1960s) had to store negative numbers. The RLR datum is
defined for each gauge site separately and the RLR at one site can not be related to the
RLR at any other site without additional knowledge on connections between TGBMs at
the different sites.

As it was commented in Chapter 2, tide gauge data require a correction for GIA. All
tide gauges series used in this thesis have been corrected using the ICE-5G VM2 model
of the GIA process described in the work of Peltier (2004) and obtained from
http://www.atmosp.physics.utoronto.ca/~peltier/data.php.

3.2 The altimetry data set

Two different satellite altimetry data sets are used along this work. The first one, used to reconstruct sea level fields (Chapter 5), is a global product, and it is used with and without the atmospheric component. We make a distinction here because satellite altimetry data are usually provided without the atmospheric component. The second data set is a specific, higher-resolution product for the Mediterranean Sea.

In the first case, gridded SLA fields were obtained at CLS (Collecte Localisation Satellites, http://www.cls.fr) by combining several altimeter missions, namely: Topex/Poseidon data spanning the 1993-2001 period, Jason-1 data (from June 2002 onwards), ERS-1/2 data (spanning from January 1993 to June 2003 with a lack of ERS-1 data from January 1994 to March 1995) and Envisat data (from June 2003 onwards). The data span the period between January 1993 and December 2005, with a spatial resolution of 1/4ºx1/4º and weekly time resolution. In order to recover the total sea level signal, we added back the atmospheric component of sea level as given by a barotropic ocean model (MOG2D, sea Chapter 4) to the SLA gridded fields. The reason why we use the global 1/4º x 1/4º gridded fields instead of the specific Mediterranean product is that the reconstruction of Mediterranean sea level fields shown in Chapter 5 was originally attempted for a domain including a sector of the NE Atlantic Ocean (a requirement imposed by the framework of the VANIMEDAT project).

In the second case, gridded SLA fields were collected from the merged AVISO products that are freely available at http://www.aviso.oceanobs.com. The AVISO regional product for the Mediterranean Sea consists of multimission gridded sea surface heights with up to 4 satellites at a given time (Jason-1 / Topex/Poseidon / Envisat / GFO between October 2002 and September 2005). The data span the period between November 1992 and December 2008, with a spatial resolution of 1/8ºx1/8º and weekly time resolution. The methodology used in AVISO (Ssalto/Duacs system, http://www.aviso.oceanobs. com/) to build up the homogeneous and inter-calibrated data set is based on a global crossover adjustment, using Topex/Poseidon as the reference mission (Le Traon and Ogor, 1998). Then, these data are geophysically corrected (tides, wet/dry troposphere, ionosphere). The atmospheric correction is also applied in order to minimize aliasing effects (Volkov et al., 2007). In the new dataset provided by AVISO, the classical Inverted Barometer correction has been replaced by the MOG2D barotropic model correction (Carrere and Lyard, 2003), which improves the representation of high frequency atmospheric forcing as it takes into account both pressure and wind effects. Then, along-track data are resampled every 7 km using cubic splines and SLA is computed by removing a 7-year mean corresponding to the 1993–1999 period. Measurement noise is reduced by applying Lanczos (cut-off and median) filters. The mapping method to produce gridded SLA fields from along-track data is described in Le Traon et al. (2003). The long-wavelength error parameters are presently adjusted according to the most recent geophysical corrections.

Adding back the atmospheric component to obtain total sea level may seem equivalent to not applying the atmospheric correction to along-track data, but it is not: the objective of correcting along-track data prior to the interpolation is to avoid the aliasing of atmospherically generated small-scale structures (not well resolved by the track sampling) onto the large scale pattern. When adding back the atmospheric signal to gridded fields no aliasing is expected, since the output grid is dense enough to resolve the atmospheric scales.

As stated in Chapter 2, satellite data, like tide gauge data, require a specific correction to compensate for the GIA. For the GIA satellite correction we also use the ICE-5G VM2 model described in the work of Peltier (2004). In this case the correction is the sum of two terms: the present-day rate of relative sea level rise due to post-glacial rebound (shown in Figure 2.4) and the rate of increase of the local radius of the solid Earth relative to the center of mass of the planet. The Peltier solutions are only available at tide gauge sites. In order to cover the whole Mediterranean basin we interpolated the values provided for tide gauges (about 100 stations) onto a regular grid covering the whole basin.

3.3 Hydrographic data bases

The steric component of sea level will be estimated from gridded temperature (T) and salinity (S) fields obtained either from model outputs (see Chapter 4) or from historical hydrographic observations. In this work we use three different hydrographic data sets, namely: the MEDAR, Ishii and EN3 data sets.

The MEDAR data set consists of yearly T and S fields on a 1/5º x 1/5º grid covering the Mediterranean basin and spanning the period 1945-2002 (Rixen et al., 2005). The vertical domain extends down to over 4000 m, with data on 25 standard levels. The fields were obtained using a variational inverse method (Rixen et al., 2001).

The Ishii data set is more recent and it consists of monthly 1ºx1º gridded global T and S fields (Ishii et al., 2009). The gridded fields span the period 1945-2006 and cover from surface to 700 m. They result from applying an objective analysis to different kinds of in situ ocean temperature and salinity data (e.g., bottle, CTD and ARGO float data); XBT and MBT data are previously submitted to the corresponding time-varying depth bias correction. The Ishii data set also includes an estimation of the errors associated with the interpolation of the temperature and salinity gridded fields.

The ENACT/ENSEMBLES version 3 (EN3) data set (Ingleby and Huddleston, 2007) was produced by objective analysis of the T and S profiles of the World Ocean Database '05, the Global Temperature and Salinity Profile Project, Argo and the Artic Synoptic Basin-Wide Oceanography Project. The data set consists of monthly gridded T and S fields with a spatial resolution of 1º x 1º covering the period 1950-2008. The vertical domain extends down to over 5000 m, with data on 42 levels.

In order to compute the steric sea level, the specific volume anomaly ($\Delta\alpha$) must be first estimated as:

$$\Delta\alpha = \frac{1}{\rho(S,T,P)} - \frac{1}{\rho(35,0,P)} \qquad (3.1)$$

where T is the temperature, S is the Salinity, P the pressure, and $\rho(35,0,P)$ is the density of a water mass at pressure P and with a temperature of 0ºC and a salinity of 35 psu. The steric component of sea level (Z_S) can then be computed as the vertical integration of the specific volume anomaly ($\Delta\alpha$):

$$Z_S = -\frac{1}{g}\int_{Pf}^{Po}\Delta\alpha \cdot dp \qquad (3.2)$$

where g is the gravitational acceleration, and P_o and P_f are the pressure values at surface and at a reference level (typically the sea bottom), respectively.

Because the Ishii data set provides error estimates for the temperature and salinity gridded fields, the uncertainty in the steric component of sea level computed from that data set can also be estimated. In a first step, the error associated with the specific volume has been computed as:

$$\varepsilon(\alpha) = \left| \frac{\partial \alpha(S,T,P)}{\partial S} \right| \cdot \varepsilon(S) + \left| \frac{\partial \alpha(S,T,P)}{\partial T} \right| \cdot \varepsilon(T) \qquad (3.3)$$

where $\varepsilon(S)$ and $\varepsilon(T)$ are the errors associated with S and T and are a function of time and space (e.g., they are larger for past decades than for recent years due to differences in the number of available observations). The derivatives $\partial\alpha/dS$ and $\partial\alpha/dT$ have been obtained from the standard UNESCO equation of state of Sea Water. To compute the error in the steric sea level ($\varepsilon(Z_s)$) we assume the worst scenario: that errors in the specific volume are vertically correlated and, therefore, that the effect of the vertical integration is an error accumulation, rather than an error cancellation. This is probably not true for bottle data, but CTD, XBT and buoy data usually do have at least a vertically correlated error component. Thus, when using the propagation error formula

$$\varepsilon(Z_S) = \left| \frac{\partial}{\partial \alpha} \left(-\frac{1}{g} \int_{P_f}^{P} \alpha \cdot dp \right) \right| \cdot \varepsilon(\alpha) \qquad (3.4)$$

we are probably obtaining a realistic upper boundary for the steric errors.

Finally, to compute the error associated with the steric sea level averaged over a selected region, we assume that errors are spatially uncorrelated; this is surely not true for small scales (adjacent grid points suffer from similar errors), but there is no reason to believe that errors are correlated at spatial scales as long as the basin scale. This means that we are assuming that positive and negative errors of the same size occur in about equal number and tend to cancel each other when we compute the mean value. The error calculation consistent with that assumption is

$$\sigma = \frac{\sqrt{\sum_{i=1}^{N} \varepsilon_i^2(Z_S)}}{N} \qquad (3.5)$$

where N is the number of horizontal grid points and $\varepsilon_i(Z_s)$ is the error associated with the steric sea level at grid point i.

3.4 GRACE data

As stated above, GRACE measures the variations in the gravity field of the Earth, then providing an independent measure of the mass contribution to sea level changes. The Level-2 Release-04 (RL04) gravity coefficients computed at the Center for Space

Research (CSR) are used to estimate global water mass variations for the period August 2002 to the end of 2008 with a spatial resolution of 1°x1°. The data include corrections to specific spherical harmonic coefficients due to solid Earth and ocean tidal contributions to the geopotential, and the solid pole tide. GRACE pre-processing also removes variability from an ocean barotropic model along with the atmospheric mass. RL04 coefficients are supplied to degree and order 60. Degree 2, order 0 coefficients from GRACE are replaced with those from the analysis of Satellite Laser Ranging (SLR) data (Cheng and Tapley, 2004).We also restore modeled rates for certain coefficients (degree 2,3, and 4 for order 0, and degree 2, order 1) as discussed in the Processing Standards Documents (Bettadpur, 2007). The last step for the obtention of the Stokes coefficients is to add the mean monthly gravity coefficients of the ocean bottom pressure (Flechtner, 2007) and also an estimate of degree 1 gravity coefficients (based on an ocean model and GRACE data, see Swenson et al., 2008). To correct GRACE data for GIA we also use the ICE-5G VM2 model.

The procedure to convert the Stokes gravity coefficients into equivalent water thickness is described in detail in Chapter 10.

3.5 Linear trends and uncertainties

When dealing with climatic datasets, the study of long term trends is one of the usual targets. Particularly, sea level trends are used as a trustful indicator of climate change and their estimation is of particular interest to policy makers and resource managers. Therefore, an accurate determination of sea level trends is of fundamental importance for understanding long-term sea level variability and hence to identify potential threats due to rising MSL. In this subsection we present the methodology used in this thesis to compute trends and the associated uncertainties.

Ordinary least squares (OLS) models provide estimates of the model parameters with the least variance among all unbiased linear estimators as long as the errors are independent and normally distributed, homoskedastic, and with no bias. Although OLS does not assume normality when calculating the coefficients, the method works better for data that do not contain a large number of random errors with extreme values, since this estimator is very sensitive to the presence of outliers. Moreover the estimates of standard errors require normally distributed errors for their validity. These assumptions do not hold in most time series encountered in climate research and, therefore, alternative trend estimation methods must be adopted to reach reliable conclusions. In this thesis, linear trends and their uncertainties are calculated by means of estimators that are robust against outlying observations and heteroskedasticity (non-constant variance), and also paying attention to the reliability of standard error estimates.

The robustness of an estimate is usually measured by means of the breakdown point, which is defined as the minimum fraction of arbitrary outliers that can take the estimate beyond any limit (Hampel, 1971; Donoho and Huber, 1983). Among the many classes of estimators, the class of M-estimators (Huber, 1981) for instance are easy to compute, but their breakdown point is zero. Another class is the S-estimators introduced by Rousseeuw and Yohai (1984), which has a breakdown point of 50% and is asymptotically normal, but its statistical efficiency is rather low. Finally there are the MM-estimators (Yohai, 1987), which combine high efficiency with high breakdown point. In this thesis we use an MM-regression estimator calculated with an initial S-estimate. Standard errors are computed by means of robust estimators whose error

estimates are designed to be robust against heteroskedasticity, autocorrelation and the presence of outliers.

Let us consider the regression model

$$y_i = \vec{x}_i^T \vec{\beta}_0 + \sigma \varepsilon_i, \quad i = 1, \ldots, n \tag{3.6}$$

where "^{T}" denotes vector transposition, y_i are independent observations, $\vec{x}_i$ is the vector of covariates, which are considered fixed, $\vec{\beta}_0$ is the vector of unknown regression coefficients, ε_i are random errors, σ is a scale parameter, and n is the number of observations. Ideally, one would like to assume that the distribution of the errors follows some specific symmetric distribution (F_0) such as the standard normal distribution with zero mean and unity variance. To allow for the occurrence of outliers and other departures from the classical model, we here assume that the actual distribution F takes the form

$$F_\varepsilon = (1 - \varepsilon) F_0 + \varepsilon \widetilde{F} \tag{3.7}$$

where $0 \leq \varepsilon < 1/2$ and $\widetilde{F}$ is an arbitrary and unspecified distribution.

MM-estimates are based on two loss functions, ρ_0 and ρ_1, which determine the breakdown point and the efficiency of the estimator, respectively. The MM-estimate $\hat{\vec{\beta}}_n$ satisfies the equation

$$\frac{1}{n} \sum_{i=1}^{n} \rho_1' \left(\frac{y_i - \vec{x}_i^T \hat{\vec{\beta}}_n}{\hat{\sigma}_n} \right) \vec{x}_i = 0 \tag{3.8}$$

where $\rho_1'(u) = \dfrac{\partial \rho_1(u)}{\partial u}$ denotes the derivative of the function ρ_1 and $\hat{\sigma}_n$ is a scale S-estimate (Rousseeuw and Yohai, 1984).

The steps to compute the MM-regression estimator are the following:

1. First we compute the S-estimators $\widetilde{\vec{\beta}}_n$ and $\hat{\sigma}_n$ as follows:

$$\widetilde{\vec{\beta}}_n = \arg \min \widetilde{\sigma}_n(\vec{\beta}) \tag{3.9}$$

where $\widetilde{\sigma}_n$ is the solution of the equation

$$\frac{1}{n} \sum_{i=1}^{n} \rho_0 \left(\frac{y_i - \vec{x}_i^T \vec{\beta}}{\widetilde{\sigma}_n(\beta)} \right) = b \tag{3.10}$$

where $b \in (0,1)$ is a tunning constant.

2. The scale S-estimate is then simply given by $\hat{\sigma}_n = \tilde{\sigma}_n(\tilde{\bar{\beta}}_n)$. To compute the S-estimate we use the fast algorithm for S-regression estimates developed by Salibian-Barrera and Yohai (2006).

3. Finally, the MM-estimator $\hat{\bar{\beta}}_n$ is computed by solving Eq. (3.8) for $\hat{\bar{\beta}}_n$ using the scale S-estimate $\hat{\sigma}_n$ obtained in Step 2.

The choices of the loss functions ρ_0 and ρ_1 are standard. We use bisquare functions for both, scale and regression estimators:

$$\rho_0(u) = \begin{cases} \dfrac{u^2}{2} - \dfrac{u^4}{2c^2} + \dfrac{u^6}{6c^4}, & if\ |u| \le c; \\[4mm] \dfrac{c^2}{6}, & if\ |u| > c \end{cases} \qquad (3.11)$$

For the robust S-estimator we use a tunning constant $c = 1.55$ (yielding a 50% breakdown point). For the regression M-estimator (Eq. 3.8) we take $\rho_1(u) = \rho_0(u)$ but we set $c = 4.685$ to have an efficiency of 95%.

The standard error of robust estimates can be estimated using their asymptotic variances. However, the asymptotic distribution of MM-estimates has mainly been studied under the assumption that $F = F_0$, which does not strictly hold in many situations. In order to obtain robust estimates of the errors associated with the trends, we use the fast robust bootstrap proposed by Salibian-Barrera (2006), which yields a consistent estimate for the variance of $\hat{\bar{\beta}}_n$ under general conditions, including the case $F \in F_\varepsilon$.

Following Salibian-Barrera (2006), the fast robust bootstrap used to estimate standard errors is computed as follows. Since the covariates are fixed, the appropriate procedure consists of bootstrapping the residuals of the robust regression. Let $r_i = y_i - \hat{\bar{\beta}}_n^T \vec{x}_i$ be the residual of the MM-estimate. The bootstrapped y_i^*'s are $y_i^* = \hat{\bar{\beta}}_n^T \vec{x}_i + r_i^*$, where $\{r_i^*\}$ is a random sample from the residuals. Now $\hat{\bar{\beta}}_n^*$ and $\hat{\sigma}_n^*$ are defined by

$$\hat{\bar{\beta}}_n^* = \left[\sum_{i=1}^n \omega_i^* \vec{x}_i \vec{x}_i^T \right]^{-1} \sum_{i=1}^n \omega_i^* \vec{x}_i y_i^*, \qquad (3.12)$$

$$\hat{\sigma}_n^* = \sum_{i=1}^n v_i^* \left(y_i^* - \tilde{\bar{\beta}}_n^T \vec{x}_i \right) \qquad (3.13)$$

where for $i = 1,...,n$: $\omega_i^* = \rho_1'(r_i^*/\hat{\sigma}_n)/r_i^*$, $v_i^* = \rho_0(\tilde{r}_i^*/\hat{\sigma}_n)/(nbr_i^*)$, $r_i^* = y_i^* - \hat{\bar{\beta}}_n^T \vec{x}_i$ and $\tilde{r}_i^* = y_i^* - \tilde{\bar{\beta}}_n^T \vec{x}_i$. The scale estimate $\hat{\sigma}_n$ is the S-scale obtained in (3.10), and $\hat{\bar{\beta}}_n$ is the

associated S-regression estimate defined in (3.9). The robust bootstrap re-calculated $\hat{\vec{\beta}}_n - \vec{\beta}$ is given by

$$\hat{\vec{\beta}}_n^{R*} - \vec{\beta} = M_n\left(\hat{\vec{\beta}}_n^* - \hat{\vec{\beta}}_n\right) + \vec{d}_n(\hat{\sigma}_n^* - \hat{\sigma}_n), \qquad (3.14)$$

where matrix M_n and vector $\vec{d}_n$ are defined as in Salibian-Barrera and Zamar (2002).

Robust standard errors for the regression coefficients are then computed as the standard deviation $\hat{\sigma}_j$ of the re-calculated estimators $\hat{\vec{\beta}}_n^{R*}$. We can also construct confidence intervals for the regression coefficients: the $(1-\alpha)100\%$ confidence interval for the jth regression coefficient $\hat{\beta}_{n,j}$ is of the form $\hat{\beta}_{n,j} \pm Z_{\alpha/2}\hat{\sigma}_j$, where $Z_{\alpha/2}$ is the standard normal quantile. In the case that the errors not due to natural variability (standard errors), such as interpolation errors and instrumental errors, are known, we can take them into account when computing the trends by simply adding an error term of the form $\sigma_i N(0,1)$ to Eq. (3.6), where σ_i is the error associated with the ith observation and $N(0,1)$ is the standard normal distribution with zero mean and unity variance. We then generate a large number of data samples and compute the error estimate for each sample. The final error estimate is the mean of all those sample errors.

Chapter 4

Basics of models

THE study of long-term sea level variability is usually undertaken either from available observations (collected by tide gauges and satellite altimeters) or from hindcasts of the last decades. Observations are obviously more accurate than models, but they are handicapped by their spatial and temporal distribution: tide gauge records can span several decades, but the need of a land mark reference makes that all them are located at coastal sites; conversely, satellite altimetry allows a complete spatial coverage of the open sea, but it only spans a short time period. An advantage of the hindcasts over sea level observations is that they give more complete information on the physical processes driving sea level variability. For instance, the steric component, resulting from changes in the volume of the water column, can be related to physical processes resulting in changes in the temperature and salinity distributions.

In this chapter we briefly review the different types of ocean models and the governing equations of motion in order to establish a minimum background on which we can discuss the results obtained in Chapters 7 and 8. We also present the selected models used in this thesis.

4.1 Types, advantages and limitations of oceans models

Before getting into the details of the particular models used in this thesis, it can be convenient to give a brief description of the different types of ocean models and to quote their advantages and limitations.

The choice of a particular ocean model depends on the intended application and on the available computational capabilities. Following Kantha and Clayson (2000), numerical ocean models can be classified as follows:

- *Global or regional models*. Global models require high performance computing capabilities, whereas regional models can be run on powerful workstations. The main factor that determines the running time of a model is the resolution (grid sizes in the horizontal and vertical). A regional model can be implemented with higher resolution, however open boundaries at which flow conditions are not

33

known will constitute a problem. Often the best solution is to nest the fine resolution regional model in a coarser resolution global model.

- *Rigid lid or free surface*. If we are interested only in long-term variations, these are mainly governed by the internal adjustment and, therefore, fast barotropic response to surface forcing (mediated by external Kelvin and gravity waves on the sea surface, and relatively slower baroclinic adjustment via internal gravity, Kelvin, planetary Rossby, and other waves) can be suppressed by imposing a rigid lid on the free surface. This results in considerable saving in computer resources. On the other hand, if sea level is considered a key variable and mass addition (from ice melting for instance) is to be taken into account, then a free surface model is required. Also for shallow water applications such as storm surge and tide modelling, free surface dynamics must be retained.

- *Hydrostatic, quasi-hydrostatic, or nonhydrostatic*. Most, if not all, large scale circulation models are based on the hydrostatic form of the incompressible Navier-Stokes equations. Hydrostatic models are adequate in modelling gyre scale (>1000 km) circulation and mesoscale eddies (10-100 km); the hydrostatic approximation only breaks down for scales less than the 10 km typical of small scale processes. In hydrostatic models the angular moment is only approximately conserved since they neglect the horizontal component of the Coriolis acceleration for energetic consistency. In Quasy-hydrostatic models the hydrostatic approximation is relaxed to the extent that the horizontal component of the Coriolis approximation is retained. Fully nonhydrostatic models can be used at all horizontal scales, but they can be computationally expensive.

- *Barotropic or baroclinic*. In a barotropic model, the density gradients are neglected so that the currents become independent of the depth in the water column. Many phenomena such as tidal sea surface elevation fluctuations and storm surges can be simulated quite adequately by a barotropic model. Since barotropic models are two-dimensional (the equations of motion are vertically integrated), they requires an order of magnitude less computing resources than a comparable baroclinic model. However, when it is important to model the vertical structure of currents, or the density field, a fully three-dimensional baroclinic model is necessary.

- *Coupled to the atmosphere or uncoupled*. For accurate simulation of long time scales processes, it is preferably to couple ocean models with atmospheric models. A cheapest option is to force the ocean model with the outputs of an atmospheric model, with no feedback to the atmosphere.

- *Deep basin or shallow coastal, Comprehensive or purely dynamical, With applications to short-term simulations or long-term climate studies, Quasi-geostrophic or primitive equation based, Purely physical or physical-chemical-biological, Process study-oriented or application-oriented, With and without coupling to sea ice, ...* That large is the range of possibilities.

In this thesis we make use of barotropic and baroclinic models to study long-term sea level variability. The main application of barotropic models is the study of the oceanic response to atmospheric pressure and wind forcing, being of particular interest the prediction of storm surge effects along the coast. Baroclinic models are used to study inter-annual variations of the steric component and of total sea level. It is worth mentioning that at present no ocean model accounts for the sea level rise due to ice

melting as a consequence of the global warming. The only solution to that is adding the contribution of ice melting estimated from other sources (e.g. from ice models) to the sea surface height given by the model, though this implies assuming that such contribution is spatially uniform, which is far from being true.

4.2 Model equations

All numerical models solve one form or another of a modified version of the Navier-Stokes equations (or more appropriately Reynolds-averaged equations for mean quantities, since the flow is invariably turbulent). The essential differences are the inclusion of the effects of the Earth's rotation, and certain simplifications. The most important simplification is to assume that the water is incompressible, which filters out acoustic waves. This is not a problem, since we are not interested in the propagation of sound, and it greatly reduces the computational time. The second most important approximation that is adopted is ignoring the density changes in the fluid except when gravitational body forces are concerned. This is the Boussinesq approximation. This approximation is also justified since changes in density are in general smaller than 0.2-0.3 %. The reason for retaining density changes in the gravitational terms while ignoring them in the other terms is that the vertical stratification of the ocean greatly inhibits vertical motions due to the fact that the motion takes place in the presence of a gravitational field, and hence gravitational forces play a key role on the motions. Apart from these simplifications, most numerical ocean models also adopt the hydrostatic approximation, which is described later in this chapter.

4.2.1 The equations of fluid motion on the rotating earth

The momentum equation and the equation of continuity (conservation of mass) for a fluid on the rotating Earth can be written as (Kantha and Clayson, 2000):

$$\frac{D\vec{v}}{Dt} + 2\vec{\Omega} \times \vec{v} = -\frac{\vec{\nabla}p}{\rho} + \vec{g} + \vec{\nabla}\Phi_t + \frac{\vec{\nabla} \cdot \overset{\Rightarrow}{\tau}}{\rho} \tag{4.1}$$

$$\frac{D\rho}{Dt} + \rho\vec{\nabla} \cdot \vec{v} = 0 \tag{4.2}$$

where ρ is the density of the fluid, $\vec{v} = \vec{v}(u,v,w)$ is the velocity, $\vec{\Omega}$ is the angular velocity vector, p is the pressure, $\overset{\Rightarrow}{\tau}$ is the turbulent stress tensor, and $\vec{\nabla}\Phi$ is the lunisolar gravitational tidal potential responsible for generating oceanic tides. The effective gravitational potential ($\vec{g}$) is defined as $\vec{g} = \vec{\nabla}\Phi = \nabla\Phi^I - \vec{\Omega} \times (\vec{\Omega} \times \vec{R})$, where the potential term $\vec{\nabla}\Phi^I$ accounts for the Earth's own gravitational forces due to the density stratification in the fluid and could include astronomical tide-generating forces due to the gravitational fields of the Moon and the Sun, the term $\vec{\Omega} \times (\vec{\Omega} \times \vec{R})$ is the centripetal force term, and $\vec{R}$ is the radius vector. D/Dt denotes the total derivative, $D/Dt = \partial/\partial t + \vec{v} \cdot \vec{\nabla}$. In addition, one needs the conservation equations for the temperature T and salinity S along with the equation of state:

$$\frac{D(T,S)}{Dt} = \vec{\nabla} \cdot (\vec{q}_T, \vec{q}_S) + So_{T,S} \tag{4.3}$$

$$\rho = \rho(T, S, p) \tag{4.4}$$

where *So* denotes the source and sink terms, and $\vec{q}_T$ and $\vec{q}_S$ are the kinematic turbulent heat and salt flux vectors.

Because of the so-called turbulence closure problem, these equations are usually simplified by adopting what is known as the zero-th order approximation for the turbulent quantities. This simplification involves assuming that the turbulent quantities have the same form as the viscous terms, but replacing the molecular values of diffusivity by constant values known as eddy diffusivities that are several orders of magnitude larger. Some other simplifications are usually made, which are described in the following subsections.

The Boussinesq approximation

The Boussinesq approximation considers that, in the ocean, variations in density are small when compared to its mean value and therefore the density can be considered to be constant except when body forces due to motion of a density-stratified fluid in a gravitational field are involved. This involves replacing ρ by a constant reference value ρ_0 (1035 kg/m^3) everywhere except in terms involving the gravitational constant g.

Incompressibility

Another approximation is to assume that the medium is incompressible. The equation describing an incompressible fluid is

$$\vec{\nabla} \cdot \vec{v} = 0 \tag{4.5}$$

The hydrostatic approximation

The hydrostatic approximation exploits the fact that at certain scales of motion, the aspect ratio of the oceans is small; hence, vertical motions are small and are further inhibited by gravitational forces under stable density stratification. Thus vertical accelerations are small, the vertical frictional forces are also small, and the fluid acts as though it is under static equilibrium as far as vertical motions are concerned.

The hydrostatic approximation therefore involves neglecting all the terms on the left hand side of Eq. (4.1) for the component *w* of the velocity, including the term involving the horizontal component of the Coriolis acceleration $2\Omega\cos\theta$ (θ being the latitude).

Unfortunately, this approximation introduces extra terms in the mechanical energy budget. These extra terms correspond to spurious sources and sinks of mechanical energy (Coriolis accelerations can not perform any work on the fluid, and hence must vanish in any energy equation). In order to recover an appropriate energy conservation statement, we must neglect the term involving $2\Omega\cos\theta$ in the Eq. (4.1) for the component *u* and *v* of the velocity.

The hydrostatic approximation is valid for most large scale motions, except for deep convection where large vertical velocities and accelerations occur when surface water is strongly cooled and descends in narrow chimney-like plumes.

4.2.2 The incompressible, hydrostatic, Boussinesq equations

Using tensorial notation and treating the horizontal coordinates separately from the vertical ones, the incompressible, hydrostatic, Boussinesq equations for a gravitational stratified fluid on the rotating earth can be written as (Kantha and Clayson, 2000):

$$\nabla \cdot \vec{U} = 0 \tag{4.6}$$

$$\frac{\partial U_i}{\partial t} + \frac{\partial}{\partial x_j}(U_j U_i) + \frac{\partial}{\partial z}(W U_i) + \varepsilon_{i3j} f U_j = -\frac{1}{\rho_0}\frac{\partial P}{\partial x_i} + \frac{\partial}{\partial xi}(\Phi_t) +$$

$$+ \frac{\partial}{\partial t}\left(K_M \frac{\partial U_i}{\partial z}\right) + \frac{\partial}{\partial x_j}\left(A_M \frac{\partial U_i}{\partial x_j}\right) \tag{4.7}$$

$$0 = -\frac{1}{\rho_0}\frac{\partial P}{\partial z} - \frac{\rho}{\rho_0} g \tag{4.8}$$

$$\frac{\partial T}{\partial t} + \frac{\partial}{\partial x_j}(U_j T) + \frac{\partial}{\partial z}(WT) = \frac{\partial}{\partial z}\left(K_H \frac{\partial T}{\partial z}\right) + So_T + \frac{\partial}{\partial x_j}\left(A_H \frac{\partial T}{\partial x_j}\right) \tag{4.9}$$

$$\frac{\partial S}{\partial t} + \frac{\partial}{\partial x_j}(U_j S) + \frac{\partial}{\partial z}(WS) = \frac{\partial}{\partial z}\left(K_H \frac{\partial S}{\partial z}\right) + \frac{\partial}{\partial x_j}\left(A_H \frac{\partial S}{\partial x_j}\right) \tag{4.10}$$

along with the equation of state (4.4). Here U_j denotes the horizontal components of mean velocity, W is the vertical component and $f = 2\Omega \sin\theta$ is the planetary vorticity. The alternating tensor ε_{ijk} is equal to 1 if indices occur in cycling order, -1 if they occur in reverse cycling order, and 0 if any two of the indices are the same. K_M and A_M are respectively the vertical and horizontal kinematic viscosity coefficients. K_H and A_H are respectively the vertical and horizontal eddy difusion coefficients, and So_T denotes a volumetric heat source such as that due to penetrative solar heating.

These equations need to be complemented by initial and boundary conditions on the prognostic variables. The oceans are forced by momentum, heat and salt fluxes at the surface that determine the boundary conditions (Kantha and Clayson, 2000):

$$K_M\left(\frac{\partial U_i}{\partial z}\right) = (\tau_{0i}) \tag{4.11}$$

$$K_H\left(\frac{\partial}{\partial z}(T, S)\right) = (q_H, q_S) \tag{4.12}$$

$$W = \frac{\partial \eta}{\partial t} + U_j \frac{\partial \eta}{\partial x_j} \tag{4.13}$$

where τ_{0i} is the kinematic shear stress acting at the free surface due to the action of winds and waves, $q_{H,S}$ are the heat and salt fluxes, and η is the sea surface height.

The conditions at the ocean bottom are of no mass, heat and salt transfer through the ocean bottom:

$$W = -U_j \frac{\partial H}{\partial x_j} \tag{4.14}$$

$$K_M \left(\frac{\partial U_i}{\partial z} \right) = (\tau_{bi}) \tag{4.15}$$

$$K_H \left(\frac{\partial}{\partial z}(T,S) \right) = (0,0) \tag{4.16}$$

where H is the thickness of the layer and τ_{bi} is bottom stress.

The lateral boundary conditions are more problematic. If the lateral boundary is a closed boundary, then it is assumed that there is no lateral mass, heat or salt flux trough the boundary and the component of the velocity perpendicular to the boundary is set equal to zero. However, for open boundaries such as those limiting regional models, it is necessary to prescribe open boundary conditions, which implies specifying complete information on several flow properties. The best strategy is to nest the model in a coarser resolution global model.

4.3 Considerations on barotropic and baroclinic models

4.3.1 Barotropic models

Many phenomena such as tidal sea surface elevation fluctuations and storm surges can be simulated quite adequately by a barotropic model. By neglecting horizontal density gradients in the governing equations, the currents in the water column away from regions of frictional influence (such as the surface and the bottom) become independent of depth. Under this condition, the governing equations can be greatly simplified by ignoring the transport equations for T and S and equations involving density. The resulting continuity and momentum equations can be vertically integrated over the depth of the water column to attend with a set of equations that govern the sea surface elevation η and the vertically averaged velocity components U_i. For a detailed deduction of such equations the reader is referred to Kantha and Clayson (2000).

The atmospheric forcing terms (i.e., the wind stress and pressure) can be presented to the model as a function of time during the model run. The sea surface height due to phenomena such as tides and storm surges is obtained by solving the vertical integrated equations. A simple solution of these equations can be found by neglecting the wind and tidal forcing, and the frictional influences. In this case the sea surface height is simply $\eta = \eta_a$, where η_a represents the atmospheric pressure forcing. That is, under the stated constraints, sea level adjusts instantaneously to changes in surface atmospheric pressure. This is the inverse barometer effect mentioned earlier in this work.

4.3.2 Baroclinic models

The applications of baroclinic models are enormous and have greatly improved our understanding of physical processes in the ocean. They have been used to study all time scale ocean variations and ocean dynamics, and to reproduce all-scale features of the circulation. They can be also used to estimate the steric sea level component from temperature and salinity distributions. However they also suffer from some deficiencies. One of these deficiencies is that they can lead to a poor representation of the mean circulation and variability. For instance, comparisons with altimetry data (McClean et al., 1997) have shown that the POP model, with a resolution of 1/6º, captures about 60% of the altimetric sea surface height variability. More realistic results can be obtained by increasing the spatial resolution of the model, but this implies increasing the computational cost. Also the upper mixed layer is often not well represented, so that an increase in the vertical resolution is desirable. Another usual problem of global circulation models is that western boundary currents are weak and do not extend as much as they should after their separation from the boundary.

Regarding the nesting of regional baroclinic models with a coarser global model, the main problem is that the parameterization of physical processes is less precise in the second than in the first. Moreover, the numerical techniques used for the nesting can introduce errors, and the propagation of these errors into the regional domain can have a significant impact on the evolution of the ocean within the domain. It seems obvious that the larger the domain surrounding the regional domain the better, since it takes longer for the errors from the lateral boundaries to propagate to the domain of interest.

When it is not possible to nest the model in a coarse global model, it is necessary the use of some sort of boundary condition that ensures that disturbances approaching the boundary from the inside are radiated out. There are several ways to prescribe such boundary conditions on open lateral boundaries. In the case that the model works in a hindcast mode, there is the possibility of using analyses to provide lateral boundary conditions. For a more complete description on lateral boundary conditions the reader is referred to Haidvogel and Beckmann (1999), and Kantha and Clayson (2000).

Free surface formulation

In free surface models, the sea surface height η describing the shape of the air-sea interface is obtained as the solution of the following prognostic equation:

$$\frac{\partial \eta}{\partial t} = -D + P - E \qquad (3.19)$$

where *P-E* is the precipitation minus evaporation budget, and $D = \frac{\partial}{xi}\left[(H + \eta)U_i\right]$.

It is worth noting that allowing the air-sea interface to move introduces external gravity waves as a solution of the governing equations. These waves are barotropic because of the hydrostatic assumption, and their phase speed is very high. Their time scale is short with respect to the other processes described by the equations. If one is only interested in low-frequency variations, it is possible to apply an explicit filter to slow down the fastest waves while not altering the slow barotropic Rossby waves. If

one is not interested in external waves at all, it is possible to use the rigid lid approximation.

Rigid lid formulation

In the rigid lid approximation it is assumed that the ocean surface ($z = 0$) is a rigid lid on which pressure p_S is exerted. This implies that the vertical velocity at the surface is equal to zero. The pressure at any depth $p(z)$ is related to the pressure against the rigid lid, p_S, by

$$p(z) = p_S + \int_z^0 \rho g dz' \qquad (3.20)$$

The main difficulty of rigid lid models is that to compute the vertically averaged velocities (or more specifically a volume transport stream function) an elliptic equation need to be solved at each time step subject to conditions imposed on lateral boundaries. The determination of the boundary condition is not an easy task. When all the coastlines are connected (i.e., when there are no islands), the value of the barotropic stream function can be arbitrarily set to zero. However, when islands are present in the domain, the value of the stream function will generally be different for each island and for the continent, and will vary with time.

Representation of steric sea level

Steric sea level changes are changes in the volume of the oceans resulting from temperature and salinity changes. Most models solve one form or another of the Boussinesq equations and they conserve volume rather than mass. It has been seen that models that use a free surface configuration compute the sea level by vertically integrating the equation for conservation of volume and hence do not account for sea level changes due to the expansion or contraction of the water body. Although expansion and contraction are included in the equation of state, it is not accounted for by the dynamical equations and, therefore, steric sea level changes are not properly represented. The solution to this problem was given by Greatbatch (1994). He showed that the total sea level can be recovered by adding the net expansion/contraction computed over the whole domain of the model to the sea level given by the model for each time step. Since the correction is spatially uniform, it creates no currents and hence does not have dynamical significance. Results obtained from rigid lid models can be corrected in exactly the same way as free surface models (Greatbatch, 1994).

4.4 Model data used in this work

In this thesis we study long-term sea level variability as given by three different baroclinic numerical models: two regional models (Somot et al., 2006; Sannino et al., 2009) and a global model (Barnier et al., 2006). The atmospheric component is also estimated from the barotropic model HAMSOM (Álvarez-Fanjul et al., 2001). A brief description of each of these models is given in the following.

4.4.1 The barotropic model

The barotropic model is used to obtain the atmospheric component of sea level in the Mediterranean Sea. The hindcast run used in this work spans the period 1958-2001 and was produced in the framework of the HIPOCAS (Hindcast of Dynamic Processes of the Ocean and Coastal Areas of Europe) project (Guedes et al., 2002). The model was the barotropic version of the HAMburg Shelf Circulation Model (HAMSOM) set-up in the same way that it is used in the operational Spanish Sea Level Forecasting System (NIVMAR), operated by Puertos del Estado (Álvarez-Fanjul et al., 1997; Alvarez-Fanjul et al., 2001; Sotillo et al., 2005). The domain covers from 30ºN to 46ºN and from 14ºW to 36ºE, with a spatial resolution of 1/4ºlat x 1/6ºlon. The atmospheric pressure and 10-m wind fields used to force the barotropic model were obtained through dynamical downscaling (1/2º x 1/2º) from the NCEP/NCAR global reanalysis using the atmospheric limited-area model REMO (Sotillo et al., 2005). The skill of the model for the complete set of hindcasted oceanographic parameters is fully evaluated in Ratsimandresy et al. (2008). Several examples of the good agreement between modelled and actual sea level are given in Gomis et al. (2006).

4.4.2 Baroclinic models

Somot et al. 2006

The OPAMED8 baroclinic model used by Somot et al. (2006) is a high resolution rigid lid model that covers the Mediterranean Sea with a resolution of $1/8°$ x $1/8°\cos(latitude)$ in the horizontal and 43 non-uniform Z-levels in the vertical. It is based on a limited-area version of the OPA model (Madec et al., 1998). The 40-year simulation (1961-2001) will be hereinafter referred to as the OM8 simulation.

The forcing was based on an ERA-40 dynamical downscaling excluding atmospheric pressure. The downscaling technique (described in Herrmann and Somot, 2008) was carried out with a regional version of the ARPEGE-Climate model (Déqué and Piedelievre, 1995) that uses a stretched and tilted grid resulting in a horizontal resolution of about 50 km over the Mediterranean Sea. When the ARPEGE model is used in a "climate mode" it does not follow the real time chronology, but for the present application it was used in a "hindcast mode", which allowed a high-resolution dynamical downscaling of the ERA40 reanalysis (Simmons and Gibson, 2000). Air-sea fluxes (heat, water and momentum) were extracted from the atmospheric simulation at a daily time scale; it is worth stating that the set of air-sea fluxes (1) have a high resolution (50 km), (2) are homogeneous over a long period of time (no change in the model configuration), (3) follow the real synoptic chronology and (4) have a realistic interannual variability. A first validation of the air-sea flux dataset has been done in Herrmann and Somot (2008) for the case study of the 1986-87 winter.

Additional forcings of the OM8 simulation are climatological values (with an annual cycle) for the river runoff, the Black Sea inflow and the Atlantic boundary conditions. The latter consist of a 3D relaxation for T and S applied in a buffer zone extending beyond the western limits of the Iberian Peninsula (11ºW). Hence, eventual sea level trends derived for instance from ice-melting occurring beyond the Atlantic boundary of the domain are not taken into account. Moreover, because the model is a

rigid lid model, volume is conserved within the Mediterranean basin. Evaporation/ precipitation are accounted for by adding/taking out salt at the sea surface. On the other hand, the zero volume exchange through Gibraltar implies a net salt outflow, since the salt content of the outflowing Mediterranean water is higher than the salt content of the same volume of incoming Atlantic water. The fact that no sea surface salinity (SSS) relaxation is applied in OM8 means that the interannual variability of the SSS is free, what represents a significant improvement compared to state-of-the-art Mediterranean Sea models.

Artale et al.. 2009

This simulation has been performed using the regional coupled system PROTHEUS (Artale et al., 2009) for the Mediterranean basin. The PROTHEUS system is composed of the RegCM3 atmospheric regional model and the MITgcm ocean model, coupled through the OASIS3 coupler. Hereinafter, we will refer to this simulation as the MITgcm simulation.

The atmospheric regional model: RegCM3

RegCM3 is a three-dimensional, sigma-coordinate, primitive equation, hydrostatic regional climate model (Giorgi and Mearns, 1999; Pal et al., 2007). The configuration used in this simulation has a horizontal spatial resolution of 30 km on a Lambert conformal projection. The model domain is centered at 41ºN and 15ºE with 160 grid points in the meridional direction, 150 grid points in the zonal direction and 16 sigma-levels. Lateral boundary conditions for the RegCM3 simulations are supplied by interpolating 6-hourly large scale horizontal wind component, temperature, specific humidity and surface pressure onto the model grid and by relaxing the prognostic model variables towards this conditions over a 12 grid point lateral buffer zone with an exponentially decreasing relaxation coefficient (Giorgi et al., 1993).

The ocean model: MITgcm

This model consists of two components: a coarse model covering the whole Mediterranean Sea and the Gulf of Cadiz, and a fine model, nested within the coarse model, whose domain is limited to the Strait of Gibraltar, part of the Alboran Sea to the east (2º 33.75'W), and part of the Gulf of Cadiz to the west (8º 21.25'W) (Sannino et al., 2009). Both models are based on the MITgcm developed by Marshall et al. (1997a,b).

The coarse model has a resolution of 1/8º x 1/8º. The bottom topography is interpolated from the 1/12º ETOPO5 database (US National Geophysical Data Centre) with some corrections made for isolated grid points located in correspondence of islands and straits; in particular the Strait of Gibraltar was modified to be represented by two grid points in latitude. It has 42 vertical levels distributed with a resolution varying from 10 m at the surface to 300 m in the deeper part of the basin, with an intermediate resolution of about 40-50 m between 200-700 m. The fine model has a spatial resolution of 1/24º x 1/24º and uses the same vertical levels as the coarse model, as well as the same vertical diffusivity and viscosity parameterization.

The simulation is initialized with MEDATLAS II (MEDAR Group, 2002)

climatology data for January. The two-way exchange through Gibraltar is achieved by means of a box located west of Gibraltar in the coarse model, where a 3D relaxation of temperature and salinity to a monthly climatology (Levitus, 1982) is applied for the Gulf of Cadiz in the first 30 grid points. The relaxation time is 5 days at the westernmost grid point, increasing up to 100 days at the thirtieth inner grid point. The period spanned by the simulation is 1958-2001.

Except for the Atlantic, where no surface forcing is applied, the model is forced through the specification of wind stress and heat fluxes computed by RegCM3. An interactive river scheme is used to provide the oceanic module with fresh water sources consistent with the atmospheric branch of the simulated hydrological cycle. Natural boundary conditions for salinity have been applied to the oceanic module, which means that the net freshwater is treated as a real fresh water flux.

Barnier et al. 2006: ORCA-R025

This simulation was developed by the DRAKKAR group (Barnier et al., 2006). The model is a free surface model based on a global configuration of the NEMO modelling system implemented on an ORCA grid with a spatial resolution of 1/4º x 1/4º. It has 46 vertical levels distributed with a resolution varying from 6 m near the surface to 250 m at the bottom. The maximum depth in the model is 5844 m. The period spanned by the simulation is 1960-2004. Hereinafter we will refer to this simulation as the ORCA simulation.

The bathymetry is derived from the 2-minute resolution Etopo2 bathymetry file of NGDC (National Geophysical Data Center). The interpolation onto the model grid has been carried out by taking all the Etopo2 grid points falling into an ORCA025 grid box, and taking the median of those points.

The atmospheric forcing is a climatological seasonal cycle forcing applied in a cycling way. Surface momentum flux is directly provided to the ocean model as a wind stress vector. A climatological daily mean wind stress vector is used. It is a combination of ERS scatterometer data (CERSAT, 2002) and NCEP/NCAR re-analysis (Kalnay et al., 1996). The daily climatology is built up using years 1992 to 2000 with a 11 days running mean filter to remove synoptic variability. Surface heat fluxes and freshwater flux are calculated by using the empirical bulk parameterization described by Goose (1997). Evaporation is derived from the latent heat flux. Climatological daily mean values of air temperature are obtained from NCEP/NCAR re-analysis; climatological monthly mean precipitation is obtained from CMAP (Xie and Arkin, 1997); monthly mean humidity and cloud cover, and climatological daily mean wind speed are from the blend of ERS and NCEP/NCAR reanalysis. River runoff was provided by MERCATOR-Ocean. No relaxation to any sea surface temperature or sea surface salinity is used.

Part II

Results

Chapter 5

Reconstruction of Mediterranean sea level fields: preliminary results

IN previous chapters we emphasized the fact that sea level observations are handicapped by their spatial and temporal distribution. Tide gauges are limited by the need for a fixed platform and thus they are installed at coastal stations, where they can be referenced to some land mark. An important consequence is that tide gauges can only measure coastal and island sea level. Conversely, satellite altimetry allows a complete coverage of sea-level, though with some handicaps. When dealing with long-term sea level variability, the crucial limitation is the short period covered by altimetry, since the first satellite measurements date back to the early nineties. These partial pictures of the actual time-space sea-level variability given by raw observations can lead to incomplete or biased results on crucial issues such as the diagnosis of sea level rise due to global warming. Obtaining an accurate reconstruction of sea level fields is therefore of key importance to improve the present knowledge on long term sea-level variability and in particular to obtain more accurate sea level trends.

Several attempts to reconstruct sea level variability over the 20th century have been carried out, both globally and regionally. The methodologies used for the reconstruction range from simple regional averaging of selected tide gauge records (e.g. Holgate and Woodworth, 2004) to more optimal interpolation methods (e.g. Church et al., 2004). These methodologies have yielded estimates of the linear rate of global MSL rise for different periods, such as the 1.8±0.3 mm/yr given by Church et al. (2004) for the period 1950-2000 or the 1.6±0.4 mm/yr given by Domingues et al. (2008) for the period 1961-2003. At regional scale, Jevrejeva et al. (2006) have used a method based on Monte Carlo Singular Spectrum Analysis to determine nonlinear long-term trends for 12 large ocean regions.

In the Mediterranean Sea the only published attempt of reconstructing the sea-level fields of the last decades has been undertaken by Tsimplis et al. (2008). They carried out an EOF analysis of Mediterranean tide gauge records and altimetry data and compared the time amplitudes of the respective leading modes (a similar analysis to that presented later in this section). They also give some examples of tide gauges

reconstructed through a very simple technique, but no basin-wide reconstruction has so far been produced.

It turns out, therefore, that all long-term sea level trends reported in the Mediterranean have been estimated from individual tide gauge records, not from a basin-wide sea level reconstruction. As an example, Tsimplis et al. (2005) evaluated sea level trends of between 0.4 – 0.8 mm/yr for the period 1958-2001. They identified two periods with marked positive trends (before 1960 and after 1994) and an intermediate period for which most tide gauges show clearly negative trends. Tsimplis et al. (2005) and Gomis et al. (2008) pointed to the atmospheric pressure as responsible for the negative trends: its contribution has been evaluated as -0.6 mm/yr for 1958-2001 and in -1.0 mm/yr for 1960-1994.

In this chapter we put the basis to reconstruct the monthly distribution of sea level in the Mediterranean Sea for the period between January 1945 and December 2000. The organization of the chapter is as follows. In the first part of the chapter we present different techniques that are commonly used to analyze climatic data sets. In particular, we focus on standard PCA and non-linear PCA. A description of the two techniques is presented in sections 5.1.1 and 5.1.2. In section 5.1.3 we show an application to altimetry data to study Mediterranean Sea level variability for the period between January 1993 and December 2005. It is important to understand how these two techniques work in order to determine the best option to reconstruct Mediterranean Sea level. In the second part of the chapter we obtain a first reconstruction of sea level fields using a simple technique that, however, did not yield satisfactory results. The problem is solved in Chapter 6 using a more sophisticated technique.

5.1 Linear and non-linear analysis of Mediterranean sea level

Climatic data sets usually involve phase spaces with thousands of dimensions, making it really difficult to interpret or understand the physical phenomena underlying the observed variability. Thus, it is important to use techniques that assist the task of analysing such massive multivariate datasets. One of the most common of such techniques used in oceanography and meteorology is PCA, also referred to as EOF analysis. Consequently, there are plenty of references describing the methodology (Preisendorfer, 1988; Wilks, 1995).

PCA is an objective technique that attempts to characterise lower-dimensional structure in large multivariate datasets. In order to resolve into simple pieces the complex variance patterns that characterize the data, PCA finds a lower-dimensional hyperplane which optimally characterize the data, such that the sum of squares of orthogonal deviations of the data points from the hyperplane is minimized. If the physical processes described by the data are linear, then PCA is an optimal technique; however, if some of those processes are nonlinear, other nonlinear techniques, such as nonlinear PCA, may be more effective in detecting the dominant structures.

5.1.1 Principal component analysis (PCA)

Following Preisendorfer (1988), PCA can be formulated as follows. We consider a real-valued, scalar, homogenously dimensioned data set Z' given in the form of an $n{\times}p$ matrix. Each element, $z'(t,x)$, of matrix Z' can be viewed as the value of sea level at

time t and location x, where $t = 1,\ldots,n$ and $x = 1,\ldots,p$.

The first step is to subtract the time mean from the values $z'(t,x)$ and write, for each $x = 1,\ldots,p$,

$$z(t, x) \equiv z'(t, x) - \bar{z}(x) \tag{5.1}$$

where

$$\bar{z}(x) = \frac{1}{n} \sum_{t=1}^{n} z'(t, x) \tag{5.2}$$

Using these t-centered values $z(t,x)$ we form a new $n \times p$ matrix Z in the manner of Z'. The rows of Z can be viewed as points in p-dimensional Euclidian space E_p, so that for each $t = 1,\ldots,n$, it can be written

$$\vec{z}(t) \equiv [z(t,1),\ldots, z(t, p)]^T \tag{5.3}$$

where "^{T}" denotes matrix transposition. The second step is to compute a symmetric pxp matrix S that will be referred to as the scatter matrix:

$$S = \sum_{t=1}^{n} \vec{z}(t)\vec{z}^T(t) = Z^T Z \tag{5.4}$$

We then find the eigenvectors and eigenvalues of the scatter matrix S. A symmetric matrix such as S generally has p eigenvectors $\vec{e}_j = [e_j(1),\ldots,e_j(p)]^T$ in E_p and p associated real, non-negative eigenvalues l_j such that

$$S\vec{e}_j = l_j\vec{e}_j \quad , \quad j = 1,\ldots, p \tag{5.5}$$

The matrix version of Equation (5.5) is

$$SE = LE \tag{5.6}$$

where $E \equiv [\vec{e}_1,\ldots,\vec{e}_p]$ is an pxp matrix and L is an pxp diagonal matrix containing the eigenvalues l_j. It is worth noting that the eigenvalues l'_j for the covariance matrix $C = (n-1)^{-1}S$ are $l'_j = (n-1)^{-1}l_j$.

The representation of the data matrix Z in terms of principal components arises then as follows. Using the property that eigenvectors $\vec{e}_j$ and $\vec{e}_k$ belonging to distinct eigenvalues l_j and l_k of S in (5.5) are orthogonal, we can write

$$Z = Z(EE^T) = (ZE)E^T \tag{5.7}$$

and define the amplitude matrix A:

$$A \equiv ZE \tag{5.8}$$

Then (5.7) can be expressed as

$$Z = AE^T \tag{5.9}$$

A vector version of (5.9) is

$$\vec{z}(t) = \sum_{i=1}^{p} a_i(t)\vec{e}_i \quad t = 1,\dots,n. \tag{5.10}$$

The vector $\vec{e}_i$ is the ith EOF and the projection of $\vec{z}(t)$ on $\vec{e}_i$ is the ith Principal Component (PC). The product of the ith PC with the ith EOF defines a vector that is usually referred to as the ith mode. Each mode explains a certain fraction of the variance of $\vec{z}(t)$. In particular, the first mode, $\hat{\vec{z}}_1(t) = a_1(t)\vec{e}_1$, is the one-dimensional linear approximation to $\vec{z}(t)$ that explains the highest percentage of variance. Increasing the number of terms in the series (5.10) increases the percentage of variance explained by the PCA approximation. The scalar version of (5.10) is

$$z(t,x) = \sum_{i=1}^{p} a_i(t)e_i(x) \quad t = 1,\dots,n \; ; \; x = 1,\dots, p \tag{5.11}$$

and the scalar version of the amplitude matrix, A, is

$$a_i(t) = \sum_{i=1}^{p} z(t,x)e_i(x) \quad t = 1,\dots,n \; ; \; x = 1,\dots, p \tag{5.12}$$

The uncentered representation can be recovered simply by recalling (5.1), so that $z'(t,x) = z(t,x) + \bar{z}(x)$.

Another interesting property of the PCA is that if the PC development is truncated after the first mode $\hat{\vec{z}}_1(t)$ then the field is separable in terms of its spatial and temporal structure. This is, it can be viewed as a fixed spatial pattern (EOF) with an amplitude that varies in time (PC). This property really makes it easy to interpret and understand the main signal driving the variability of the data set. However, this approximation assumes that the optimal one-dimensional approximation to the data set can be separable in terms of its spatial and temporal variability, which may not be the case in reality. This motivates the definition of the nonlinear PCA.

5.1.2 Nonlinear principal component analysis

Let's consider the same $n \times p$ matrix Z used in Section 5.1.1. The optimal one-dimensional nonlinear approximation $\hat{\vec{z}}_1^{NL}(t)$ to $\vec{z}(t)$ can be defined as

$$\hat{\vec{z}}_1^{NL}(t) = \left(g \circ f\right)\left(\vec{z}(t)\right) \tag{5.13}$$

where the functions $f: \Re^p \to \Re$ and $g: \Re \to \Re^p$ must be estimated under the constraint that the sum of squared residuals,

$$J = \left\langle \left\| \vec{z}(t) - \hat{\vec{z}}_1^{NL}(t) \right\|^2 \right\rangle \tag{5.14}$$

is minimized (Monahan, 2001). The function f maps the original data, of dimension p, to a one-dimensional space, while g is a map from this space back to $\Re^p$. If the functions f and g are constrained to be linear, then the problem reduces to traditional PCA. However, we can generalize PCA to allow the estimation of non-linear one-dimensional structures by allowing the function f and g to be nonlinear. This is referred to as nonlinear PCA.

Nonlinear PCA can be implemented by means of a five-layer feed-forward neural network such as that represented in Figure 5.1 (Freeman and Skapura, 1991; Kramer, 1991). The first (input) and fifth (output) layers each contain p neurons, while the third (bottleneck) layer contains only a single neuron. Layers 2 and 4, denoted respectively as the encoding and decoding layers, both contain L neurons. Each neuron can have many inputs, but it has a single output, which can fan out to many other neurons in the network. An input vector, $\vec{z}(t) = [z(t,1),...,z(t,p)]^T$, is applied to the input layer of the network. The input units distribute the values to the encoding layer neurons. Each connection to the jth neuron of the encoding layer has a quantity called 'weight' associated with it. The weight on the connection from the ith input neuron to the jth neuron of the encoding layer is denoted as ω_{ji}^e.

Each neuron determines a net-input value based on all its input connections. This net-input is calculated as the sum of the input values multiplied by their corresponding weights:

$$net_{tj}^e = \sum_{i=1}^{p} z_{ti} \omega_{ji}^e + \theta_j^e \tag{5.15}$$

where θ_j^e is a bias term that can be included as a weight on a connection that has its input value always equal to 1, and $z_{ti} \equiv z(t,i)$. The "e" superscript refers to quantities on the encoding layer.

The output value of the jth neuron of the encoding layer is

$$i_{tj} = f_j^e \left(net_{tj}^e \right) \tag{5.16}$$

where f_j^e is referred to as the transfer function of the jth neuron of the encoding layer. In the case of our neural network (Fig. 5.1), the transfer functions of the layers 2 and 4 are hyperbolic tangent functions, while the transfer functions of the bottleneck and output layers are linear.

Since the transfer function of the bottleneck is linear, the equation for its output is given by

$$q_{t1} = \sum_{j=1}^{L} i_{tj} \omega_{1j}^b + \theta_1^b \tag{5.17}$$

where the "*b*" superscript refers to quantities on the bottleneck layer. The net-input corresponding to the *r*th neuron of the decoding layer is then

$$net_{tr}^d = q_{t1}\omega_{r1}^d + \theta_r^d \tag{5.18}$$

where the "*d*" superscript refers to quantities on the decoding layer. The output of the *r*th neuron of the decoding layer is

$$v_{tr} = f_r^d\left(net_{tr}^d\right) \tag{5.19}$$

Finally, the equations for the *k*th neuron of the output layer are

$$net_{tk}^o = \sum_{r=1}^{L} v_{tr}\omega_{kr}^o + \theta_k^o \tag{5.20}$$

$$o_{tk} = f_k^o\left(net_{tk}^o\right) \tag{5.21}$$

where $o_{tk} \equiv o(t,k)$ and the "*o*" superscript refers to quantities on the output layer.
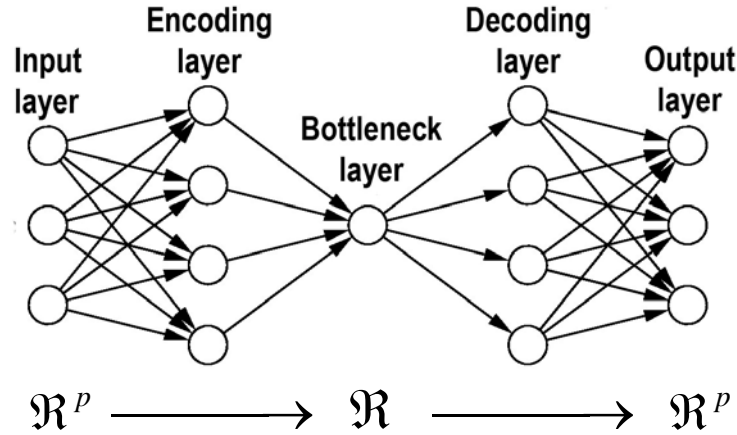
Figure 5.1. The autoassociative neural network used to perform nonlinear PCA.

The initial set of weight values represents a first guess to the proper weights for the problem. The basic procedure for training the network is as follows:

1. Apply an input vector $\vec{z}(t)$ to the network and calculate the corresponding output, $\vec{o}(t) = [o(t,1),...,o(t,p)]^T$.
2. Compute the error by means of (5.14).
3. Determine in which direction to change each weight in order to reduce the error.
4. Determine the amount by which to change each weight.
5. Apply the corrections to the weights.

6. Repeat points 1 through 5 with all the training vectors until the error for all vectors in the training set is reduced to an acceptable value.

Update of output-layer weights

We shall define the error at a single output neuron to be $\delta_{tk} = (z_{tk} - o_{tk})$, where the subscript "$t$" refers to the tth training vector and "k" refers to the kth output neuron. In this case, z_{tk} is the desired output value, and o_{tk} is the actual output from the kth neuron. Because the output of the network is adjusted until it matches the input as closely as possible, the network is said to be *autoassociative*. The error that is minimized is the sum of the squares of the errors for all output neurons:

$$E_t = \frac{1}{2} \sum_{k=1}^{p} (z_{tk} - o_{tk})^2 \qquad (5.22)$$

The factor 1/2 in Eq. (5.22) is there for convenience in calculating derivatives later. To determine the direction in which to change the weights, we calculate the negative of the gradient of E_t, ∇E_t, with respect to the weights ω_{kr}^o. To keep things simple, each component of ∇E_t is considered separately. From Eqs. (5.21) and (5.22),

$$\frac{\partial E_t}{\partial \omega_{kr}^o} = -(z_{tk} - o_{tk}) \frac{\partial f_k^o}{\partial (net_{tk}^o)} \frac{\partial (net_{tk}^o)}{\partial \omega_{kr}^o} \qquad (5.23)$$

The last factor in Eq. (5.23) is

$$\frac{\partial (net_{tk}^o)}{\partial \omega_{kr}^o} = \frac{\partial}{\partial \omega_{kr}^o} \left(\sum_{r=1}^{L} v_{tr} \omega_{kr}^o + \theta_k^o \right) = v_{tr} \qquad (5.24)$$

Combining Eqs. (5.23) and (5.24), the negative gradient is given by

$$-\frac{\partial E_t}{\partial \omega_{kr}^o} = (z_{tk} - o_{tk}) \frac{\partial f_k^o}{\partial (net_{tk}^o)} v_{tr} \qquad (5.25)$$

To update the output weights we consider that the weight change is proportional to the negative gradient. Thus, the weights on the output layer are updated according to

$$\omega_{kr}^o(m+1) = \omega_{kr}^o(m) + \eta \left((z_{tk} - o_{tk}) \frac{\partial f_k^o}{\partial (net_{tk}^o)} v_{tr} \right) \qquad (5.26)$$

where the factor η is called the learning-rate parameter. Usually, η must be a small number (on the order of 0.05 to 0.3) to ensure that the network will settle to a solution. Since the transfer function of the output layer is linear,

$$\frac{\partial f_k^o}{\partial \left(net_{tk}^o \right)} = 1 \qquad (5.27)$$

Eq. (5.26) can then be written as

$$\omega_{kr}^o(m+1) = \omega_{kr}^o(m) + \eta \left(z_{tk} - o_{tk} \right) v_{tr} \qquad (5.28)$$

Finally we define a quantity, referred to as error term,

$$\delta_{tk}^o = \left(z_{tk} - o_{tk} \right) \frac{\partial f_k^o}{\partial \left(net_{tk}^o \right)} = z_{tk} - o_{tk} \qquad (5.29)$$

We can then write then the weight-update equation as

$$\omega_{kr}^o(m+1) = \omega_{kr}^o(m) + \eta \delta_{tk}^o v_{tr} \qquad (5.30)$$

Update of hidden-layers weights

If the same type of calculation done for the output layer is repeated for the hidden layers, a similar expression for the weight-update equations is obtained. From Eqs. (5.15) to (5.21) it is obvious that the total error E_t depends on the output values on the hidden layers. This can be exploited to calculate the gradient of E_t with respect to the hidden-layer weights.

The first step is the computation of the gradient of E_t with respect to the decoding-layer weights. Eq. (5.22) can be written as:

$$E_t = \frac{1}{2} \sum_{k=1}^{p} \left(z_{tk} - o_{tk} \right)^2 = \frac{1}{2} \sum_{k=1}^{p} \left[z_{tk} - f_k^0 \left(\sum_{r=1}^{L} v_{tr} \omega_{kr}^o + \theta_k^o \right) \right]^2 \qquad (5.31)$$

Since v_{tr} depends on the weights on the decoding layer through Eqs. (5.18) and (5.19), the gradient of E_t with respect to the decoding-layer weights can be written as

$$\frac{\partial E_t}{\partial \omega_{r1}^d} = -\sum_{k=1}^{p} \left(z_{tk} - o_{tk} \right) \frac{\partial f_k^o}{\partial f_r^d \left(net_{tr}^d \right)} \frac{\partial f_r^d \left(net_{tr}^d \right)}{\partial net_{tr}^d} \frac{\partial net_{tr}^d}{\partial \omega_{r1}^d} \qquad (5.32)$$

One of the differences with respect to the output layer is that the transfer functions of the encoding and decoding layers are hyperbolic tangent functions instead of linear functions and, therefore, the derivative of the transfer function is not equal to 1. Thus, the derivative of the transfer function of the decoding layer neurons is

$$\frac{\partial f_r^d \left(net_{tr}^d\right)}{\partial \left(net_{tr}^d\right)} = 1 - \left[f_r^d \left(net_{tr}^d\right)\right]^2 \tag{5.33}$$

The other factors in Eq. (5.32) are

$$\frac{\partial f_k^o}{\partial f_r^d \left(net_{tr}^d\right)} = \omega_{kr}^o \tag{5.34}$$

$$\frac{\partial net_{tr}^d}{\partial \omega_{r1}^d} = q_{t1} \tag{5.35}$$

By using Eqs. (5.33), (5.34) and (5.35), Eq (5.32) becomes

$$\frac{\partial E_t}{\partial \omega_{r1}^d} = -\sum_{k=1}^{p} \left(z_{tk} - o_{tk}\right) \omega_{kr}^o \left\{1 - \left[f_r^d \left(net_{tr}^d\right)\right]^2\right\} q_{t1} \tag{5.36}$$

The decoding-layer weights are updated proportionally to the negative of Eq. (5.36):

$$\omega_{r1}^d(m+1) = \omega_{r1}^d(m) + \eta \left(\sum_{k=1}^{p} \left(z_{tk} - o_{tk}\right) \omega_{kr}^o \left\{1 - \left[f_r^d \left(net_{tr}^d\right)\right]^2\right\} q_{t1}\right) \tag{5.37}$$

Using (5.29) we can rewrite Eq. (5.37) as

$$\omega_{r1}^d(m+1) = \omega_{r1}^d(m) + \eta \left\{1 - \left[f_r^d \left(net_{tr}^d\right)\right]^2\right\} q_{t1} \sum_{k=1}^{p} \delta_{tk}^o \omega_{kr}^o \tag{5.38}$$

Notice that every weight update on the decoding layer depends on all error terms δ_{tk}^o on the output layer. The known errors on the output layer are propagated back to the hidden layer to determine the appropriate weight changes on the layer. By defining a decoding-layer error term in a similar way as (5.37)

$$\delta_{tr}^d = \left\{1 - \left[f_r^d \left(net_{tr}^d\right)\right]^2\right\} \sum_{k=1}^{p} \delta_{tk}^o \omega_{kr}^o \tag{5.39}$$

the weight update equation for the decoding-layer weights becomes analogous to Eq. (5.30):

$$\omega_{r1}^d(m+1) = \omega_{r1}^d(m) + \eta \delta_{tr}^d q_{t1} \tag{5.40}$$

Repeating the same calculation for the bottleneck and encoding layers, similar weight update equations can be computed for these layers. Once the errors terms have been computed, the weight-update equations for the bottleneck and encoding layers can be written as

$$\omega_{1j}^{b}(m+1) = \omega_{1j}^{b}(m) + \eta \delta_{t1}^{b} i_{tj} \qquad (5.41)$$

$$\omega_{ji}^{e}(m+1) = \omega_{ji}^{e}(m) + \eta \delta_{tj}^{e} z_{ti} \qquad (5.42)$$

where the error terms are given by

$$\delta_{t1}^{b} = \sum_{k=1}^{p} \left(\delta_{tk}^{o} \sum_{r=1}^{L} \omega_{kr}^{o} \left\{ 1 - \left[f_{r}^{d}\left(net_{tr}^{d}\right) \right]^{2} \right\} \omega_{r1}^{d} \right) \qquad (5.43)$$

$$\delta_{tj}^{e} = \sum_{k=1}^{p} \delta_{tk}^{o} \sum_{r=1}^{L} \omega_{kr}^{o} \left\{ 1 - \left[f_{r}^{d}\left(net_{tr}^{d}\right) \right]^{2} \right\} \omega_{r1}^{d} \omega_{1j}^{b} \left\{ 1 - \left[f_{j}^{e}\left(net_{tj}^{e}\right) \right]^{2} \right\} \qquad (5.44)$$

It is important to remark that the error terms on the hidden neurons are calculated before the connection weights to the output layer neurons have been updated. Once all the weights have been updated, the error E_t is computed again. When the error is acceptably small for each of the training-vector pairs, training can be discontinued.

Practical considerations

In order to avoid overfitting, we have used a technique called early stopping, as in Monahan (2000). In early stopping, the training is terminated before the error function is minimized, according to a stopping criterion. The strategy used here consisted of holding aside a fraction (20%) of randomly selected data points in a validation set not used to train the network. While training the network, we compute the error on the validation set and training is discontinued when such an error begins to increase. Due to the existence of multiple minima in the error function (5.22), we carried out 30 training runs starting from different, randomly chosen, initial weights for each run. The results from those runs were examined and we selected the one with a lower error.

Regarding the number of neurons in the hidden layers, it is not required that the encoding and decoding layers have the same number of neurons, but the numbers are fixed to be the same in our case ($L = 3$) so as to have only one free parameter in the model architecture.

As we commented in section 5.1.1, PCA partitions variance in the sense that if $\hat{\vec{z}}_{p}(t)$ is the p-dimensional linear approximation to $\vec{z}(t)$, then the total variance of $\vec{z}(t)$ is the sum of the total variance of $\hat{\vec{z}}_{p}(t)$ and the total variance of the residual $\vec{z}(t) - \hat{\vec{z}}_{p}(t)$. Monahan (2000) found empirically that nonlinear PCA also partitions variance in this sense. However, unlike traditional PCA, nonlinear PCA usually does not have the additive structure shown by Eq. (5.10). To find the *P*-dimensional nonlinear PCA, the one-dimensional approximation $\hat{\vec{z}}_{1}(t)$ is first comnputed and subtracted from the original data to give the residual $\vec{r}_{1}(t) = \vec{z}(t) - \hat{\vec{z}}_{1}(t)$. Then, computing the one-dimensional approximation of $\vec{r}_{1}(t)$ we determine the second mode, $\hat{\vec{z}}_{2}(t)$, and iterating this procedure *P*-times we find all the *P*-modes. The resulting *P*-dimensional approximation will be the sum of the successive i-order approximations.

5.1.3 Application to Mediterranean Sea level

To inspect how these two techniques can assist the study of climatic data sets, they have been applied to the study of Mediterranean Sea level variability. The primary objective of this section is to compare both techniques and to determine whether the use of nonlinear techniques brings significant improvements in comparison with traditional PCA in the case of Mediterranean Sea level data. It is important to remark that the application of nonlinear PCA is far more complicated than the use of traditional PCA, not only in terms of implementation but also in terms of interpreting results. Thus, it is no surprise that the use of traditional PCA is much more extended than nonlinear PCA.

The sea level data used to test PCA analysis is the standard 1/4º x 1/4º gridded altimetry data set provided by CLS and described in section 3.2, with the atmospheric component added to SLA. Prior to the analysis, a linear trend and the mean seasonal cycle was removed from each grid point series by means of a harmonic analysis.
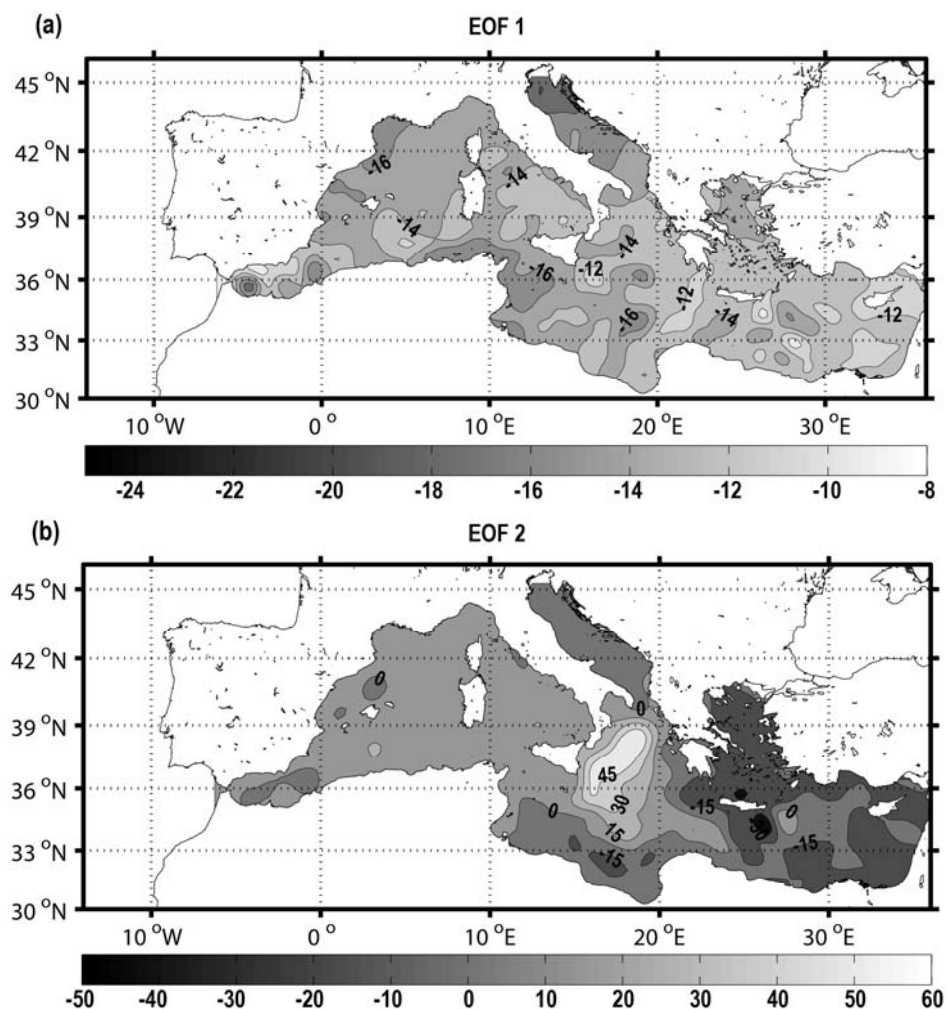
Figure 5.2. The two leading linear EOFs of the altimetry data set (1993-2005) obtained after the removal of the seasonal cycle and a linear MSL trend: (a) EOF 1, (b) EOF 2.

The data set has over 5000 spatial grid points covering the whole Mediterranean basin. Such a large amount of grid points is not a problem when implementing the traditional PCA, but it makes unattainable the implementation of nonlinear PCA. In order to afford the nonlinear problem we pre-processed the data set by projecting it on the space of its first 15 EOF modes, which altogether explain 88.1% of the total variance. In this way, each training vector $z(t)$ has only 15 components. Figure 5.2 shows the two leading EOFs of Mediterranean sea level, which explain 61.6% and 9.2% of the variance, respectively (the EOF3, not shown, explains only 3.4%). The EOF1 has the same sign all over the basin, which represents an oscillation of the basin as a whole. EOF2 has a dipole structure, changing sign between the Ionian Sea and the Aegean Sea. The two times series corresponding to these two modes are shown in Figure 5.3.
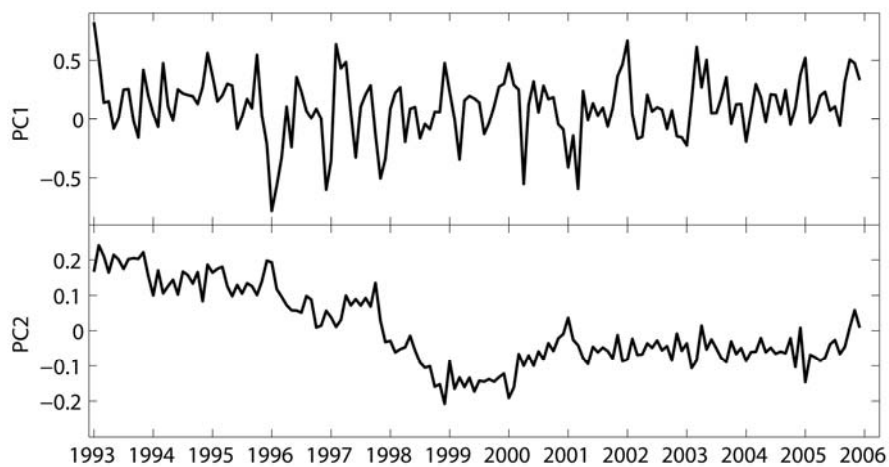
Figure 5.3. The time amplitudes of the two leading linear EOFs estimated from altimetry (1993-2005): amplitude 1(top) and amplitude 2 (bottom).

The correlation between the two time series of Figure 5.3 is non-significant. However, a projection of the data onto the plane spanned by the two leading EOFs shows that they are not totally independent (Fig. 5.4). Nearly zero values of PC1 are more associated with negative values of PC2 than with positive values, for instance (there are twice as many negative values as positive values).

When considering a nonlinear PCA of the data, the first nonlinear mode explains 70.7% of the variance in the 15-dimensional EOF space, and thus 62.3% of the variance of the original data set. Figure 5.5 shows the projection of the nonlinear mode 1 approximation (circles) together with alimetry data (dots) onto the subspace spanned by the two leading EOFs. The curve differs slightly from a straight line due to fact that nearly zero values of PC1 results in more negative values of PC2. This behaviour is reflected in the U-shaped form of the curve.

The output of the neuron in the bottleneck layer is the time series associated with the nonlinear mode. Figure 5.6 shows this time series (standardized) together with the time series associated with the first linear mode. The resemblance between the two series is well apparent, indicating that the structure of the data set is mainly linear.
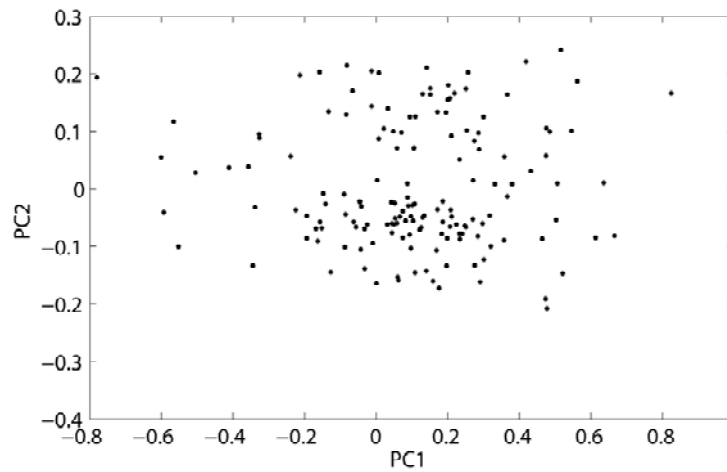
Figure 5.4. Scatterplot of satellite altimetry data (1993-2005) projected onto the plane spanned by the two leading linear EOFs.
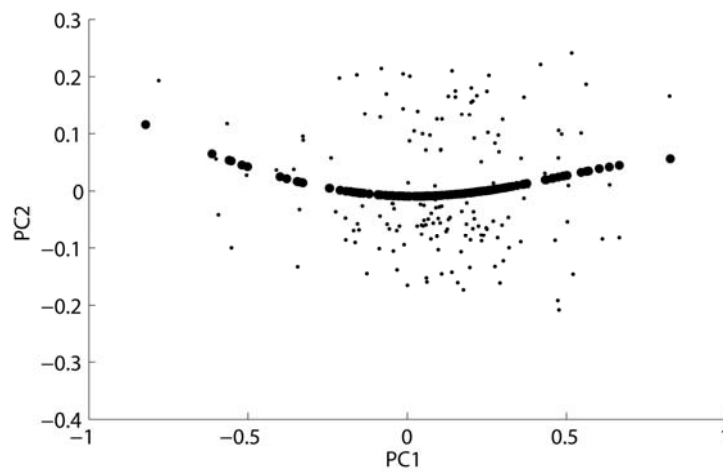
Figure 5.5. Scatterplot of satellite altimetry data (dots) and nonlinear mode 1 approximation (circles) projected onto the plane spanned by the two leading EOFs.
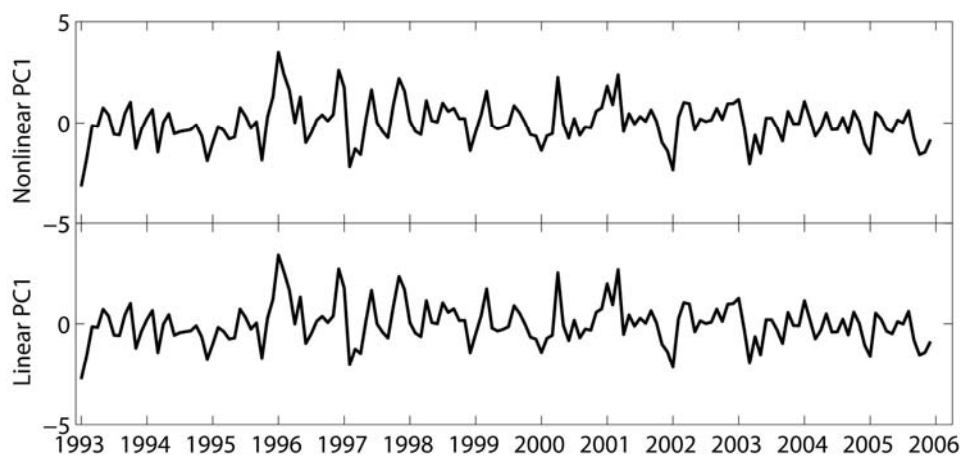
Figure 5.6. The time amplitudes associated with nonlinear (top) and linear (bottom) modes 1.
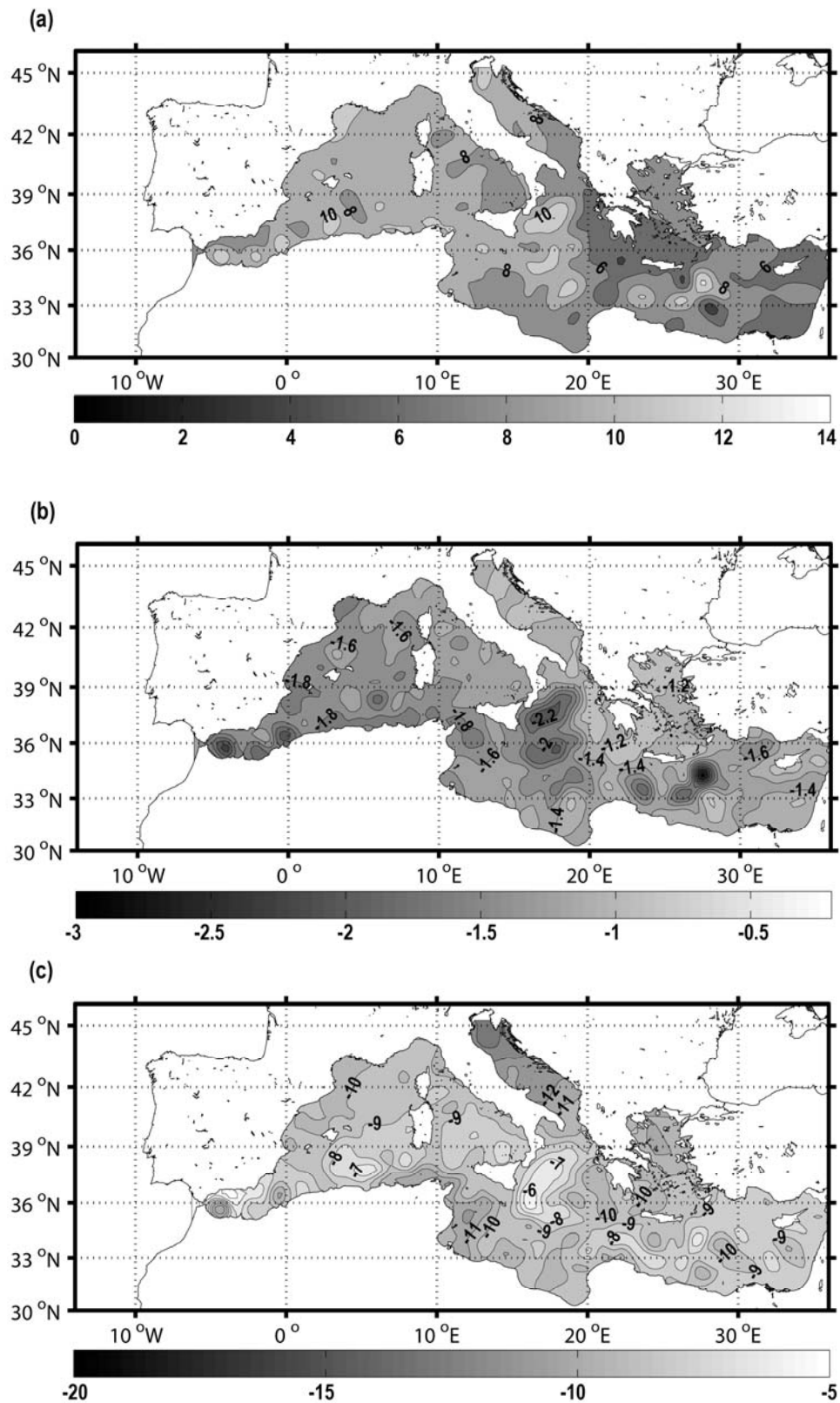
Figure 5.7. Sequence of spatial maps characterising nonlinear mode 1 for different values of the associated time amplitude: (a) -2.5; (b) 0; (c) 2.5.

Unlike traditional PCA, no single spatial pattern is associated with the nonlinear mode. However, following Monahan (2000), we can represent the nonlinear approximation $\hat{z}_1(t)$ as a sequence of patterns that can be visualized sequentially. All linear modes represent oscillations that have fixed spatial structures (Fig. 5.2a) and corresponding time amplitudes (Fig. 5.3a). If the data set contains any structure more general than just a standing oscillation, it should be detected by nonlinear PCA and made apparent in the sequence of patterns representing the first nonlinear mode. Figure 5.7 shows maps of the first nonlinear mode $\hat{z}_1(t)$ that correspond to different values of the nonlinear time series (-0.5, 0, 0.5). These values have been chosen to provide a representative sample of spatial patterns associated with the first nonlinear mode. It is important to note that all nonlinear patterns show the same sign all over the basin, just as the linear EOF1 does. However, the nonlinear mode does not only describe the oscillation of the basin as a whole, but also some of the features found in the linear EOF2. In fact, nonlinear patterns bear a remarkable resemblance to both EOF1 and EOF2 (Fig. 5.2). Figure 2.7a shows a pattern with larger values in the Western Mediterranean and a maximum in the Ionian Sea. This structure is very similar to the one shown by linear EOF2. Also Figure 5.7c shows features belonging to both EOF1 and EOF2, indicating that nonlinear mode 1 mixes linear PCA modes 1 and 2.

The variance explained by the nonlinear mode 2 is 10.1%, as compared to the 9.2% explained by the second linear PCA mode. Figure 5.8 shows the time series corresponding to the nonlinear mode 2 (top panel) and linear mode 2 (bottom panel). The correlation between the two series is 0.94. Time series associated with nonlinear modes 1 and 2 are uncorrelated. Spatial patterns associated with the nonlinear mode 2 are shown in Figure 5.9: they also show the dipole structure shown by linear EOF2. When the associated time series is strongly negative, nonlinear mode 2 is characterized by positive anomalies in the Western Mediterranean, with a maximum in the Ionian Sea and negative anomalies in the Eastern Mediterranean. As the values of the time series increase and become positive, the anomalies decrease in magnitude. For values of the time series near the positive extreme, the pattern associated with nonlinear mode 2 becomes the opposite of that obtained for values near the negative extreme: negative anomalies in the Western Mediterranean, more marked in the Ionian Sea, and positive anomalies in the Eastern Mediterranean.
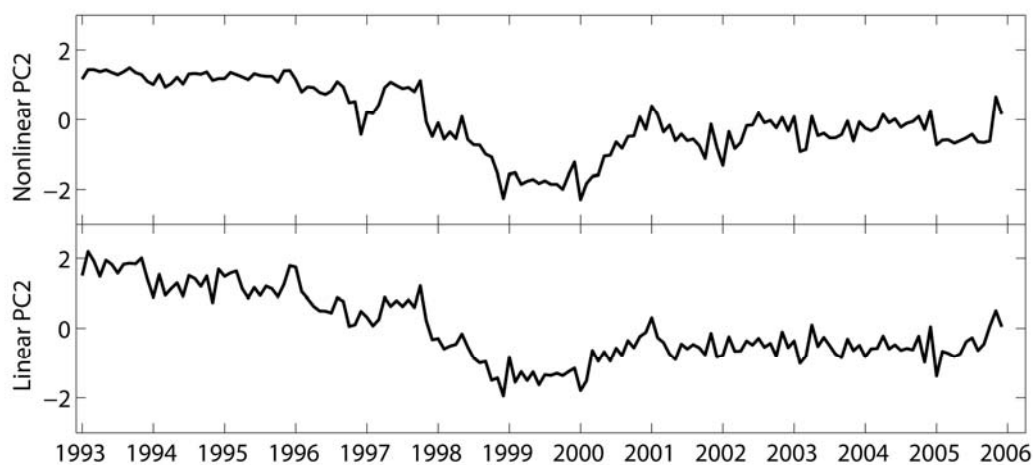
Figure 5.8. The time amplitudes associated with nonlinear (top) and linear (bottom) modes 2.
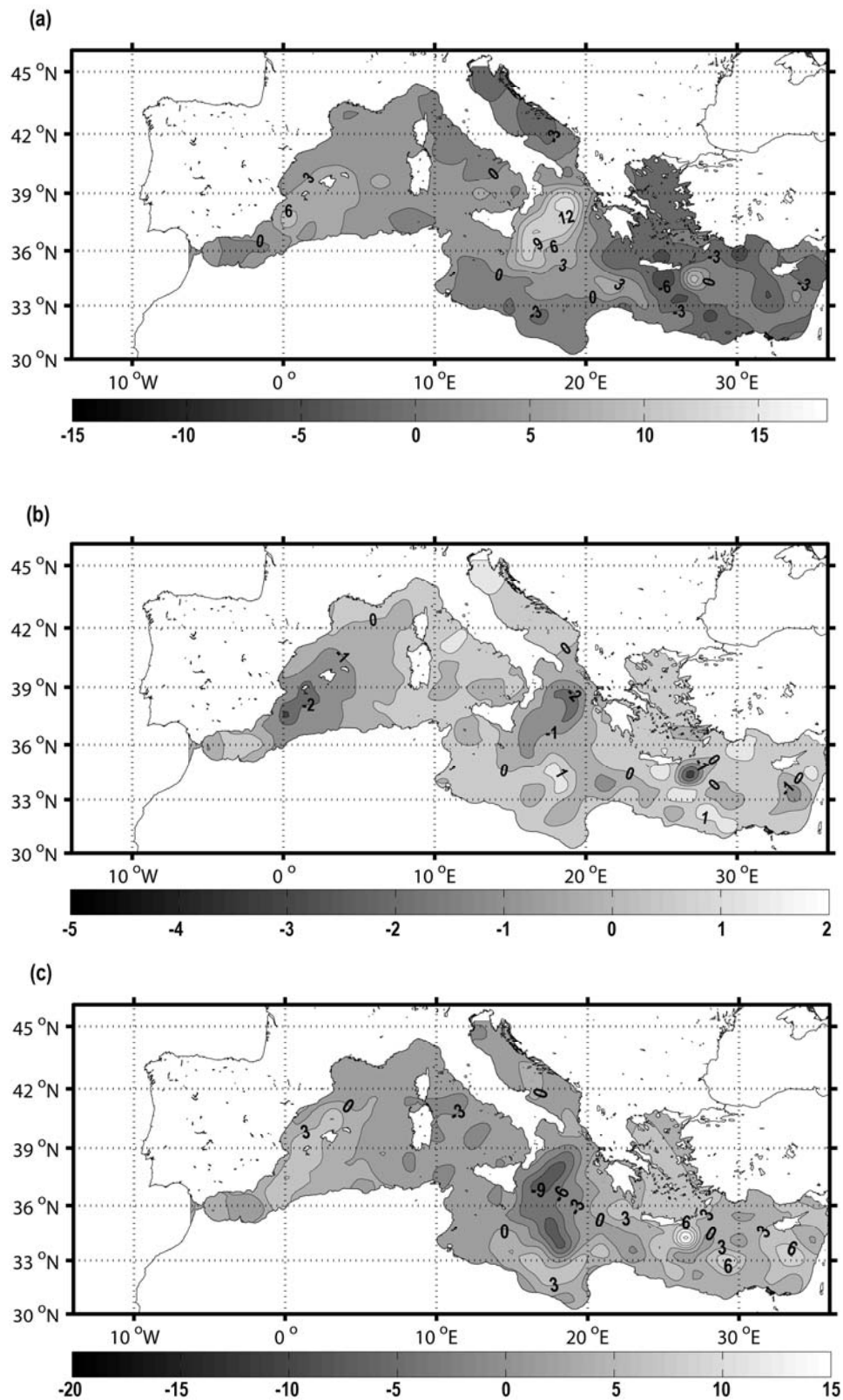
Figure 5.9. Sequence of spatial maps characterising nonlinear mode 2 for different values of the associated time amplitude: (a) -2; (b) 0; (c) 1.5.

Summary and discussion

In this section we have studied Mediterranean sea level variability by applying linear and nonlinear PCA to altimetry data. We have found that nonlinear mode 1 explains 62.3% of the total variance, as compared to the 61.6% explained by the one-dimensional PCA approximation. The difference is not significant. The time series describing linear and nonlinear mode 1 are highly correlated (0.99). Regarding the spatial patterns, the linear PCA mode 1 describes a standing oscillation of the basin as a whole, whereas the linear PCA mode 2 shows a dipole structure with the same sign in the Western Mediterranean and the Ionian Sea, and opposite sign in the Eastern Mediterranean. Nonlinear mode 1 mixes linear PCA modes 1 and 2, but the dominant dipole structure shown by linear PCA mode 2 is not actually in nonlinear mode 1 (it has the same sign all over the basin). Regarding the nonlinear mode 2, it explains 10.1% of the total variance, as compared to the 9.2% explained by the linear PCA mode 2. The time series associated with the linear and nonlinear modes 2 are also highly correlated (0.94). Moreover, nonlinear mode 2 bears a strong resemblance to linear PCA mode 2, both showing a similar dipole structure.

   The results obtained in this section will be used in the following in a first attempt of reconstructing Mediterranean sea level fields (both linear and nonlinear PCA analysis will be tested).

5.2 First attempt: reconstruction by using linear and nonlinear PCA

In this section we present two simple methodologies that use linear and nonlinear PCA to reconstruct Mediterranean sea level. The main objective is to determine whether it is worth using nonlinear PCA to reconstruct sea level or not. The preliminary results obtained in the last section suggest that the differences between the two methods could not be significant when applied to Mediterranean sea level data, but this must be confirmed by the final results of the reconstruction.

   The data set used in this section consists of the same satellite altimeter data used in Section 5.1.3 (covering the period January 1993 to December 2005) and tide gauge data covering the period January 1955 to December 2000, obtained from the PSMSL (see Chapter 3). Namely, the tide gauge records used in this section are Venezia (45.433ºN, 12.333ºE), Trieste (45.65ºN, 13.75ºE), Ceuta (35.9ºN, 5.317º W), Bakar (45.3ºN, 14.533º E) and Split (43.5ºN, 16.433ºE). The mean seasonal cycle was removed from both the satellite altimeter data and the tide gauge data by means of a harmonic analysis.

5.2.1 Reconstruction by using linear PCA

The first attempt to reconstruct Mediterranean sea level for the period 1955-2000 is based on a very simple technique. First, PCA is applied to tide gauge records and altimeter data in an independent way. Considering that tide gauge observations are a spatial subset of the whole sea level field measured by the altimeters, and assuming that the sampling is good enough to reproduce the leading spatial modes, it derives that the leading tide gauge EOFs should be a spatial subsampling of the leading altimetry EOFs and that the time amplitudes should be similar for both data sets.
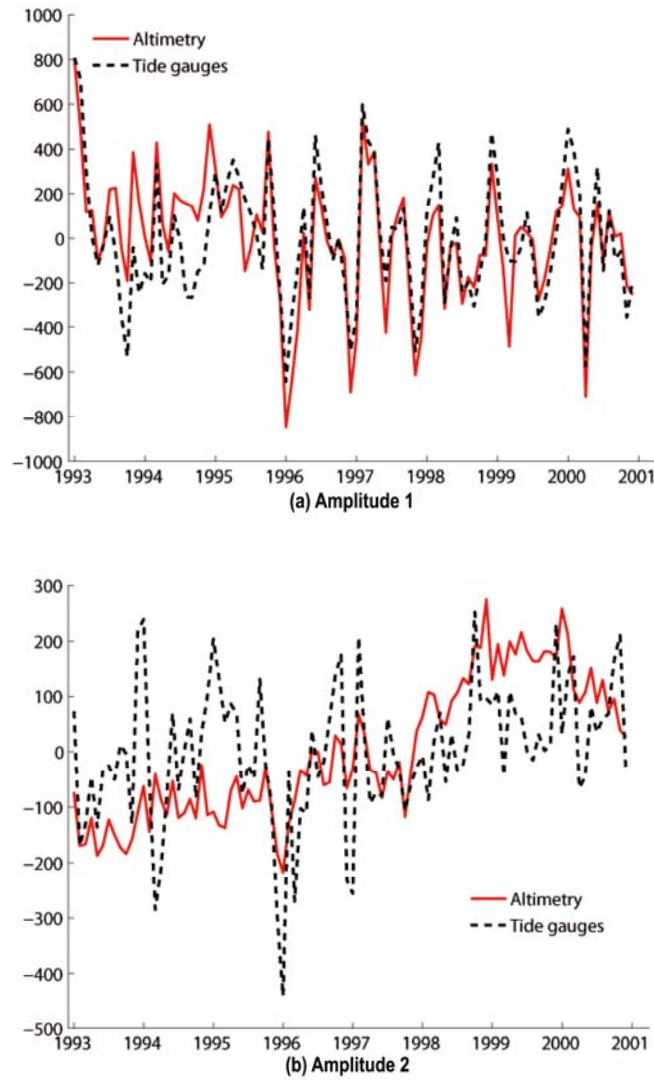
Figure 5.10. The time amplitudes of the two leading EOFs estimated from altimetry (solid line) and tide gauges (dashed line): (a) amplitude 1; (b) amplitude 2.

Results reveal that the correlation between the amplitudes of the leading modes (EOF1, Fig. 5.10a) is 0.81, while it goes down to 0.45 for the amplitudes of EOF 2 (Fig. 5.10b); both correlations are significant at the 99% confidence level. The correlation between the amplitudes of EOF 3 (not shown) is no significant. These results indicate that a convenient choice to obtain the reconstruction would be using Eq. (5.9) and truncating the expansion by including only the lowest 2 EOFs

$$\hat{Z}_2 = A_2 E_2^T \tag{5.45}$$

where E_2 contains the two leading spatial modes obtained from the altimetry data set and A_2 is a matrix containing the amplitudes of the two leading modes obtained from tide gauge records. Since the spatial modes from satellite altimetry data cover the whole Mediterranean Sea and the amplitudes obtained from tide gauge data span the period January 1955 to December 2000, $\hat{Z}$ will give Mediterranean sea level fields covering

the whole basin and spanning the long period covered by tide gauge data. We will refer to this approach as the 'substitution approach', since the basis of the method consists of substituting the short amplitudes of the altimetry leading modes by the corresponding longer tide gauge amplitudes.

Results

In order to test the goodness of the reconstruction over the whole domain we compare the reconstructed field with observations from altimetry for the period 1993-2000. This is not an independent test, since EOFs were estimated from satellite altimeter data, but will give some hints on the accuracy of the reconstruction.

The spatial distribution of the correlation between the observed and reconstructed fields (Fig. 5.11) shows correlations close to 0.8 in the Adriatic Sea and in the northern-sector of the Western Mediterranean. In the Ionian, Aegean Sea, south of Creta, and near the coast of Morocco the correlation is smaller but still larger than 0.5 in most areas. Also the distribution of sea level trends derived from the reconstruction for the period 1993-2000 can be compared with the trends estimated directly from altimetry data. The distribution of reconstructed sea level trends (Fig. 5.12b) shows a similar spatial pattern to the observed trends (Fig. 5.12a), but the magnitude of the trends is rather different, especially in the Ionian and Aegean Sea. Altimetry data shows marked negative trends in the Ionian Sea (up to -20 mm/yr) and large positive trends in the Aegean Sea (up to 20 mm/yr); trends are positive almost everywhere else, with larger positive values in the Eastern Mediterranean (up to 15 mm/yr) than in the Western Mediterranean (nearly zero). The distribution of reconstructed sea level trends shows also negative trends in the Ionian Sea, but they are much smaller (up to -3 mm/yr). In the Aegean Sea the reconstruction also underestimates the trends (up to 6 mm/yr). In contrast, in the Western Mediterranean the reconstruction overestimates the trends, reaching about 6 mm/yr in this region.
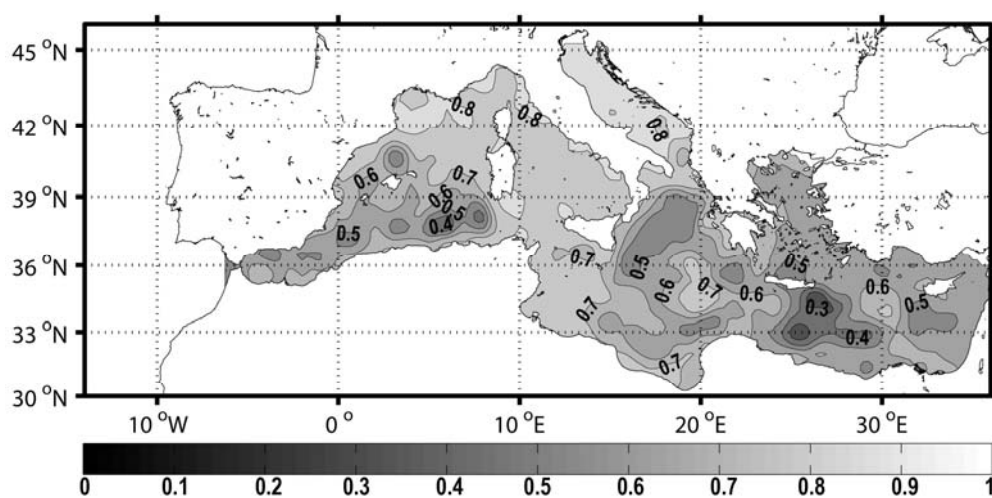
Figure 5.11. Correlation between the reconstructed sea level fields (using linear PCA) and satellite altimeter observations over the period 1993-2000 (the contour interval is 0.1).
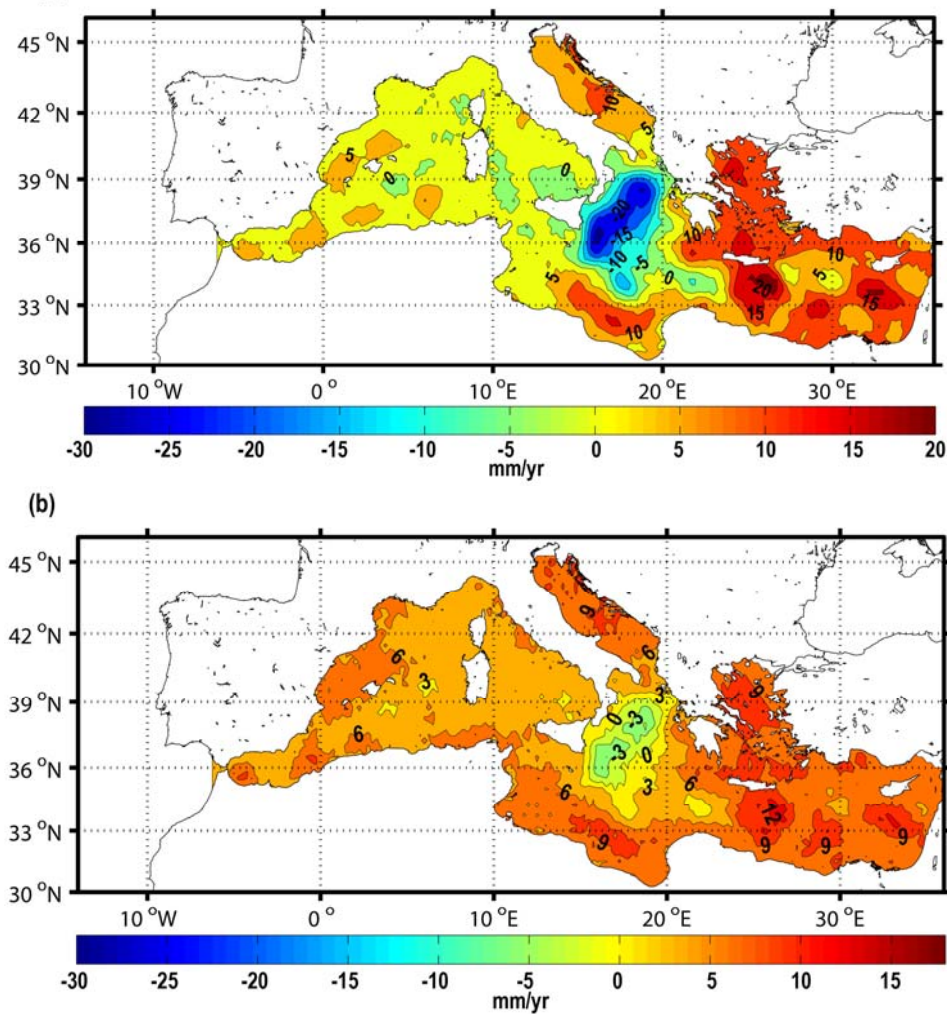
Figure 5.12. The distribution of sea level trends for the period 1993-2000 as estimated from (a) satellite altimetry data (the contour interval is 5 mm/yr); (b) the reconstructed fields, obtained using the substitution approach based on linear PCA (the contour interval is 3 mm/yr).

Also the basin MSL was computed for both, the reconstruction and altimetry values. The correlation between the two series is 0.8 and the root mean square difference between the two series is 0.7 cm. The MSL rise for the period 1993-2000 is 4.5±0.7 mm/yr when computed from the reconstruction and 3.9±0.7 mm/yr when derived from satellite altimeter data. All sea level trends have been estimated by using the MM-estimator described in Chapter 3. Errors on the MSL trends represent random errors computed by means of a robust bootstrap (Chapter 3).

For the sea level fields spanning the whole period 1955-2000, the trend is 0.4 mm/yr. The distribution of sea level trends (not shown) shows a uniform pattern with small positive trends all over the basin.

5.2.2 Reconstruction by using nonlinear PCA

The same principle used in Section 5.2.1 can be used to reconstruct Mediterranean sea level fields from nonlinear PCA. Tide gauge data are used to compute temporal

amplitudes that are then combined with spatial patterns estimated from satellite altimetry data. The reconstruction can be obtained carrying out the following steps:

1. the function $f: \Re^p \to \Re$ is first estimated from tide gauge data. In Section 5.1.2 it was shown that f is a function that maps the original data onto a one-dimensional space. Applying f to tide gauge data will give the time series associated with the nonlinear mode 1. This time series will span the same period as tide gauge data.

2. the function $g: \Re \to \Re^p$ is estimated from altimetry data. As described in Section 5.1.2, g is a function that, given a time series (output of the bottleneck neuron), maps it back to the same space as the original data.

3. the last step is to apply function g, estimated in Step 2, to the time series computed in Step 1. This will give a reconstruction of the field covering the same spatial domain as altimetry data and spanning the same period as tide gauge data (1955-2000).

Results

The reconstruction is again compared with satellite altimetry observations for the period 1993-2000. The spatial distribution of the correlation between observed and reconstructed fields (Fig. 5.13) shows that the highest correlations are found in the Adriatic Sea (up to 0.8). The reconstruction performs poorly in the Ionian, where correlation is smaller than 0.2 at some points. In the other regions of the Mediterranean Sea, the reconstruction shows correlations of about 0.6. The distribution of sea level trends derived from the reconstruction (Fig. 5.14) is rather different from the one given by altimetry (Fig. 5.12a), with positive trends (up to 6 mm/yr) all over the basin.

The correlation between the reconstructed and observed basin MSL series is 0.8 and the root mean square difference between the two series is 0.7 cm. The MSL rise obtained from the reconstruction is 4.5±0.7 mm/yr for the period 1993-2000.
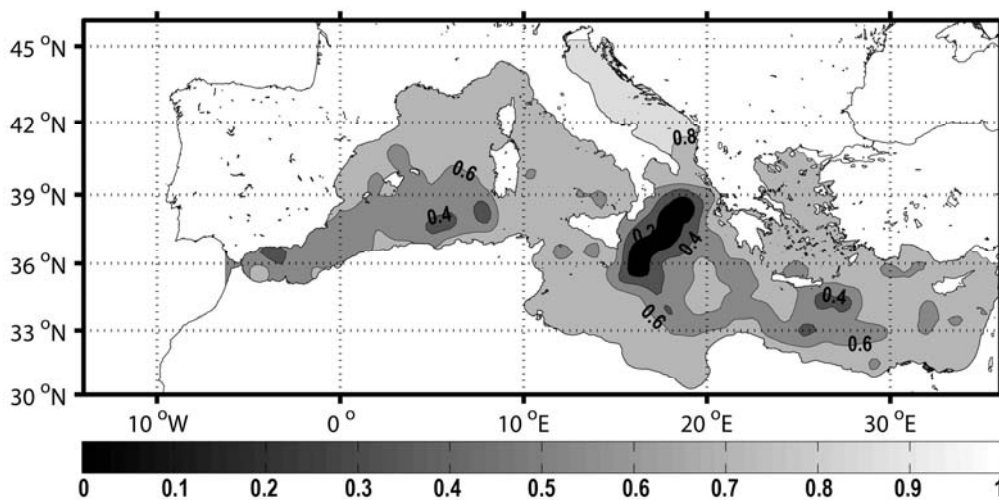
Figure 5.13. Correlation between the reconstructed sea level fields (using nonlinear PCA) and satellite altimeter observations over the period 1993-2000 (the contour interval is 0.2).
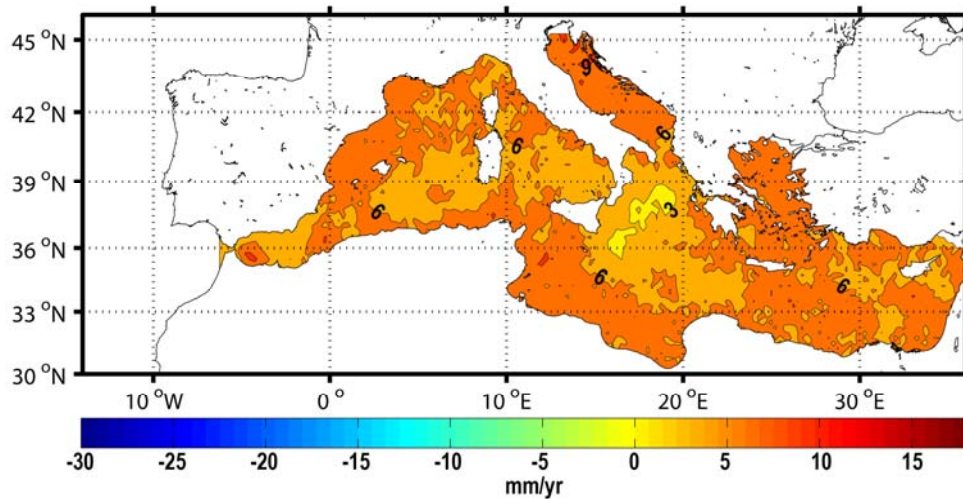
Figure 5.14. The distribution of sea level trends for the period 1993-2000 as estimated from the reconstructed fields, obtained using the nonlinear PCA (the contour interval is 3 mm/yr).

The MSL rise obtained for the reconstructed period 1955-2000 is 0.4 mm/yr. The distribution of sea level trends (not shown) shows again a very uniform pattern with positive trends all over the basin.

5.2.3 Summary and discussion

Mediterranean sea level fields have been reconstructed by means of two different techniques: standard PCA and nonlinear PCA. The primary objective was to determine whether the use of non-linear techniques is necessary in the case of reconstructing Mediterranean sea level. In order to validate the results, both reconstructions have been compared with observation from satellite altimetry data for the period 1993-2000. First we have looked at the correlations between the reconstructed and observed fields, finding that the reconstruction obtained by using standard PCA performs better than the nonlinear one, especially in the Ionian Sea, where linear PCA shows correlations larger than 0.5, as compared to correlations smaller than 0.2 given by the nonlinear PCA. The highest correlations given by the PCA are found in the Adriatic Sea and the northern sector of the Western Mediterranean (up to 0.8), while the smallest correlations are found to the south of Crete (0.3) and near the coast of Morocco (0.5). It is not surprising that the highest correlations are found in the Adriatic Sea since most tide gauges used in this analysis are located in that region. However, the fact that the nonlinear approach gives correlation of 0.8 only in such region indicates that this technique is quite sensitive to the location of the tide gauges. This is a serious handicap, since the spatial distribution of tide gauges in the Mediterranean Sea is rather heterogeneous.

With respect to the distribution of sea level trends, linear PCA reproduces the patterns observed in altimetry data, though the magnitude of the trends is rather different. The main features shown by altimetry observations are marked negative trends in the Ionian Sea (up to -20 mm/yr) and large positive trends in the Aegean Sea (up to 20 mm/yr). These features have already been reported by several authors

(Cazenave et al., 2002; Fenoglio-Marc, 2002; Larnicol et al., 2002) and they are described in detail in Chapters 8 and 9. Trends are positive almost everywhere else, with larger values in the Eastern Mediterranean (up to 15 mm/yr) than in the Western Mediterranean (nearly zero). The reconstruction obtained from linear PCA shows also negative trends in the Ionian Sea, but they are much smaller (up to -3 mm/yr). In the Aegean Sea the reconstruction also underestimates the trends (up to 6 mm/yr). In contrast, in the Western Mediterranean the linear reconstruction overestimates the trends, giving values of about 6 mm/yr. The distribution of sea level trends obtained from the reconstruction based on nonlinear PCA shows positive trends everywhere (up to 6 mm/yr), with a rather uniform spatial pattern that does not match the one obtained from altimetry observations.

Mediterranean MSL rise for the period 1993-2000 has also been estimated from both reconstructions. The correlation between the reconstructed and the observed MSL is 0.8 for both reconstructions. The MSL trend given by both reconstructions is 4.5 ± 0.7 mm/yr, while the one obtained from altimetry data is 3.9 ± 0.7 mm/yr.

Although the previous results rise serious doubts on the skill of the reconstruction methods, we have also computed the distribution of sea level trends for the whole reconstructed period 1955-2000. Both reconstructions show a uniform spatial pattern with positive trends everywhere in the basin, which might indicate that the approaches are not capable of recovering distinct regional features. The MSL rise for the period 1955-2000 given by both reconstructions is 0.4 mm/yr.

The results presented so far suggest, first, that the use of nonlinear techniques to study Mediterranean sea level variability is not more accurate than the standard linear PCA and does not necessarily lead to a better understanding of physical phenomena. Using standard PCA we have obtained equivalent results to nonlinear PCA and in the particular application of the reconstruction the linear results are even better than the ones obtained with nonlinear PCA. This is partly due to the fact that nonlinear PCA seems to be quite sensitive to the time series to which one applies the function g to map back to the space of the original data. Considering moreover that linear techniques are much simpler than nonlinear ones, the conclusion seems to point to standard PCA as the best choice to reduce the dimensionality of the original sea level data set.

The second major conclusion is that the reconstructions obtained following the simple approach described at the beginning of this section are not satisfactory. The tests against altimetry data show differences that are too large as to rely on the results obtained for the pre-altimetric period. The next task will be to carry out a more refined reconstruction of Mediterranean sea level fields following a much more sophisticated methodology (though still based on PCA as a first step): the reduced spaced optimal interpolation described by Kaplan et al. (1997, 1998, 2000).

Chapter 6

Reconstruction of Mediterranean sea level fields for the period 1945-2000 using a reduced-spaced optimal interpolation

IN[1] the previous chapter we set the basis of the reconstruction and carried out a first attempt using a simple technique. However, results were not satisfactory enough as to ensure the reliability of the key parameters that can be derived from the reconstruction (e.g., the regional distribution of long-term trends).

In this chapter we present a more sophisticated methodology to reconstruct sea level variability in the Mediterranean Sea: a reduced space optimal interpolation analysis proposed by Kaplan et al. (1997; 1998; 2000) and used by Church et al. (2004) to recover global scale sea level fields. The method intends to combine in an optimal way the benefits of the available long tide gauge series with the complete spatial coverage offered by satellite altimetry and it gives a theoretical estimate of the errors associated to the reconstructed field. The details of the data sets and of the methodology are presented in Sections 6.1 and 6.2, respectively. In Section 6.2 we also carry out some sensitivity sets to ensure the robustness of the reconstruction. Results are presented in Section 6.3 for two different periods: 1993-2000 and 1945-2000. For the period 1993-2000 the results are compared with observations from satellite altimetry, which allows testing the results over the whole domain, whereas for the period 1945-2000 the reconstruction can be validated only against tide gauges. As particularly valuable products we obtain the time evolution of Mediterranean MSL and its trend, as well as the spatial distribution of sea level trends for the period 1945-2000. A brief summary of the results and the main conclusions of the analysis are given in Section 6.4.

---

[1] This chapter is based on the paper:
Calafat, F. M., and D. Gomis (2009), Reconstruction of Mediterranean Sea level fields for the period 1945-2000, *Global Planet. Change*, *66*(3-4), 225-234.

6.1 Details on the specific data sets

6.1.1 The tide gauge data set

The tide gauge dataset used to carry out the reconstruction consists of monthly MSL series from the PSMSL as described in Chapter 3. The period of the reconstruction was determined as a trade-off between the length of the period and the number of tide gauges spanning it. A reasonable choice was the period from January 1945 to December 2000. Tide gauge records with large gaps were discarded and also the tide gauge located in Malaga was discarded because of its unrealistically large trend (8 mm/yr over the period 1965-2000). All nearby stations have correlation larger than 0.7 and trend differences smaller than 1 mm/yr. We broke the period of the reconstruction 1945-2000 into 6 smaller periods and selected tide gauges with useful data for each period. This left a total of 3 tide gauges for the period 1945-1954, 6 for the period 1955-1964, 8 for the period 1965-1974, 10 for the period 1975-1984, 11 for the period 1985-1994 and 12 for the last 6 years. Gaps of 1-2 months were filled by using splines; gaps larger than 2 months were filled by means of a multiple linear regression using nearby records. The distribution of tide gauges over the selected domain is not uniform: most of them are located at the northern Mediterranean shores, whereas we barely find a single tide gauge along the African Coast (Fig. 6.1). This can be a serious handicap to resolve local events taking place close to the southern shores.

Prior to any computation the mean seasonal cycle was removed from tide gauge records by means of a harmonic analysis. Because the annual cycle is not constant in time (see Marcos and Tsimplis, 2007b) a common period (1975-2000) was selected to compute the annual cycle of most tide gauge records. The time variability of the annual amplitude of each tide gauge record has been computed by Marcos et al. (2007b) and range from 0.26 to 0.69 cm (for amplitudes ranging from 3.15 to 8.90 cm).

Finally, since the reconstruction method minimizes for changes in sea level, the reference frame of tide gauge data is not relevant. However, when recovering sea level, changes are integrated backward in time and then a reference frame is to be defined for the reconstruction. We set the reconstruction to be in the same reference frame as the altimeter data.

6.1.2 The satellite altimetry data set

For the reasons pointed out in Chapter 3, the satellite altimetry data set used for the reconstruction is the non-specific Mediterranean data set, with the atmospheric component added back to sea level anomalies. The mean seasonal cycle was removed from satellite altimeter data by means of a harmonic analysis. A Mediterranean MSL trend was also removed, not because it is spurious or unreliable, but in order to make the EOF representation more effective and unbiased (see Kaplan et al., 1997). Obviously this does not prevent the reconstruction from having a trend: the EOFs only give the dominant spatial pattern of sea level variability; the time variability is obtained when projecting the tide gauge records onto the spatial EOFs, so that if those records have a trend, this will be projected onto the reconstruction.
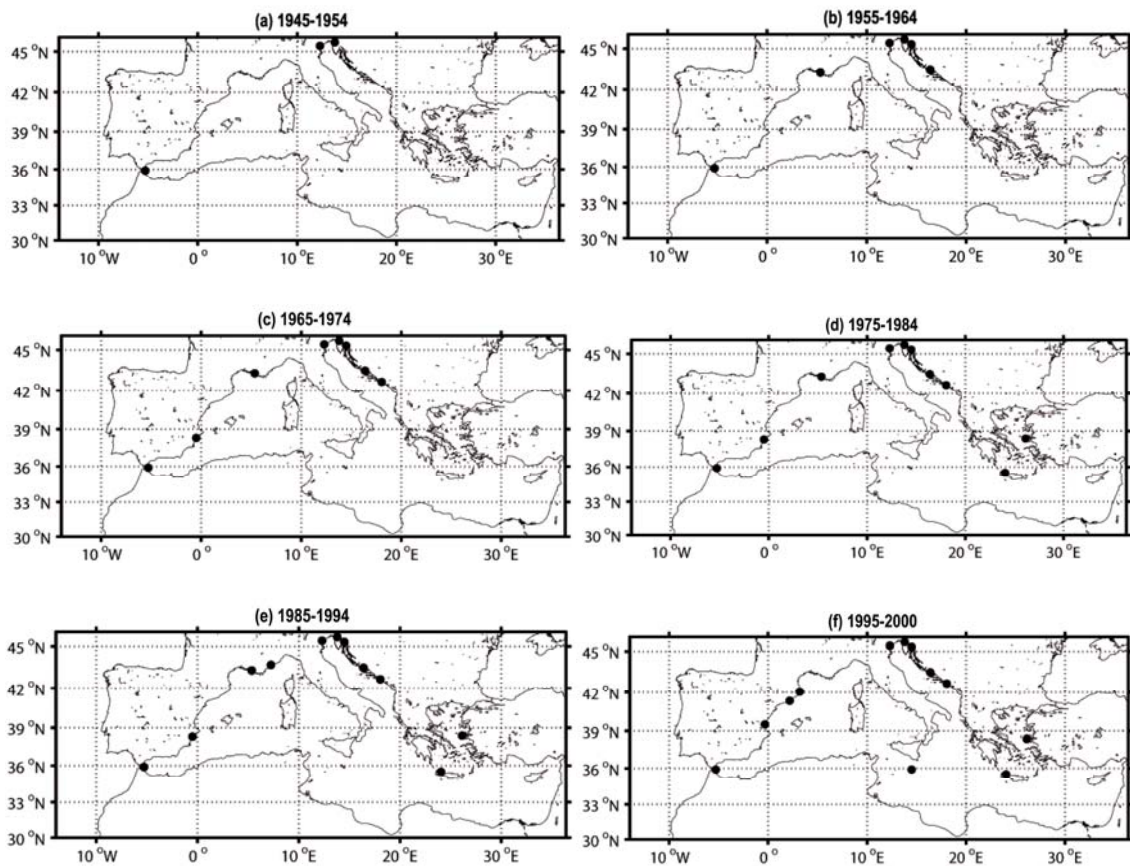
Figure 6.1. The distribution of tide gauges for different periods of the reconstruction: (a) 1945-54, (b) 1955-64, (c) 1965-74, (d) 1975-84, (e) 1985-1994, and (f) 1995-2000.

6.1.3 Comparison between both data sets

A key assumption of the methodology is that altimetry and tide gauge data are different spatial samplings of the same field. Before starting with the analysis we wanted to compare tide gauge records with the altimetry time series at the closest grid point. For the tide gauges located in Dubrovnik and Split, for instance, the distances to the nearest altimetry point are 47 and 13 km, respectively. The correlation and relative RMSE (RMS differences divided by the standard deviation of the series) between tide gauge records and the corresponding altimetry series are 0.81 and 0.61 for Dubrovnik and 0.89 and 0.47 for Split. Therefore, although altimetry and tide gauges measure in principle the same signal, there are some differences. These figures must be kept in mind when evaluating the skill of the reconstructing technique.

6.2 Methodology

In this subsection we present the technical aspects of the reduced optimal interpolation that we use to reconstruct sea level, as well as some assumptions that must be done regarding some of the parameters that are involved in the methodology.

6.2.1 Reduced-space optimal interpolation

In the previous chapter it was shown that nonlinear PCA was not superior to the standard linear PCA for the obtention of the modes that explain Mediterranean sea level variance. Hence, for this second reconstruction attempt the modes will be only constituted by linear spatial EOFs and temporal amplitudes. An interesting property of PCA is that the lower-order modes contain the largest spatial structures, and therefore it can be used to filter small spatial structures that are significantly affected by noise and that can hardly be resolved with the tide gauge distribution. This can be achieved by truncating the number of modes to a smaller number such that it still captures most of the signal.

For the reconstruction we use the reduced space optimal interpolation described by Kaplan et al. (1997, 1998, 2000) and used by Church et al. (2004) to recover global sea level. This method combines feature extraction and least squares optimal estimation, and provides theoretical error estimates for analyzed values. As in Church et al. (2004), we minimize for changes in sea level between subsequent time steps and then integrate over time to obtain sea level, in order to avoid the problem of locating all stations in a single, consistent vertical reference frame. This approach is an extension of the technique used by Smith et al. (1998) and Chambers et al. (2002).

The first step of the method (feature extraction) involves computing the spatial EOFs from satellite altimeter data. Unlike in the previous chapter and to strictly follow the methodology of Church et al. (2004), here we removed the spatial MSL for each time step prior to the EOF computation. The advantage of this procedure is that it avoids pouring spatially uniform sea level changes into different EOFs. The disadvantage is that a spatially-constant EOF (named as EOF0 in Church et al., 2004) has to be added to those obtained from the EOF analysis in order to account for spatially uniform sea level changes. A test carried out without removing the spatial mean (and hence without adding the EOF0) resulted in a different modal distribution of the variability, but in practically the same reconstruction. This is due to the fact that in the Mediterranean basin the EOF1 computed as in the previous chapter has the same sign all over the basin (Fig. 5.2a) and, therefore, it plays the role of an EOF0. In the case of a global reconstruction (Church et al., 2004), adding an EOF0 is more determinant than in the case of the Mediterranean Sea, due to the fact that the global EOF1 does not have the same sign everywhere in the ocean.

The longer the period used to estimate covariance patterns the more faithful the reconstruction will be. Here we use 13 years of altimetry data spanning from January 1993 to December 2005. In order to obtain the EOFs we construct an *mxn* matrix *Z* containing the satellite altimeter data, where *m* is the number of spatial grid points (5022) and *n* is the number of months (156). The matrix Z can be separated into three matrices by using a singular value decomposition (Preisendorfer, 1988):

$$Z = ULV^T \tag{6.1}$$

where *U* is an *mxn* matrix whose columns are the EOFs, *V* is an *nxn* matrix whose columns are the orthogonal time series (the amplitudes) of the modes, and *L* is an *nxn* diagonal matrix whose elements are the square root of the eigenvalues of the spatial covariance matrix. This is, the columns of *U* are functions of space only and the amplitudes of *V* are functions of time only. The EOF expansion of the dataset can be truncated to a smaller subset by including only the lowest *M* EOFs:

$$Z_M(x, y, t) = U_M(x, y) \cdot L_M \cdot V_M^T(t) \tag{6.2}$$

where subindex "M" indicates matrices that only contain the lowest M modes. Expression (6.2) can be rewritten as:

$$Z_M(x, y, t) = U_M(x, y) \cdot \alpha(t) \tag{6.3}$$

where $\alpha(t) = L_M \cdot V_M^T(t)$ is an Mxn matrix whose rows are the time series of the amplitudes of the lowest M EOFs.

The second step of the method is the optimal interpolation described by Kaplan et al. (2000). The reduced space optimal interpolation solution for $\alpha(t)$ is the one minimizing (for each time step) the cost function

$$S(\alpha) = (HU_M\alpha - Z^o)^T R^{-1}(HU_M\alpha - Z^o) + \alpha^T \Lambda^{-1}\alpha \tag{6.4}$$

where Z^o is a matrix of available tide gauge observations, H is a sampling operator equal to 1 where and when tide gauge data are available and 0 otherwise, and Λ is a diagonal matrix which contains the M largest eigenvalues of the covariance matrix. R is the error covariance matrix and consists of two terms:

$$R = \Sigma + HU'\Lambda'U'^T H^T \tag{6.5}$$

The term Σ is the data error covariance matrix accounting for the instrumental error. We assumed spatially uncorrelated errors of the order of 20 mm. This implies that $\Sigma = \sigma\, I$, where I is the identity matrix and σ is the observational error variance. The second term in R contains the covariance of the truncated modes; it accounts for the errors introduced by ignoring higher-order EOFs in the reconstruction (the prime indicates matrices of the omitted EOFs and eigenvalues).

The second term on the right-hand side of the cost function (6.4) can be written as:

$$\alpha^T \Lambda^{-1}\alpha = \sum_{i=1}^{M} \frac{\alpha_i^2}{\lambda_i} \tag{6.6}$$

Thus the second term of the cost function (6.4) is a constraint on the EOF spectrum of the solution. It prevents the solution from giving too much energy to the features described by higher modes: the higher the mode, the smaller is the associated eigenvalue λ_i and therefore the more severe is the punishment for deviations of its amplitude from zero. If this term is not used, the reconstruction can bring too much variance to grid points with no nearby observations, particularly when a large number of EOFs are used. In our case, a reconstruction obtained without using this term showed exaggerated variance in areas with no tide gauge data, a feature that was corrected when adding the term. In the simpler approach used by Smith et al. (1998) and by Chambers (2002) this term is omitted and matrix R is simply the identity matrix.

Since tide gauge measurements are all made relative to their own local datum, we will solve for changes in sea level between adjacent time steps. Following Church et al. (2004), for adjacent times t_n and t_{n+1}, (6.3) can be written as

$$\Delta Z_M = U_M(x, y)(\alpha(t_{n+1}) - \alpha(t_n)) = U_M(x, y)\Delta\alpha(tn) \tag{6.7}$$

Because of the first term in the cost function (6.4), the minimization of S will constrain the solution to be close to the observations. The second term confines the distribution of energy over the modes of variability to that found in the data. Thus, the change in the amplitudes of the leading EOFs between each time step can be estimated by minimizing the cost function (6.4). The solution is

$$\Delta\alpha = PU_M^T H^T R^{-1} \Delta Z^o \tag{6.8}$$

where $\Delta Z^o = Z^o(x, y, t_{n+1}) - Z^o(x, y, t_n)$, and $P = \left(U_M^T H^T R^{-1} H U_M + \Lambda^{-1}\right)^{-1}$ is a theoretical estimate for the error covariance of the solution.

Once the change in the amplitudes has been obtained for each time step, the amplitudes themselves can be recovered by integrating backward in time. This approach introduces an arbitrary constant for each EOF amplitude. Since we have split the period of reconstruction into 6 smaller periods, we have to fix a constant for each one of these periods. For the periods overlapping totally or partially the period covered by altimetry, the average amplitude of each EOF is set equal to the average amplitude of the corresponding EOF of the altimeter data over the common period. For the other periods, we have computed another reconstruction spanning the period 1955-2000 by using only tide gauges covering the whole period, then the average amplitude of each EOF is set equal to the average amplitude of the corresponding EOF of this reconstruction over the common period. Since matrix Z^o contains the tide gauge observations of the period 1945-2000, the amplitudes obtained by minimizing the cost function (6.4) will also span this period. Finally, the whole reconstruction of sea level is obtained by substituting the estimated amplitudes $\alpha(t)$ in (6.3).

6.2.2 Assumptions, error sources, and EOFs used in the analysis

The approach used to recover sea level fields assumes that EOFs are reasonably stationary in time, i.e., that the dominant modes of the period 1993-2005 are not very different from the dominant modes of the period 1945-2000. In this work the covariance pattern is estimated using 13 years of satellite altimeter data; that is slightly more than the 12 years of altimeter data used by Church and White (2006) to estimate global sea level and the 12 years of SST data used by Smith et al. (1998) to estimate surface temperature variations in the tropical Pacific. The 13 years of satellite data should give a reasonably accurate estimate of covariance patterns, but do not truly ensure the stability of the EOFs. In next subsection we carry out an empirical test consisting of the computation of EOFs for different subperiods of the altimetric period and comparing the reconstructions that result for each EOF set. In any case it is worth stating that because the minimization of the cost function (6.4) constrains the solution to be close to observations, even if the EOFs are not fully stationary, the analysis could reconstruct sea level successfully at the expense of the amplitudes losing their physical meaning.

The distribution of tide gauges within the domain is another crucial issue and probably the main error source. Optimal interpolation naturally accounts for irregular distribution, giving less relative weights to redundant stations (in mathematical terms, stations that are highly correlated among them). However, the method will never be able to recover the signal in regions where sea level is not correlated with any tide gauge station. Both the effect of assuming the stationarity of EOFs and the impact of the tide gauge distribution are investigated in next subsection.

Regarding the distribution of the field variance into the leading modes, the EOF0 (not shown) explains 58% of the variance. As stated above, it is set strictly constant over the whole domain and therefore it only accounts for changes in MSL. EOF1 explains 10% of the variance. It has a dipole structure, changing sign between the Western and Eastern basins of the Mediterranean Sea; maximum (opposite) values are reached in the Ionian Sea and in the Aegean Sea (Fig. 6.2a). EOF2 explains 4% of the variance and has a more complex structure; the Ionian and Aegean Sea appear now in phase and in opposite phase to the Algerian basin (Fig. 6.2b). EOF 3 (not shown) only explains 2.5% of the variance.
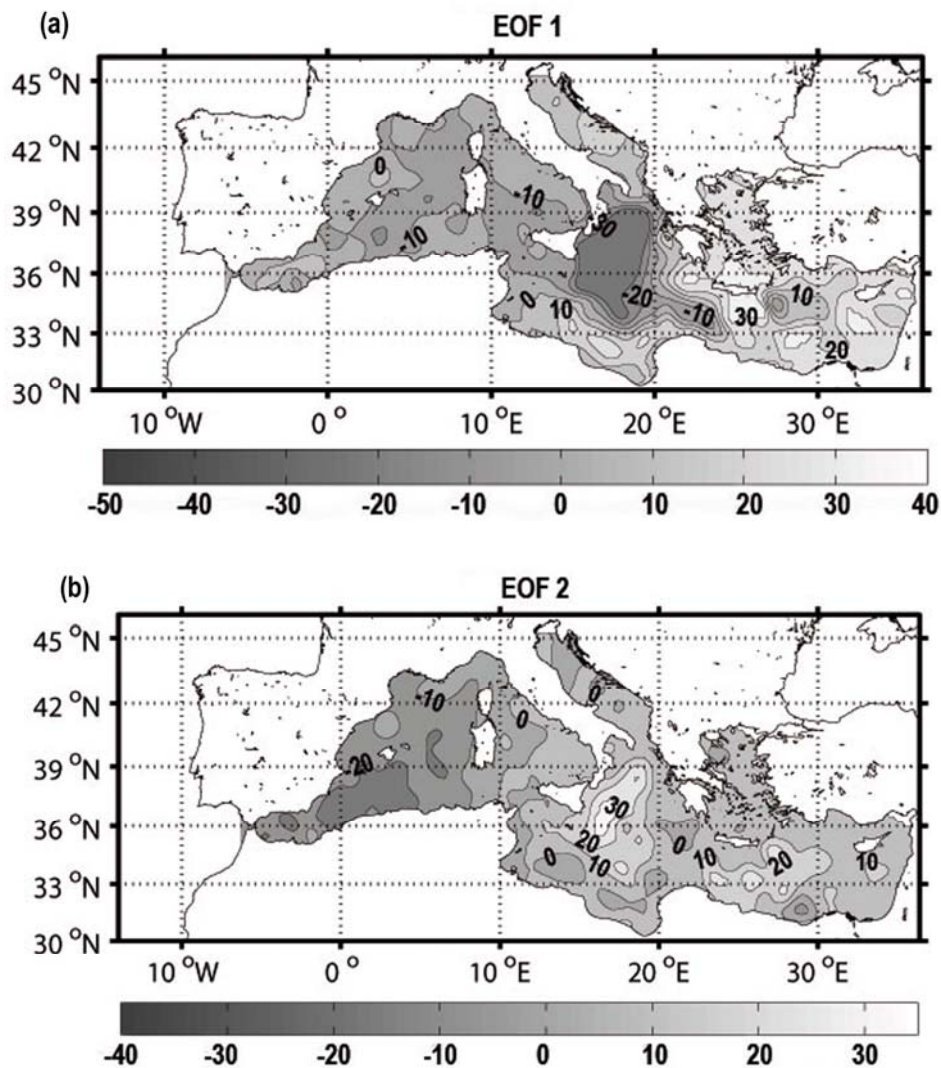
Figure 6.2. The two leading EOFs of the altimetry data set (1993-2005) obtained after the removal of the seasonal cycle, a linear mean trend and a spatial mean: (a) EOF 1, (b) EOF 2.

Following Church et al. (2004), we test the effect of increasing the number of EOFs by quantifying the reduction of the residual variance in terms of the reduction in the degrees of freedom. First, only the lowest mode is considered; when adding a second mode, the reduction of the residual tide gauge variance is of 48 mm^2 per degree of freedom. When adding a third mode the reduction is of 20 mm^2 per degree of freedom, and when adding a fourth mode it is only 9 mm^2 per degree of freedom. Additionally, the distribution of sea level trends resulting from the use of 1, 2, 3, 4 and 5 EOFs have been compared with altimetry trends for a common period (1993-2000). All results suggest that for the application of the optimal interpolation method, using 3 EOFs is the best option, in order to avoid overfitting while reducing the residual variance.

6.2.3 Sensitivity study

In order to investigate the effect of assuming that EOF modes are reasonably stationary in time, we obtained two different reconstructions: one using EOFs computed from the period 1993-1998 and another one using EOFs computed from the period 1999-2005. The cut in 1999 coincides with a clear change in the Eastern Mediterranean dynamics and sea level trend (see Vigo et al., 2005), in an attempt to obtain EOFs corresponding to different regimes. Figure 6.3 shows the leading EOFs corresponding to each case; they are similar but not exactly the same. The correlations between the observed and reconstructed fields for the period 1993-2000 are similar for both reconstructions; average values of 0.73 and 0.72 are obtained when using EOFs from 1993-1998 and from 1999-2005, respectively. The rate of MSL rise for the period 1945-2000 is 0.6 ± 0.1 mm/yr for both reconstructions. We have also computed the distribution of sea level trends obtained from the two reconstructions for the period 1993-2000 (Fig. 6.4): both are very similar to the distribution of sea level trends obtained from altimetry for the same period (Fig. 5.12a). These results suggest either that the assumption of stationarity is reasonable at least for the leading EOFs, or that the changes in time of the leading EOFs do not critically affect the reconstruction.
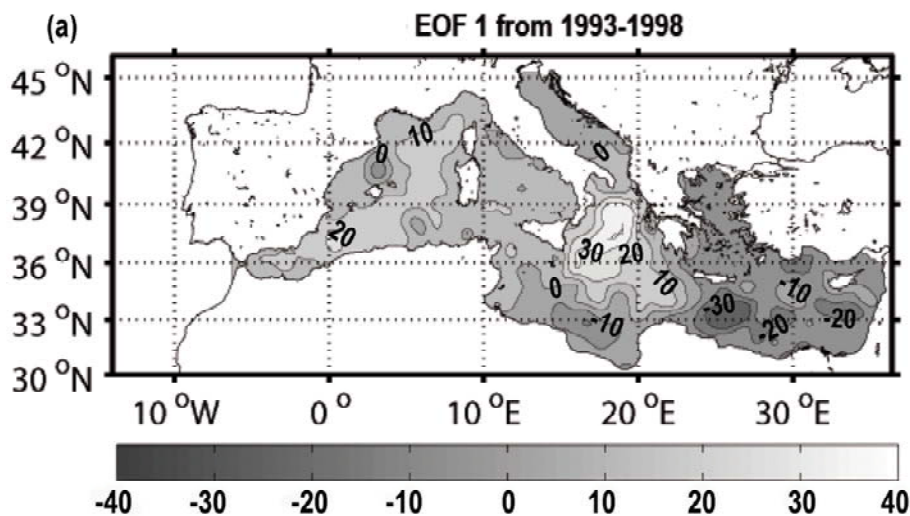
Figure 6.3 (continue in next page)
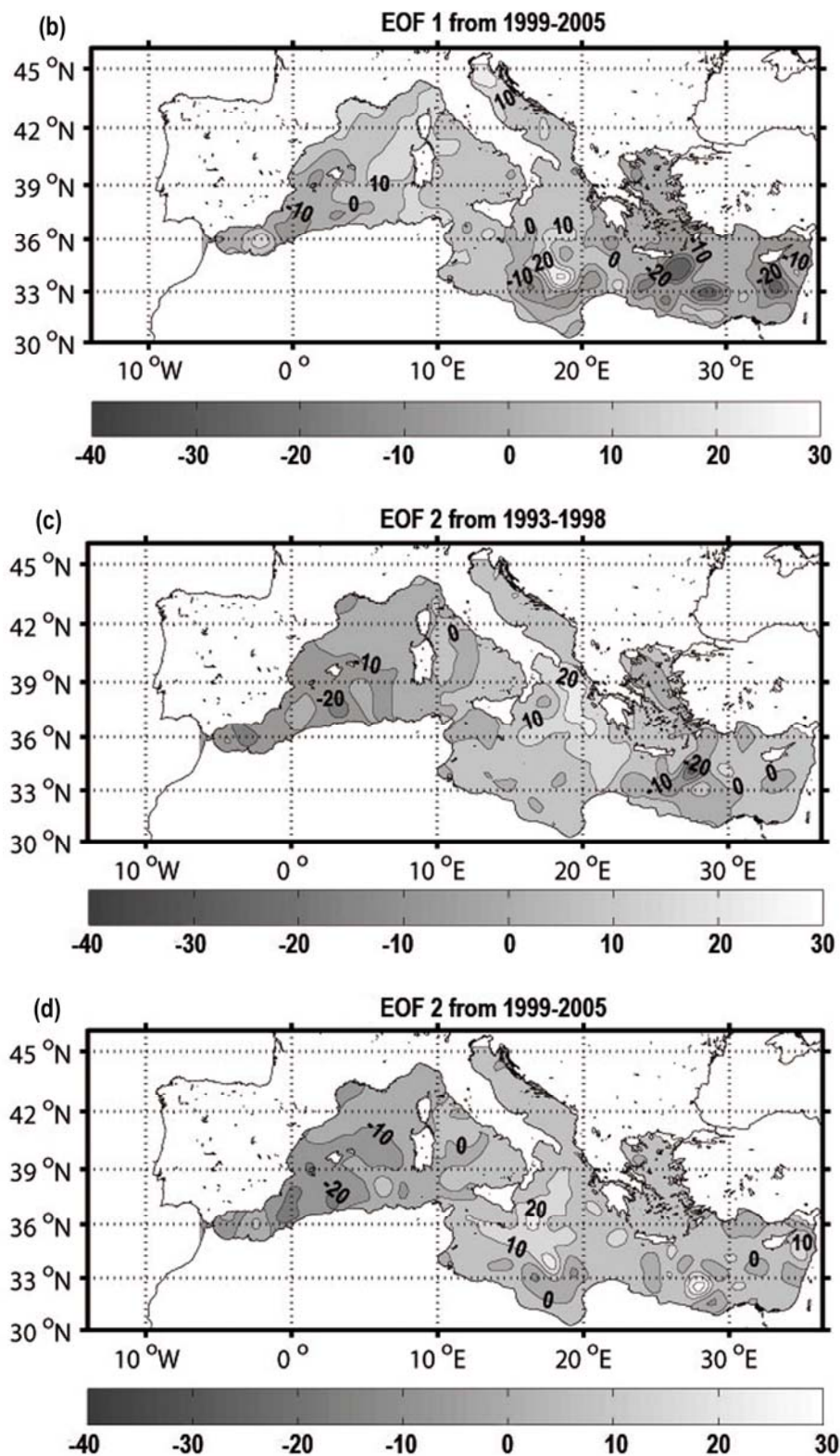
Figure 6.3. The two leading EOFs of satellite altimeter data obtained for two different subperiods: (a) EOF 1 for 1993-1998; (b) EOF 1 for 1999-2005; (c) EOF 2 for 1993-1998; and (d) EOF 2 for 1999-2005.
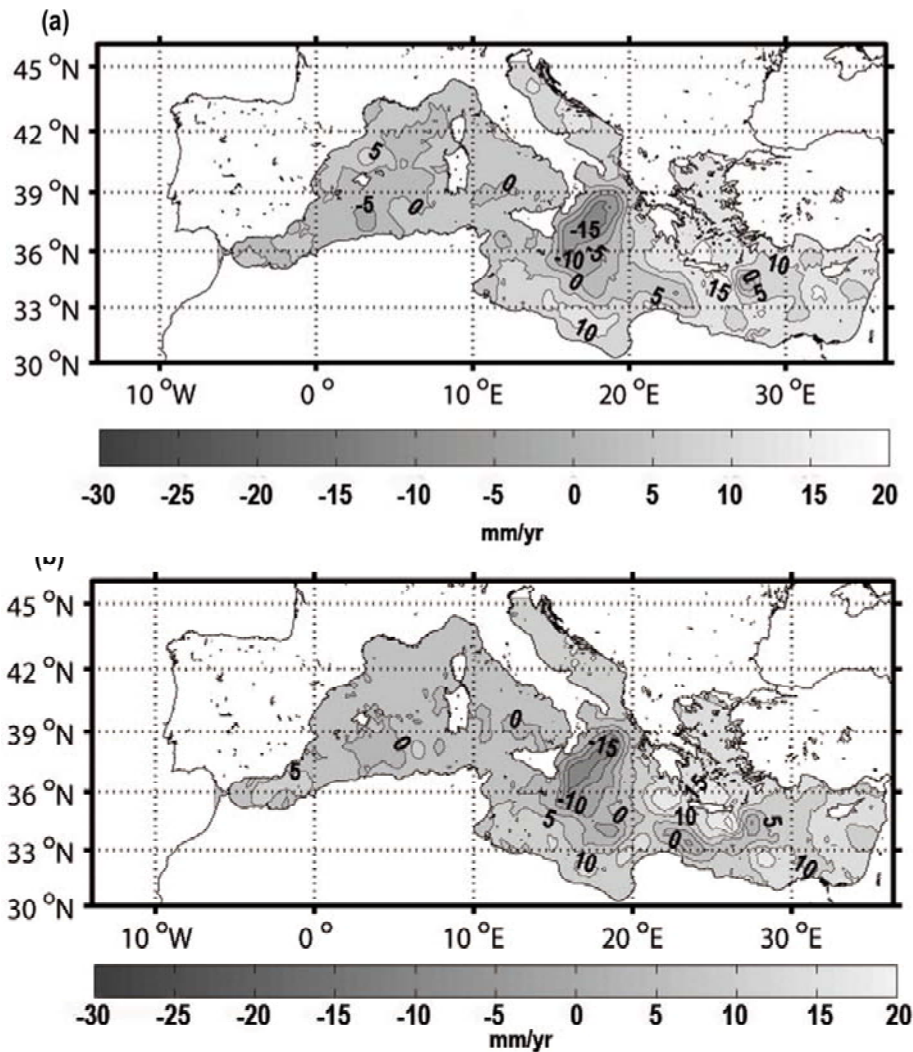
Figure 6.4. The distribution of sea level trends for the period 1993-2000 estimated from two different reconstructions: (a) from the EOFs obtained for the period 1993-1998; (b) from the EOFs obtained for the period 1999-2005. The contour interval is 5 mm/yr.

One of the strengths of optimal interpolation is that it provides statistical error estimates for the interpolated fields. These estimates are computed under some ideal conditions (e.g., that the correlation model reflects true correlations) and they are therefore considered as a lower boundary. Hence, we can use now the results obtained above to ensure that the errors estimated by the method are a realistic measure at least of the order of magnitude of the uncertainty of the reconstruction. We have used the reconstruction obtained from the EOFs computed for the period 1999-2005 to compute the Mediterranean MSL and we have compared the result with the MSL obtained from satellite altimetry data. The root mean square (rms) difference between the reconstructed and the measured Mediterranean MSL is 1.5 cm, similar to the largest errors (1.3 cm) given by the optimal interpolation method.

To test the effect of the distribution and the number of tide gauges entering the computations, reconstructions obtained using different distributions of tide gauges are compared. Namely, we reconstructed sea level fields using only tide gauges from the

Adriatic Sea, using all tide gauges except the ones located in the Adriatic Sea and using all tide gauge records available (see Section 6.1). The averaged correlation between satellite altimeter observations and the reconstructed fields for the 1993-2000 period is 0.70 when using only tide gauges from the Adriatic Sea, 0.72 when using all tide gauges except the ones from the Adriatic and 0.80 when using all tide gauges available. The rates of MSL rise obtained for the period 1945-2000 are 0.6±0.2 mm/yr, 0.5±0.2 mm/yr and 0.7±0.2 mm/yr, respectively. Again, the results are similar and, therefore, the reconstruction does not appear to be very sensitive to the number or distribution of tide gauges used in terms of correlations and rate of MSL.

The above results do not imply that additional tide gauge records would not improve the reconstruction; the correlations shown in Figure 6.5 (see next section) are clearly lower in the southern Mediterranean shores due to the absence of tide gauge records. What results suggest is that of the whole set of available tide gauges, a reasonable subset appears to do a similar job than using the whole set.

6.3 Results

In this section we present the results obtained from the reconstruction for two different periods. First we compare the results from the reconstruction to the observations from satellite altimetry data for the period 1993-2000. Next we show the results for the period 1945-2000 and we check the reconstruction at some independent tide gauge locations.

6.3.1 Reconstruction for the period 1993-2000

The only way to test the goodness of the reconstruction over the whole domain is to compare the observed and reconstructed fields for the period 1993-2000, since this is the period spanned by satellite altimeter data. As already stated in the previous chapter, this is not an independent test due to the fact that EOFs were estimated from satellite altimeter data, but it will be useful to validate important aspects of the results. This test complements the more independent validation carried out in Section 6.2, where the altimeter data set was broken into 2 periods and the validation was carried out for the whole period all over the domain.

The spatial distribution of the correlation between the observed and reconstructed fields (Fig. 6.5a) shows correlations close to 0.9 in the north-western region of the Mediterranean Sea, the Adriatic Sea and in the Gulfs of Gabes and Sirte. In the Ionian and Aegean Sea and near the coast of Morocco the correlation is smaller but still larger than 0.7 in most areas. The spatial mean of the correlation is 0.8. As expected, the reconstruction cannot recover the altimetric signal (the 'true' field in the test) in regions of high mesoscale activity such as the Algerian basin. Tsimplis et al. (2008) showed that Algerian mesoscale eddies are poorly correlated with sea level of nearby regions, which explains why their variability can hardly be reconstructed from discrete coastal data. A map of the percentage of variance explained (Fig. 6.5b) shows that the highest percentage is achieved in the same regions where correlation is high. The percentage of variance explained is above 60% in these region, and larger than 40% in all regions.

Also the distribution of sea level trends derived from the reconstruction (Fig. 6.6) can be compared with the trends estimated directly from satellite altimeter data (Fig. 5.12a). The reconstructed and observed trends are very similar, showing positive values

above 10 mm/yr in the Eastern Mediterranean and smaller rates (less than 5 mm/yr) in the Western Mediterranean. The reconstruction also reproduces the marked negative trend of more than -15 mm/yr observed in the Ionian Sea. The major features observed in the sea level trends for the period 1993-2000 are consequence of the circulation changes that occurred in the Eastern Mediterranean after 1987 (the EMT) and they are described in detail in Chapters 8 and 9.

MSL was also computed for both, the reconstruction and altimetry values, obtaining very similar results (Fig. 6.7). The correlation between the reconstructed and observed MSL time series is 0.9 and the root mean square difference between the two series is 0.5 cm. The error bars of Figure 6.7 are obtained from the error distribution produced by the optimal interpolation method. The method gives an estimate for the statistical error covariance matrix of the interpolated values; the diagonal of that matrix is the variance of interpolation errors at each point of the output grid. The error bars of MSL have been obtained simply as the average of the standard deviation of the interpolation errors at each grid point.
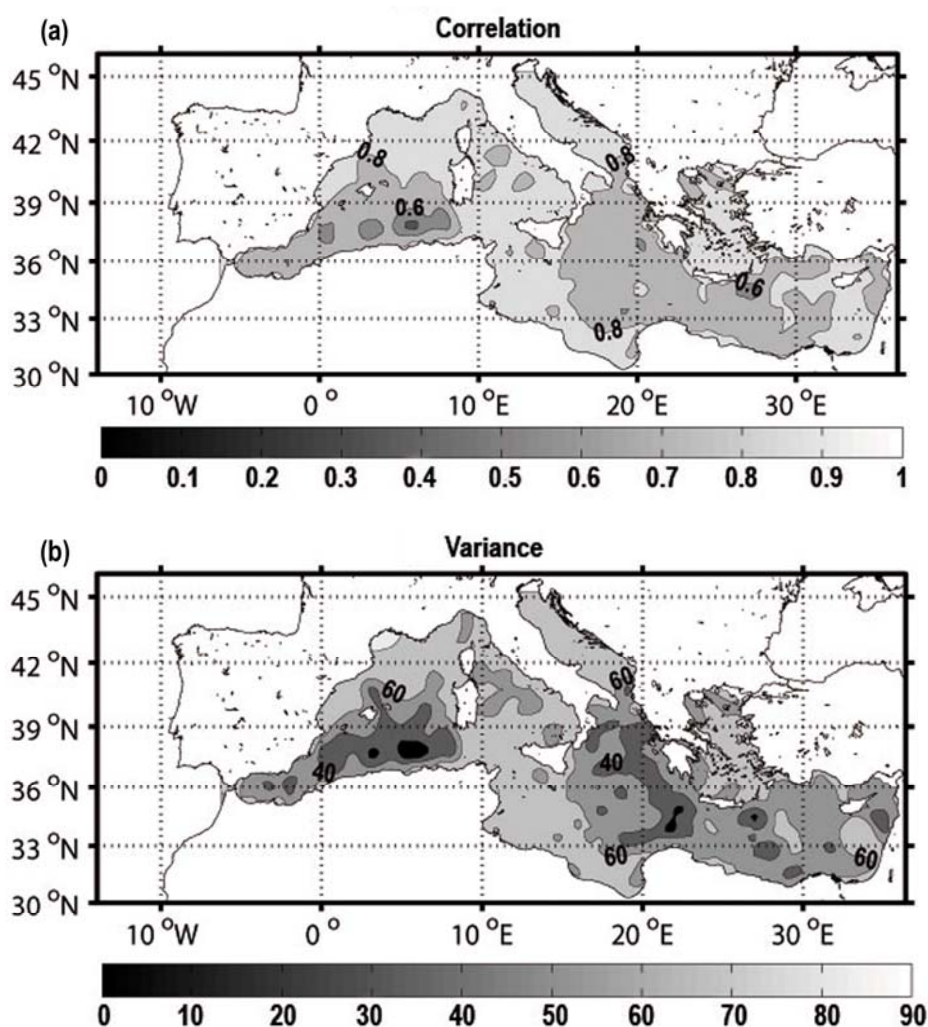
Figure 6.5. (a) Correlation between the reconstructed sea level fields and satellite altimeter data over the period 1993-2000 (the contour interval is 0.2). (b) Percentage of the altimetry variance explained by the reconstruction over the same period (the contour interval is 20%).
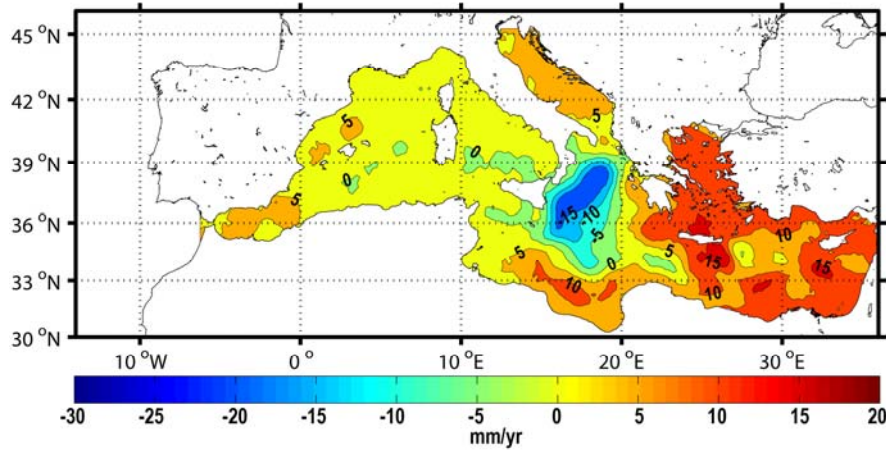
Figure 6.6. The distribution of sea level trends for the period 1993-2000 as estimated from the reconstructed fields, obtained using EOFs computed for the whole altimetric period (1993-2005). The contour interval is 5 mm/yr.

The MSL rise for the period 1993-2000 is 3,5±0.7 mm/yr when computed from the reconstructed fields and 3.9±0.7 mm/yr when derived from satellite altimeter data. The uncertainty of the trends is estimated by means of the robust bootstrap method described in Chapter 3. The errors associated with the reconstruction obtained from the interpolation analysis have been taken into account in the trend analysis by using the MM-estimator, also presented in Chapter 3. The error bars of MSL are of the order of 1.1 cm (see Fig. 6.7), while for altimetry data we have considered error zero. The fact that the uncertainties obtained for the reconstruction and for altimetry (±0.6 mm/yr) are equal indicates that the errors inherent to the reconstruction have a small impact on the computed trends (i.e., the main source of uncertainty comes from the length and variability of the series).
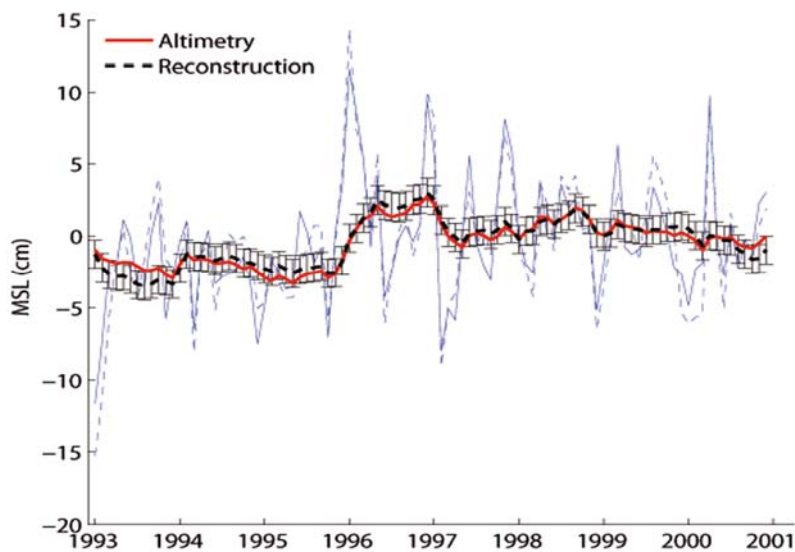
Figure 6.7. MSL for the period 1993-2000 estimated from the reconstructed fields (dashed lines) and from satellite altimeter data (solid lines). Thin lines correspond to the original monthly data; thick lines are one year moving averages of the thin lines.

A last comparison is with the reconstruction obtained using the simple substitution approach described in Section 5.2.1. When that approach is applied retaining the first 2 EOFs, the resulting rate of MSL rise is 4.5±0.7 mm/yr (where the bootstrap method has been applied without considering the uncertainty of the series). The averaged correlation between this reconstruction and altimetry data is 0.75. Both results indicate that optimal interpolation is more accurate than the substitution approach.

6.3.2 Reconstruction for the period 1945-2000

The only way to validate the reconstruction beyond the period covered by satellite altimetry is checking it at tide gauge locations. To do it, we used tide gauge records that did not enter the computations because of their large amount of data voids and that can therefore be used as fully independent test sites. The tide gauges of Rovinj, in the Adriatic Sea, and Alexandria, in the northern coast of Africa, were selected for the test. The time periods used for each record were 1974-1990 and 1960-1976, respectively.

Figure 6.8 show the observed and reconstructed sea level at the two selected locations. Correlations are 0.85 and 0.70, respectively, and the percentages of variance explained by the reconstruction are 85% and 50%. The reason why the highest correlation and explained variance are obtained at Rovinj must be attributed to the fact that several tide gauges located in the Adriatic Sea were used for the reconstruction, while none was used in the southern shores of the Mediterranean Sea. These values are comparable to those obtained for the altimetric period, which suggests that the reconstruction is fairly stable for the pre-altimetric period and hence that the open-sea correlations shown in Figure 6.5a can be expected to be valid for the whole period.

The regional distribution of sea level trends for the period 1945-2000 is shown in Figure 6.9. The main features are the maximum positive rate in the Ionian Sea (up to 1.2 mm/yr) and the nearly zero trends in the Aegean Sea, with a negative peak of -0.5 mm/yr to the south-east of Crete. In general we find small positive trends in the Western Mediterranean (between 0.5 and 1 mm/yr) and even smaller trends in the Eastern Mediterranean, especially in the Aegean Sea (between 0 and 0.5 mm/yr).
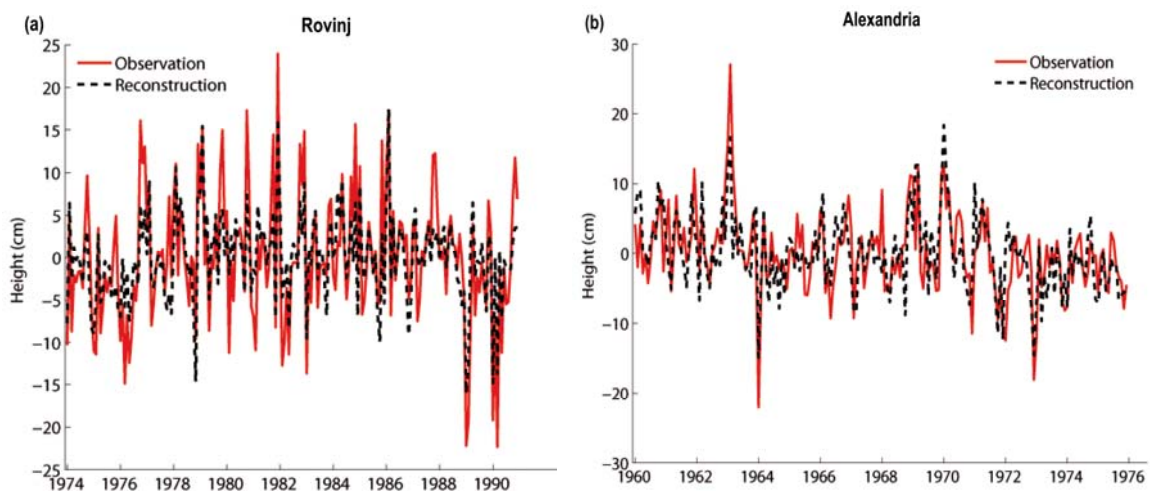
Figure 6.8. Comparison between reconstructed fields and tide gauge observations at (a) Rovinj; (b) Alexandria.

The time evolution of MSL is presented in Figure 6.10. It clearly shows the three different periods outlined by Tsimplis et al. (2005): marked positive trends before 1960 and after 1994 and an intermediate period with negligible or negative trends. For the whole period the MSL rise is 0.6±0.1 mm/yr.

As for the altimetric period, we also reconstructed sea level fields by using the simpler, substitution approach (Section 5.2.1) for the period 1945-2000. Results give a trend of 0.6±0.2 mm/yr for MSL, that is, exactly the same as for the optimal approach. We also computed the rate of regional averaged sea level rise for different values of tide gauge errors but results showed little or no difference with respect to the values given above.
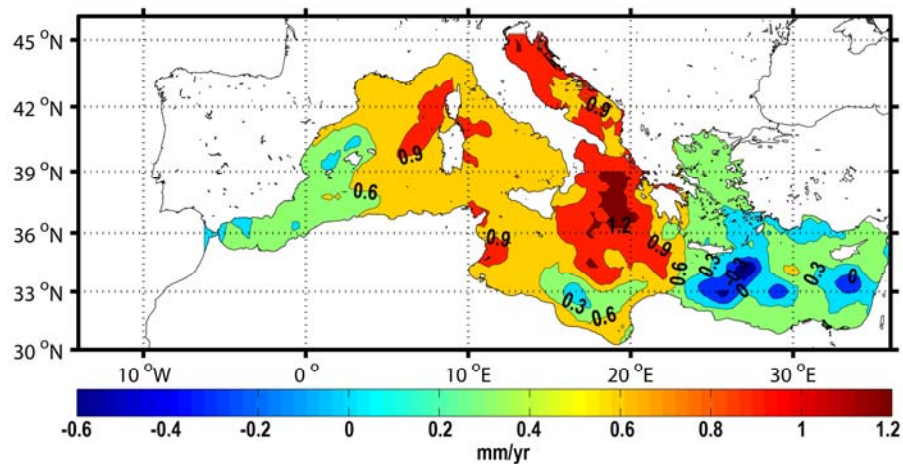
Figure 6.9. Distribution of sea level trends estimated for the whole reconstructed period 1945-2000. The contour interval is 0.3 mm/yr.
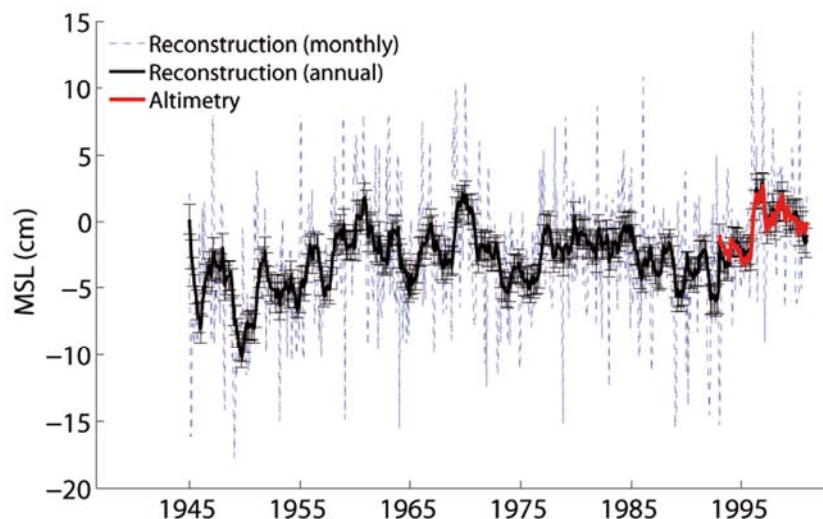
Figure 6.10. MSL for the whole reconstructed period 1945-2000. The dashed line corresponds to original monthly data; the thick lines is a one year moving average of the thin line. The red line is the MSL computed from the altimeter data set for the period 1993-2000.

6.4 Summary and conclusions

The reduced space optimal interpolation approach described by Kaplan et al. (1997, 1998, 2000) and used by Church et al. (2004) to reconstruct global MSL has been successfully used to reconstruct the distribution of sea level in the Mediterranean Sea for the period 1945-2000. The much simpler technique presented in Section 5.2 has been used to compare results.

The robustness of the reconstruction has been checked by means of several tests. A crucial assumption is that EOFs computed for the period 1993-2005 are also representative for the whole period 1945-2000. We have tested the validity of that assumption by computing EOFs for the periods 1993-1998 and 1999-2005 and then obtaining the reconstruction for both sets. Results are quite similar, though further tests should be carried out as soon as new altimetric data are available. The sensitivity of the reconstruction to the number and distribution of tide gauges has also been tested. Results do not appear to be very sensitive to reasonable modifications in the tide gauge sites. However, in the regions where there are no tide gauges (i.e., Aegean Sea and southern Mediterranean) only the large scale structures can be expected to be recovered. Other complementary tests carried out, such as the sensitivity of the reconstruction to tide gauge errors, showed little impact on the results.

To quantify the goodness of the reconstruction over the whole domain we have compared the reconstructed fields with satellite altimeter observations for the period 1993-2000. For this period, reconstructed and observed results are remarkably similar. The spatially averaged correlation between the reconstructed and observed fields is 0.80 when using the optimal choice of parameters. The basin MSL rise for this period is 3.5±0.7 mm/yr, which agrees with the rate of 3.9±0.7 mm/yr obtained from altimetry fields. The distribution of sea level trends is also remarkably similar to altimetry trends except in regions with high mesoscale activity such as the Algerian basin. The substitution approach gives similar results for the basin MSL rise (4.5±0.7 mm/yr), though the distribution of trends is less accurate.

The validation of the reconstruction for the period 1945-2000 is based on local comparisons with tide gauge records that were not used to obtain the reconstruction. The correlation between the reconstruction and these independent tide gauge records is higher than 0.7 for all cases. These values are comparable to those obtained for the altimetric period, which suggests that the accuracy of the reconstruction is fairly stable during the whole period.

Our best estimate for the Mediterranean MSL rise occurred during the period 1945-2000 is 0.6±0.1 mm/yr. The uncertainty of the trend (±0.1 mm/yr) is mostly due to the statistical properties of the series (length and variability), with a small impact of the errors associated with the interpolation process. The five Mediterranean tide gauge records that span most of the 20th century show positive trends between 1.2±0.1 and 1.5±0.1 mm/yr (Marcos and Tsimplis, 2008). When using the 21 longest records (>35 years) for the period 1960-2000, the obtained trends are much smaller in the Mediterranean (−0.7±0.3 mm/yr to 0.3±0.4) than in the neighbouring Atlantic sites (1.6±0.5 to 1.9±0.5 mm/yr) for the period 1960-2000. As expected, our trends are therefore consistent with previous estimates from tide gauges. The progress beyond the state of the art is that the rate of MSL rise derived in this work corresponds to a basin average and therefore it should be in principle more representative of

Mediterranean MSL than individual tide gauges.

Results confirm that during the second half of the 20th century Mediterranean MSL has been rising at a smaller rate than global MSL. According to the most recent estimate, global MSL has been rising at a rate of 1.6±0.4 mm/yr for the period 1961-2003, of which 0.9±0.2 mm/yr would correspond to the melting of glaciers and ice caps and 0.7±0.4 mm/yr would correspond to thermal expansion (Domingues et al., 2008). The closest period we can evaluate from our reconstruction is 1961-2000, for which we obtain 0.3±0.2 mm/yr. The atmospheric contribution to sea level estimated (Gomis et al.. 2008, see next chapter) is −0.7±0.1 mm/yr, so that the remaining components (steric and mass increase) would contribute with 1.0±0.2 mm/yr. It turns out, therefore, that the rising of atmospheric pressure over the region would explain a significant part but not all the difference between global and Mediterranean trends. The partition of total sea level into the different components will be addressed with detail in the next chapter.

The reconstruction also gives, for the first time in the Mediterranean, the spatial distribution of trends spanning more than five decades. A main feature of that distribution is the maximum positive trend obtained in the Ionian Sea (up to 1.2 mm/yr), precisely where maximum negative trends were observed for the altimetric period 1993-2000. Minimum values are obtained in the Aegean Sea, where trends are nearly zero; a negative peak of -0.5 mm/yr is obtained to the south-east of Crete. In general we find small positive trends in the Western Mediterranean (between 0.5 and 1 mm/yr) and even smaller trends in the Eastern Mediterranean (between 0 and 0.5 mm/yr).

Chapter 7

Quantification of the different physical processes driving sea level variability

IN Chapter 6 we have successfully reconstructed total sea level in the Mediterranean basin for the past decades using satellite altimetry and tide gauge data. The reconstruction has been used to estimate Mediterranean MSL trends for the period 1945-2000 as well as the distribution of sea level trends in the basin. While the information derived from the reconstruction is essential to know how much the Mediterranean sea level has been rising as a whole during the past decades and whether the rise has been uniform or not, it is also very important to identify and quantify the different contributions of such a rise. As it was described in Chapter 2, the long-term variations are due to changes in the water content of the oceans (mass component), and to changes in the volume of the oceans resulting from an expansion or a contraction of the water body (steric component). At regional scale, the impact of long-term atmospheric pressure variations and, to a lesser extent, changes in the ocean circulation derived from winds and other non-geostrophic processes can also play an important role.

The steric sea level can be estimated directly from hydrographic data sets or from model data. On the other hand, the mass contribution to sea level variability for the past decades is usually estimated by subtracting the steric and atmospheric contribution from total sea level, since the first satellite gravimetry measures have not been obtained until the 21th century and very few models contemplate the long-term melting of continental ice. Several works have already been published on the steric component of Mediterranean sea level, but Chapters 8 and 9 intend to go beyond the present state of the art. The long-term mass component had never been addressed in the Mediterranean Sea; we do it in Chapter 10, where we intend to close the budget of sea level variability.

The atmospheric component has already been estimated from barotropic models by other authors (e.g., Tsimplis et al., 2005; Gomis et al., 2008). The present state of the art on this component is good enough to close the budget of Mediterranean sea level variability and therefore we will not address this topic. What we will do in this chapter is to summarize the results obtained by others authors for the sake of completeness.

7.1 The atmospheric component: executive summary

The atmospheric component of Mediterranean sea level was recently studied by Gomis et al. (2008). They used 44 years (1958-2001) of model data to quantify the contribution of atmospheric pressure and wind to Mediterranean sea level variability. The simulation used by those authors was produced in the framework of the HIPOCAS project and obtained from a barotropic run of the HAMSOM model (see Chapter 4). They examined the inter-decadal trends and they also characterized the seasonal cycle.

They found that the atmospheric contribution has a clear negative inter-decadal trend of about -0.60±0.04 mm/yr (ranging from -0.5 mm/yr in the Levantine basin and in the vicinity of Gibraltar to less than -0.7 mm/yr in the Adriatic) for the period 1958-2001. The trend is more marked (mean value of -1.0 mm/yr) for the period 1960-1994. These results would explain a significant part of the difference found in Chapter 6 between the rate of Mediterranean sea level rise (0.6±0.1 mm/yr for the period 1945-2000) and the global estimates (1.8±0.2 mm/yr for the period 1950-2000). The other part should be explained by the contribution of other processes such as the steric and mass components.
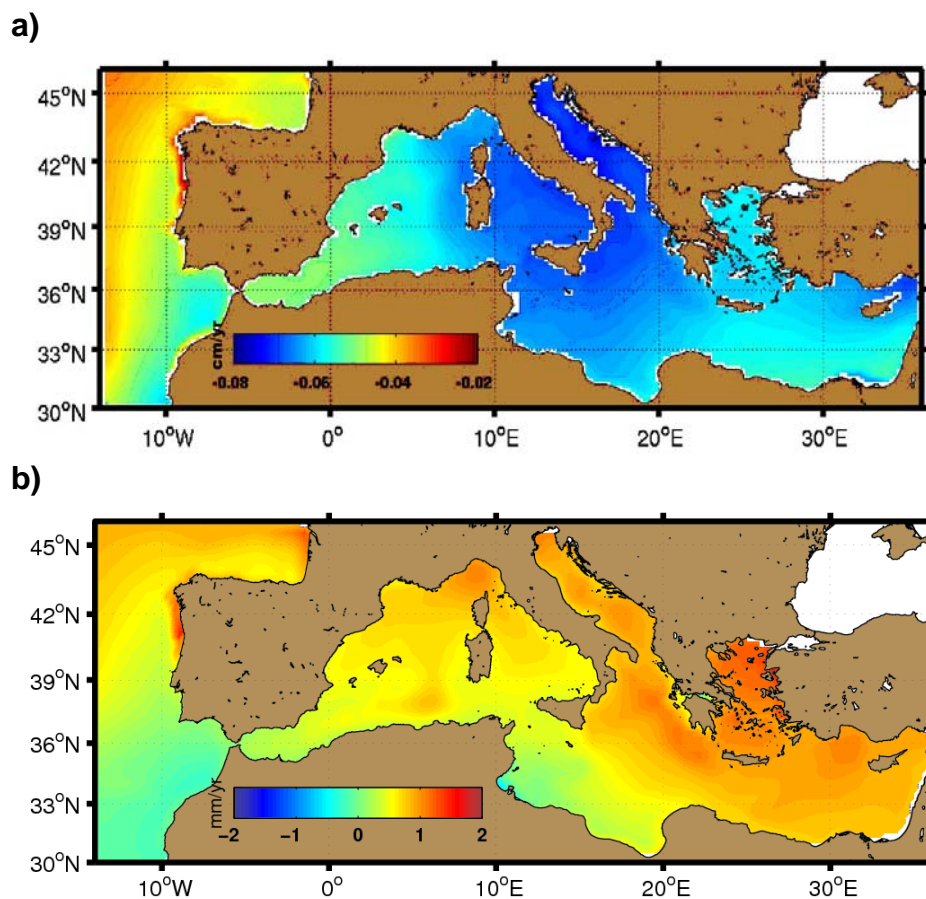
Figure 7.1. Spatial distribution of trends of the atmospheric contribution to sea level as obtained from HAMSOM outputs: (a) for the whole modeled period (1958-2001); (b) for the period (1993-2001). Note the different units: (a) cm/yr; (b) mm/yr. (from Gomis et al., 2008).

The same authors also estimated the atmospheric trends for the period 1993-2001 and the results that they found were rather different. The trend of the contribution of atmospheric pressure and wind computed for the period 1993-2001 is positive, having a mean value of 0.6 mm/yr compared with a trend of 3.9±0.7 mm/yr estimated for the total sea level from altimetry data (Chapter 5). Hence, unlike for the previous decades, the atmospheric component has contributed in the same sense of the marked sea level rise observed in the last decade of the 20th century.

Figures 7.1a,b show the spatial distribution of trends of the atmospheric contribution for the period 1958-2001 and 1993-2001. The distribution shows a rather homogenous pattern, as it can be expected from a large scale atmospheric variable, but it still shows some local interesting phenomenon. One of them is the fact that the most marked negative trends corresponding to the period 1958-2001 are found in the central Mediterranean and in the Adriatic Sea. It is worth recalling, however, that Pascual et al. (2008) found that one of the weakest points of the HIPOCAS barotropic modeling was precisely the northern Adriatic Sea, probably due to a misrepresentation of local winds. For the period 1993-2001, positive trends are found almost everywhere in the basin, with the largest values in the Aegean Sea.
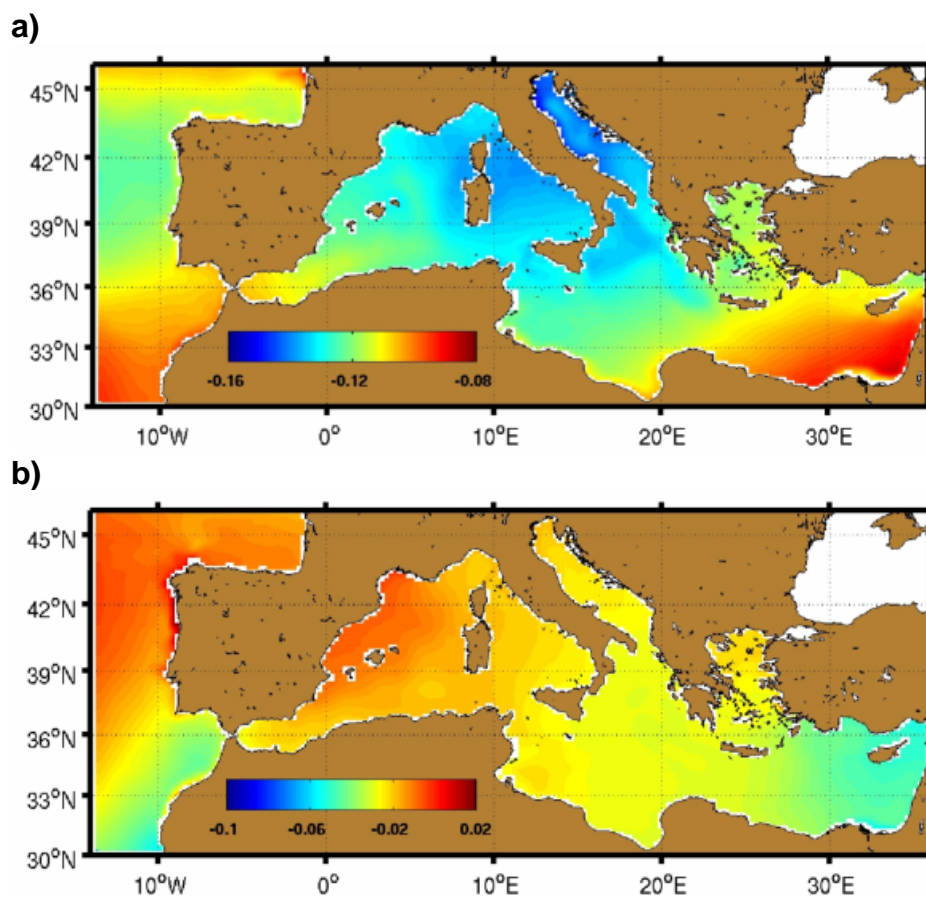
Figure 7.2. Spatial distribution of winter (a) and summer (b) trends (cm/yr) of the atmospheric contribution to sea level for the period 1958-2001 (from Gomis et al., 2008).

Gomis et al. (2008) also characterized the seasonal differences of long term trends and their contribution to the seasonal cycle. The spatial distribution of the winter and

summer trends is shown in Figures 7.2a,b. In winter (Fig. 7.2a) the most pronounced trends are found again in the Adriatic, with values up to -1.5 mm/yr, and in the central Mediterranean. Less negative trends values (of the order of -1.0 mm/yr) are obtained in the Eastern Mediterranean. In summer (Fig. 7.2b) the situation is rather different: the most pronounced trends (of the order of -0.5 mm/yr) are found in the Eastern Mediterranean, and the less negative trends (about -0.1 mm/yr) are obtained in the Western Mediterranean. From these results, it seems clear that winter is the season driving the overall negative trends obtained for the period 1958-2001. Since the minimum of observed sea level is reached in winter and the maximum by the end of the summer, the seasonality of the trends obtained from the mechanical atmospheric contribution could result in a strengthening of the seasonal cycle by up to 1 mm/yr (the difference between winter and summer trends). However since the steric and atmospheric contributions are not in phase, the strengthening of the observed seasonal cycle during the last decades has been smaller.

The marked seasonality of the trends can be explained in terms of the seasonal trends of the NAO and in particular of the Mediterranean Oscillation Index (MOI). Both the NAO and MOI indices show a clear trend (0.032 NAO-units/yr and -0.035 MOI-units/yr, respectively) in winter and less significant trends in the other seasons. The NAO index is significantly correlated with the atmospheric contribution to sea level only in winter. The MOI is highly correlated all year round, though maximum values are also reached in winter.

Finally, and although this thesis is mainly devoted to interannual and interdecadal variability, two further results from other authors are worth being quoted. The first one is that Gomis et al (2008) quantified the amplitude of the seasonal cycle of the atmospheric component in about 2 cm over most of the basin (ranging between 1.5 and 4 cm), while the semi-annual component is much smaller (amplitude of about 0.6 cm). This means that the seasonal cycle accounts for about 30% of the standard deviation of the atmospheric component when this is estimated from monthly mean data. Although the contribution of the atmospheric component cycle to the observed sea level cycle is not very large, it can explain why the seasonal cycle estimated from altimetry is usually larger than the cycle estimated from tide gauges: 7-8 cm (Fenoglio-Marc, 2001; Larnicol et al., 2002; Fenoglio-Marc et al., 2006; García et al., 2006) in front of 4-7 cm (Tsimplis and Woodworth, 1994; García-Lafuente et al., 2004). A first reason is that the atmospheric component, not included in the altimetry data, is offset from the steric cycle by about 6 months, then reducing the amplitude of the annual cycle when fitting a harmonic function to tide gauge data. A second reason could be that altimetry data only cover the last decade of the 20th century, the period for which the seasonal cycle is slightly more marked due to the seasonality of the trends detected in the atmospheric component. A third reason could be that tide gauges are located pointwise along the coast, while the 7-8 cm cycle estimated from altimetry is a basin average value.

The second result relevant for this work is the comparison of the sea level response to pressure and wind forcing of two barotropic model runs against tide gauge and altimetry data carried out by Pascual et al (2008). Although it does not focus particularly on long term sea level variability, it contains interesting hints regarding the atmospheric correction of satellite altimetry data. The two runs compared by Pascual et al. (2008) are the HIPOCAS run with the HAMSOM model and the MOG2D run used by AVISO to correct altimetry data sets (both have already been referred in this work).

They found that the HIPOCAS run reproduces observed (TG recorded) sea level better than MOG2D (residual variance of 70.81 ± 0.69 cm^2 versus 74.05 ± 0.68 cm^2) except in the northern Adriatic, where HIPOCAS gives higher residual variance than MOG2D (118.80 ± 0.60 cm^2 versus 107.15 ± 0.60 cm^2). At low frequencies (T>20 days) the atmospherically induced coastal sea level is better reproduced by HIPOCAS in the entire domain (23.43 ± 0.34 cm^2 versus 32.35 ± 0.33 cm2), while at high frequencies (T<20 days) MOG2D and HIPOCAS perform similarly (37 ± 0.5 cm^2). Basing on their results, these authors recommend to use either MOG2D or HIPOCAS for the correction of altimetry, and to use HIPOCAS for studies aimed to determine the atmospheric contribution to sea level variability.

7.2 Conclusions

In this short chapter we have presented a brief summary from other papers about the atmospheric contribution to Mediterranean sea level for the last decades. The main conclusion is that the atmospheric contribution played a key role in the lower-than-global trend estimated in Chaper 6 for the averaged total sea level in the Mediterranean Sea. If we remove the contribution of the atmospheric (-0.6 mm/yr) component from the total sea level (0.6 mm/yr) the resulting trend (1.2 mm/yr) does not completely explain the difference with respect to the global trend (about 1.8 mm/yr). This difference should come from the other two contributions, the steric and mass components, that are quantified in the following chapters.

Chapter 8

Steric and total sea level as given by a baroclinic model: comparison with the reconstruction

$\mathbf{I}$N[1] this chapter two Mediterranean Sea level distributions spanning the last decades are examined. The first one is the reconstruction of sea level obtained in Chapter 6 by a reduced-space optimal interpolation applied to tide gauge and altimetry data. The second distribution is obtained from a 3D (baroclinic) regional circulation model. Results are presented for two different periods: 1993-2000 (for which altimetry data are available) and 1961-2000 (the longest period common to both distributions). The interest of the comparison is not only the validation of the model against the reconstruction, but also the estimation of the steric component from the model.

8.1 Introduction

The study of the total and steric long-term sea level variability is usually undertaken either from available observations (tide gauge records and satellite altimetry for total sea level and hydrographic data bases for the steric component) or from hindcasts of the last decades. The partial pictures of the actual time-space sea level variability given by observations can be improved when tide gauge records and satellite altimetry data are combined to reconstruct sea level fields as already described in Chapter 6. Hydrographic data are usually optimally interpolated on regular grids.

Regarding long-term sea level hindcasts, they are usually obtained from the output of global or regional baroclinic circulation models. In the Mediterranean Sea, global models are handicapped by their low resolution, which usually prevents an accurate representation of key processes such as deep water formation or the water exchange through Gibraltar. On the other hand, regional hindcasts have enough spatial resolution;

---

[1] This chapter is based on the paper:
Calafat, F. M., D. Gomis, M. Marcos, (2010). Comparison of Mediterranean sea level fields for the period 1961-2000 as given by a data reconstruction and a 3D model, *Global Planet. Change*, *68*(3), 175-184.

Their drawback is that sea level variations inside the Mediterranean basin depend, at least to some extent, on the boundary conditions imposed at the Strait of Gibraltar and/or in the Atlantic boundary of the domain; these are usually taken either from a climatology or from a global model. An advantage of the hindcasts over sea level reconstructions is that they give a much more complete information on the physical processes driving sea level variability. Hence, changes in the mass content of a semi-enclosed basin such as the Mediterranean Sea can in principle be related to the evaporation-precipitation-river runoff (E-P-R) budget and the mass exchanges through Gibraltar. The steric component, resulting from changes in the volume of the water column, are computed from and therefore can be related with changes in temperature and salinity distributions. It is worth noting here that, in a strict sense, the mass and the steric components are not fully independent, since salinity changes are obviously related to the freshwater budget.

The objective of this chapter is, first, to compare the 1945-2000 reconstruction of Mediterranean sea level carried out in Chapter 6 with the 1961-2000 OM8 simulation carried out by Somot et al. (2006) (see section 4.4.2). The two representations are fully independent and based on different hypotheses. On one hand, the reconstruction entirely relies on sea level observations; basic hypotheses are that the dominant (usually large-scale) spatial modes inferred from the altimetric period are almost stationary in time (i.e., that they are valid for the whole reconstructed period) and that at least the overall pattern of these modes can be reconstructed from the discrete tide gauge spatial sampling. The validation of these hypotheses was presented in Chapter 6 altogether with other sensitivity tests. On the other hand, the hindcast is forced by a downscaled meteorological analysis and does not assimilate any oceanographic observation; the basic hypotheses are that the heat, fresh water and momentum forcings are accurate and that the model equations can account for the most important processes driving the dynamics of the Mediterranean Sea. The characteristics of the OM8 simulation were given in Chapter 4, but it is worth recalling here that the Atlantic boundary of the domain is set to match a monthly climatology and therefore the observed warming of Atlantic waters or the eventual mass increase and water freshening derived from ice-melting are not accounted for by the model. This implies that the mass exchanges through Gibraltar and hence the Mediterranean sea level variability will not be affected by remote influences.

The second objective of this chapter is to characterize the steric component of sea level given by the model. In fact, it is worth recalling that the sea level provided by the model does neither account for sea level changes due to remote mass changes (i.e., mass increase due to ice melting) nor for the atmospheric pressure. Hence, what we will refer to as total sea level given by the model, only reflects the steric changes and the smaller changes due to the wind and other non-geostrophic parts of the circulation.

The comparison between the reconstruction and the hindcast is performed for two different periods: 1993-2000 (for which altimetry data are available) and 1961-2000 (the longest period common to both distributions). For the first period the reconstruction has already been validated against altimetry data, while before that period it has only been validated locally, against a few independent tide gauges that were not included in the reconstruction process (Chapter 6). It is therefore of great interest to compare both sea level representations and to determine their strengths and weaknesses for the pre-altimetric period. The ultimate aim is to end up with a reliable representation of the spatial and temporal variability of Mediterranean sea level spanning the last decades.

The key magnitudes intended to be derived are the usual ones: basin mean and regional trends for both, total sea level and the steric component. At global scale, widely accepted values for total sea level trends are the 1.8 mm/yr given by Church et al. (2004) for the period 1950-2000 and the 1.7 mm/yr given by Church and White (2006) for the whole 20th century, both obtained from reconstructions based on altimetry and tide gauge records. More recently, Domingues et al. (2008) have considered the bias affecting part of the historical observations and have given an updated value of 1.6±0.4 mm/yr for the period 1961-2003. The rate of the thermosteric (i.e., due to temperature only) component of global sea level rise has usually been evaluated from gridded ocean temperature data sets (Levitus et al., 2000; Ishii et al., 2003; Levitus et al., 2005). Antonov et al. (2005) estimated the thermosteric trend to be 0.33 mm/yr for the period 1955-2003. For the same period, Ishii et al. (2006) give values of 0.31±0.07 and 0.04±0.01 mm/yr for the thermosteric and the halosteric sea level, respectively. However, a recent result obtained by Domingues et al. (2008) from in-situ hydrographic measurements spanning the period 1961-2003 increases the thermosteric sea level trend up to 0.52±0.08 mm/yr. All those estimates correspond to the thermosteric contribution for the upper 700 m. Estimates of the thermal expansion of the ocean below 700 m are much more uncertain and they vary from the 0.07 mm/yr computed from observations spanning the period 1961-2003 given by Domingues et al. (2008) to the 0.3 mm/yr given by the German Consortium for Estimating the Circulation and Climate of the Ocean Model for the period 1962-2001. At global scale, the differences between total sea level rise and the steric component must be attributed to other contributions such as the ocean mass increase derived from the melting of continental ice, but also to errors in the estimated trends.

At regional scale sea level shows a high spatial variability even at subbasin scale. For instance, Antonov et al. (2005) give values of 0.60, 0.25 and 0.22 mm/yr for the Atlantic, Indian and Pacific Oceans, respectively, for the period 1955-2003. In the Mediterranean Sea, Tsimplis et al. (2008) found steric sea level trends of -0.16±0.06 and -0.26±0.06 mm/yr in the Western Mediterranean and in the Adriatic, respectively, for the period 1960-2000. Bethoux et al. (1990) and Rixen et al. (2005) showed that the temperature and salinity of deep waters of the Mediterranean Sea are not constant, and therefore long-term sea level changes derived from changes in the temperature, salinity and circulation are expected. Moreover, transient events such as the EMT can strongly modify the internannual sea level variability.

The EMT is described in detail in Chapter 9, but here it is worth giving some details with the aim of establishing a background on which to discuss the results obtained in this chapter. The Mediterranean Sea is believed to have had the Adriatic Sea as the major source of deep waters in the Eastern Mediterranean during most of the last century. However, between 1987 and 1995 the location of the Eastern Mediterranean Deep Water Formation (EMDW) changed and the Aegean became the major source of deep water formation (Roether et al. 1996; Theocharis et al., 1999; Roether et al., 2007). This change is what we refer to as the EMT and it was due to anomalous meteorological conditions over the Aegean Sea and also in the region of the Adriatic (Josey, 2003), with very cold winters in 1992 and 1993. After 1995 the situation returned back to normal: the Aegean Sea returned to pre-EMT conditions, exporting small amounts of dense water that do not reach the bottom of the Ionian and the Levantine basins (Theocaris et al., 2002) while the Adriatic Sea became again the main contributor to the dense waters of the Eastern Mediterranean (Klein et al., 2000; Manca et al., 2006). The marked sea level dropping observed in the altimetry maps of the Ionian Sea during the nineties (Cazenave et al., 2001; Fenoglio-Marc, 2002; Criado-Aldeanueva et al., 2008)

are now thought to be a consequence of the EMT. Other regional trends have been estimated from the 1945-2000 reconstruction obtained in Chapter 6. When averaged over the whole Mediterranean basin, sea level rise has been estimated in 0.6±0.1 mm/yr for the period 1945-2000.

The chapter is organized as follows. The details on the specific data sets used in this chapter are presented in section 8.2. Section 8.3 is devoted to present the results of the comparison between the reconstruction and the hindcast; that section is divided in two different periods: the altimetric period (1993-2000) and the total period 1961-2000. The regional distribution of trends and the time variability of selected regionally-averaged sea level (both for total sea level and for the steric component) are shown for both periods. All results are discussed and summarized in section 8.4.

8.2 Datasets

8.2.1 Reconstructed sea level fields

Here we just need to recall that the reconstruction obtained in Chapter 6 consists of monthly 1/4º x 1/4º gridded total sea level fields covering the Mediterranean Sea for the period 1945-2000 and that it contains the atmospheric contribution.

8.2.2 The atmospheric contribution

The reconstruction undertaken from sea level observations has all the components in it, while the hindcast described in the next section is not forced by atmospheric pressure. Hence, the atmospheric component of sea level has to be estimated in an independent way and subtracted from the reconstruction (it could also be added to the hindcast) before comparing the two sea level representations. The data set used here is the HIPOCAS run of the HAMSOM model described in section 4.4.1.

8.2.3 The baroclinic model

The baroclinic model used in this chapter is the OM8 model described in Chapter 4. It is a high resolution rigid lid model for the Mediterranean Sea with a resolution of 1/8° x 1/8°cos(*latitude*) in the horizontal and 43 non-uniform vertical levels based on an area limited version of the OPA model (Madec et al., 1998). The simulation spans the period 1961-2000. Sea surface height is computed from the pressure gradient at the surface layer. The steric sea level is computed from the modeled temperature and salinity as described in Chapter 3.

8.2.4 The altimetry dataset

Altimetry data are used as a reference to validate the reconstruction and the model for the period 1993-2001. In this chapter we use the AVISO regional product for the Mediterranean Sea presented in Chapter 3. The AVISO data consist of multimission (up

to four satellites for some periods) gridded sea surface heights. The data span the period between November 1992 and December 2008, with a spatial resolution of 1/8º x 1/8º and weekly time resolution.

8.3 Results

The results of the comparison between the reconstruction (with the atmospheric component subtracted) and the hindcast is divided into two different periods: the altimetric period (1993-2000) and the total period 1961-2000. The regional distribution of sea level trends and the time variability of selected regionally-averaged sea level are shown for both periods.

8.3.1 Total and steric sea level trends for the period 1993-2000

The reconstruction has already been compared with altimetry data in Chapter 6; the spatial distributions of trends (Figs. 8.1a-b) are shown here for the sake of completeness and because they differ from those shown in Chapter 6 in that those included the atmospheric forcing. Figures 8.1c-d show the trends for total sea level and the steric component derived from the model. In the Western Mediterranean the model shows a pattern with both negative (-5 mm/yr) and markedly positive (10 mm/yr) values and that does not match the pattern obtained from altimetry and the reconstruction. The positive trends obtained in the Eastern Mediterranean are more similar, but the values are smaller with respect to altimetry and the reconstruction. The model shows negative trends (-2 mm/yr) in the Ionian Sea, but they are much weaker than the observed trends and only cover a reduced sector to the south of the Ionian basin (Fig. 8.1c). The steric trends (Fig. 8.1d) inferred from the model show a spatial pattern similar to total sea level trends, but with small positive trends in the Ionian Sea and slightly larger positive trends in the Levantine basin.
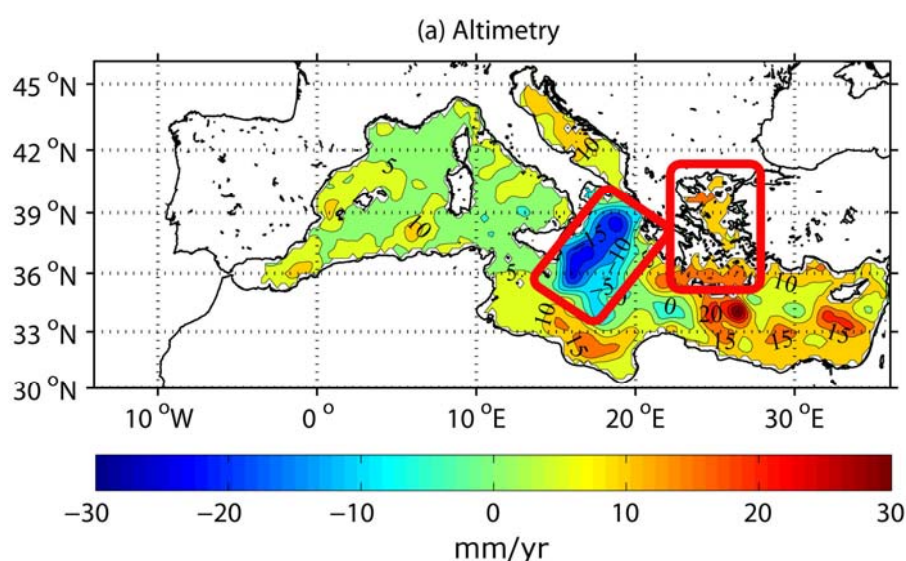
Figure 8.1. The distribution of sea level trends for the period 1993-2000 estimated from (a) altimetry data. Panels (b), (c) and (d) and the full figure caption are shown in next page..
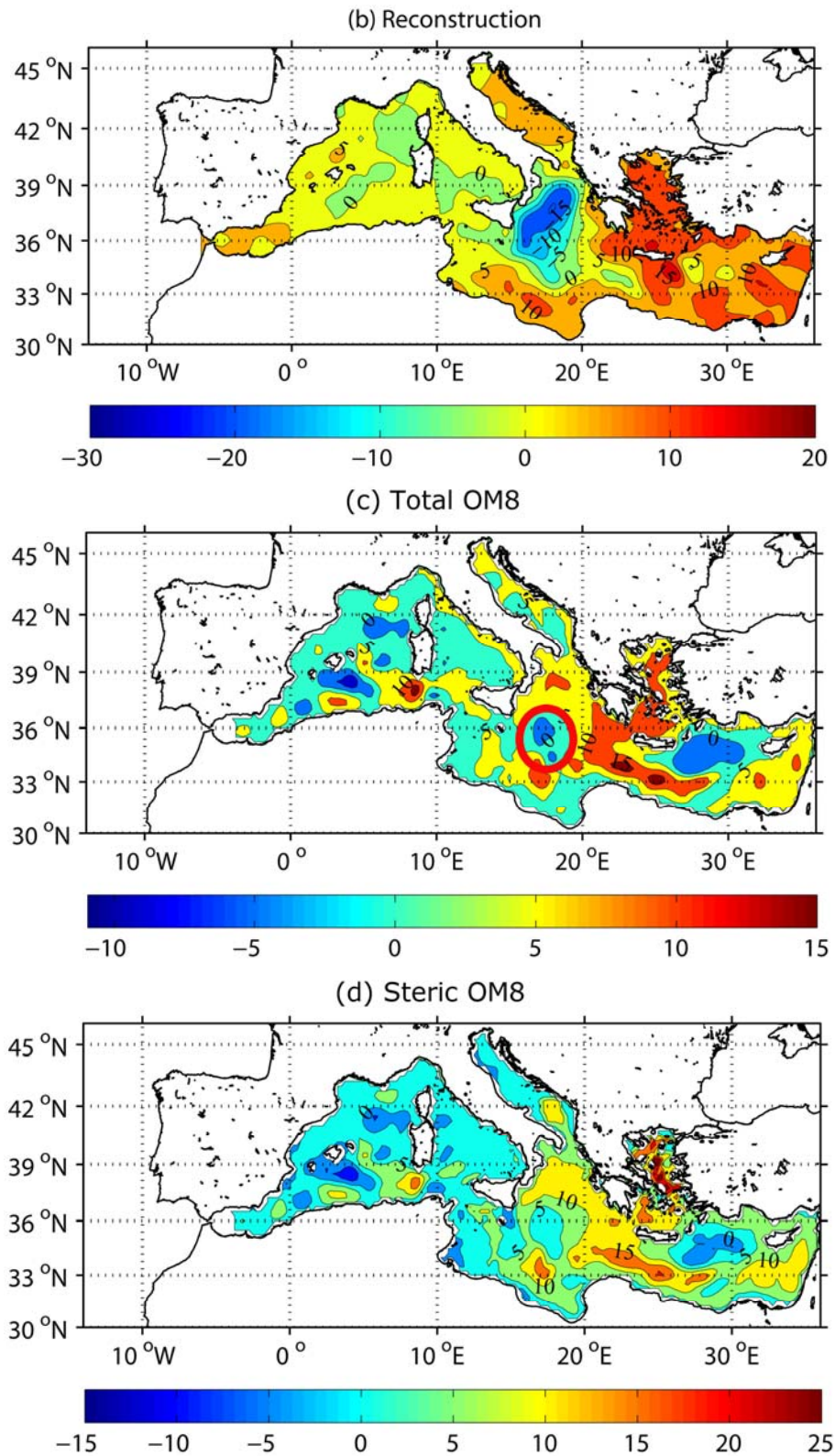
Figure 8.1. (Continued). The distribution of sea level trends for the period 1993-2000 estimated from (b) reconstructed sea level fields; (c) total sea level derived from the OM8 simulation; (d) the steric component of sea level derived from the OM8 simulation. The contour interval is 5 mm/yr. Note the different scale ranges (units are mm/yr in all cases). The enclosed regions in figures (a) and (c) denote the Aegean and Ionian domains averaged in Figures 3 and 6 (note that for the latter the averaged domain is different for the reconstruction (a) and for the model (c)).

The temporal sea level variability has been examined for the whole Mediterranean basin and for regions showing distinct features. Yearly time series of observed and reconstructed sea level averaged over the entire basin together with averaged total and steric sea level from the 3D model are plotted in Figure 8.2. The interannual variability of the reconstruction is in good agreement with altimetry; the model (both total sea level and the steric component) shows an overall similar behaviour, but the interannual variability departs from observations. The trends computed for the four curves of Figure 8.2 are given in Table 8.1. It must be stressed that for such a short period, trends undergo significant variations just by adding or taking out one year from the computations (e.g., Criado-Aldeanueva et al., 2008, give altimetric trends of 6.3±0.8 mm/yr for the period 1993-2001, in front of the 3.8±0.4 mm/yr given in Table 8.1 for the period 1993-2000). Correlations between altimetry and the reconstruction, the total and the steric sea level computed from the model are given in Table 8.2.
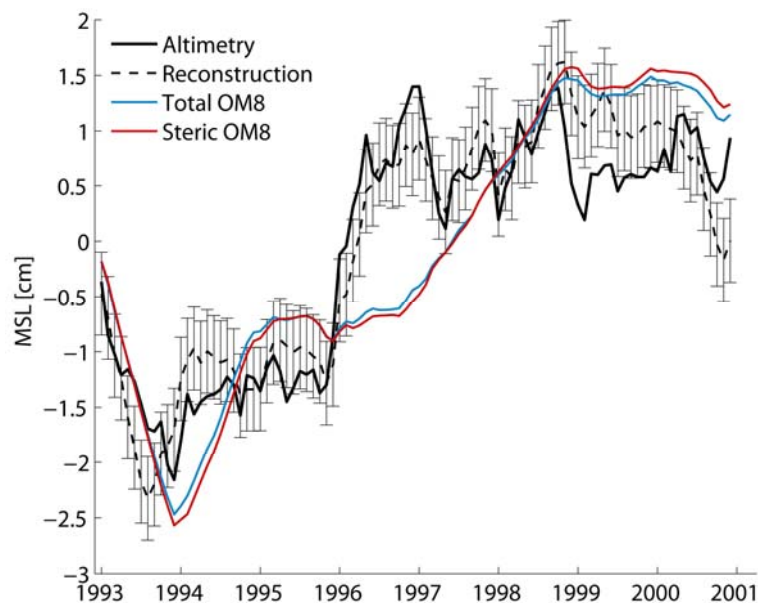
Figure 8.2. Yearly Mediterranean MSL for the period 1993-2000 estimated from altimetry data, reconstructed sea level fields (with error bars), total OM8 sea level and the steric component of OM8 sea level.

Figure 8.3 shows yearly sea level time series averaged over the Aegean Sea, the Ionian Sea, the central Western Mediterranean (excluding the Alborán Sea and the Tyrrhenian Sea) and the whole Eastern Mediterranean basin. The limits of the averaged domains are shown in Figure 8.1, while the derived linear trends are listed in Table 8.1. Note that the limits of the domain averaged in the Ionian Sea are different for the reconstruction (Fig. 8.1a) and the model (Fig. 8.1c). The reason is that in the model the negative trends appear displaced to the south (with respect to the reconstruction and altimetry) and the aim of the average was to reflect the time evolution of the main features observed in the trend distribution. Correlations between altimetry and the reconstructed sea level, the total and the steric from the model are given in Table 8.2 for all regions.

The Aegean Sea (Fig. 8.3a) is the region showing the closer behaviour to the basin MSL (Fig. 8.2) and also the region for which all estimations are closer to each other. All signals show a marked sea level rise until 1999, when sea level starts to decrease. The model clearly departs from altimetry only between 1994 and 1996, but these two years are enough to yield slightly different trends (Table 8.1). In the Ionian Sea (Fig. 8.3b) the model reflects some of the major features of the altimetric interannual variability, but it fails to reproduce the marked sea level decrease observed between 1998 and 2000. The reconstruction follows the altimetric variability much more closely and gives a negative trend that, although smaller, it is very close to the altimetric one. The model total sea level shows a negative trend, but it is much weaker than the reconstructed and altimetric ones (Table 8.1).
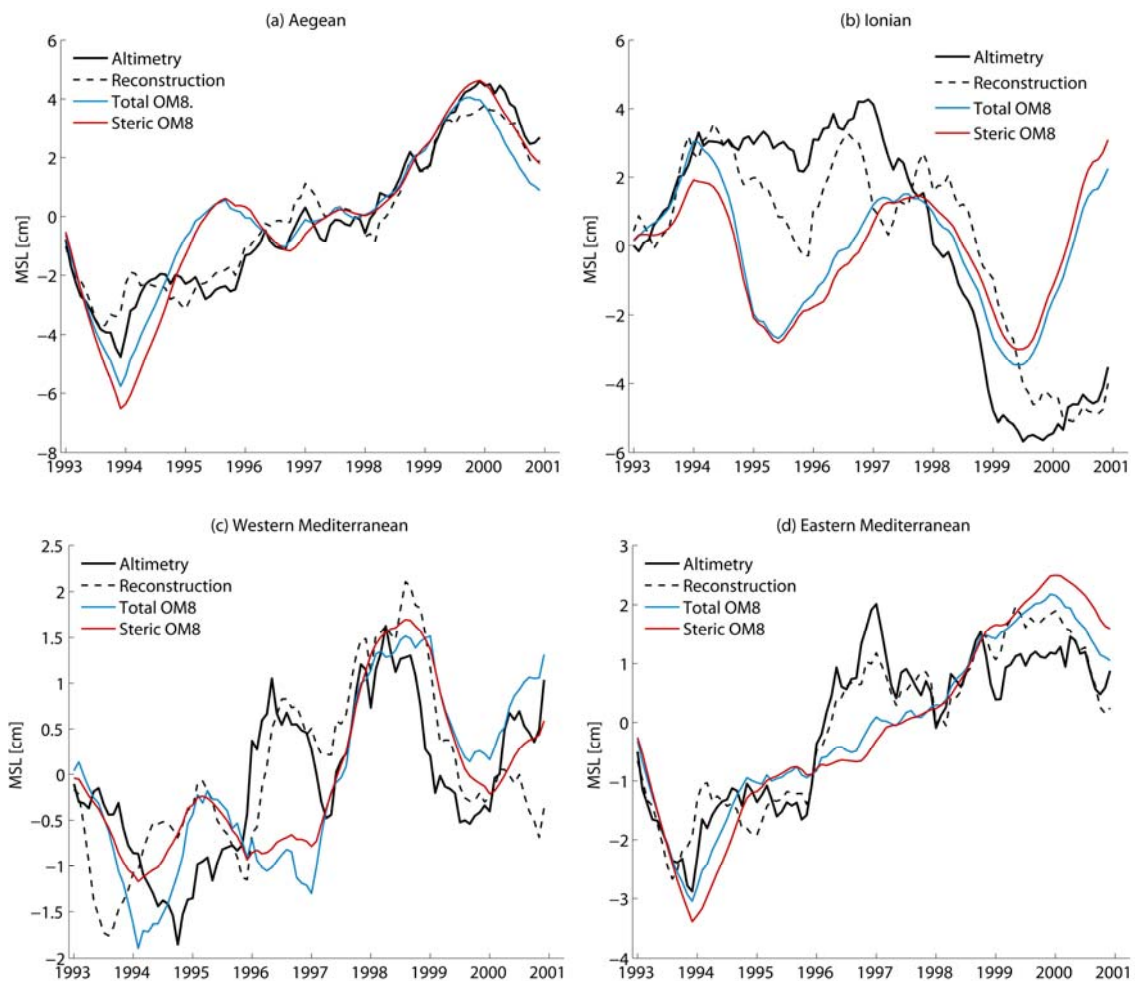
Figure 8.3. Yearly regional-averaged sea level for the period 1993-2000 estimated from altimetry data, reconstructed sea level fields, total OM8 sea level and the steric component of OM8 sea level for: (a) the Aegean Sea; (b) the Ionian Sea; (c) the Western Mediterranean and (d) the Eastern Mediterranean. The domains of the averages are shown in Figure 8.1.

The changes observed in the Aegen and Ionian Sea have been related to changes in the regional circulation associated with the EMT. Vigo et al. (2005) already found this sort of time-space oscillation between the Ionian Sea and the Levantine basin in which

before 1999 a sea level rise and drop is observed in the Levantine basin and the Ionian Sea, respectively, while after 1999 the behaviour seems to be the opposite. This description is however handicapped by the short coverage of the altimetric period, which starts about six years after the onset of the EMT. The described features will be re-visited when examining the whole 1960-2000 period.

The Western Mediterranean (Fig. 8.3c) is the only region where the model follows the observed interannual variability, sometimes even more closely than the reconstruction (in 1994-1996 for instance). The reconstruction and steric trends are both in agreement with the altimetric trend (within the statistical uncertainty; see Table 8.1), but the model total sea level shows larger trends. Regarding the Eastern Mediterranean (Fig. 8.3d), the reconstruction follows the altimetric variability much more closely than the model. The trend given by the reconstruction is in good agreement with the altimetric one. The model trends (both the total and steric ones) are larger than the altimetric one (Table 8.1).

Table 8.1. Sea level trends for the period 1993-2000 estimated from altimetry data, reconstructed sea level fields, total OM8 sea level and the steric component of OM8. Trends are given for the whole Mediterranean, the Aegean Sea, the Ionian Sea and the Western and Eastern basins.

1993-2000 [mm/yr]	MED	Aegean Sea	Ionian Sea	Western MED	Eastern MED
Altimetry data	3.8±0.4	10.7±0.5	-11.7±1.2	1.9±0.3	4.7±0.4
Reconstruction	4.1±0.4	9.8±0.4	-9.1±1.0	1.9±0.5	5.2±0.4
Total OM8	5.4±0.2	8.9±0.7	-2.3±0.9	3.0±0.3	6.5±0.3
Steric OM8	5.5±0.2	10.7±0.8	-0.5±0.8	1.7±0.3	7.3±0.3

Table 8.2. Correlations for the period 1993-2000 estimated between altimetry data and reconstructed sea level fields, total OM8 sea level and the steric component of OM8. Correlations are given for the whole Mediterranean, the Aegean Sea, the Ionian Sea and the Western and Eastern Mediterranean basins. Time series have been detrended before computing correlations.

Correlation	MED	Aegean Sea	Ionian Sea	Western MED	Eastern MED
Reconstruction	0.81	0.81	0.74	0.59	0.80
Total OM8	NS	0.50	0.3	0.41	0.42
Steric OM8	NS	0.49	NS	0.47	NS

8.3.2 Total and steric sea level trends for the period 1961-2000

The regional distributions of sea level trends for the period 1961-2000 estimated from the reconstruction and the model (total sea level and the steric component) are shown in Figure 8.4. The distribution estimated from the reconstructed fields (Fig. 8.4a) shows positive trends everywhere, but larger in the Western Mediterranean (up to 1.2 mm/yr) than in the Eastern Mediterranean (up to 0.6 mm/yr). A prominent feature is the relative maximum in the Ionian Sea (up to 1.8 mm/yr), while almost zero trends are observed in the Levantine basin. The trend distribution obtained from the OM8 simulation (Fig. 8.4b) is also positive everywhere; the overall differences with respect to the
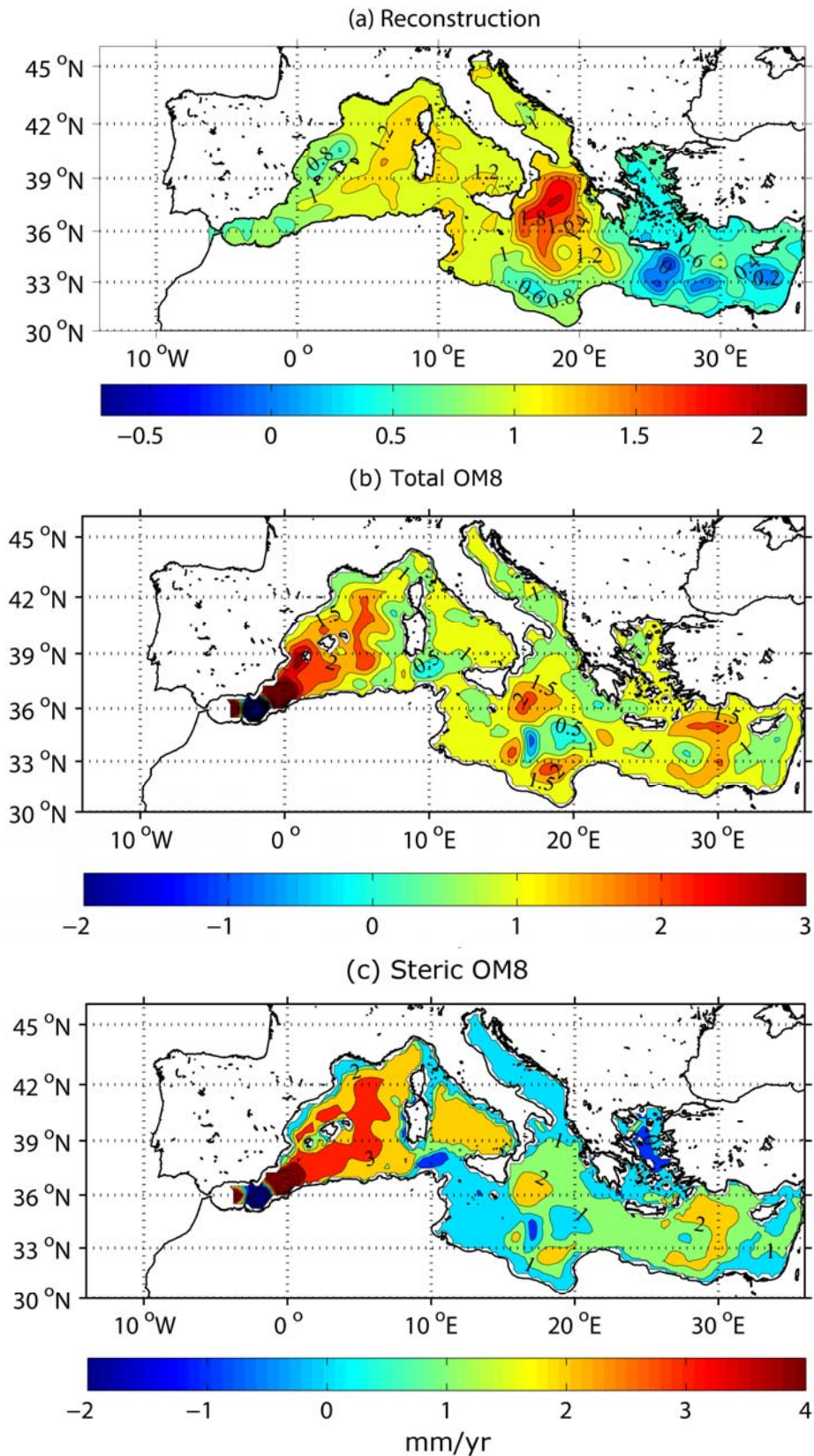
Figure 8.4. The distribution of sea level trends for the period 1961-2000 as estimated from (a) reconstructed sea level fields; (b) total sea level derived from the OM8 simulation; (c) the steric component of sea level derived from the OM8 simulation. The contour interval is 0.3 mm/yr in (a) and 0.5 mm/yr in (b) and (c). Note the different scale ranges (units are mm/yr in all cases).

reconstruction are that trends are less homogeneous and values are slightly higher than in the reconstruction (up to 1.5 mm/yr in the Western Mediterranean and larger than 0.5 mm/yr in the Eastern basin). The OM8 simulation also reproduces the positive peak in the Ionian Sea, though it covers a smaller area and it appears surrounded by other mesoscale structures

The distribution of trends derived from the model steric contribution (Fig. 8.4c) resembles model total sea level trends except in that values are significantly larger in the Western Mediterranean (above 2 mm/yr everywhere) and also, though to a lesser extent, in the Eastern basin (up to 1.5 mm/yr). The positive peak in the Ionian Sea is similar to the one obtained for total sea level (up to 2 mm/yr). Higher values of steric and total sea level trends in the model are obtained in the Alboran Sea.

It is worth noting that the steric trend distribution appears to follow the most prominent bathymetric changes. This is due to the fact that steric changes are integrated over the whole water column (see Eq. (3.2)) and therefore they depend on depth. This does not mean that, in the case of a hypothetical homogeneous warming, sea level would remain much higher where the water column is deeper (i.e., over larger depths); as the water would warm up and start to be higher over larger depths, it would flow over shallower depths, where sea level would be lower. This mass redistribution (associated with changes in the circulation) is part of the circulation or dynamical component.

The temporal sea level variability of the whole period 1961-2000 has also been examined for the whole Mediterranean basin and for regions showing distinct features. Yearly time series of reconstructed sea level averaged over the entire basin together with averaged total and steric sea level from the 3D model are plotted in Figure 8.5. Like for the altimetric period, the reconstructed and modelled MSL show a similar overall behaviour, though some details of the interannual variability are rather different (see for instance the disagreement in 1970 and in 1982-1985); the correlation between the two series is 0.8 (quoted correlations are always significant at the 95% confidence level, unless otherwise stated). The rate of MSL rise for the reconstruction and for the total sea level derived from the model are very similar (around 1 mm/yr, see Table 8.3). The evolution of the steric contribution closely follows the modelled total sea level, though the linear trend is slightly larger (Table 8.3).

The overall comments pointed out for the comparison of reconstructed and modelled basin MSL can be extended to the time evolution of the Aegean Sea, the Ionian Sea, the Western Mediterranean and the Eastern Mediterranean (Fig. 8.6). In the Aegean Sea (Fig. 8.6a), the evolution of the reconstructed sea level can be broken into three different periods: negligible trends for the period 1961-1987, a marked sea level lowering for the period 1987-1995 (the EMT) and a pronounced rebound for the period 1995-2000. The modelled sea level reproduces the first period and the 1995-2000 sea level rebound, but fails to reproduce the sea level fall associated with the EMT (the correlation between the two series is 0.6). The trends estimated in the Aegean Sea for for the total OM8 sea level fields are higher than those estimated from reconstructed fields (Table 8.3). The difference is mainly due to the departure between both signals during the EMT period (1987-1995). The steric component closely follows the total modelled sea level and hence the associated steric trend is also similar to that of total sea level (Table 8.3).
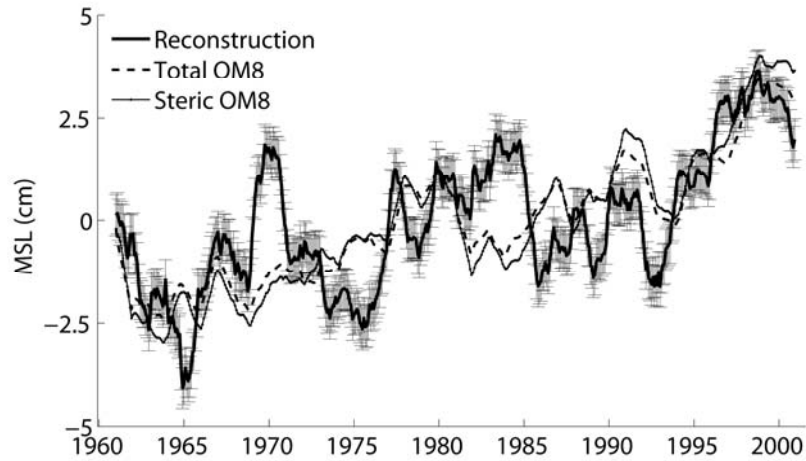
Figure 8.5. Yearly Mediterranean MSL for the period 1961-2000 estimated from reconstructed sea level fields, total OM8 sea level and the steric component of OM8 sea level.
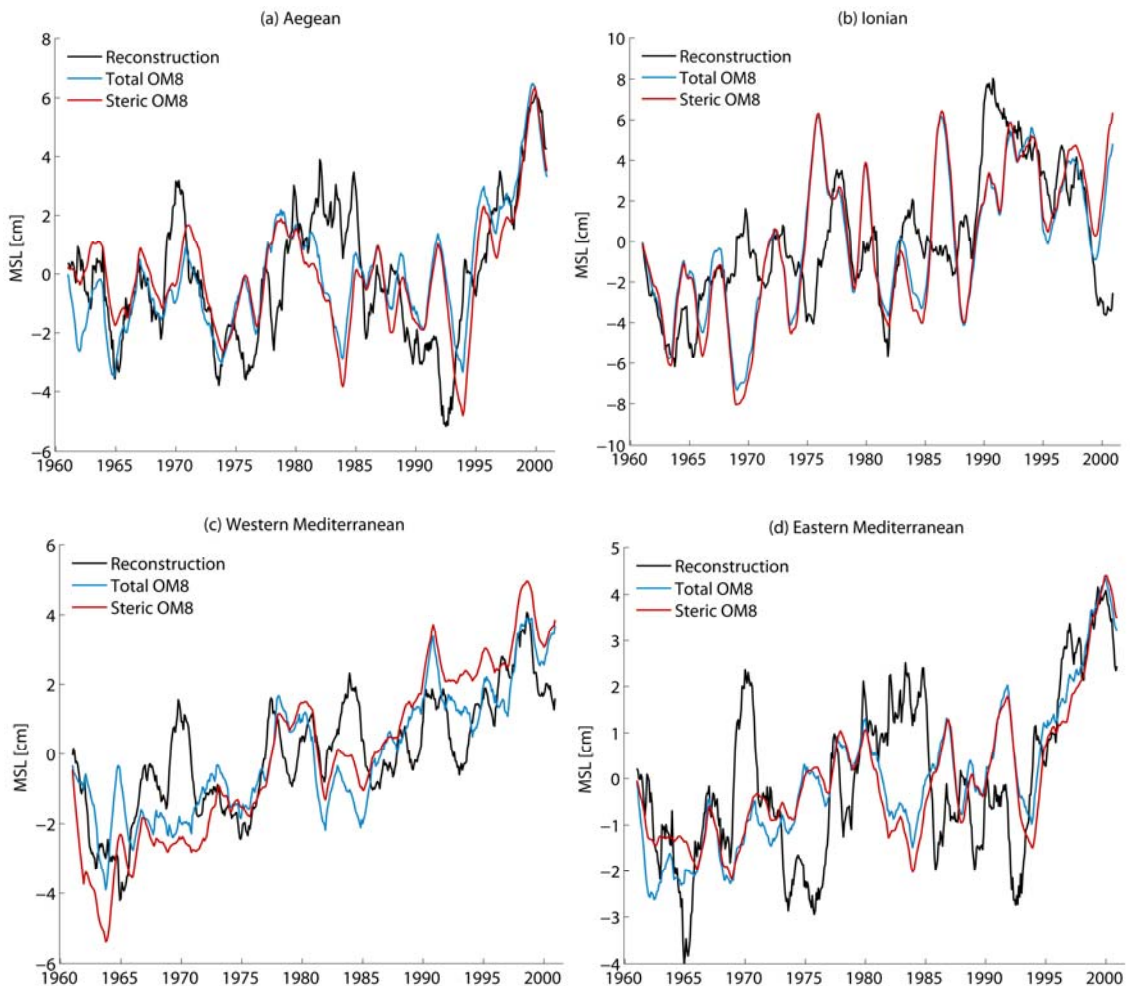
Figure 8.6. Yearly regional-averaged sea level for the period 1961-2000 estimated from reconstructed sea level fields, total OM8 sea level and the steric component of OM8 sea level for: (a) the Aegean Sea; (b) the Ionian Sea; (c) the Western Mediterranean and (d) the Eastern Mediterranean. The domains of the averages are shown in Figure 8.1.

Also the Ionian sea level evolution can be split into three distinct periods attending to the reconstruction: a smooth sea level increase from 1961 to 1987, values much higher than normal during the EMT years (1987-1995) and values lower than normal after the EMT (Fig. 8.6b). For the first period the reconstructed and modelled sea level are rather similar, though with some localized departure (e.g. in 1969). Consequently the trends are similar for this period (1.6±0.2 mm/yr for the reconstruction and 1.4±0.2 mm/yr for the OM8 simulation). The behaviour of both representations diverges after 1987. While the reconstruction shows a sudden sea level increase during the EMT years (peaking in 1991) followed by a fall down to values that are several cm smaller than pre-EMT values, the OM8 simulation does not show significant variations, neither during the EMT nor for the post-EMT years. The correlation between the reconstructed and total OM8 MSL in the Ionian Sea is 0.5 and the trends for the whole period 1961-2000 are shown in Table 8.3. The steric sea level resembles total model sea level for the whole period 1961-2000, with only a few localized disagreements.

In the Western Mediterranean (Fig. 8.6c) the reconstructed and the total OM8 sea level fields show similar positive trends (Table 8.3). However, the agreement between the two series is only fair at the interannual scale (the correlation between the two series is 0.7). A distinct feature with respect to the Aegean and the Ionian Sea is that here the steric sea level departs more significantly from the modelled total sea level. The steric component is smaller than total sea level in the 60s and larger in the 90s, which results in a larger trend (2.5 mm/yr for the whole period 1961-2000). The correlation between the reconstruction and the steric sea level in the Western Mediterranean is 0.8.

Finally, the 1961-2000 time evolution in the Eastern Mediterranean (Fig. 8.6d) resembles the variability found in the Aegean Sea (Fig. 8.6a), though the variations during the EMT and post-EMT periods are obviously smoothed. Another difference is that the variability of the reconstruction and the model (for both total sea level and the steric component) are more similar, which translates in more similar trends (Table 8.3).

Table 8.3. Sea level trends for the period 1961-2000 estimated from the reconstruction, total OM8 sea level and the steric component of OM8 sea level. Trends are given for the whole Mediterranean, the Aegean Sea, the Ionian Sea and the Western and Eastern Mediterranean basins.

1961-2000 [mm/yr]	MED	Aegean Sea	Ionian Sea	Western MED	Eastern MED
Reconstruction	1.0±0.1	0.6±0.1	1.8±0.1	1.1±0.1	0.8±0.1
Total OM8	1.2±0.1	0.9±0.1	1.7±0.1	1.3±0.1	1.1±0.1
Steric OM8	1.3±0.1	0.5±0.1	2.0±0.1	2.0±0.1	0.8±0.1

8.4 Discussion and conclusions

We have compared the reconstruction of Mediterranean sea level fields carried out in Chapter 6 with the sea level fields obtained from the output of a regional 3D baroclinic model. The comparison covers the four decades common to both sea level representations (1961-2000) and has been divided in two periods: the period for which altimetry data are available (1993-2000) and the whole period 1961-2000.

The fact that the overall trends of MSL given by the reconstruction and the model are similar must not hide the significant differences between the two representations. First

of all it must be recalled that the model uses a (monthly) climatology at the boundary of the Atlantic sector covered by the domain. It is clear that by using such condition the model cannot account for mass increments derived from continental ice melting, mass redistribution in the Atlantic Ocean or any other remote source of sea level changes. On the other hand, the reconstruction bases on the interpolation of actual sea level data and therefore it implicitly accounts for the eventual impact of such remote sources. Hence, unless the mass increase in the nearby Atlantic region has a negligible impact on Mediterranean sea level, the trends derived from the reconstruction should be larger than the trends derived from the model.

The crucial question is which of the two representations gives the best approach to actual sea level fields. For the altimetric period the reconstruction is clearly superior, but this was an expected result, since altimetry data are used to build up the reconstruction. For the whole period the only available sea level observations are tide gauge records. In order to be compared with the model and the reconstruction, the atmospheric contribution can be estimated at tide gauge stations from the output of the barotropic model described in section 8.2.3 (taking the closest HAMSOM gridpoint) and subtracted from tide gauge records. The result for the longest tide gauge records available in the Mediterranean Sea is shown in Figure 8.7 (from Tsimplis et al., 2005 and reproduced here for the sake of completeness). The comparison between Figures 8.5 and 8.7 reveals that the time evolution of MSL as given by the reconstruction is much more similar to tide gauge records than the MSL computed from the model. Prominent features common to most tide gauges such as the relative maxima recorded around 1960 and 1970 or the minima recorded in the middle 60s and the middle 70s are well recovered by the reconstruction, but not by the model.
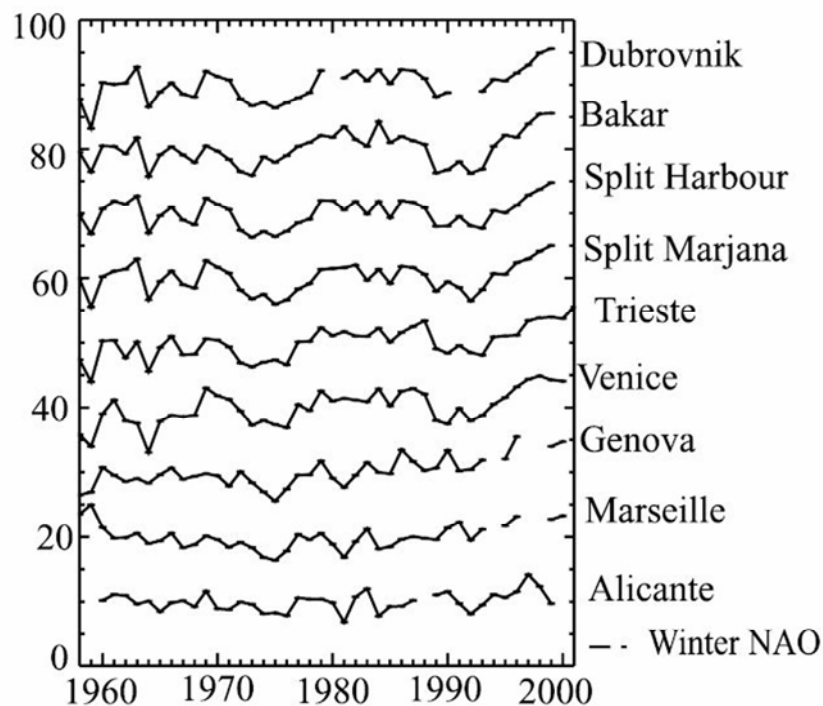
Figure 8.7. The longest tide gauge records in the Mediterranean Sea after removal of the atmospheric contribution (from Tsimplis et al., 2005).

There are also evidences that the reconstruction does a better job at regional scale. During the EMT (1987-1995) sea level dropped in the Aegean Sea and rose in the Ionian Sea, following the shift in the location of the main source of deep water formation from the Adriatic to the Aegean Sea (Roether et al. 1996; Theocharis et al., 1999; Roether et al., 2007). A first explanation for the impact of the described physical processes on regional sea level would be that the onset of deep water formation in the Aegean Sea implies densities higher than normal and, consequently lower sea level (sometimes linked to cyclonic circulation, depending on bathymetric constraints). Conversely, in the Ionian Sea, a transit basin for deep waters formed in the Adriatic, the stop of deep water formation would imply a lowering of isopycnals, with the consequent sea level rise and the triggering of anticyclonic circulation. The minimum/maximum values in the Aegean/Ionian Sea were achieved in 1991-1992, getting back to 'normal' values by 1995 (when the EMT was over, according to Klein et al., 2000, and Manca et al., 2006). In terms of sea level, however, after 1995 both the Aegean Sea and the Ionian Sea show a clear positive/negative rebound that affected the whole Eastern basin and that apparently ended in 1999 (Vigo et al., 2005). The physical processes underlying the observed rebounds would need of a carefully interpretation of the hydrographic data available in the region during the post-EMT years.

All these features are well reproduced by the reconstruction (Figs. 8.6a-b) but not by the model. It is worth noting that the period 1987-1992 is not covered by altimetry, so that the successful recovery of sea level fields for that period must be attributed to the proper methodology used for the reconstruction and not to the advantage of using contemporary altimetry data.

There may be several reasons why the model does not properly reproduce some of the major sea level features observed in the Mediterranean Sea during the last decades. Using climatological boundary conditions beyond the Atlantic sector might not only exclude the influence of remote features; it could also affect the water exchange through Gibraltar (which depends on the pressure gradients at the Strait) and hence influence Mediterranean MSL. A second model feature that might constrain the long-term evolution of hydrographic variables within the basin is the condition of zero net volume flux through Gibraltar (a consequence of using a rigid-lid model). The large trends of the steric component found in the Western Mediterranean could actually be attributed to a spurious warming of deep waters (S. Somot, personal communication), but the ultimate cause of the warming has not yet been explained. Simple (box) models could help to investigate the effects of model constraints on the mean temperature and salinity of the basin and find out whether they may be causing spurious trends as a response to changes in the heat and freshwater budgets within the basin.

At regional scale, the difficulties of the model to reproduce sea level changes derived for instance from the EMT are more likely due to the heat and freshwater forcing. Beuvier et al. (2008) have recently shown that considering the inter-annual variability of the river runoff and the Black Sea outflow (instead of considering just an annual cycle) has a significant impact on the EMT. In particular, the Black Sea runoff impacts the Aegean convection during the years preceding the EMT, though the timing of the EMT seems more related to the atmospheric forcing.

Regarding the reconstruction, it is worth recalling that the atmospheric contribution was subtracted from the original values shown in Chapter 6 in order to be compared with the model. The trend associated with the atmospheric contribution has a basin mean value of -0.7±0.2 mm/yr, which implies that the total sea level trend for the period

1961-2000 would be 0.3±0.1 mm/yr. Figure 8.8 shows the reconstructed MSL with and without the atmospheric contribution, as well as the atmospheric contribution itself. It shows that the negative trend of the atmospheric contribution lasted until 1990, when it started to recover.

The sea level reconstruction is surely submitted to significant uncertainties. However, the fact that not only the inferred basin MSL follows the behaviour of tide gauge records, but also key regional sea level features such as those associated with the EMT are reproduced, suggests that the reconstruction can be used to check further improvements in the output of regional models. This is particularly important for regions and periods for which historical hydrographic data are sparse.
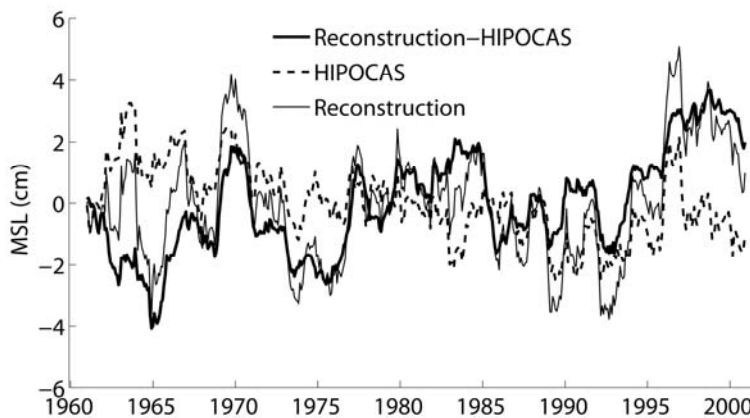
Figure 8.8. Total Mediterranean MSL obtained from the reconstruction with and without the atmospheric contribution. The latter is plotted with a zero mean value.

In the next chapter we attempt to throw some light on the reasons why the model is not able of reproducing some of the major sea level features observed in the Mediterranean Sea. To do this we extend the inter-comparison to 3 baroclinic models, focusing not only on sea level changes, which for instance in the case of the EMT are simply a manifestation of such an event, but also on the hydrodynamic variables that are directly responsible for such changes. In particular, we compare the model outputs with hydrographic data bases and complete our estimation of the steric component of sea level.

Chapter 9

Comparison of results from three baroclinic models of the Mediterranean Sea

T HE[1] marked negative sea level trends in the Ionian Sea and the large positive trends in the Aegean Sea that are shown by satellite altimetry data during the last decade are consequence of the variations during the post-EMT period. In Chapter 8 we have examined Mediterranean sea level variability as estimated by the reconstruction of sea level fields carried out in Chapter 6 and by the OM8 simulation. We have found that while the reconstruction is able to reproduce the major features shown by altimetry during the years after the EMT, the OM8 simulation does not perform so well. In this chapter we compare the results of three different baroclinic models (OM8, MITcgm, ORCA) focusing on the changes in the thermohaline circulation and their impact on sea level, particularly during the EMT. Model results are compared against hydrographic observations for mass properties and steric sea level, and against satellite altimetry data and the reconstruction for sea level.

9.1 Introduction

On average, the Mediterranean Sea loses mass to the atmosphere through an excessive evaporation over precipitation and river runoff. The exchanges with the atmosphere also result in a buoyancy lost, due to the negative surface heat budget. These mass and buoyancy fluxes make that if the basin was not connected to the Atlantic through the Strait of Gibraltar, the Mediterranean sea level would be sinking by over 1 m/year. If this does not occur is because the two negative budgets are compensated by a two-layer lagoonal type thermohaline circulation. Low salinity (36.2 psu) and warmer (15 ℃) Atlantic water gets into the basin in the upper layer through the Strait of Gibraltar.

---

[1] This chapter is based on the paper:
Calafat, F. M., B. Jordà, D. Gomis, M. Marcos. Comparison of results from three baroclinic models of Mediterranean sea. Submitted (2010).

Within the basin, this fresher and warmer Atlantic water is transformed into colder (13.5 ºC) and saltier (38.4 psu) water that subsequently gets out of the basin to the Atlantic through the lower layer. This out-flowing water consists of two distinct water types: the Western Mediterranean Deep Water (WMDW) and the Levantine Intermediate Water (LIW); the second is the main contributor to the Mediterranean outflow and can be found all around the basin at intermediate depths (200-400 m). The transformation of the surface Atlantic water into LIW constitutes the main cell of the Mediterranean thermohaline circulation. Two closed secondary cells, one in each subbasin, complement the main cell: they transform surface and intermediate water into WMDW in the Western basin and into EMDW in the Eastern basin. Although WMDW and EMDW are not directly connected, they are coupled by means of the LIW layer.

Recent observations have shown that the classical pattern of the Mediterranean circulation described above is not as stable as thought before. Indeed, between 1987 and 1995 a new pattern of thermohaline circulation developed in the Mediterranean, with particularly marked changes in the deep thermohaline circulation of the Eastern basin (Roether et al., 1996, 2007). The deepest parts of the Eastern basin were filled by very dense water of Aegean origin that lifted up the older bottom waters of Adriatic origin and changed in a few years the water mass structure of the region. Hydrological observations showed that the marked increase in dense water formation in the Aegean Sea started in 1987 and reached maximum values in 1993 (Theocharis et al., 1999). It was found to be the result of an increase in salinity and a decrease in temperature in the water masses of the Aegean triggered by the extremely cold winter of 1987 (Zervakis et al., 2000) and the reduced Black Sea water outflow during the early nineties. In the previous chapters it has been shown that such change in the thermohaline circulation of the basin clearly reflected on regional sea level changes such as the marked negative trends observed in the Ionian Sea and the strong positive trends observed in the Aegean Sea during the altimetric period 1993-2000.

Several authors have attempted to reproduce the processes and mechanisms involved in the EMT by means of numerical simulations. Lascaratos et al.(1999) reviewed hydrological observations of the last decade and presented some results from numerical simulations. They found that the intensity of the atmospheric forcing is a major factor in the formation of dense water in the Aegean Sea. From 1986 the dense water formation increased during almost every winter. They also found that the dense water of Aegean origin is stored in the deep basins of the south Aegean (in the form of Cretan Deep Water, CDW) and outflows to the Levantine basin first through the eastern strait of the Cretan Arc and then through the western straits. Numerical studies carried out by Stratford and Haines (2002) showed that the role of wind is secondary to the role of buoyancy forcing and that the cooling occurred during the winters of 1987, 1992 and 1993 can trigger the formation of deep water. Nittis et al. (2003) not only point to the very cold winters of 1987, 1992 and 1993, but also to the dry period 1989-1993 that affected the whole Eastern Mediterranean as the main driving mechanisms, being responsible for the 50% and 32%, respectively, of the deep water formed in the Aegean after 1987. The reduced Black Sea Water outflow observed during the same dry period accounted for a 18% of the total formation, while the increase inflow of saline waters from the Levantine Sea after 1992 is recognized as an additional preconditioning factor.

The motivation of this chapter is to gain insight into the reasons why the model used in the previous chapter was unable to reproduce the sea level patterns shown by observations after the EMT. To accomplish such a goal, we compare the outputs of three baroclinic models focusing on water mass formation and on the derived steric and

total sea level. This is why we first present a brief overview of water mass formation processes in the Mediterranean Sea. Then we show results on averaged temperatures and salinities, rates of water formation in selected areas, and total and steric sea level. The outputs of the models are validated against temperature, salinity and sea level observations. A major objective is to end up with the most reliable estimate of steric sea level. Finally we summarize the main conclusion and results.

9.2 A review of water mass formation processes in the Mediterranean Sea

The processes of water mass formation occur in selected areas where deep water formation is favored by oceanic conditions and extreme air-sea interaction processes. This section is devoted to summarize the main water masses formed in the Mediterranean Sea including the water mass changes observed in the Eastern Mediterranean during the EMT. This description intends to help understanding the sea level patterns obtained from the models and to set the stage for a deeper analysis of model results.

9.2.1 Western Mediterranean Deep Water

The WMDW is formed in the Gulf of Lions during winter time by excess cooling and evaporation. The main intensive studies were carried out by the MEDOC group through several oceanographic surveys conducted during the late sixties (MEDOC Group, 1960) and, more recently, by the Theoretical and Experimental Tomography of the Sea (THETIS) Group (Scott et al., 1994, 1996). A main precondition for the formation of WMDW is the presence of a cyclonic gyre in the center of the Gulf of Lions that reduces the stability of the surface layer. The convection area has a diameter of about 100 km and defines the area of dense water formation. Another important factor is the presence of salty LIW at intermediate depths. The occurrence of Mistral (cold and dry northerly winds) events that persist for a few days triggers the mixing of cold surface water with the warmer but saltier LIW, which results in a well-mixed water column that sometimes reaches the ocean bottom (about 2500 m). Convection occurs in plumes with horizontal scales of less than 1 km (Jones and Marshall, 1993) and can end up with a homogeneous water column of newly formed WMDW about 2 weeks after the onset of the Mistral (the water mass characteristics of the WMDW are shown in Table 9.1). The homogeneity of the water column can break up and turn into a rapid stratification of surface water in other 2 weeks. The newly formed WMDW leaves the area, while waters advected by the Ligurian-Provençal Current replace the surface and intermediate waters, leading again to a three-layer stratification.

Table 9.1. Water mass characteristics of Western Mediterranean Deep Water as reported by different authors (from Castellari et al. 2000).

Authors	T (ºC)	S (psu)	σ_θ (kg/m^3)
MEDOC Group (1970)	12.70 - 12.90	38.42 – 38.45	29.10
Ovchinnikov et al. (1987)	12.85	38.45	29.10
Leaman and Schott (1991)	12.80	38.44	29.10
Rohling and Bryden (1992)	12.70	38.40	29.10

9.2.2 Eastern Mediterranean Deep Water

The EMDW is mainly formed to the south of the Adriatic Sea, with small contributions from the dense water formed in the northern Adriatic. The latter forms during the winter season and flows to the south along the western coast, where deep convection and mixing with the incoming LIW takes place. The newly formed deep water, referred to as the Adriatic Deep Water (ADW), has a typical temperature of 13ºC and salinity of 38.65 psu (Gacic et al., 1996). The ADW exits the Adriatic through the Strait of Otranto, filling the deepest parts of the Ionian Sea and then of the Levantine basin, where it becomes EMDW. This water mass is very homogenous in temperature and salinity (see Table 9.2) and can be found everywhere in the Eastern Mediterranean below an average depth of 1200 m.

The Aegean Sea has also been suggested as a possible source of deep water by many authors (Wüst, 1961; Miller, 1963; Malanotte-Rizzoli and Hecht, 1988). However results show that it has at most been an occasional and minor contributor to EMDW (Theocaris et al., 1999). Hydrographic and tracer data obtained in 1987 (Schlitzer et al., 1991) provided evidence of water of Aegean origin, but this water was identified as the intermediate water referred to as Cretan Intermediate Water (CIW) and its properties are intermediate between those of LIW and EMDW (Malanotte-Rizzoli et al., 1999).

As it has been commented before, the role played by the Aegean Sea changed significantly in 1987 due to the EMT event. This new state of the thermohaline circulation in the Eastern Mediterranean is described in more detail in subsection 9.2.4.

Table 9.2. Water mass characteristics of Eastern Mediterranean Deep Water as reported by different authors (from Castellari et al. 2000).

Authors	T (ºC)	S (psu)	σ_θ (kg/m^3)
Pollak (1951)	13.60	38.70	29.10
Ovchinnikov et al. (1987)	13.44 – 13.75	38.70-38.85	29.20 – 29.24

9.2.3 Levantine Intermediate Water

LIW is the main contributor to the Mediterranean outflow into the Atlantic and it is found all around the basin at intermediate depths (200-400 m). It is also the major component of the westward flow through the Strait of Sicily. The characteristics of LIW as reported by different authors are shown in Table 9.3. The main formation area (but not the only one) is thought to be the center of the Rhodes gyre (Lascaratos et al., 1993). Lascaratos and Nittis (1998) reached the same conclusion when they studied the Levantine basin by means of a three-dimensional oceanic model and found that LIW was only formed where the doming of isopycnals inside the Rhodes gyre facilitates deep mixing. However, Nittis and Lascaratos (1998) also found that during cold winters intermediate water was formed all over the north Levantine basin, while deep water was formed inside the Rhodes gyre. They showed that these processes are mainly controlled by the variability of the mean buoyancy loss and the characteristics of the synoptic scale atmospheric events over the area.

Table 9.3. Water mass characteristics of Levantine Intermediate Water as reported by different authors (from Castellari et al. 2000).

Authors	T (ºC)	S (psu)	σ_θ (kg/m^3)
Wust (1961)	15.50	39.10	29.05
Lacome and Tchernia (1972)	15.70	39.10	28.98
Ozturgut (1976)	16.20 – 16.40	39.12 – 39.15	28.85 – 28.86
Ovchinnikov (1984)	14.70 – 14.90	39.03 – 39.06	29.12 – 29.15
Plakhin and Smirnov (1984)	14.50	38.85	29.06
Hecht (1986)	15.50 ± 0.40	39.02 ± 0.05	28.91 – 29.01
Lascaratos et al. (1993)	15.00 – 16.00	38.95 – 39.05	28.85 – 29.10

9.2.4 The Eastern Mediterranean Transient

Hydrological observations showed that the increased in dense water formation in the Aegea Sea started in 1987 and reached maximum values in 1993 (Theocharis et al., 1999). Roether et al. (1996) showed that by 1995 as much as 20% of the EMDW below 1200 m had been replaced by this new dense Aegean overflow. Lascaratos et al.(1999) found that the waters of the Cretan Sea located at 1000 m depth increased their density throughout the period 1987-1995, first (1987-1992) due to an increase in salinity and later (1992-1995) due to a decrease in temperature (about 0.4ºC). They estimated the average formation rate of deep water of Aegean origin to be 1.2 Sv (taking 1989 as the starting year of the EMT). Theocharis et al. (1999) found very similar results when they showed that the σ_θ = 29.2 kg/m^3 level in the Cretan Sea shoaled from 1988 up to 1992 when it reached a minimum depth. After 1992 it deepened again. The isopycnal 29.2 kg/m^3 has been considered as the lower limit of the CDW (Theocharis et al., 1999).

After 1995 the situation returned back to normal: the Aegean Sea returned to pre-EMT conditions, exporting small amounts of dense water that do not reach the bottom of the Ionian and the Levantine basins (Theocaris et al., 2002) while the Adriatic Sea became again the main contributor to the dense waters of the Eastern Mediterranean (Klein et al., 2000; Manca et al., 2006).

9.3 Results

The model intercomparison extends to the whole common period 1961-2000, paying particular attention to the EMT as one of the most relevant features of the steric and total Mediterranean sea level variability of the last decades. The baroclinic models used for this analysis were described in Chapter 4: MITgcm, OM8 and ORCA. The three models have recently been validated by several authors (references are given in Chapter 4). Here we present additional comparisons against hydrographic observations and also in terms of sea level.

The comparison is presented in two parts: the first one is devoted to the study of dense water formation processes in the Aegean and Adriatic seas, and it is aimed to understand why the models reproduce better or worse the sea level changes observed during the EMT. Model results are compared with the MEDAR climatology described in Chapter 3, which spans the full water column.

The second part focuses on total and steric sea level variability. In the case of total sea level, results are presented for two different periods: 1993-2000 and 1961-2000. For

the first period (1993-2000) results are compared against altimetry observations, while for the total period (1961-2000) we use the reconstruction obtained in Chapter 6. Steric sea level obtained from models is validated against the steric sea level computed from hydrographic observations. The Ishii data set is used here instead of MEDAR data for two reasons. First, the Ishii data set provides an error estimate for both temperature and salinity, which can be used to obtain an estimation of the error associated with the steric sea level, as described in Chapter 3. Second, the Ishii data has a monthly time resolution, while MEDAR provides only annual values. The drawback is that the Ishii data only span the upper 700 m of the ocean.

9.3.1 Water mass properties

Potential temperature and salinity from the models are compared with the MEDAR climatology in terms of basin averages. The comparison is carried out for the whole Mediterranean basin, for the Eastern and Western subbasins and since we are particularly interested in the study of the EMT also for the Aegean and Adriatic Seas.

Averaged temperature and salinity

The 3D average of a given variable ($\langle X \rangle$) has been computed by means of the formula:

$$\langle X \rangle = \frac{\iiint\limits_{V} X(x, y, z)\, dx\, dy\, dz}{\iiint\limits_{V} dx\, dy\, dz} \tag{9.1}$$

where X represents temperature, salinity or density, and V is the volume of the water basin where the average is carried out. The different volume of the cells of the model grid is to be taken into account when computing (9.1). In Table 9.4 the 3D basin-averaged temperature and salinity obtained from the models are also averaged in time (over the period 1961-2000) and compared with MEDAR climatological values. Good agreement is found between all models and MEDAR, both for temperature and salinity. The closest results to MEDAR values are given by the MITgcm model, with a difference in temperature of only -0.04ºC and no difference at all in salinity. Largest biases are found for the ORCA model (0.22ºC in temperature and -0.03 in salinity).

Table 9.4. Temperature and salinity averaged over the whole Mediterranean basin (from surface to bottom) and over the time period 1961-2000 for the three baroclinic models. The equivalent values for the MEDAR climatology are also given.

	MEDAR	MITgcm	ORCA	OM8
T (ºC)	13.90	13.86	14.12	13.99
S (psu)	38.62	38.62	38.59	38.61

Figure 9.1 shows the 3D basin-averaged temperature and salinity computed over the

period 1961-2000 as given by the three models and the MEDAR climatology. In temperature, the interannual variability shown by the models is very similar; all them reproduce the main features, particularly the peaks. On the other hand, the bias between the models is well apparent and, most importantly, all models show a positive trend that is not observed in MEDAR data. This is attributed to a spurious drift in the temperature of intermediate and deep layers that is more important in the Western basin.

With regard to salinity, the three models show a much smoother variability than observations. In fact, the most significant variation is the absolute salinity minimum obtained around 1997 by the MITgcm model, followed by an increase of about 0.02 psu. The salinity biases quantified in Table 9.4 are clearly visible in Figure 9.1. Unlike for temperature, the models do not show a clear salinity trend, while observations do show a clear increase along the sampled period.
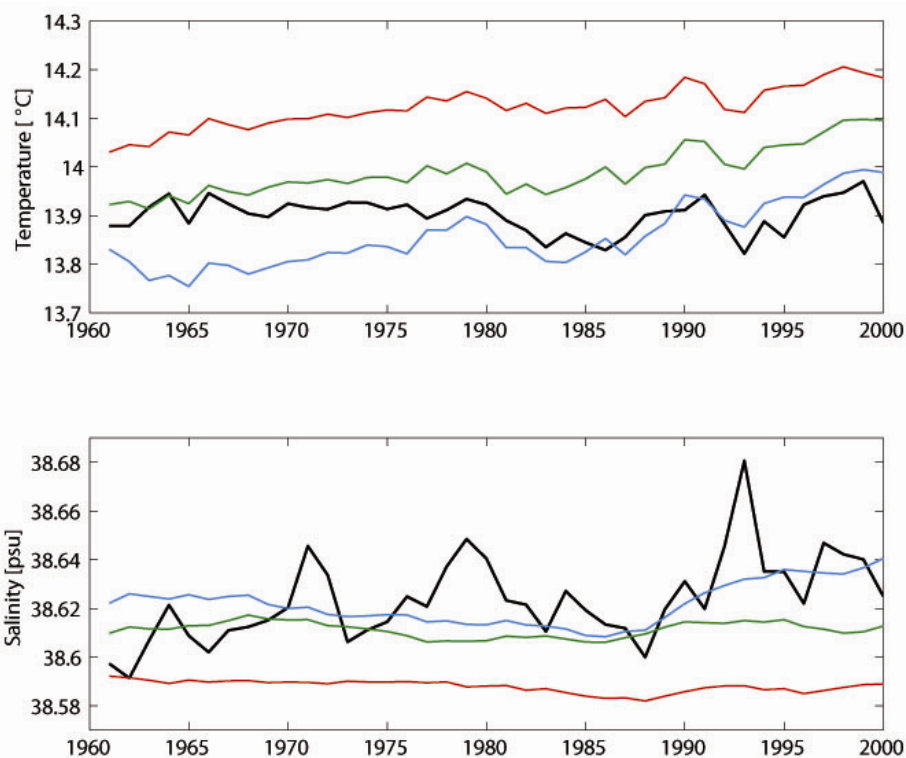
Figure 9.1. 3D basin-averaged temperature (top) and salinity (bottom) computed over the period 1961-2000 for the MITgcm (blue line), the ORCA (red line) and the OM8 (green line) models. The black line has been obtained from MEDAR data.

Temperature and salinity have also been averaged for the Western and Eastern basins. The comparison is shown in four layers: 0-100 m, 100-500 m, 500-1000 m and 1000-2000 m and the linear trend has been subtracted from each series for an easier comparison (Fig. 9.2). We have also computed the correlations (Table 9.5) and biases (Table 9.6) between the three models and MEDAR, and the temperature and salinity trends (Table 9.7) obtained from the models and MEDAR.

For the top 100 m and for both the Eastern and Western basins (Figs. 9.2a,b) the observed temperature variability is, on average, larger than the variability of the models. It is worth noting here that there are two versions of the MEDAR climatology; one, in

which the mean annual cycle is removed prior to the computation of the annual means and one in which no correction is applied. In the second, part of the intra-seasonal variability can be poured into interannual scales when the spatial and temporal distribution of the data is particularly sparse. Obviously the comparison between models and this second version of MEDAR is not as good as when the corrected MEDAR version is used (Tsimplis et al., 2009). Here we have used the uncorrected version because it is the only one that is available.

Correlations between models and MEDAR for the top 100 m are lower than 0.43 (Table 9.5) in both the Eastern and Western subbasins. When the seasonally corrected MEDAR version is used, the correlation with the OM8 model increases up to 0.7 (Tsimplis et al., 2009). When using the Ishii data set, the correlation between upper layer temperatures is over 0.8 in both subbasins and for all models. Regarding biases, the MITgcm model shows the largest bias in both the Eastern and the Western subbasins (-1.00 ºC and -0.64 ºC, respectively, see Table 9.6). This cold bias is in good agreement with the -0.7 ºC bias found by Sannino et al. (2009) for the sea surface temperature computed over the whole basin. The OM8 is the model that shows smaller bias in both subbasins (-0.06 ºC and 0.23 ºC).

For the layer 100-500 m, the models and the MEDAR averaged temperature variability is in good agreement in both subbasins (Figs. 9.2a,b). The OM8 is the model showing the highest correlations (0.73 and 0.92 in the Eastern and Western subbasins, respectively, see Table 9.5) and the MITgcm is the model that better represents the time-mean temperature, with biases of only -0.11ºC and 0.01ºC in the Eastern and Western Mediterranean, respectively (Table 9.6). A major feature observed in this layer is the cooling of the Western Mediterranean between 1980 and 1990, which is clearly shown by MEDAR and by the models.

For the layer 500-1000 m, the model that better reproduces the major features of the averaged temperature variability in the Eastern Mediterranean (Fig. 9.2a) is the MITgcm, showing a correlation of 0.5 (Table 9.5) and a bias of 0.18 ºC (Table 9.6). The other two models do not describe this layer successfully in the Eastern Mediterranean, although the time-mean temperature simulated by ORCA is in very good agreement with MEDAR (the bias is only of 0.04ºC), the variability is by far too smoothed. In the Western Mediterranean both the MITgcm and the OM8 show a very good agreement when compared with MEDAR (Fig. 9.2b), with correlations of 0.82 and 0.86, respectively. The ORCA model does not show a significant correlation with the MEDAR temperature, again because of the smooth variability. The MITgcm shows the smallest temperature bias (0.23 ºC), while the OM8 shows the largest one (0.63 ºC).

For the layer below 1000 m none of the models reproduce the MEDAR temperature variability; the three of them and particularly ORCA show a very smooth behaviour (Figs. 9.2a,b). The biases with respect to MEDAR are all small, the smallest one being that of the MITgcm model in both the Eastern and Western basins (-0.02ºC and 0.01ºC respectively, see Table 9.6).
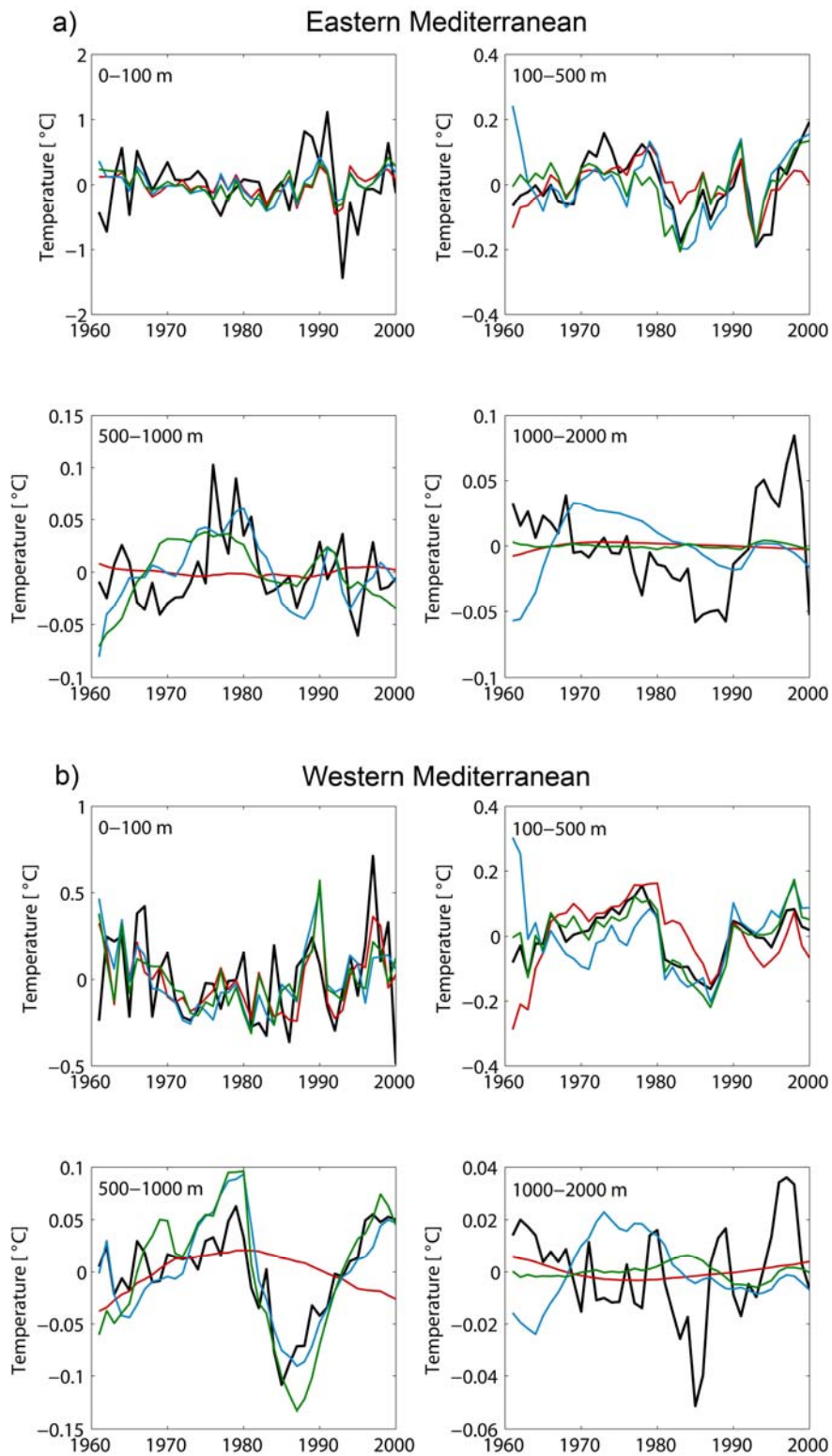
Figure 9.2. Temperature and salinity anomalies over the period 1961-2000 averaged over the Eastern Mediterranean (a,c) and the Western Mediterranean (b,d) for four different layers: 0-100 m, 100-500 m, 500-1000 m and 1000-2000 m. They have been estimated from MEDAR (black line) and from the three models: MITgcm (blue line), ORCA (red line) and OM8 (green line). Linear trends have been removed from all time series.
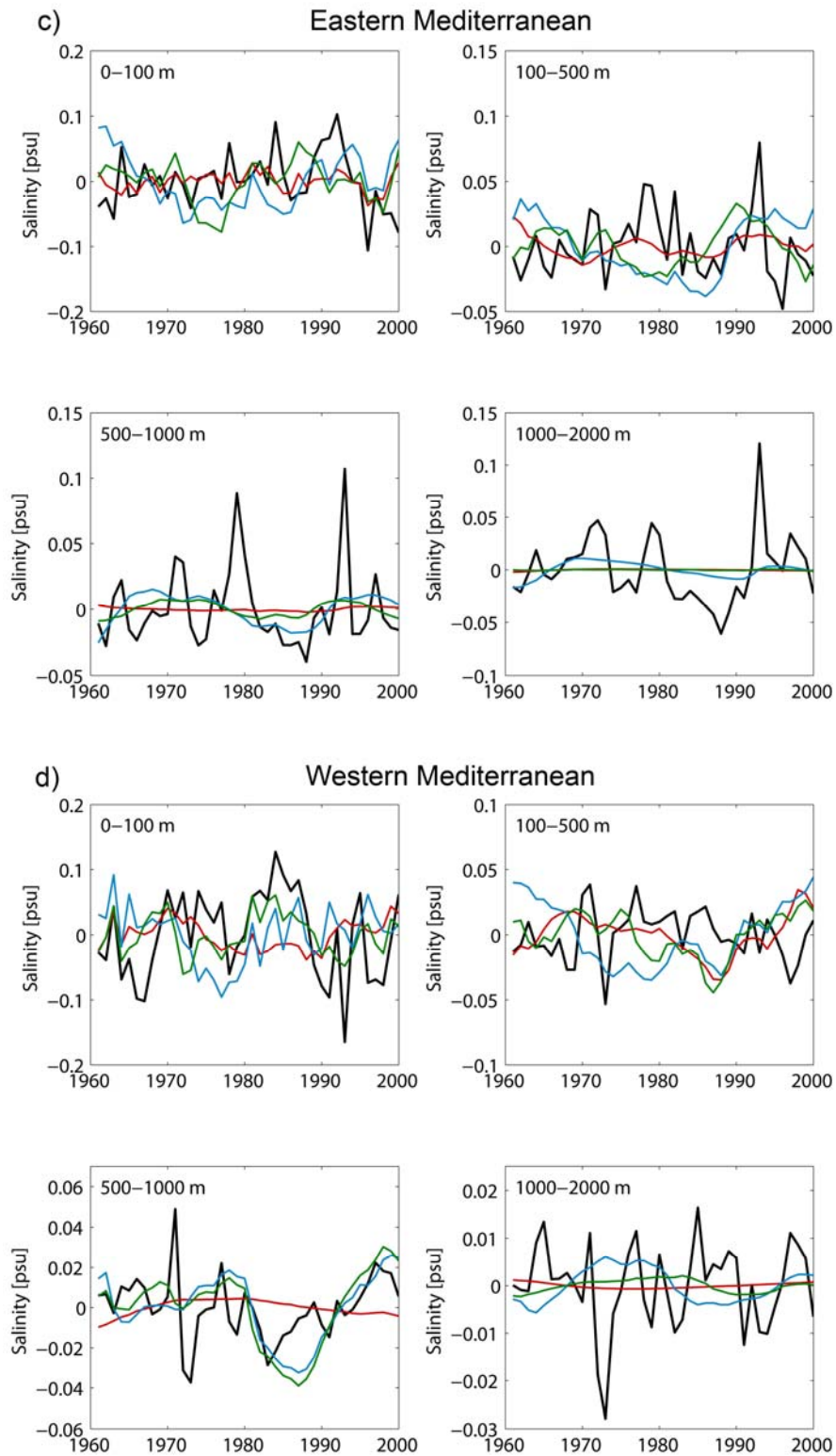
Figure 9.2. (Continued).

With regard to temperature trends, the most remarkable feature is the warming drift shown by all models in the intermediate and deep layers, especially in the Western Mediterranean (Table 9.7). In the layer 500-1000 m all models show large trends of up to 0.0130 ºC/year in the Western subbasin, while the MEDAR trend is of only 0.0022ºC/year. Below 1000 m only the MITgcm and OM8 models show such a drift (0.0097 ºC/year and 0.0062 ºC/year). The reason for the drifts is a too weak average surface heat loss with respect to the Gibraltar Strait net heat transport (Somot and Colin, 2008). The warming trend will lead to unrealistic large steric sea level trends shown later in this chapter.

The agreement between the salinity variability computed from the models and from MEDAR is not as good as for the temperature (Figs. 9.2c,d). In the Eastern Mediterranean none of the models show significant correlations with MEDAR at any layer (Table 9.5). In the Western Mediterranean, the OM8 model shows a significant correlation of 0.5 in the upper layer, and in the layer 500-1000 the MITgcm and OM8 models show correlations of 0.4 and 0.5, respectively. No significant correlation is found in the other layers. In the top 500 m, the ORCA model shows much fresher waters than MEDAR and the other two models in both subbasins, with a maximum bias of -0.37 psu with respect to MEDAR (in the upper layer of the Western Mediterranean). It is also worth noting that models show very little inter-annual variability compared to MEDAR, especially the ORCA model. For the upper layer the discrepancies can be attributed to the fact of using the non-corrected version of MEDAR (salinity data are spatially sparser than temperature observations), but arguing the same reason for intermediate and deeper layers is more risky, since the intra-seasonal variability is much smaller at these layers than for the upper layer.

Table 9.5. Correlations (computed over the period 1961-2000) between basin mean temperature and salinity given by the models and by MEDAR. They have been computed for the Western and Eastern Mediterranean basins. NS means that the correlation is non-significant.

	TEMPERATURE CORRELATION					
Layer	**Western Mediterranean**			**Eastern Mediterranean**		
	MITgmc	**ORCA**	**OM8**	**MITgmc**	**ORCA**	**OM8**
0-100	0.39	0.43	0.28	0.29	NS	0.29
100-500	0.47	0.69	0.92	0.65	0.72	0.73
500-1000	0.82	NS	0.86	0.50	NS	NS
1000-2000	NS	NS	NS	NS	NS	NS

	SALINITY CORRELATION					
Layer	**Western Mediterranean**			**Eastern Mediterranean**		
	MITgmc	**ORCA**	**OM8**	**MITgmc**	**ORCA**	**OM8**
0-100	NS	NS	0.48	NS	NS	0.28
100-500	-0.35	NS	NS	NS	NS	NS
500-1000	0.40	NS	0.47	NS	NS	NS
1000-2000	NS	NS	NS	NS	NS	NS

Table 9.6. Bias between the basin mean temperature and salinity given by the models and MEDAR. They have been computed for the Western and Eastern basins for the period 1961-2000.

	TEMPERATURE		BIAS [ºC]			
Layer	**Western Mediterranean**			**Eastern Mediterranean**		
	MITgmc	**ORCA**	**OM8**	**MITgmc**	**ORCA**	**OM8**
0-100	-0.64	0.32	0.23	-1.00	0.21	-0.06
100-500	0.01	0.85	0.69	-0.11	0.32	0.43
500-1000	0.23	0.33	0.63	0.18	0.04	0.33
1000-2000	0.01	0.05	-0.08	-0.02	0.12	-0.13

	SALINITY		BIAS [psu]			
Layer	**Western Mediterranean**			**Eastern Mediterranean**		
	MITgmc	**ORCA**	**OM8**	**MITgmc**	**ORCA**	**OM8**
0-100	0.043	-0.37	-0.124	0.013	-0.220	-0.046
100-500	-0.142	-0.080	-0.056	-0.074	-0.110	-0.058
500-1000	0.020	0.013	0.058	0.035	-0.043	0.017
1000-2000	0.035	0.006	0.012	0.040	0.018	-0.013

Table 9.7. Linear trends and their associated uncertainty (computed with a robust bootstrap) for the basin mean temperature and salinity estimated from the models and from MEDAR. They have been computed for the Western and Eastern Mediterranean basins over the period 1961-2000.

	WESTERN MEDITERRANEAN [ºC/year]			
Layer	**0-100**	**100-500**	**500-1000**	**1000-2000**
MEDAR	-0.0019 ± 0.0042	0.0000 ± 0.0011	0.0022 ± 0.0005	0.0027 ± 0.0002
MITcgm	0.0060 ± 0.0026	0.0041 ± 0.0012	0.0080 ± 0.0006	0.0097 ± 0.0004
ORCA	0.0002 ± 0.0029	0.0081 ± 0.0012	0.0132 ± 0.0006	0.0006 ± 0.0001
OM8	0.0083 ± 0.0022	0.0058 ± 0.0011	0.0129 ± 0.0008	0.0062 ± 0.0001

	EASTERN MEDITERRANEAN [ºC/year]			
Layer	**0-100**	**100-500**	**500-1000**	**1000-2000**
MEDAR	-0.0216 ± 0.0077	-0.0076 ± 0.0014	-0.0003 ± 0.0004	0.0005 ± 0.0003
MITcgm	0.0014 ± 0.0028	-0.0024 ± 0.0015	0.0037 ± 0.0005	0.0067 ± 0.0002
ORCA	0.0000 ± 0.0023	0.0033 ± 0.0008	0.0035 ± 0.0001	0.0002 ± 0.0004
OM8	0.0003 ± 0.0030	-0.0038 ± 0.0011	0.0060 ± 0.0003	0.0044 ± 0.0001

	WESTERN MEDITERRANEAN [psu/year]			
Layer	**0-100**	**100-500**	**500-1000**	**1000-2000**
MEDAR	0.0028 ± 0.0009	0.0018 ± 0.0002	0.0011 ± 0.0002	0.0011 ± 0.0001
MITcgm	-0.0017 ± 0.0006	-0.0011 ± 0.0006	0.0006 ± 0.0002	0.0014 ± 0.0001
ORCA	-0.0018 ± 0.0003	-0.0012 ± 0.0003	0.0012 ± 0.0001	0.0001 ± 0.0001
OM8	-0.0008 ± 0.0005	0.0004 ± 0.0002	0.0009 ± 0.0001	0.0004 ± 0.0001

	EASTERN MEDITERRANEAN [psu/year]			
Layer	**0-100**	**100-500**	**500-1000**	**1000-2000**
MEDAR	-0.0005 ± 0.0007	0.0003 ± 0.0003	0.0002 ± 0.0003	0.0004 ± 0.0004
MITcgm	-0.0022 ± 0.0006	-0.0043 ± 0.0002	0.0003 ± 0.0002	0.0006 ± 0.0001
ORCA	-0.0002 ± 0.0003	-0.0009 ± 0.0001	-0.0001 ± 0.0001	0.0000 ± 0.0001
OM8	-0.0028 ± 0.0004	0.0017 ± 0.0002	0.0005 ± 0.0001	0.0007 ± 0.0001

Because the Ishii climatology is used later in this chapter to estimate the steric sea level, it is also worth comparing the model averaged temperature and salinity with the Ishii data set. In that case the comparisons are restricted to the upper 700 m, since this is the maximum depth covered by Ishii data. Namely, we have computed the temperature and salinity average only for the layers 0-100 m and 100-500 m.

The averaged temperature obtained from the Ishii data set is in very good agreement with models in both subbasins and for both layers (Fig. 9.3). In the upper layer, all models show correlations over 0.85 in both subbasins. The reason for the higher correlation with Ishii data than with uncorrected MEDAR data seems clear: the upper layer is the one most affected by the seasonal cycle and therefore by the eventual aliasing of seasonal variability onto larger time scales reported for the MEDAR data set. The Ishii data set does not suffer for this problem, since observations are gridded on a monthly basis (the annual means are computed later on from monthly values). This reflects for instance in the smaller interannual variability of Ishhi data (Figs. 9.3a,b) with respect to uncorrected MEDAR data (Figs. 9.2a,b).

For the layer 100-500 m correlations are also high, although there are some differences. In the Western Mediterranean the MITgcm model shows a correlation of 0.45 as compared to the 0.91 obtained for the OM8 model. In the Eastern Mediterranean correlations are more similar ranging from the 0.7 obtained for the MITgcm model to the 0.84 obtained for the ORCA model. For this layer the Ishii and MEDAR averaged temperatures (Figs. 9.3a,b and Figs. 9.2a,b) are almost identical, since the impact of the seasonal cycle (and therefore of the eventual bias onto larger scales in the MEDAR data) is small below 100 m.

With regard to salinity, none of the models reproduce the Ishii inter-annual variability successfully (Figs. 9.3a). When comparing Ishii (Figs. 9.3a,b) and MEDAR (Figs. 9.2c,d) salinities, they coincide in the major features, but they are far from being identical. This is likely a consequence of the small number of salinity observations, which translates in a larger dependence on which observations are included in each data base and on the interpolation method. On the other hand, the differences between the two data bases are not larger for the 0-100 m layer than for the 100-500 layer; this is likely a consequence of the smaller salinity seasonal cycle with respect to temperature.

Dense water formation rates

In Chapter 8 we showed that the OM8 model is unable to reproduce the sea level changes associated with the EMT. Now we pretend to understand the reasons why the model does not reproduce those changes, and this implies to analyze the driving mechanisms. It is reasonable to assume that models that show the increase in deep water formation observed in the Aegean during the years between 1987 and 1995 will also perform better in reproducing the sea level changes observed during those years. We will then focus on the different model results for water formation rates in the Adriatic and Aegean Seas.

The dense water formation process is often visualized using the depth of selected isopycnal surfaces. When an isopycnal that characterizes intermediate or deep layers outcrops the surface it indicates that the corresponding layer is ventilated and that dense water is formed. In order to quantify the inter-annual variability of dense water formation in the Adriatic and Aegean Seas, we have computed the annual formation rates following the methodology of Lascaratos and Nittis (1998). This methodology
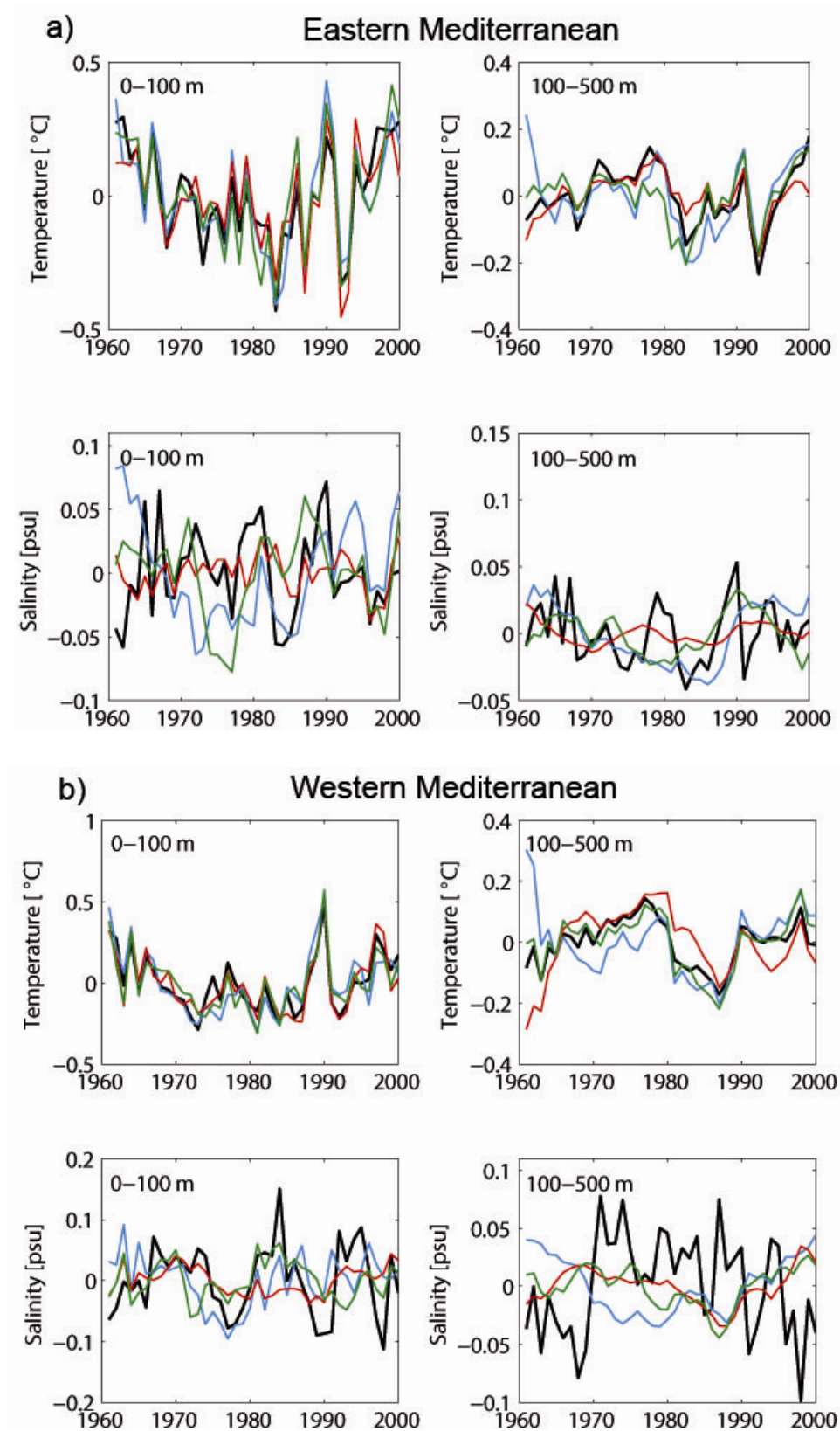
Figure 9.3. Temperature and salinity anomalies over the period 1961-2000 averaged over the Eastern Mediterranean (a) and the Western Mediterranean (b) for two different layers: 0-100 m and 100-500 m. They have been estimated from the Ishii data set (black line) and the three models: MITgcm (blue line), ORCA (red line) and OM8 (green line). Linear trends have been removed from all time series.

consists of computing the volume of water with potential density greater than a selected value for every month of the simulation. Then for every year the difference between the maximum volume after the winter season and the minimum volume before the winter season is computed and divided by the number of seconds in a year to obtain the formation rate. In order to make the comparison between models as reliable as possible, we have introduced a slight modification in that methodology: we will quantify mass instead of volume by multiplying the volume of each cell by its potential density. This is to take into account the fact that denser water in a model cell can diffuse to other cells resulting in a higher volume of dense water.

Formation rates have been estimated for deep and intermediate waters. The characteristics of the two mass waters can be obtained from Section 9.2, where we reported that the isopycnal 29.2 kg/m^3 is considered to be the lower limit of the CDW (Theocharis et al., 1999) and that LIW has a potential density ranging between 28.85 and 29.15 kg/m^3 (Table 9.3). A further consideration is needed before quantifying the rates: models have been shown to have some biases in temperature and salinity and hence in potential density. Therefore, using the same value of the potential density for all models could lead to wrong conclusions, since it might not correspond to the model limit between intermediate and deep waters, for instance. In order to overcome this problem, we use different values of the potential density for each model, basing on the averaged potential density of selected layers. For deep waters we computed the time-mean of the averaged potential density corresponding to the waters below 2000 m in the Eastern Mediterranean. The values of the potential density obtained are: 29.18 kg/m^3, 29.13 kg/m^3 and 29.18 kg/m^3 for the MITgcm, ORCA and OM8 models, respectively. The minimum potential density for the formation of intermediate waters will be computed as the time-mean of the averaged potential density in the layer 200-500 m. For this layer, the obtained values are: 29.01 kg/m^3, 28.93 kg/m^3 and 28.93 kg/m^3 for the MITgcm, ORCA and OM8 models, respectively.

Figure 9.4 shows the computed dense water formation rates in the Aegean and Ionian Seas for the three models. In the Aegean Sea the only model that shows a significant formation of deep water is MITgcm (Fig. 9.4a, top). For this model, the maximum deep water formation rates in the Aegean are found during the extreme winters of 1992-1993. The OM8 model also shows a deep water formation peak during those years, but it is much smaller than the one shown by the MITgcm model. The ORCA model does not show formation of deep water in this area at all. In the Adriatic Sea (Fig. 9.4a, bottom), a regular formation of deep water is shown by all models. The MITgcm model is again the one showing larger rates, though the differences between the MITgcm and OM8 models are smaller than for the Aegean Sea. The ORCA model shows a much smaller formation rate than the other two models in this region too.

With regard to the formation of intermediate water in the Aegean Sea (Fig. 9.4b, top), both the OM8 and MITgcm models show similar rates. The formation rate given by the ORCA model are again much lower. The most prominent features are the two maximum peaks obtained in 1983 (not shown by the ORCA model) and during the period 1992-1993. It is worth noting that for the intermediate waters, the maximum values of formation rates during those years are shown by the OM8 rather than by the MITgcm model. In the Adriatic Sea (Fig. 9.4b, bottom), the MITgcm and OM8 models show similar overall formation rates of intermediate water. While the formation of intermediate water shown by the ORCA model is also regular, it is much less intense than for the other two models.
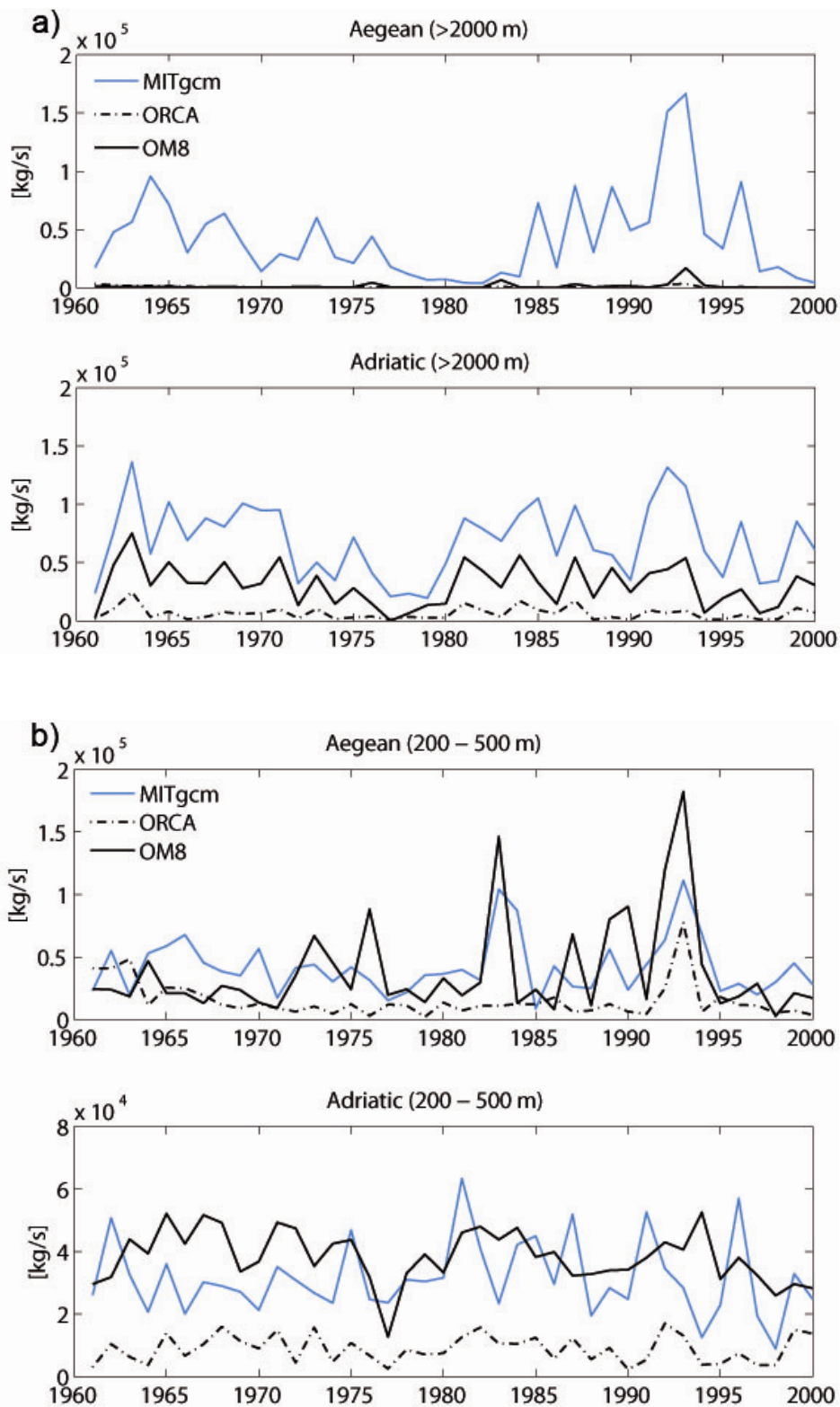
Figure 9.4. Time series of dense water annual formation rates (kg/s) in the Aegean and Ionian Seas as obtained from the MITgcm (blue line), ORCA (dashed-dotted line) and OM8 (black line) models. The formation rates have been estimated for (a) deep (>2000 m) water; (b) intermediate (200-500 m) water.

Summarizing, the MITgcm is the only model showing a significant formation of deep water in the Aegean Sea, especially during the years of the EMT event. This model also shows important rates of intermediate water formation in this area. The OM8 model also shows formation of dense water in the Aegean Sea, but most of it in the form of intermediate water. The newly formed Aegean Sea dense water obtained by this model is not dense enough to sink to the bottom of the Levantine basin.. Finally, the ORCA model shows very weak formation rates for either the deep and intermediate water both in the Aegean and Adriatic Seas.

For a better assessment of the dense water formation mechanisms, annual averaged water properties such as temperature, salinity and potential density, have been estimated in the Aegean Sea over the period 1961-2000. The averages have been computed for the layers 0-100 m, 100-500 m, 500-1000 m and 1000-2000 m (Fig. 9.5), as we did for the Eastern and Western basins. Results are very clarifying and explain why the MITgcm model is the only one showing formation of deep water in the Aegean Sea during the years of the EMT.

As it was commented in Section 9.2.4, Lascaratos et al. (1999) showed that the waters located at about 1000 m depth in the Cretan Sea (to the south of the Aegean Sea) increased their density during the period 1987-1995. The MITgcm model clearly shows a pronounced density increase in the layers 100-500 m and 500-1000 m during that period, with a maximum peak in 1993 (Fig. 9.5c). The OM8 model also shows a density increase and a maximum peak in 1993 in the layer 100-500 m, but they are not observed in the layer 500-1000 m. Apart from a weak peak in 1993, the ORCA model does not show any increase in density during that period.
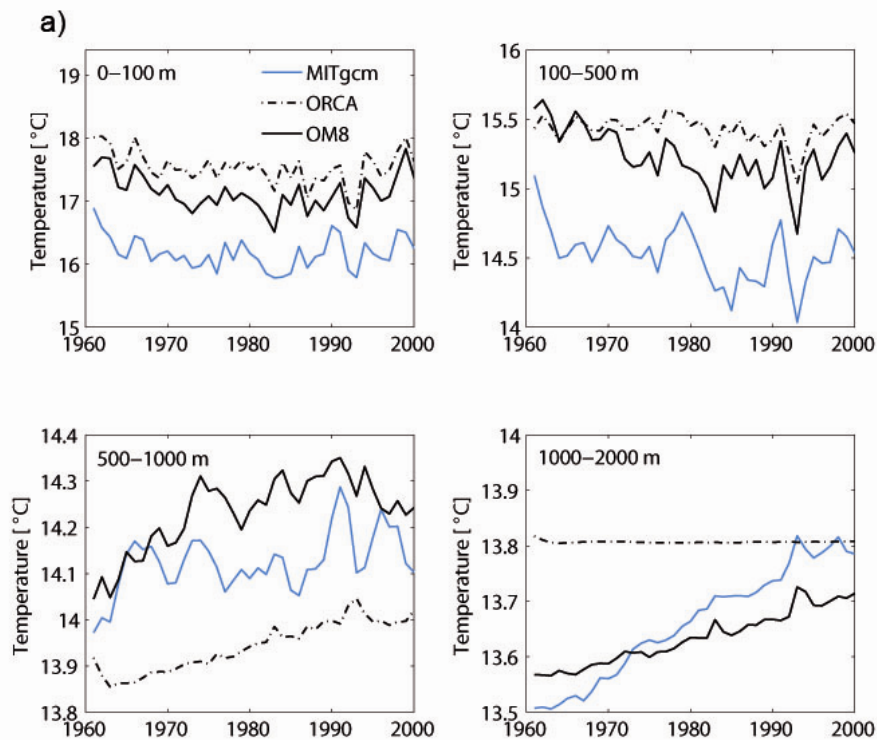
Figure 9.5. Annual averaged temperature (a), salinity (b) and potential density (c) in the Aegean Sea over the period 1961-2000 for the layers 0-100 m, 100-500 m, 500-1000 m and 1000-2000 m as given by the MITgcm (blue line), ORCA (dashed-dotted line) and OM8 (black line).
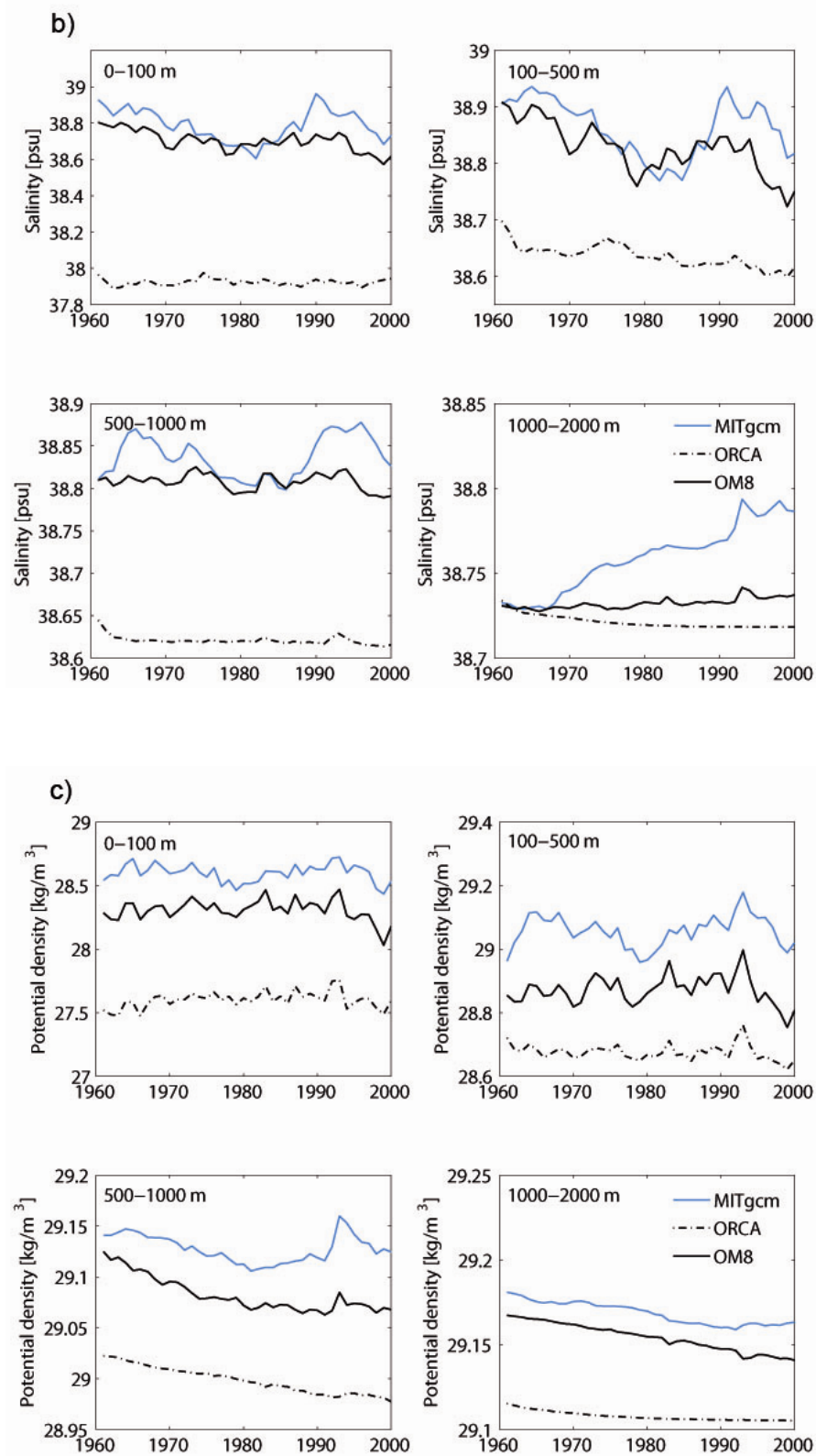
Figure 9.5. (continued)

The increase in density was first due to an increase in salinity during the period 1987-1992 and later (1992-1995) to a decrease in temperature (Lascaratos et al, 1999). This is well reproduced by the MITgcm, which shows both, a salinity increase throughout the whole water column from 1986 to 1992 and a pronounced decrease in temperature in the top 1000 m during the years 1992-1993. The other two models also show a decrease in temperature for the top 500 m during the years 1992-1993, but they do not show any salinity increase for the period 1987-1992. Nittis et al. (2003) showed that the dry period 1989-1993 that affected the whole Eastern Mediterranean and the derived salinity increase were important preconditioning mechanisms for dense water formation in the Aegean Sea during the EMT years. This would explain why the MITgcm model is the only one showing deep water formation in the Aegean Sea, while the other two models only show intermediate water formation in this area. Moreover, the MITgcm model reproduces the increased water formation rates not only during the cold winters of 1987 and 1992-1993 but also during the period in between, characterized by relatively mild winters. This is in good agreement with the results based on observations shown by Theocharis et al. (1999) and with the numerical simulation carried out by Nittis et al. (2003) and should be attributed to the preconditioning of the 1987 winter and to the increased buoyancy loss due to the freshwater anomaly that took place during the period 1989-1990.

9.3.2 Sea level variability and trends

The results obtained in the last section show that the MITgcm model is the only one reproducing the major features of the EMT. Consequently, we also expect this model to be the only one reproducing the sea level changes associated with the EMT that were captured by satellite altimetry during the period 1993-2000. In this section we show a comparison of the sea level variability and trends obtained from the three models. Results are presented for two different periods; for the period 1993-2000, total sea level from the models is compared to total sea level obtained from satellite altimetry; for the period 1961-2000, total sea level from the models is compared to the reconstruction obtained in Chapter 6. It is worth recalling again that sea level provided by the models does not account either for remote mass changes (i.e., mass increase due to ice melting) or the atmospheric component; it only account for steric changes and circulation changes. Hence, the atmospheric component has been removed from the reconstructed sea level by using the HIPOCAS data (in the same way as it was done in Chapter 8). Also the steric component of sea level has been computed for all models. Again, particular attention will be devoted to the regions that played a major role in the general picture of the EMT: the Aegean and Ionian basins.

Sea level trends for the period 1993-2000

The OM8 has already been compared with altimetry data and with the reconstruction in Chapter 8 and thus maps of the OM8 trend distributions are not shown here. Figures 9.6a,b show the distribution of sea level trends for the period 1993-2000 as obtained from the MITgcm and ORCA models. The main features of the distribution of sea level trends obtained from altimetry data (Fig. 8.1a) are well reproduced by the MITgcm. Indeed, it shows strong negative trends (up to -13 mm/yr) in the Ionian Sea and marked positive trends in the Levantine basin with a maximum peak to the south of Crete (up to

20 mm/yr). The values of the trends in the Aegean Sea are of the same order as the ones shown by altimetry data and the ones in the Ionian Sea are only slightly smaller. Moreover, the negative trends cover a wide part of the Ionian Sea, in good agreement with altimetry. The trend pattern shown by the ORCA model (Fig. 9.6b) is more similar to the OM8 one (Fig. 8.1c) than to the altimetry pattern. It reproduces the strong positive trends in the Levantine basin found with altimetry, though the trends are weaker. However it does not succeed to reproduce the strong negative trends in the Ionian Sea (instead, it shows marked positive trends in that region).
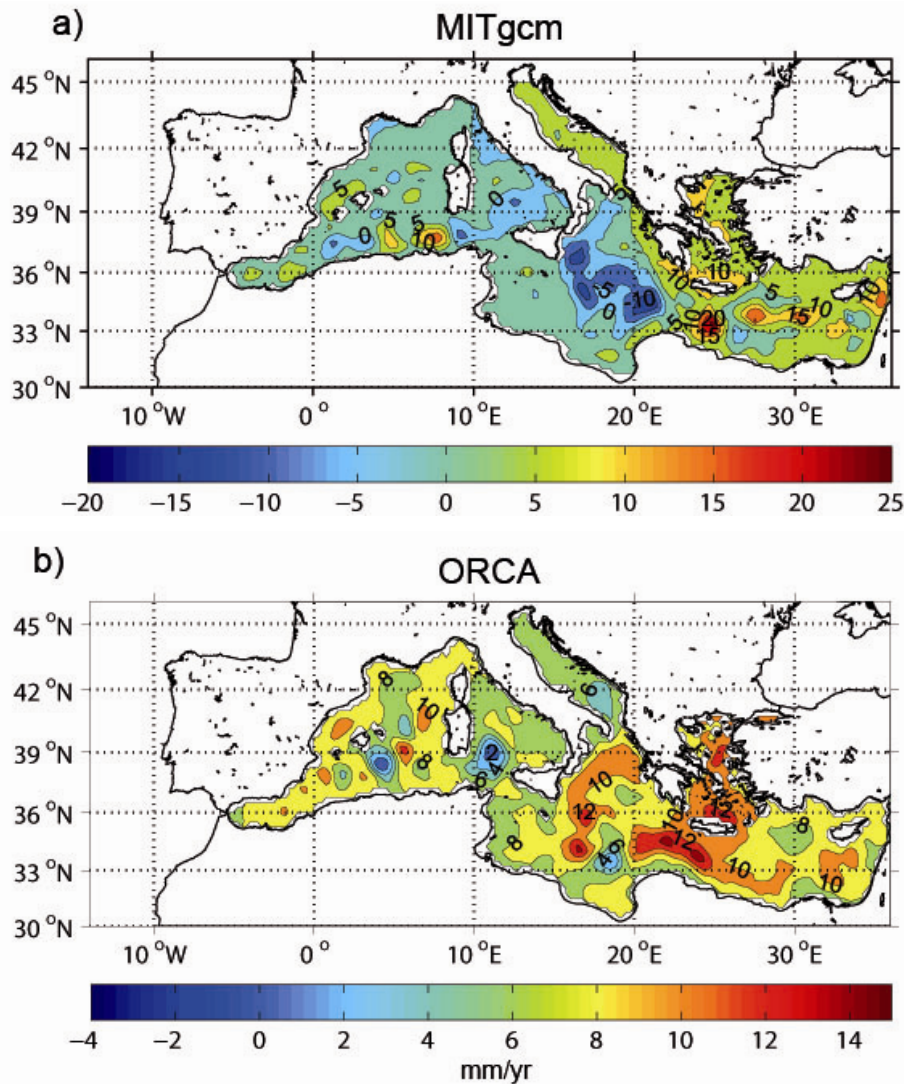
Figure 9.6. Distribution of total sea level trends for the period 1993-2000 as obtained from: (a) the MITgcm model; (b) the ORCA model. The contour interval in (a) and (b) is 5 and 2 mm/yr, respectively. Note the different scale ranges (units are mm/yr in all cases).

The distribution of steric sea level trends for the period 1993-2000 as estimated from the MITgcm and ORCA models is shown in Figure 9.7. The steric trends from the MITgcm model (Fig. 9.7a) shows a spatial pattern similar to total sea level trends, but with smaller negative trends in the Ionian and slightly larger positive trends in the Levantine basin. A similar behaviour was observed for the OM8 model, which also

showed a spatial pattern with larger positive trends in the Levantine basin and slightly positive trends in the Ionian (Figs. 8.1c,d). Conversely, the steric sea level trends from ORCA are smaller everywhere in the basin (Fig. 9.7b).
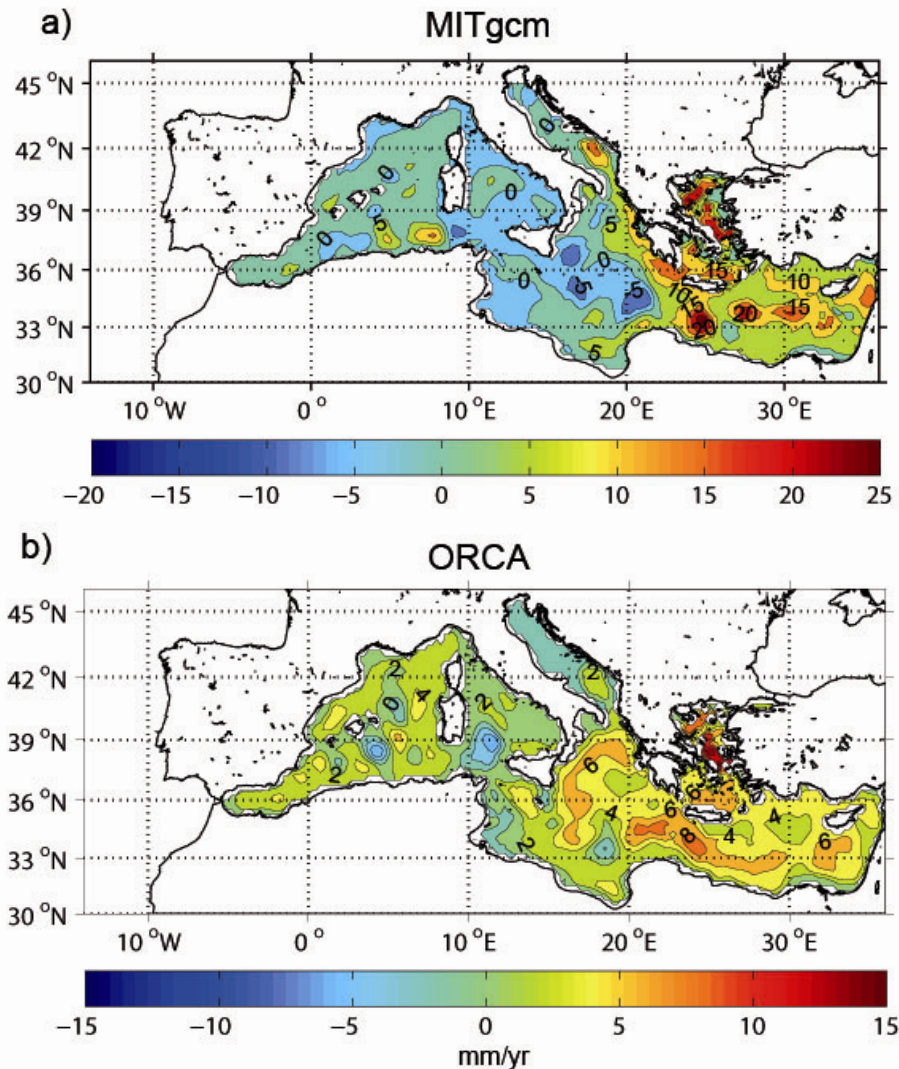
Figure 9.7. Distribution of steric sea level trends for the period 1993-2000 as obtained from: (a) the MITgcm model; (b) the ORCA model. The contour interval in (a) and (b) is 5 and 2 mm/yr, respectively. Note the different scale ranges (units are mm/yr in all cases).

The temporal sea level variability has also been examined for the Ionian and Aegean Seas. Figures 9.8a,b show the yearly sea level time series obtained from the three models and from altimetry data. The limits of the averaged domain in the Ionian Sea are not the same for all models. For the ORCA and the MITgcm models, the limits are the same as for altimetry (Fig. 8.1a), although for the MITgcm we selected the grid points with trends smaller than -5 mm/yr within the selected area, while for the OM8 model the limits are the same as used in Chapter 8 (Fig. 8.1c). The reason is that in the OM8 model the negative trends in the Ionian Sea appear displaced to the south (with respect to altimetry) and the aim of this analysis is to show the time evolution of the main features found in the distribution of sea level trends. The derived linear trends are listed in Table 9.8.
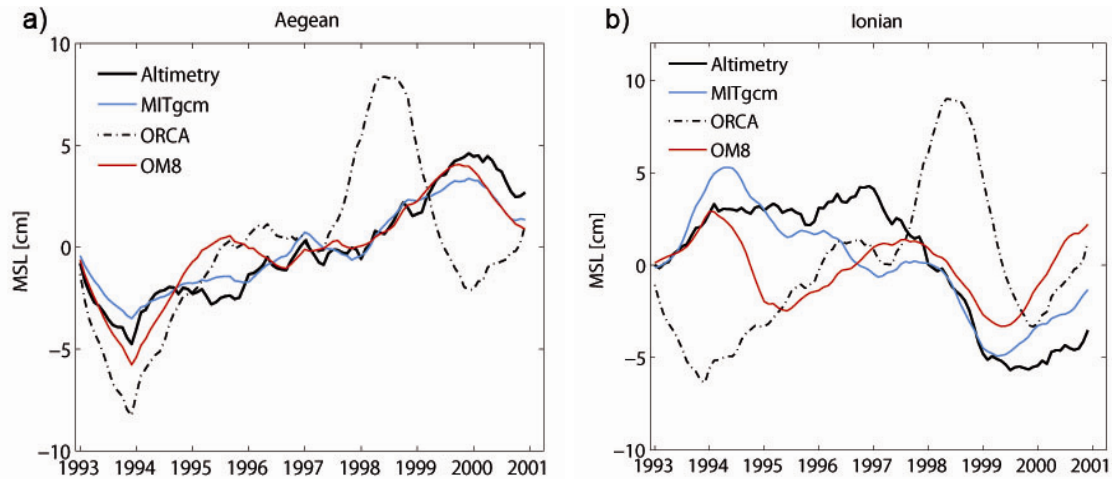
Figure 9.8. Yearly regional-averaged total sea level for the period 1993-2000 estimated from altimetry data (black line) and the three models: MITgcm (blue line), ORCA (dashed-dotted line) and OM8 (red line) for: (a) the Aegean Sea; (b) the Ionian Sea. The averaging domains are stated on the text.

The Aegean Sea (Fig. 9.8a) is the region where all estimations are closer to each other. The inter-annual variability shown by the MITgcm model is in good agreement with the variability observed by altimetry, with a correlation of 0.82 (estimated from the detrended time series). The OM8 model also reflects most of the major features of the observed variability, although its correlation with altimetry is lower (0.50). The ORCA model is the one performing poorer, not showing a significant correlation with altimetry. With regard to trends (Table 9.8), all models show large positive trends in good agreement with altimetry; the MITgcm model is the one that better approximates the observed trend (9.5±0.5 mm/yr as compared to the 10.7±0.5 given by altimetry).

Table 9.8. Total and steric sea level trends in the Aegean and Ionian seas for the periods 1993-2000 and 1961-2000 estimated from the three models, the reconstruction, altimetry and Ishii data.

TOTAL SEA LEVEL TRENDS [mm/yr]				
	Aegean Sea		**Ionian Sea**	
Period	**1993-2000**	**1961-2000**	**1993-2000**	**1961-2000**
Altimetry	10.7 ± 0.5	-	-11.7 ± 1.2	-
Reconstruction	9.8 ± 0.4	0.6 ± 0.1	-9.1 ± 1.0	1.8 ± 0.1
MITgcm	9.5 ± 0.5	0.6 ± 0.1	-11.7 ± 1.3	1.7 ± 0.1
ORCA	8.8 ± 1.8	7.8 ± 0.2	6.5 ± 2.1	7.8 ± 0.2
OM8	8.9 ± 0.7	0.9 ± 0.1	-2.3 ± 0.9	1.7 ± 0.1

STERIC SEA LEVEL TRENDS [mm/yr]				
	Aegean Sea		**Ionian Sea**	
Period	**1993-2000**	**1961-2000**	**1993-2000**	**1961-2000**
Ishii	11.5 ± 0.6	-0.3 ± 0.1	4.6 ± 1.1	-0.33 ± 0.1
MITgcm	9.1 ± 0.6	0.2 ± 0.1	-7.4 ± 0.6	2.3 ± 0.1
ORCA	4.3 ± 0.8	0.2 ± 0.1	4.6 ± 0.7	0.8 ± 0.1
OM8	10.7 ± 0.8	0.3 ± 0.1	-0.5 ± 0.8	2.0 ± 0.1

In the Ionian Sea (Fig. 9.8b) all models perform poorer than in the Aegean Sea. Again the MITgcm is the model reproducing with a higher degree of accuracy the observed sea level variability, although the correlation with altimetry is lower than in the Aegean Sea (0.60). Despite it reproduces exactly the sea level trend estimated from altimetry (-11.7±1.3 mm/yr), there are some important differences. The main one is that the pronounced sea level drop shown by the MITgcm model begins between 1994 and 1995, while in the altimetric time series it beings in 1997. The OM8 also gives a negative sea level trend in this region (-2.3±0.9 mm/yr), but it is much weaker than those obtained from the MITgcm model and altimetry. Moreover the interannual variability is rather different, showing two sea level drops in 1994 (until middle 1995) and in 1998 (until 1999) leading to a w-shaped time series. The time series estimated from the ORCA model is very similar to the one obtained for the Aegean Sea and it is uncorrelated with the other models and altimetry.

The temporal variability of the steric sea level in the Aegean and Ionian Seas for the period 1993-2000 is shown in Figures 9.9a,b. The derived sea level trends are listed in Table 9.8. It is worth noting that the steric sea level (Fig. 9.9) estimated from the MITgcm and OM8 models shows a very similar inter-annual variability to the corresponding total sea level (Fig. 9.8) in both the Aegean and the Ionian Sea. The sea level trends are also very similar, especially in the Aegean Sea (Table 9.8). The most striking feature is that the behaviour of the MITgcm and OM8 models is very different from the steric sea level computed from the Ishii data set. The explanation may be that since Ishii data only span the upper 700 m, they cannot fully account for the steric changes associated with intermediate and deep water formation. Another feature to be considered is that the uncertainty of the steric sea level derived from Ishii data is very high, particularly in the Ionian Sea. It turns out, therefore, that the model steric sea level might be more reliable than Ishii during the EMT and post-EMT years.

The steric sea level estimated from the ORCA model shows a rather different behaviour compared to the total sea level obtained from the same model. This is rather surprising, since the dynamic component is supposed to be a small contribution when compared with the steric one.
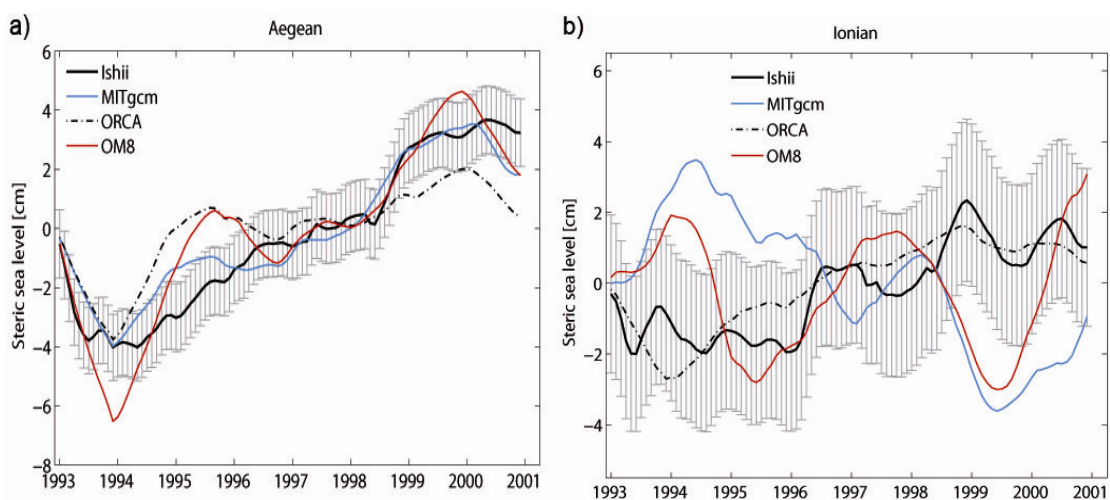
Figure 9.9. Yearly regional-averaged steric sea level for the period 1993-2000 estimated from the Ishii data set (black line) and the MITgcm (blue line), ORCA (dashed-dotted line) and OM8 (red line) models for: (a) the Aegean Sea; (b) the Ionian Sea. Error bars are shown for the Ishii time series. The averaging domains are stated on the text.

Sea level trends for the period 1961-2000

The regional distributions of sea level trends for the period 1961-2000 estimated from the MITgcm and ORCA models are shown in Figure 9.10. The distribution estimated from the MITgcm simulation (Fig. 9.10a) shows positive trends almost everywhere. A prominent feature is the relative maximum in the Ionian Sea (up to 2 mm/yr), while almost zero trends (about 0.5 mm/yr) are observed in the Aegean Sea. The marked positive trend found in the Ionian is also found in the distribution of sea level trends derived from the reconstruction (Fig. 8.4a) and the OM8 simulation (Fig.8.4b), although it covers a smaller area than in the reconstruction and it appears surrounded by other mesoscale structures. In the Adriatic Sea it shows a trend of about 1 mm/yr everywhere, which is also in very good agreement with the reconstructed trends. The spatial patterns in the Western Mediterranean shown by the MITgcm and OM8 models are very similar. The trend distribution obtained from the ORCA simulation (Fig. 9.10b) shows unrealistic large positive trends (between 7 and 10 mm/yr) everywhere.
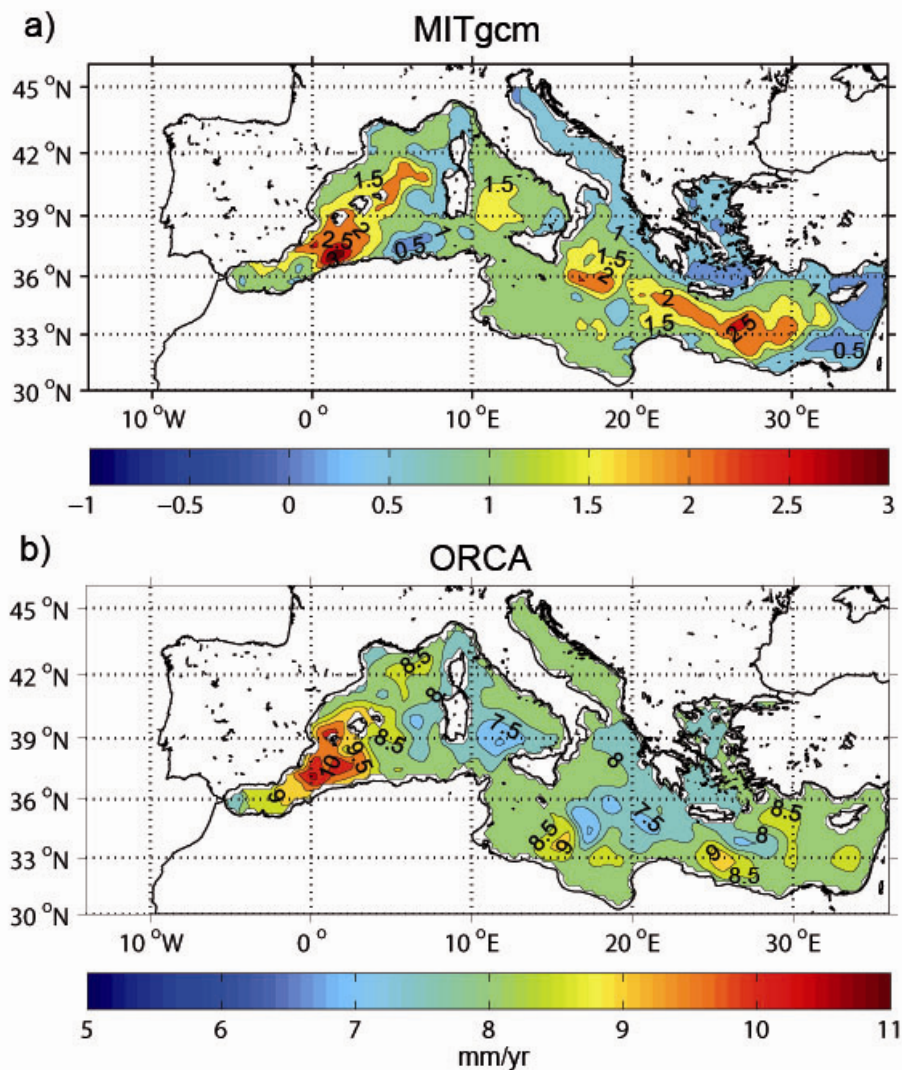
Figure 9.10. Distribution of total sea level trends for the period 1961-2000 as obtained from: (a) the MITgcm model; (b) the ORCA model. The contour interval is 0.5 mm/yr. Note the different scale ranges (units are mm/yr in all cases).

The regional distributions of steric sea level trends for the period 1961-2000 estimated from the MITgcm and ORCA models are shown in Figure 9.11. The MITgcm distribution (Fig. 9.11a) resembles total sea level trends given by the same model except in that values are significantly larger in the Western Mediterranean (above 2 mm/yr everywhere) and also, though to a lesser extent, in the Eastern basin. The positive peak in the Ionian Sea is similar to the one obtained for total sea level (up to 2 mm/yr). This unrealistic large trends found in the Western Mediterranean seem to be a recurrent problem in all models and they are related to the warming drift found in the deepest layers of this region. The steric trends derived from the ORCA model do not resemble the corresponding total sea level trends. In fact, it gives more realistic smaller trends everywhere in the basin, which indicates that the problem pointed out above arises from the mass redistribution (dynamical component) associated with the changes in the circulation or with the derivation of the sea surface height itself rather than from the evolution of the temperature or salinity.
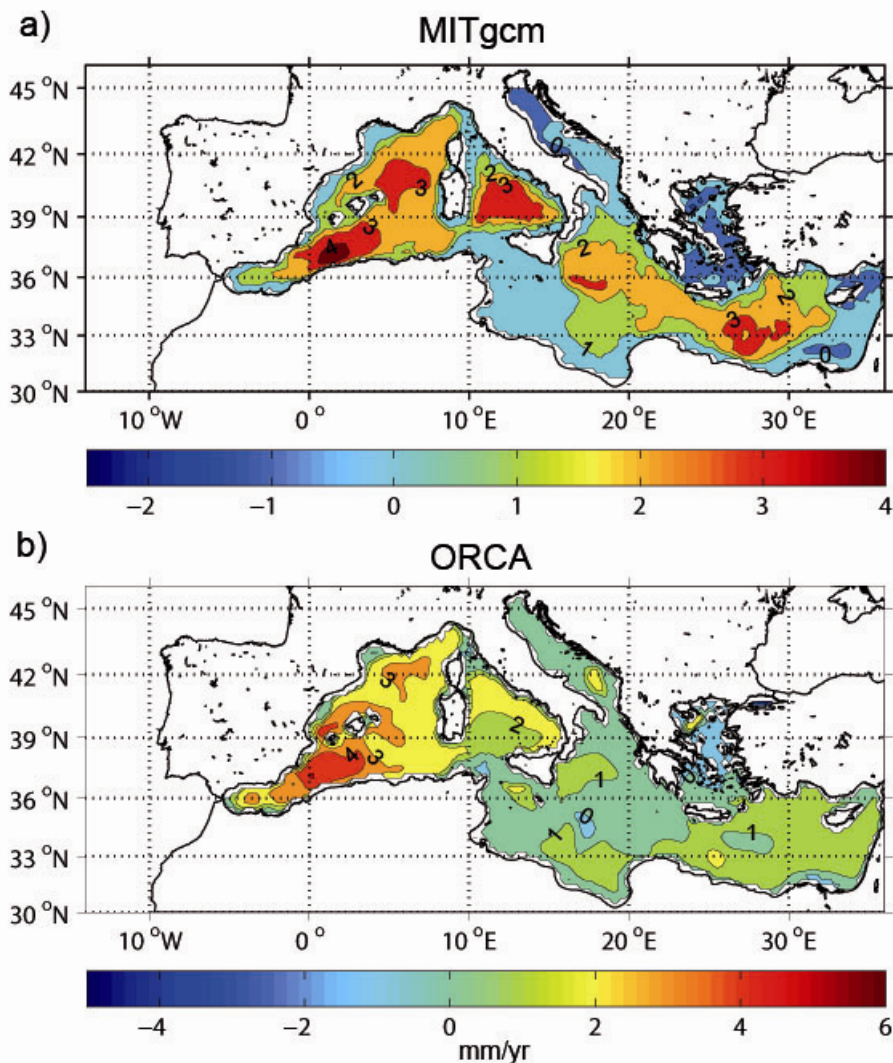
Figure 9.11. Distribution of steric sea level trends for the period 1961-2000 as obtained from: (a) the MITgcm model; (b) the ORCA model. The contour interval is 1 mm/yr. Note the different scale ranges (units are mm/yr in all cases).

The time evolution of total sea level in the Aegean Sea and the Ionian Sea for the period 1961-2000 as estimated from the three models and the reconstruction is shown in Figure 9.12. In the Aegean Sea (Fig. 9.12a), both the MITgcm and OM8 total sea level are well correlated with the reconstructed time series (0.5 and 0.6, respectively) and they also show similar trends (see Table 9.8); however, the MITgcm simulation reproduces the sea level drop during the years 1985-1993 (the EMT) and the subsequent rebound after 1993 slightly better. The total sea level derived from the ORCA model shows an unrealistic large trend and no correlation with the reconstruction.

In the Ionian Sea the situation is rather different. While the total sea level derived from the MITgcm and OM8 models shows similar trends to the reconstructed sea level (Table 9.8), only the MITgcm total sea level is well correlated with the reconstructed sea level (0.7). The MITgcm model reproduces quite accurately the sea level jump shown by the reconstruction during the major part of the EMT (1987-1992) and the subsequent sea level drop after 1992. These features are not captured by the other two models. In this region, the OM8 total sea level shows a larger variability than the MITgcm and the reconstructed sea level. Again the ORCA model is the one performing poorer, showing an unreliable large positive trend.
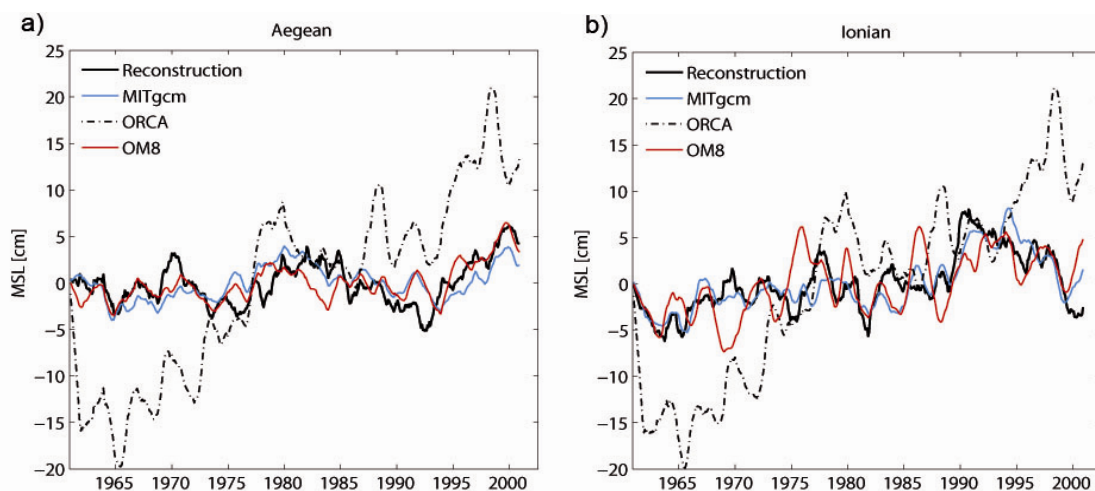
Figure 9.12. Yearly regional-averaged total sea level for the period 1961-2000 estimated from the reconstruction (black line) and the three models: MITgcm (blue line), ORCA (dashed-dotted line) and OM8 (red line) for: (a) the Aegean Sea; (b) the Ionian Sea. The averaging domains are stated in the text.

Figure 9.13 shows the time evolution of the steric sea level in the Aegean Sea and the Ionian Sea for the period 1961-2000 estimated from the three models and the Ishii data set. In the Aegean Sea all models reproduce the inter-annual variability shown by the Ishii steric sea level (the highest correlation, 0.6, is for OM8). However, the strong sea level drop shown by the Ishii steric sea level during the period 1987-1991 (coinciding with the very cold 1987 winter and the relatively dry period mentioned above) is not reproduced by any of the models. The extent to which this is due to the fact that Ishii only accounts for the upper 700 m or to a model misrepresentation is not clear. The steric sea level given by ORCA resembles the estimates of the other two models and, despite it gives a lower trend than the other models (Table 9.8), it seems to provide reasonable results unlike the total sea level.

In the Ionian Sea the situation is more complicated. Surprisingly ORCA is the model that better reproduces the Ishii steric sea level. Both signals are reasonably correlated (0.5) and give the same steric trend (Table 9.8). The main features shown by the Ishii steric sea level are the strong sea level rise during the period 1967-1973, and the sea level rise between 1987 and 1992 that was followed by a marked sea level drop during the period 1992-1995. These features are visible in the ORCA steric sea level, although they are much less pronounced than in the Ishii steric sea level. The MITgcm also reproduces some of the major features, such as the increases in sea level during the periods 1967-1973 and 1987-1992; however, the sea level drop observed in the Ishii steric sea level during 1992-1995 appears some years later in the MITgcm steric sea level. The OM8 steric sea level shows in this region a larger inter-annual variability than the other simulations.
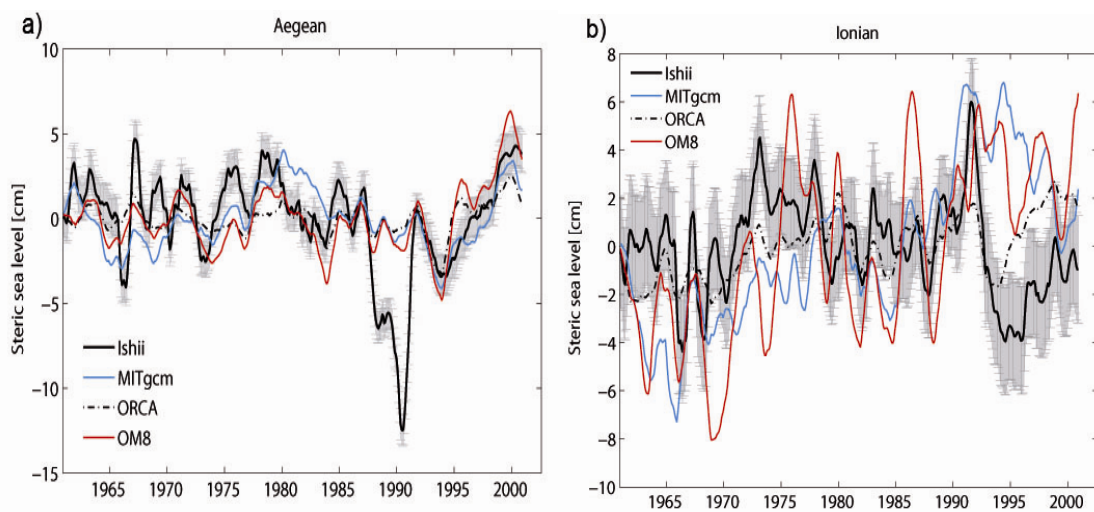
Figure 9.13. Yearly regional-averaged steric sea level for the period 1961-2000 estimated from the Ishii climatology (black line) and the three models: MITgcm (blue line), ORCA (dashed-dotted line) and OM8 (red line) for: (a) the Aegean Sea; (b) the Ionian Sea. The averaging domains are stated in the text.

9.4 Discussion and conclusions

In this chapter we have compared three different baroclinic models (MITgcm, ORCA and OM8) in the Mediterranean Sea for the period 1961-2000 with the aim of understanding and explaining some of the OM8 weaknesses found in Chapter 8, especially during the EMT years. First, a comparison between the models and with the MEDAR climatology has been carried out as a complementary validation of the models. When averaged over the whole Mediterranean basin and over the whole time period, temperature and salinity are in good agreement with the values obtained from MEDAR (see Table 9.4): the smallest biases are for the MITgcm model (-0.04ºC and no difference at all in salinity), while the largest biases are for ORCA (0.22ºC in temperature and -0.03 in salinity).

The analysis has also been carried out for the Eastern and Western basins, on four different layers: 0-100 m, 100-500 m, 500-1000 m and 1000-2000 m. For the top 1000 m in the Western Mediterranean and the top 500 m in the Eastern Mediterranean,

averaged temperatures from all models are well correlated with MEDAR (Table 9.5), although the correlations decrease for the uppermost (0-100 m) layer due to inaccuracies in the interannual variability of the non-corrected MEDAR data base. At deeper layers models do not show significant correlations with MEDAR, although the time-mean properties do not show large biases. The most noticeable characteristic is the warming drift that all models present in the deeper layers, especially in the Western Mediterranean (see Table 9.7); the drift is more pronounced for the regional models (MITgcm and OM8) than for the global model (ORCA).

With regard to salinity, models do not successfully reproduce the inter-annual variability shown by the MEDAR data at any layer (Table 9.5), although the biases are rather small (Table 9.6).

We have also computed dense water formation rates in the Aegean and Ionian Seas for the three models, paying especial attention to the EMT years. In the Aegean Sea the only model that shows a significant deep water formation is the MITgcm model (Fig. 9.4a, top), which shows maximum formation rates in the Aegean Sea during the extreme winters of 1992-1993. The OM8 model also shows a deep water formation peak during those years, but it is much smaller than for the MITgcm model; most of the dense water formation shown by OM8 in the Aegean Sea corresponds to intermediate water (Fig. 9.4b, top). The ORCA model does not show formation of deep water at all in the Aegean Sea.

For a better assessment of the dense water formation mechanisms, we have also computed the average temperature, salinity and potential density in the Aegean Sea and the Ionian Sea for the period 1961-2000 and the layers 0-100 m, 100-500 m, 500-1000 m and 1000-2000 m (Fig. 9.5). This analysis shows that the MITgcm results are in good agreement with other studies on the EMT (Lascaratos et al., 1999), which showed that the density increase in the Aegean Sea during the EMT period was first due to an increase in salinity during the period 1987-1992 followed by a temperature decrease in 1992-1995. The other two models also show a decrease in temperature for the top 500 m during the years 1992-1993, but they do not show any salinity increase for the period 1987-1992. The salinity increase during the first years of the EMT has been proven an important preconditioning mechanism for the formation of deep water in the Aegean Sea during the EMT period (Nittis et al., 2003). The fact that the OM8 and ORCA models do not show such a salinity increase would explain at least partially why they do not perform well in reproducing the formation of deep water in this region during the EMT years. The MITgcm model also reproduces the increased water formation rates not only during the cold winters of 1987 and 1992-1993, but also during the period in between, which was characterized by relatively mild winters. This is in good agreement with the results based on observations shown by Theocharis et al. (1999) and the results obtained from numerical simulation by Nittis et al. (2003). After 1995 the situation returned back to normal: the Aegean Sea returned to pre-EMT conditions, exporting small amounts of dense water that did not reach the bottom of the Ionian and the Levantine basins (Theocaris et al., 2002), while the Adriatic Sea became again the main contributor to the dense waters of the Eastern Mediterranean (Klein et al., 2000; Manca et al., 2006).

The described changes are clearly reflected in the decadal sea level trends computed from satellite altimetry (Cazenave et al., 2001; Fenoglio-Marc, 2002; Criado-Aldeanueva et al., 2008). In the second part of the chapter we have computed the total (steric + dynamic part of the circulation) and steric sea level from the models and

compared the results with altimetry (for the period 1993-2000), with the reconstruction (1961-2000) and, in the case of the steric sea level, with the steric component computed from the Ishii data set. As expected from the above considerations, for the period 1993-2000 the MITgcm mode is the only one that reproduces successfully the major features shown by altimetry: marked negative and positive trends in the Ionian and the Aegean seas, respectively. Indeed, these features are related to a normalization of the thermohaline circulation in the Eastern Mediterranean after the EMT. The fact that the OM8 and ORCA models do not properly reproduce this process would explain why these models do not correctly reproduce the major sea level features shown by altimetry. Namely, the OM8 shows a small peak related to deep water formation in the Aegean Sea during the years 1992-1993 (Fig. 9.4a, top), which would explain why the model shows slightly negative sea level trends in the Ionian for the period 1993-2000 (the situation going back to normal after a weak EMT). The ORCA model shows large unrealistic trends everywhere in the Mediterranean.

Regarding the inter-annual variability of total sea level for the period 1993-2000 in the Ionian and Aegean Sea, all models perform better in the Aegean Sea than in the Ionian Sea. Both the MITgcm and OM8 models show high correlations with total sea level from altimetry in the Aegean Sea. In the Ionian Sea the sea level trend given by the MITgcm model is in good agreement with altimetry, but the correlation is lower than in the Aegean.

With regard to steric sea level, it is worth noting that all models perform well in the Aegean Sea when compared to the steric sea level computed from the Ishii data set. All models show high correlation with the observation and give high positive trends in good agreement with the observations, although the trends given by the ORCA model are smaller. In the Ionian Sea, the behaviour of the MITgcm and OM8 models is very different from the steric sea level computed from the Ishii data set. The explanation may be that since Ishii data only span the upper 700 m, they cannot fully account for the steric changes associated with intermediate and deep water formation. Another feature to be considered is that the uncertainty of the steric sea level derived from Ishii data is very high, particularly in the Ionian Sea.

For the whole period 1961-2000 there are several results that are worth commenting. First, all models show large steric sea level trends in the Western Mediterranean derived from the spurious warming drift in the deeper layers. Second, a major feature of the distribution of sea level trends for this period is the positive maximum obtained in the Ionian Sea, shown by the reconstruction and reproduced by the MITgcm and OM8 models. Third, the inter-annual variability of the reconstructed sea level averaged over the Aegean and Ionian Seas clearly reflects the sea level changes that affected those regions during and after the EMT years. These sea level changes are only fully captured by the MITgcm model, which shows a sea level rise (fall) during the years of the EMT (1986-1995) followed by a sea level drop (rise) after 1995 in the Ionain (Aegean) Sea, in good agreement with the reconstruction.

The relation between sea level changes and the EMT was already explained in Chapter 8; here we will get back to it only to relate them with the new results found in the first part of this chapter. The significant salinity increase from 1985 to 1992 and the temperature decrease during the years 1992-1993 shown by the MITgcm model, result in densities higher than normal in the region and, consequently, in a sea level decrease. After 1995, there is a pronounced decrease in salinity in the top 1000 m (Fig. 9.5b) that results in sea level rising. In Chapter 8, it was commented that the difficulties of the OM8 model to reproduce sea level changes derived from the EMT could be due to the

heat and freshwater forcing. The results obtained in this chapter suggest that the difficulties are more related to the freshwater forcing than to the heat forcing, since the main differences between the MITgcm model and the other two models come mainly from the salinity fields. A plot of the net surface heat fluxes used by the three models averaged over the Aegean Sea and Adriatic Sea shows no significant differences (Fig. 9.14). Instead, the freshwater budget (Evaporation (E)-Precipiation (P)-Runoff (R)) are not that similar. Figure 9.15 shows the anomalies of the E-P-R net flux averaged over the Aegean Sea as given by the MITgcm and OM8 models. The MITgcm freshwater forcing clearly shows a more pronounced increase in the E-P-R net budget (the opposite in salinity) for the period 1985-1993, followed by a sharp decrease after 1993. This is the extended dry period 1989-1993 that affected the whole Eastern Mediterranean and reduced the Black sea water outflow during the same period (Nittis et al., 2003). The subsequent pronounced salinity decrease shown by the MITgcm after 1995 is what explains the large positive trends in sea level captured by satellite altimetry observations for the period 1993-2000. The fact that the OM8 model uses climatological values for the river runoff and the Black Sea while the MITgcm uses an Interactive River Scheme (IRIS) that provides fresh water sources consistent with the atmospheric branch of the simulated hydrological cycle (so that the E-P-R budget is treated as a real fresh water flux) could explain some of the differences between both models. Also Beuvier et al. (2008) have shown that considering the inter-annual variability of the river runoff and the Black Sea outflow (instead of considering just an annual cycle) has a significant impact on the simulation of the EMT.
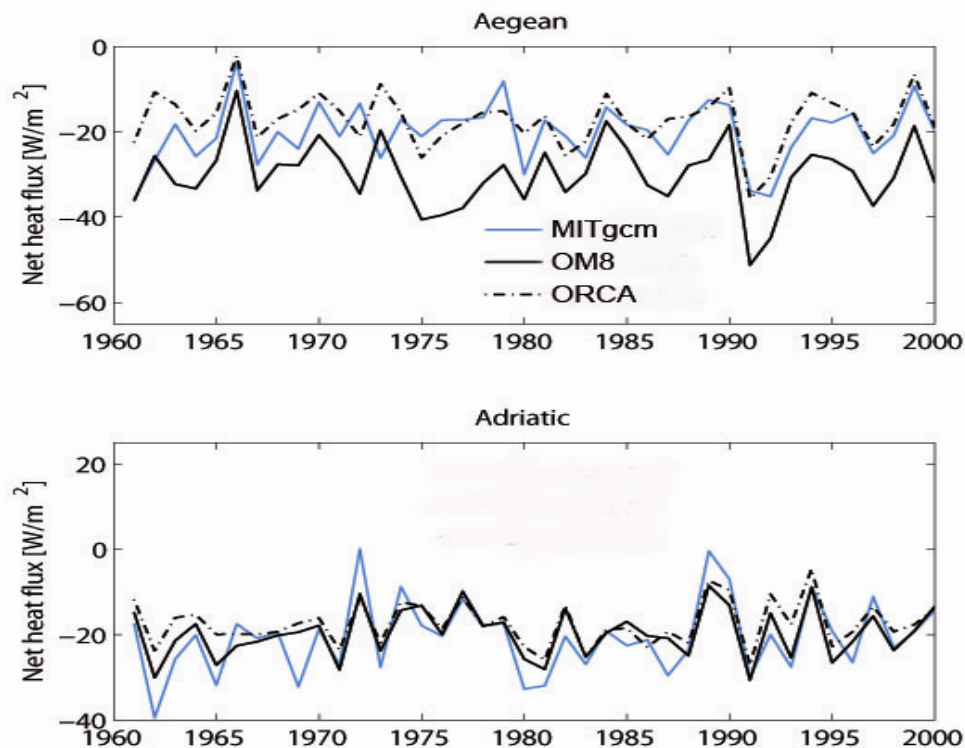
Figure 9.14. Yearly regional-averaged net surface heat flux for the period 1961-2000 as given by the three models: MITgcm (blue line), OM8 (black line) and ORCA (dash-dotted line) in: (a) the Aegean Sea; (b) the Adriatic Sea.
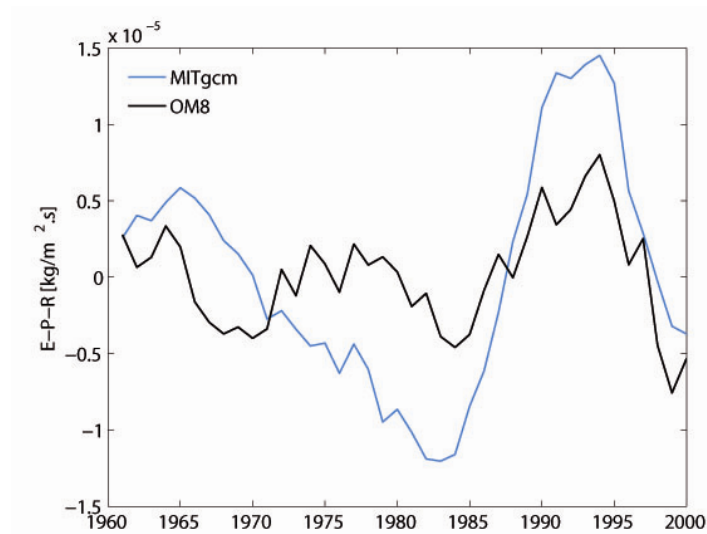
Figure 9.15. Yearly regional-averaged E-P-R net flux for the period 1961-2000 as given by the MITgcm (blue line) and OM8 (black line) models over the Aegean Sea.

Major conclusions regarding the overall Mediterranean sea level budget are, first, that the best model to estimate the steric component of sea level seems to be the MITgcm model, since it is able to successfully reproduce a major sea level feature of the last decades such as the EMT. The drawback of model data is the spurious warming drift that all tested models show in the deep waters of the Western Mediterranean. Regarding the option of using hydrographic data, we have found that the non-corrected version of MEDAR is not reliable in the upper (0-100 m) layer, particularly for the temperature, and this can lead to errors in the steric component of sea level; another, minor problem of MEDAR is that it only gives annual values. Conversely, the Ishii data set is given on a monthly base, which avoids the aliasing problems in the upper layer. The drawback of the Ishii data set is that it only spans the upper 700 m; although most of the interannual steric sea level variability is expected to be related with density changes occurring within that layer, wrong results can be obtained where deep waters suffer significant changes, as in the Aegean and Ionian seas during the EMT and post-EMT period.

Chapter 10

Mass contribution to Mediterranean sea level variability for the period 1948-2000

$\mathbb{A}$T[1] the beginning of this thesis we formulated a series of questions whose answers were crucial to understand long-term sea level variability in the Mediterranean Sea during the past decades. Many of these questions have already been given an answer in the previous chapters. However, there is still an important question that remains unanswered: can the mass contribution to sea level be determined and hence to close the budget of Mediterranean MSL?. As stated before, none of the models accounts for remote mass changes, so that the answer to this question requires either an estimation of the mass component from observations or some robust proof that it can be reliably determined as total minus steric sea level. This chapter is devoted to investigate these requirements.

10.1 Introduction

At global scale, water mass changes essentially derive from changes in the terrestrial storage of freshwater (i.e., melting rate of continental glaciers and ice-sheets and river run-off), since the precipitation-evaporation rates are assumed to keep constant. At regional scale, the mass content of a basin is affected by fresh water fluxes and by the exchanges with adjacent basins (which are in turn driven by the freshwater budget and by the atmospheric pressure).

---

[1] This chapter is based on the papers:

Calafat, F. M., M. Marcos, D. Gomis. Mass contribution to the Mediterranean sea level variability for the period 1948-2000. Global and Planetary Change, submitted (2010).

Marcos, M., F. M. Calafat, W. Llovel, D. Gomis, B. Meyssignac. Regional distribution of steric and mass contributions to sea level changes. Global and Planetary Change, submitted (2010).

The long-term trend of the global mean steric component has been estimated in different works. Fewer estimates have been published for the mass contribution to total sea level. Due to the lack of direct, independent observations, the mass component has been estimated in two different ways: i) from estimations of the components of the hydrological budget, e.g., basin on models of continental ice melting; ii) computing the non-steric (total minus steric) sea level. The first method has the problem that the components of the hydrological budget are subjected to large uncertainties. The second method has the problem that, on a long term basis, total sea level has only been recorded by tide gauges located at coastal sites which may not be representative of the basin averaged sea level.

Since 1992, satellite altimetry provides a global coverage of total sea level. This opened the door to combine altimetric fields and long tide gauge records to obtain reconstructions of sea level fields, such as the global one obtained by Church et al. (2004) or the Mediterranean reconstruction obtained in Chapter 6. Domingues et al. (2008) used the global reconstruction to estimate total sea level rise in 1.6±0.2 mm/yr for the period 1961-2003; subtracting their estimate of the thermosteric contribution for the upper 700 m from that value they concluded that the mass component of sea level change is of the order of 1.1±0.3 mm/yr for the same period. Estimates of the thermal expansion of the ocean below 700 m are much more uncertain and they vary from the 0.07 mm/yr computed from observations spanning the period 1961-2003 (Domingues et al., 2008) to the 0.3 mm/yr given by the German Consortium for Estimating the Circulation and Climate of the Ocean Model for the period 1962-2001. This implies that taking into account the thermal expansion of the deep-ocean, the contribution of the mass component to global sea level rise would range between 0.8 and 1.1 mm/yr for the period 1961-2003 (Domingues et al., 2008).

Since 2002, the Gravity Recovery and Climate Experiment (GRACE) Mission measures the variations in the gravity field caused by changes in the water mass of the Earth, then providing the first direct and independent measures of the mass contribution to sea level change. GRACE data have also been used to validate the estimation of the mass component as non-steric sea level. Willis et al. (2008) presented an analysis of altimetry, steric sea level and GRACE observations and concluded that the 4-year trends of the three signals were not consistent. Conversely, Leuliette and Miller (2009) stated that total sea level trends are not statistically different from the sum of the steric and mass trends.

In this chapter we first use altimetry, GRACE and hydrographic observations spanning the period 2002-2006 to assess the consistency between total sea level and its two components (steric and mass) in the Mediterranean Sea. This is not the first attempt: Fenoglio-Marc et al. (2006) and García et al. (2006) carried out similar works for the period 2002-2004, but they only focused on the seasonal sea level cycle Here we consider both intra and inter-annual variability. Other differences with respect to those works are that they use model data (not hydrographic observations) to estimate the steric cycle and that an improved and longer GRACE data set is presently available.

Provided we find a good agreement between GRACE observations and steric-corrected altimetry in the Mediterranean Sea, it would support the quantification of the mass contribution in terms of non-steric sea level for the past decades, using the sea level reconstruction as total sea level (with the atmospheric component subtracted) and estimating the steric sea level either from a model or from historical hydrographic measurements (Ishii et al., 2009; Ingleby and Huddleston, 2007). When quantifying the

referred agreement it is crucial to have reliable estimates of the uncertainties of all sea level components. Hence, particular attention will be devoted to error computations.

10.2 Data processing

10.2.1 Grace data

In Chapter 3 we described the main functioning principles of the GRACE mission and its objectives, but it is appropriate to briefly recall them here. The primary goal of the GRACE project is to determine variations in the Earth's gravity field at monthly intervals and at a spatial resolution of several hundred km. This objective is achieved by making continuous measurements of the change in the distance between twin spacecraft, co-orbiting in ~ 500 km altitude, near circular, polar orbit, spaced ~ 220 km apart, using a microwave ranging system. The satellite orientation and position are accurately measured using twin star cameras and a GPS receiver, respectively.

Spatial and temporal variations in the Earth's gravity field affect the orbits of the twin spacecrafts differently. These differences result in changes in the distance between the spacecrafts, as they orbit the Earth, which in turn reflecte in the time-of-flight of microwave signals transmitted and received nearly simultaneously between the two spacecraft. The change in this time of flight is continuously measured by tracking the phase of the microwave carrier signals. The so-called dual-one way range change measurements can be reconstructed from these phase measurements. This range change, along with other mission and ancillary data, are subsequently analyzed to extract the parameters of an Earth gravity field model.

In this section we will describe how the gravity coefficients provided by the GRACE project are converted into sea level variations. We will also describe how the surface density field is smoothed in order to reduce satellite measurement errors.

Stokes gravity coefficients

The Level-2 Release-04 (RL04) gravity coefficients (C'_{lm}, S'_{lm}) computed at the Center for Space Research (CSR) are used to estimate global water mass variations for the period August 2002 to the end of 2006 with a spatial resolution of 1°x1°. The data include corrections to specific spherical harmonic coefficients due to solid Earth and ocean tidal contributions to the geopotential, the solid pole tide and a correction for the atmospheric mass. Moreover, a barotropic model is used to correct for water mass displacements due to atmospheric forcing. That is, GRACE data do not account for water mass displacements due to changes in atmospheric pressure and wind, so that when added to the steric component it will not result in total sea level, but in atmospherically corrected total sea level. RL04 coefficients are supplied to degree and order 60.

Several other important corrections must be made to RL04 gravity field coefficients (C'_{lm}, S'_{lm}) before converting them into water mass variations. Those corrections have been described in Chapter 3 (Section 3.3) and thus they will not be presented here again. The corrected gravity coefficients (C_{lm}, S_{lm}) can be converted into water mass variations following the methodology that we present in the following sections.

Equations relating surface mass to gravity

The Earth's gravity field is usually represented in terms of the shape of the geoid, the equipotential surface that most closely coincides with MSL over the ocean. It is usual to expand the geoid N as a sum of spherical harmonics (Wahr et al., 1998)

$$N(\theta,\phi) = a\sum_{l=0}^{\infty}\sum_{m=0}^{l} P_{lm}(\cos\theta)\left[C_{lm}\cos(m\phi) + S_{lm}\sin(m\phi)\right] \tag{10.1}$$

where P_{lm} are normalized associated Legendre polynomials, θ and ϕ are colatitude and longitude, and a is the radius of the Earth. Although theoretically the series is exact only if the summation is carried out to an infinite degree, in practice it is truncated at some value $l=N_{max}$, since the GRACE project provides estimates of the gravity field coefficients up to degree l=60 every month.

Using the Stokes coefficients provided by the GRACE project, it is possible to infer monthly changes in the gravity field and so to study processes involving the redistribution of water mass over the Earth's surface. Assuming that for periods less than several hundred years the primary cause of temporal changes in the Earth's gravity field is the movement of water mass within the Earth's relatively thin fluid envelope, a local change in surface mass density $\Delta\sigma(\theta,\phi)$ can be related to changes in the Stokes coefficients ΔC_{lm} and ΔS_{lm} by (Wahr et al., 1998)

$$\Delta\sigma(\theta,\varphi) = \frac{a\rho_E}{3}\sum_{l=0}^{\infty}\sum_{m=0}^{l}\frac{(2l+1)}{(1+k_l)} P_{lm}(\cos\theta)\left[\Delta C_{lm}\cos(m\varphi) + \Delta S_{lm}\sin(m\varphi)\right] \tag{10.2}$$

where ρ_E is the average density of the solid Earth and k_l are the load love numbers representing the effects of the Earth's response to surface loads. The load love numbers have been obtained from Wahr et al. (1998).

Swenson and Wahr (2002) showed that for values of l greater than 5, the GRACE satellite error estimates increase rapidly with increasing l. Because RL04 coefficients are supplied only to degree 60, the sums in equation (10.2) will be truncated at $l = 60$. Although neglecting the contribution of coefficients with $l > 60$ will reduce the impact of satellite errors on the estimate of $\Delta\sigma(\theta,\phi)$, the errors from the larger remaining values of l will still seriously degrade the solutions. On the other hand, using a truncated sum in equation (9.2) will make that $\Delta\sigma(\theta,\phi)$ lacks components having length scales less than about 300 km. Both types of errors can be reduced by spatial averaging $\Delta\sigma(\theta,\phi)$ over a region (spatial averaging reduces the contributions from large l to the summation in equation (10.2), then reducing the effects of both satellite error and misrepresentation of the gravity field due to the truncation error).

Spatial averaging

The mass contribution to Mediterranean MSL is computed by using an averaging kernel for $\Delta\sigma(\theta,\phi)$. The basin average can be represented as

$$\overline{\Delta\sigma} = \frac{1}{\Omega_{Med}} \int \Delta\sigma(\theta,\phi)\,\vartheta(\theta,\phi)\,d\Omega \tag{10.3}$$

where $d\Omega = \sin\theta\,d\theta\,d\phi$ is an element of solid angle, $\Omega_{Med} = \int \vartheta(\theta,\phi)d\Omega$, and

$$\vartheta(\theta,\phi) = \begin{cases} 1 & inside\ the\ Mediterranean \\ 0 & outside\ the\ Mediterranean \end{cases} \tag{10.4}$$

By expanding the exact averaging kernel $\vartheta(\theta,\phi)$ in terms of spherical harmonic coefficients, Eq. (10.2) can be written as follows (Swenson and Wahr, 2002)

$$\Delta\sigma(\theta,\phi) = \frac{a\rho_E}{3\Omega_{Med}} \sum_{l=0}^{60} \sum_{m=0}^{l} \frac{(2l+1)}{(1+k_l)} \Big[\vartheta_{lm}^c \Delta C_{lm} + \vartheta_{lm}^s \Delta S_{lm}\Big] \tag{10.5}$$

where ϑ_{lm}^c and ϑ_{lm}^s are the spherical harmonic coefficients describing $\vartheta(\theta,\phi)$:

$$\vartheta(\theta,\phi) = \frac{1}{4\pi} \sum_{l=0}^{60} \sum_{m=0}^{l} P_{lm}(\cos\theta)\Big[\vartheta_{lm}^c \cos(m\phi) + \vartheta_{lm}^s \sin(m\phi)\Big] \tag{10.6}$$

$$\begin{Bmatrix} \vartheta_{lm}^c \\ \vartheta_{lm}^s \end{Bmatrix} = \int \vartheta(\theta,\phi)\,P_{lm}(\cos\theta)\begin{Bmatrix} \cos(m\phi) \\ \sin(m\phi) \end{Bmatrix} \tag{10.7}$$

The use of the exact averaging kernel reduces the error due to truncation, however it increases the basin-averaged satellite measurements errors due to the presence of short-wavelength ϑ_{lm}^c and ϑ_{lm}^s in the expansion of $\vartheta(\theta,\phi)$. Swenson and Wahr (2002) showed that the expansion of an averaging kernel which varies smoothly across the basin boundary decreases the satellite errors in the estimates of basin-averaged surface mass change without increasing the error due to truncation. To compute the mass contribution to Mediterranean MSL we will use a Gaussian filter.

The approximate basin average, $\overline{\overline{\Delta\sigma}}$, can be computed by replacing the exact averaging kernel, $\vartheta(\theta,\phi)$, by the approximate averaging kernel, $W(\theta,\phi)$, in Eq. (10.3):

$$\overline{\overline{\Delta\sigma}} = \frac{1}{\Omega_{Med}} \int \Delta\sigma(\theta,\phi)W(\theta,\phi)\,d\Omega \tag{10.8}$$

Expanding the approximate averaging kernel, $W(\theta,\phi)$, in terms of spherical harmonic coefficients as

$$W(\theta,\phi) = \frac{1}{4\pi} \sum_{l=0}^{60} \sum_{m=0}^{l} P_{lm}(\cos\theta)\Big[W_{lm}^c \cos(m\phi) + W_{lm}^s \sin(m\phi)\Big] \tag{10.9}$$

the approximate basin average can be expressed in terms of Stokes coefficients as

$$\overline{\overline{\Delta\sigma}} = \frac{a\rho_E}{3\Omega_{Med}} \sum_{l=0}^{60} \sum_{m=0}^{l} \frac{(2l+1)}{(1+k_l)} \left[W_{lm}^c \Delta C_{lm} + W_{lm}^s \Delta S_{lm} \right]$$ (10.10)

The smooth averaging kernel $W(\theta,\phi)$ is created by convolving the exact kernel $\vartheta(\theta,\phi)$ with a Gaussian filter:

$$W(\theta,\phi) = \int \omega(\theta,\phi,\theta',\phi')\,\vartheta(\theta',\phi')\,d\Omega'$$ (10.11)

where,

$$\omega(\theta,\phi,\theta',\phi') = \frac{b}{2\pi} \frac{\exp\{-b[1-(\cos\theta\cos\theta' + \sin\theta\sin\theta'\cos(\phi-\phi'))]\}}{1-e^{-2b}}$$ (10.12)

$$b = \frac{\ln(2)}{(1-\cos(r_{1/2}/a))}$$ (10.13)

and $r_{1/2}$ is the half width of the Gaussian smoothing function. The Stokes coefficients in Eq. (10.10) are defined as

$$\begin{Bmatrix} W_{lm}^c \\ W_{lm}^s \end{Bmatrix} = 2\pi W_l \begin{Bmatrix} \vartheta_{lm}^c \\ \vartheta_{lm}^s \end{Bmatrix}$$ (10.14)

where W_l are computed recursively by the following relation:

$$W_0 = \frac{1}{2\pi}, \quad W_1 = \frac{1}{2\pi}\left[\frac{1+e^{-2b}}{1-e^{-2b}} - \frac{1}{b}\right], \quad W_{l+1} = -\frac{2l+1}{b}W_l + W_{l-1}$$ (10.15)
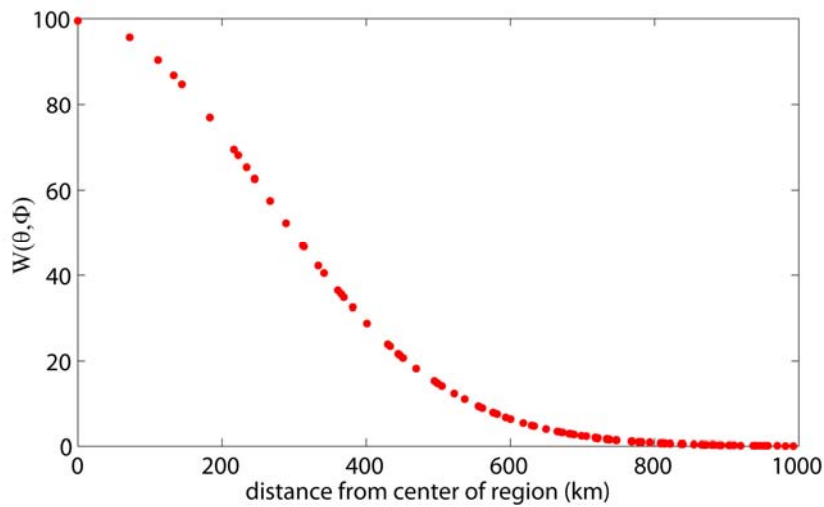
Figure 10.1. Gaussian averaging $W(\theta,\phi)$ as a function of separation distance for an averaging radius of 300 km.

The smoothing radius used for our analysis is 300 km (Fig. 10.1), significantly shorter than for most global applications. The resulting Gaussian averaging kernel for the estimation of the Mediterranean mean mass variation is shown in Figure 10.2.

Finally, the mass variations can be easily translated into sea level as $\overline{\overline{\Delta\sigma}} / \rho_W$, where ρ_W is the density of fresh water.
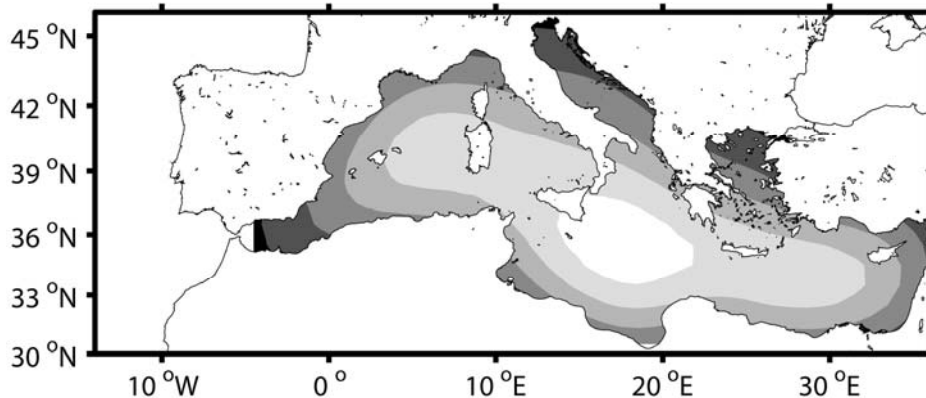
Figure 10.1. Gaussian averaging kernel used to calculate the Mediterranean averages of all fields.

A problem of applying a spatial averaging on global spherical harmonics is that large mass variations ocurring over land but within the smoothing radius of the kernel average will contribute to the basin average. This problem, referred to as leakage, is very relevant in all coastal regions, since the hydrology signal over land tends to be larger than the oceanic signal. In the case of the Mediterranean Sea it can significantly contaminate the sea signal of almost the whole basin, since the width of the basin is only of the order of several hundred km. In the following we show how it can be corrected.

Hydrology and leakage correction

There are several ways to reduce the leakage. Some authors simply mask not only all grid points on land, but also all ocean grid points located within a certain distance of coastlines (Chambers, 2006); in the Mediterranean Sea, however, this would mean living unmasked only a very small part of the basin. Another way consists of using GRACE data to first solve for the continental mass distribution, then removing the effects of that mass distribution from the GRACE geoid and finally using the residual data to compute the oceanic signal. But perhaps the best methodology is to use a hydrological model to remove the hydrology signal that contaminates the oceanic signal (Fenoglio-Marc et al., 2006). Using a hydrological model is particularly preferred when dealing with small basins such as the Mediterranean Sea.

In this work we have used the Climate Prediction Center (CPC) hydrological model to correct for the effect of land waters $\overline{\overline{\Delta\sigma}}_{Hydro}$ (Fan and van den Dool, 2004). The CPC model is a one-layer "bucket" water balance global model with a spatial resolution of

0.5º x 0.5º; the driving input fields are CPC monthly global precipitation data over land, for which it uses observations from over 17,000 gauges worldwide, and monthly global temperature from global reanalysis. The output consists of global monthly soil moisture, evaporation, and runoff, starting from January 1948 and extending up to present.

In order to correct for the leakage, the basin average computed using Stokes coefficients from GRACE is written as the sum of the ocean signal and the hydrological signal that has leaked into it:

$$\overline{\overline{\Delta\sigma}} = \overline{\overline{\Delta\sigma}}_{true} + \overline{\overline{\Delta\sigma}}_{Hydro} \tag{10.16}$$

The leakage $\overline{\overline{\Delta\sigma}}_{Hydro}$ is computed from CPC model data and subtracted to the signal computed from GRACE data, $\overline{\overline{\Delta\sigma}}$, to finally obtain the true signal, $\overline{\overline{\Delta\sigma}}_{true}$. In order to be consistent with GRACE data, the same averaging kernel (10.11) is to be applied to the hydrology signal over land $\overline{\overline{\Delta\sigma}}_{Hydro}$ prior to subtracting it from the GRACE signal.

The GIA correction

A final correction must be applied to obtain the mass contribution to Mediterranean Sea level. Not only the hydrology signal can leak into the oceanic signal, but also solid Earth processes leak into the gravimetric satellite solutions. The largest time-varying signal caused by a solid Earth process comes by far from the GIA, the continuing rebound of the Earth in response to the melting of the ice at the end of the last ice age. The GIA signal that the GRACE satellite observes is the sum of two contributions (referred to as the time rate of change of geoid height): the present-day rate of sea level rise relative to the deforming surface of the solid Earth and the time rate of change of radial displacement with respect to the center of mass of the planet. To GRACE, the GIA signal appears as a long term trend in the gravity field. This signal is not due to the redistribution of water over the Earth's surface and must therefore be removed.

For the GIA correction we use the ICE-5G VM2 model of the GIA process described in the work of Peltier (2004), which accounts for the two contributions mentioned above. The Peltier solutions are only available for tide gauge sites (they can be downloaded from http://www.atmosp.physics.utoronto.ca/~peltier/data.php); we therefore interpolated the values provided for tide gauges in the Mediterranean Sea (about 100 stations) onto a 1º x 1º regular grid covering the whole basin.

To correct GRACE data from GIA we need to convert the time rate of change of geoid height, $\dot{G}(\theta,\phi,t)$, to mass rate. To do this, we first compute the spherical harmonical coefficients from the gridded field of the GIA correction as described above

$$\dot{C}_{lm} = \frac{1}{\Omega_{Med}} \int_{\Omega} \dot{G}(\theta,\phi,t) P_{lm}(\cos\theta) \cos m\phi \, d\Omega$$

$$\dot{S}_{lm} = \frac{1}{\Omega_{Med}} \int_{\Omega} \dot{G}(\theta,\phi,t) P_{lm}(\cos\theta) \sin m\phi \, d\Omega \tag{10.17}$$

The coefficients are computed for all degrees and orders from 0 to 120. Using these Stokes coefficients that represent the time rate of change of geoid height, the average mass rate correction that is applied to GRACE data can then be computed using the same averaging function as GRACE (Eqs. 10.5 and 10.8). The average GIA correction obtained for the Mediterranean Sea is of -0.7 mm/yr of equivalent water. This is the value to be subtracted from the hydrologically-corrected GRACE average.

10.2.2 The altimetry, reconstruction and steric data sets

The total sea level fields contemporary to the GRACE period are obtained from the AVISO gridded SLA regional product for the Mediterranean Sea (see Section 3.2). That data set spans the period between November 1992 and December 2008, with a spatial resolution of 1/8°x1/8° and weekly time resolution. The GIA correction to be applied to altimetry data is only the contribution of the time rate of change of geoid height $\dot{G}(\theta,\phi,t)$. The average GIA correction for altimetry data computed by using the same averaging function as for GRACE data is -0.1 mm/yr. The overall accuracy of MSL for a single 10-d cycle of the altimeter is estimated in about ±5 mm (Leuliette et al., 2004). Assuming that the errors of subsequent cycles are not correlated, the uncertainty associated with monthly mean values will be $\pm 5/\sqrt{3}$ mm.

The total sea level fields used to infer the mass component for the period 1948-2000 come from the reconstruction obtained in Chapter 6. The uncertainty associated with the reconstructed Mediterranean MSL is ±1.5 cm (see the sensitivity study in section 6.3.2).

Finally, the steric contribution to Mediterranean sea level variability can be obtained from models or from hydrographic observations. It has been seen in Chapters 8 and 9 that all models show unrealistic large trends in the Western Mediterranean due to a warming drift in the deeper layers of that basin. On the other hand, hydrographic data are unevenly distributed in space and time. Since in this chapter we target to Mediterranean MSL values rather than to regional distributions, we considered that the handicap of hydrographic data is preferable to the handicap of models for the purpose of this study. Thus, the steric sea level is computed from the monthly 1°x1° gridded temperature and salinity fields produced by Ishii et al. (2009) by means of Eq. (3.2). The Ishii gridded fields span the period January 1945 to December 2006 and cover from surface to 700 m. The most important reason to use Ishii data instead of MEDAR data is that the first includes an estimation of the errors associated with the temperature and salinity gridded fields. These errors can be used to obtain the error associated with the steric contribution to Mediterranean MSL by means of the propagation methodology presented in Section 3.3. The errors associated with the basin mean steric sea level were found to vary from ±2.3 to ±3.8 cm for the period 1945-2006. For the GRACE period (2002-2006) the steric errors vary from ±2.3 to ±3.2 cm.

10.3 Results

10.3.1 Validation of the mass component against GRACE data for the period August 2002 to December 2008

The mass contribution to sea level as provided by GRACE is compared with the non-steric sea level estimation obtained by subtracting steric sea level from altimetric

observations for the period August 2002 to December 2006. Both total sea level (with the atmospheric forcing excluded) and steric sea level have been computed using the same smoothing spatial averaging kernel as the one applied to GRACE data (Eq. 10.8), so that the comparison is consistent. The spatial averaging kernel reduces the errors of all components; for the steric component, for instance, the uncertainty of the averaged series ranges between ±1.0 and ±1.5 cm.

Figure 10.3 shows the monthly time series of Mediterranean MSL and its components. Black lines show the atmospherically-corrected sea level from altimetry (upper panel), the steric component of sea level derived from the Ishii dataset (middle panel) and the mass component of sea level obtained from GRACE observations (bottom panel). Grey lines show the estimates resulting from adding or subtracting the two observational components of sea level other than the one shown in each panel. Thus, the comparison between the grey and black lines gives different views of the accuracy of the closure of the sea level budget.
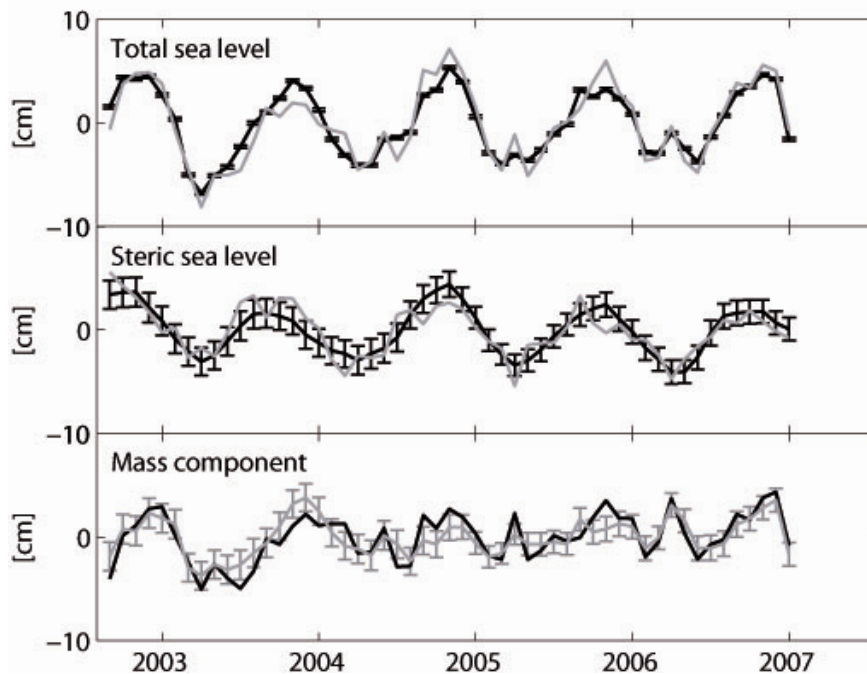
Figure 10.3. Mediterranean MSL variability and its components with error bars for the period August 2002 to December 2006: (atmospherically-corrected) total sea level (top), the steric component of MSL (middle), and the mass component of sea level (bottom). Black lines show the observed estimates from satellite altimetry (top), the Ishii dataset (middle) and GRACE (bottom), respectively. Grey lines show the estimates obtained by adding or subtracting the two observational components of sea level other than the one shown in each panel.

The most energetic signal of the atmospherically-corrected total sea level and the steric sea level is the seasonal cycle. Amplitudes and phases of the annual cycle for all components computed from August 2002 and December 2006 are listed in Table 10.1. Errors for the amplitudes and phases have been computed as a 95 % confidence interval by using bootstrapping. The unfiltered Mediterranean average of the atmospherically-corrected altimetry has an annual amplitude of 7.5±0.8 cm, peaking by the middle of October. The unfiltered averaged steric sea level has a smaller annual amplitude

(5.8±0.7 cm) and peaks early in October. That is, they are almost in phase, as expected, since the heating/cooling of the water column is the main forcing of the annual sea level cycle. It is remarkable that the amplitudes and phases of the independent estimates of atmospherically-corrected total sea level and steric sea level obtained from the other two components (grey lines in Fig. 10.3) are very similar to those obtained from observations: both the annual amplitude and the phase agree to within the computed error bounds (see Table 10.1).

For the mass component in particular (Fig. 10.3, bottom panel), the annual amplitude and phase of GRACE observations are 2.0±0.6 cm and 303±22 degrees, respectively; the amplitude and phase of the steric-corrected altimetry are 1.6±0.6 cm and 292±22 degrees, respectively. The observed mass component from GRACE and the estimated contribution from non-steric sea level have a correlation of 0.81 (significant at the 95% confidence level) and an rms difference of 1.3 cm. The largest difference between the two curves is found during the second half of 2006, when GRACE observations are higher than non-steric sea level by 2.9 cm.

Table 10.1. Seasonal cycle annual amplitudes and phases of Mediterranean MSL (as given by atmospherically-corrected altimetry) and of the different sea-level components estimated for the period from August 2002 to December 2006. The overbar denotes filtered basin average (i.e., using the averaging Kernel suitable for GRACE data). Errors associated with amplitudes and phases have been computed as a 95 % confidence interval by using bootstrapping.

Field	Amplitude [cm]	Phase [degree]
Altimetry	7.5±0.8	264±3
Steric (Ishii)	5.8±0.7	248±3
$\overline{Altimetry}$	4.1±0.4	263±7
$\overline{Steric}$ (Ishii)	2.9±0.3	248±6
$\overline{GRACE}$	2.0±0.6	303±22
$\overline{Steric}$ (Ishii) $+ \overline{GRACE}$	4.4±0.7	270±10
$\overline{Altimetry} - \overline{GRACE}$	2.9±0.5	237±8
$\overline{Altimetry} - \overline{Steric}$ (Ishii)	1.6±0.6	292±22

An analysis of the percentage of variance explained by the seasonal cycle shows that the 95% confidence interval is (77%, 91%) for the atmospherically-corrected altimetry and (79%, 93%) for the steric sea level. For the mass component estimated from GRACE observations, however, the 95% confidence interval is (8%, 52%). This indicates that the existence of a seasonal cycle in the mass component of Mediterranean MSL is not evident and, if it exists, it is not the most energetic signal.

This can be illustrated by removing the seasonal cycle from all time series (Fig. 10.4). The residual of the mass component (Fig. 10.4, bottom panel) is very similar to the mass component with the seasonal cycle included (Fig. 10.3, bottom panel), while both the residual of total sea level (Fig. 10.4, top panel) and the residual of steric sea level (Fig. 10.4, middle panel) are very different from the corresponding time series

with the seasonal cycle included (Fig. 10.3). It is also worth noting that the interannual variability is less pronounced for steric sea level than for the mass component, so that the second resembles more total sea level than the first (Fig. 10.4); the correlation between the interannual variability of the mass component from GRACE and of the (atmospherically-corrected) altimetry is 0.7.

Finally, we have also computed the linear trends of the different de-seasoned sea level components, bearing in mind that a 5-year trend reflects mainly the inter-annual variability and can obviously not be extrapolated to longer periods. Prior to the computation of the linear trends, time series were filtered with a 6-month running average. The linear trend of the steric-corrected altimetry and that obtained from GRACE are fully consistent: their values are 4.9±2.7 mm/yr and 5.1±1.4 mm/yr, respectively. All trends have been estimated using the MM-regression estimator calculated with an initial S-estimate that was presented in Section 3.4. Errors associated with the total and steric sea level have been taken into account in the analysis of the trend uncertainty carried out by means of the robust bootstrap described in Section 3.4.
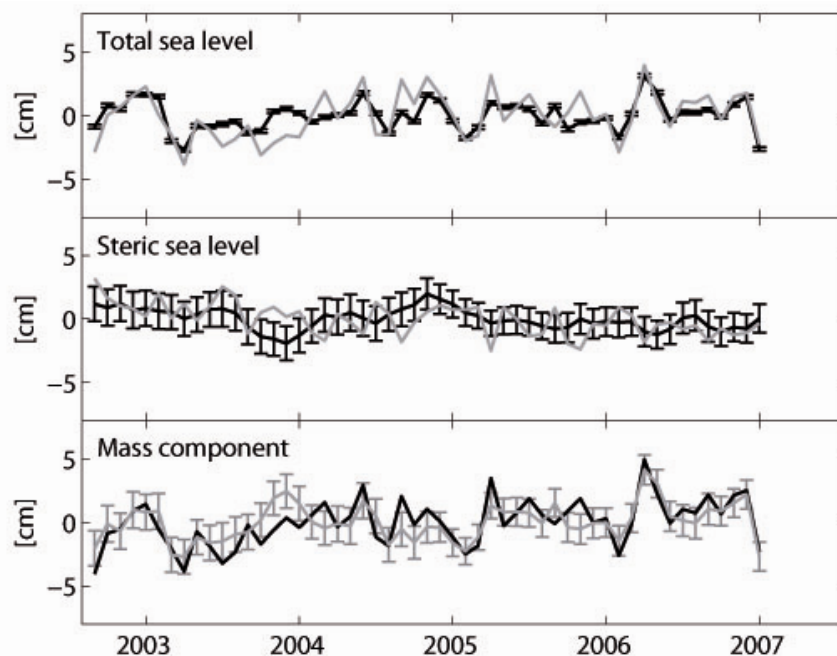
Figure 10.4. Same as Figure 10.3, but with the seasonal cycle removed.

As a complementary validation test we have computed the steric-corrected total sea level for a longer period by using the EN3 data set (see Section 3.3). The EN3 does not provide error estimates for the temperature and salinity gridded fields, but it spans the period 1950-2008 and thus it can be used to compute the steric sea level until December 2008. This additional validation will be useful to check whether the good agreement found between steric-corrected altimetry and GRACE for the period August 2002 to December 2006 holds for a longer period.

Figure 10.5 shows the monthly time series of Mediterranean MSL and its components for the period August 2002 to December 2008 in which the steric contribution to Mediterranean MSL has been computed from the EN3 data set. The

good agreement between GRACE and steric-corrected total sea level found for the period 2002-2006 also holds for this longer period. The two signals have a correlation of 0.78 (significant at the 95% confidence level) and an rms difference of 1.2 cm. Amplitudes and phases of the annual cycle for all components computed from August 2002 and December 2008 are listed in Table 10.2. The amplitudes and phases of the independent estimates of atmospherically-corrected total sea level and steric sea level obtained from the other two components (grey lines in Fig. 10.5) are in very good agreement with those obtained from the observations. In fact, the annual amplitudes are exactly equal for the filtered total and steric sea level (4.0 and 2.8 cm, respectively), and almost equal for the filtered mass component (Fig. 10.5, bottom panel): 1.3 ± 0.4 cm from GRACE and 1.5 ± 0.5 cm from the steric-corrected total sea level. Phases also agree within the computed error bounds.
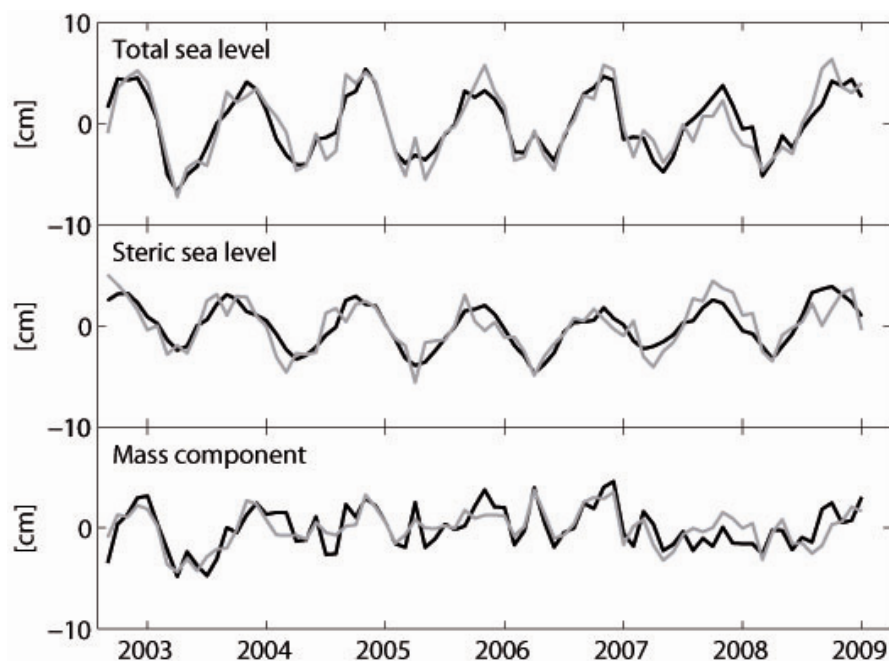
Figure 10.5. Mediterranean MSL variability and its components with error bars for the period August 2002 to December 2008: (atmospherically-corrected) total sea level (top), the steric component of MSL (middle), and the mass component of sea level (bottom). Black lines show the observed estimates from satellite altimetry (top), the EN3 dataset (middle) and GRACE (bottom), respectively. Grey lines show the estimates obtained by adding or subtracting the two observational components of sea level other than the one shown in each panel.

For this longer period, an analysis of the percentage of variance explained by the seasonal cycle shows that the 95% confidence interval is (79%, 89%) for the atmospherically-corrected altimetry and (79%, 89%) for the steric sea level. For the mass component estimated from GRACE data the 95% confidence interval is (5%, 41%), which confirms the result obtained before: the seasonal cycle of the mass contribution to Mediterranean MSL is rather weak. This can be visualized again by removing the seasonal cycle from all time series (Fig. 10.6). The residual of the mass component (Fig. 10.6, bottom panel) bears a strong resemblance to the mass component with the seasonal cycle included (Fig. 10.5, bottom panel).

Table 10.2. Seasonal cycle amplitudes and phases of Mediterranean MSL (as given by atmospherically-corrected altimetry) and of the different sea-level components estimated for the period from August 2002 to December 2008. The overbar denotes filtered basin average (i.e., using the averaging Kernel suitable for GRACE data). Errors associated with amplitudes and phases have been computed as a 95 % confidence interval by using bootstrapping.

Field	Amplitude [cm]	Phase [degree]
Altimetry	7.3±0.7	263±6
Steric (EN3)	5.2±0.5	246±5
$\overline{Altimetry}$	4.0±0.4	263±5
$\overline{Steric}$ (EN3)	2.7±0.3	249±6
$\overline{GRACE}$	1.6±0.5	301±24
$\overline{Steric}$ (EN3) $+ \overline{GRACE}$	4.0±0.6	267±10
$\overline{Altimetry} - \overline{GRACE}$	2.8±0.5	243±9
$\overline{Altimetry} - \overline{Steric}$ (EN3)	1.5±0.5	291±20
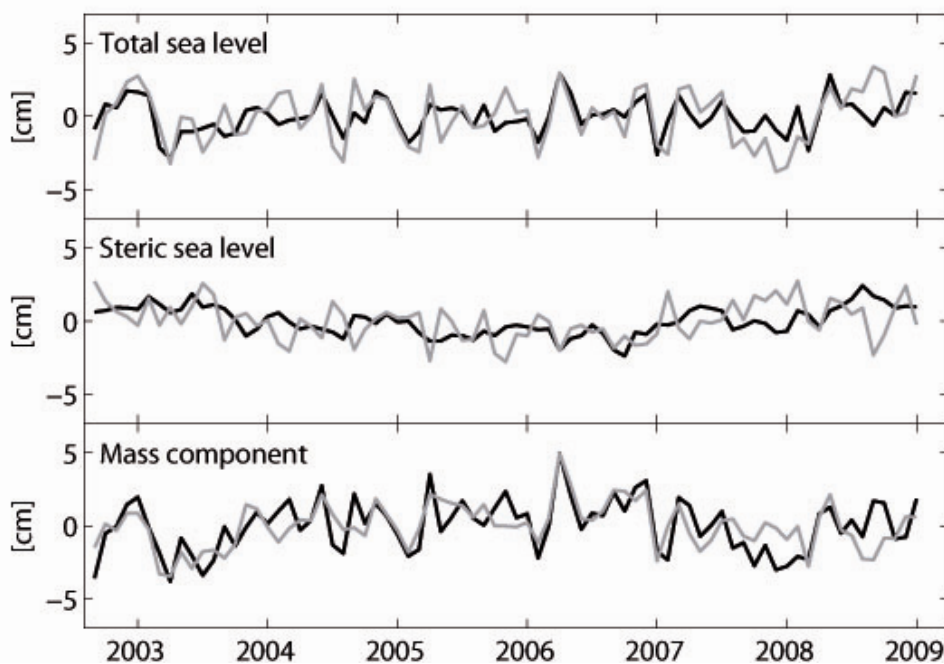
Figure 10.6. Same as Figure 10.5, but with the seasonal cycle removed.

The linear trends of the mass component from GRACE and from the steric-corrected altimetry for the period August 2002 to December 2008 are also fully consistent: their values are -0.8±0.8 mm/yr and -0.6±0.9 mm/yr, respectively.

10.3.2 Mass contribution to Mediterranean sea level for the period 1948-2000

The major point of the previous section is not the value of the trend of the mass component, which has little value due to the short period considered in the analysis, but the consistency between non-steric sea level and GRACE observations. Such a consistency supports that the mass component can be obtained as the non-steric contribution of Mediterranean sea level for a longer period, provided that total and steric sea level fields are available.

Total sea level fields (including the atmospheric contribution) covering the last decades are available from the reconstruction obtained in Chapter 6. Atmospherically-induced sea level variability must be removed from the total signal to make it consistent with the comparisons shown in the previous section. The atmospheric contribution to sea level has been quantified (using the inverted barometer approach) from a NCEP/NCAR reanalysis spanning the period 1948-2000 (Kalnay et al., 1996). The reason for not using the HIPOCAS data set is that it begins in 1958, while here we intend to determine the mass component starting a decade before. The steric contribution to sea level, on the other hand, has been quantified using the Ishii hydrographic data base.

Figure 10.7 shows the basin mean values of atmospherically-corrected total sea level as given by the reconstruction (upper panel), the steric sea level obtained from the Ishii data set (middle panel) and the non-steric (or mass) component resulting from the difference of the two (bottom panel). As in Figure 10.4, the interannual variability of the steric component is smoother than for the mass component, which is therefore more similar to the atmospherically-corrected total sea level.

The time period spanned by Figure 10.7 can be divided into three periods with different behaviors in the steric and atmospherically-corrected total sea level. Until the beginning of the 60s, the steric component does not show significant trends, so that the increase observed in total sea level (3.7±0.4 mm/yr for the period 1948-1960) would be entirely due to the mass component. From the early 60s to the early 90s, the steric sea level shows negative trends (-0.7±0.1 mm/yr for the period 1961-1992) while the atmospherically-corrected total sea level shows slightly positive trend (0.3±0.1 mm/yr). Finally, from the early 90s to the end of the sampled period the steric sea level shows a clear positive trends (6.3±0.4 mm/yr for the period 1993-2000), which coincides with a sharp increase in total sea level. The overall trends computed for the period 1948-2000 are -0.25±0.04 mm/yr for the steric component and 0.96±0.05 mm/yr for the atmospherically-corrected total sea level. The net mass contribution to sea level trends would then be of the order 1.2±0.2 mm/yr.

In all the above considerations the atmospheric component has been excluded from all computations. In order to visualize actual total sea level, the atmospheric component has now been included in Figure 10.8. For the first sub-period, until the early 60s, the total sea level (top panel) shows a larger positive trend (5.0±0.5 mm/yr for the period 1948-1960) when the atmospheric contribution is included. From the early 60s to the early 90s, the negative steric (Figure 10.7, middle panel) and atmospheric (Figure 10.8, middle panel) trends (-0.7±0.1 mm/yr and -0.8±0.2 mm/yr respectively) would compensate and even exceed the positive trend of the mass component, then resulting in the slight decrease observed for total sea level (-0.5±0.1 mm/yr). For the last years of the period, the total sea level shows a clear positive trend (5.4±0.7 mm/yr for the period 1993-2000).
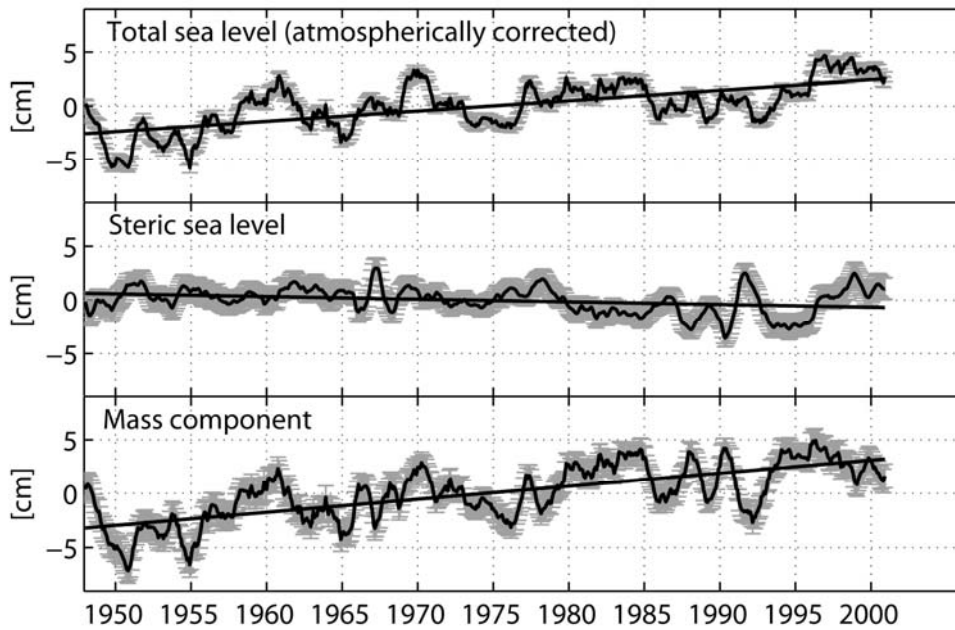
Figure 10.7. Mediterranean MSL variability and its components with error bars for the period 1948-2000: (atmospherically-corrected) total sea level reconstructed from a reduced-space optimal interpolation of altimetry tide gauge records (top), the steric component of MSL computed from the Ishii dataset (middle), and the steric- (and atmospherically-) corrected total sea level (bottom). Mean values are removed from each series and they are smoothed using a 12-month running average.
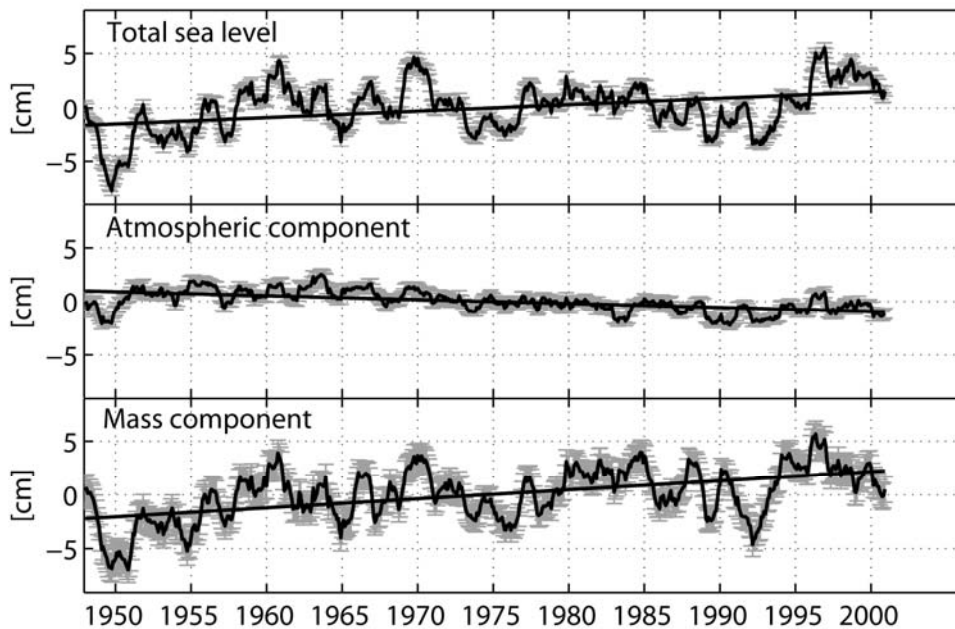
Figure 10.8. Mediterranean MSL variability and the mass and atmospheric components with error bars for the period 1948-2000. Total sea level (with the atmospheric component included) obtained from the reconstruction (top), the atmospheric component of sea level as given by the NCEP/NCAR reanalysis (middle), and the steric-corrected total sea level (bottom). The steric component is not shown since it is the same as in Figure 10.7. Mean values are removed from each series and they are smoothed using a 12-month running average.

The trends corresponding to the total period 1948-2000 (when the atmospheric component is included) are: 0.59±0.05 mm/yr for total sea level and 0.8±0.1 mm/yr for the mass component (which now also accounts for the mass exchanges through Gibraltar due to differential atmospheric pressure at each side of the Strait. The values are rather different from those reported before due to the negative trend of the atmospheric component (-0.37±0.07 mm/yr for the whole period 1948-2000), which is particularly marked from the 60s to the 90s (-0.8±0.1 mm/yr for the period 1960-1990).

10.4 Summary and Conclusions

The mass contribution to Mediterranean sea level variability measured by GRACE is consistent with the estimation obtained by subtracting the steric sea level (from the Ishii data set) from the atmospherically-corrected altimetry for the period August 2002 to December 2006. The correlation between monthly observed and estimated mass variations is 0.75 and the rms difference is 1.4 cm. Once the atmospheric component is removed from total sea level, the seasonal sea level cycle is mainly annual and caused by the expansion/contraction of the water column. Thus atmospherically-corrected altimetry and steric annual sea level signals are found to be in phase, as expected. We have presented an additional validation test for a longer period (2002-2008) using a different hydrographic data base (EN3), which does not include error estimates for the temperature and salinity gridded fields but provides data up to December 2008; the very good agreement between GRACE observations and the steric-corrected total sea level also holds for that period.

The seasonal cycle of mass variations in the Mediterranean has been examined on the basis of altimetric observations and modeled steric sea level in previous works (García et al., 2006; Fenoglio-Marc et al., 2006; Fenoglio-Marc et al., 2007). Fenoglio-Marc et al. (2007) found that the annual amplitude of atmospherically-corrected total sea level was 8.3±0.2 cm, whereas modeled steric sea level was 5.0±0.4 cm for the period April 2002 to July 2004. Our estimates for annual amplitudes are 7.5±0.8 cm and 5.8±0.7 cm for the unfiltered atmospherically-corrected total sea level and the steric component, respectively, computed for the period from August 2002 to December 2006 (Table 10.1). To reconcile both results, the annual amplitudes have also been computed for the same period than in Fenoglio-Marc et al. (2007): from August 2002 to August 2004; the results are 8.0±1.4 cm and 5.2±1.0 cm for the unfiltered atmospherically-corrected total sea level and steric sea level, respectively, which are consistent with those obtained by Fenoglio-Marc et al. (2007). Regarding the phase, Fenoglio-Marc et al. (2007) found it to be 284±2 degree for atmospherically-corrected total sea level and 256±4 degree for modeled steric sea level. Our estimates for the unfiltered fields are 264±3 degree for total sea level and 248±3 degree for steric sea level, when computed for the period August 2002 to December 2006 (Table 10.1); for the period August 2002 to August 2004 the values are 270±4 and 233±5 degree (i.e., they differ in 15-25 degrees with respect to those computed by Fenoglio-Marc et al., 2007).

The seasonal cycle of the mass component is less clear. A bootstrap analysis of the annual amplitude of the mass component (filtered with a 300 km filter radius) applied to GRACE observations spanning the period August 2002 to December 2006 gives a 95% confidence interval of (1.3, 2.5) cm. This range is smaller than the 2.8±0.6 cm obtained by Fenoglio-Marc et al. (2007) from GRACE data spanning the period from April 2002 to July 2004 and filtered with a 400 km filter radius. A bootstrap analysis of the annual amplitude for a similar period (August 2002 to August 2004) provides a 95%

confidence interval of (1.6, 3.4) cm. Although the result (with its associated uncertainty) given by Fenoglio-Marc et al. (2007) falls within our 95% confidence interval, it is placed at the upper bound of the interval.

Bootstrapping can also be used to obtain a confidence interval for the percentage of the variance of the mass component explained by the seasonal cycle. Using GRACE data spanning the whole period August 2002 to December 2006, a 95% confidence interval for the variance explained is (8%, 52%), whereas it is (5%, 75%) from August 2002 to August 2004. These big differences between the seasonal cycles estimated for different periods are observed neither for total sea level nor for steric sea level. Our conclusion is that the seasonal cycle of the mass component in the Mediterranean Sea is not clear and that it may have been overestimated in the past.

Regarding the interannual variability, the most noticeable feature is the smoothness of the steric component when compared to (atmospherically-corrected) total sea level. This makes that the mass component exhibits a variability that resembles total sea level. This feature is confirmed by the independent GRACE observations.

A major point of the analysis of the period 2002-2008 is the good agreement found between GRACE observations and steric-corrected sea level, which suggests that the mass component could be estimated for a longer period as far as total and steric sea level are available. This is however limited by the reliability of total and steric sea level fields for the past decades. The reconstruction of total sea level used in this work had been submitted to several tests (Chapter 6) and compared against model data (Chapters 8 and 9). The reliability of steric sea level has required more attention, specially taking into account that as we go back in time it is computed on the basis of fewer and sparser observations. A careful and rigorous uncertainty analysis has been applied in order to overcome this limitation. Therefore the mass contribution for the period 1948-2000 and the associated uncertainty estimated in this work are probably the best estimates that can be obtained using the presently available data.

The trends of the different components of sea level have also been obtained. The trend of the steric component has been found to be negative for the period 1948-2000. This makes that the trend of the (atmospherically-corrected) mass component (1.2±0.2 mm/yr) is larger than the trend of (atmospherically-corrected) total sea level (0.97±0.07 mm/yr). When the atmospheric component is included, the trends for total sea level and the mass component are 0.59±0.05 mm/yr and 0.8±0.1 mm/yr, respectively.

The value obtained for the atmospherically-corrected mass contribution is in agreement with the global mean value obtained by Domingues et al. (2008) for the period 1961-2003 (between 0.8 and 1.1 mm/yr). Also Marcos and Tsimplis (2007a) found a similar trend (1.2 mm/yr) for the atmospherically- and steric-corrected sea level inferred from Mediterranean tide gauge records for the period 1961-2000.

A major conclusion is that the small sea level increase observed in the Mediterranean during the second half of the 20th century (0.6±0.1 mm/yr for the period 1948-2000, 0.3±0.1 mm/yr between 1961-2000) relative to the global ocean trend (1.6±0.2 mm/yr for the period 1961-2003) would not be due to a smaller mass component, but to the negative steric and atmospheric contributions to sea level. The negative contribution of atmospheric pressure had already been reported (see for instance Gomis et al., 2008). The steric contribution has been more controversial, as the estimated trends range between zero and slightly negative values.

Chapter 11

Concluding remarks and future work

SEA level variability has a significant environmental and socio-economic impact on coastal regions. Presently, one of the most important risks comes from the possibility of a significant increase in MSL over this century as a result of global warming. This work was initially motivated by the will to achieve a better understanding on MSL changes in the Mediterranean Sea, which is a compulsory requirement to predict its impact and, if necessary, to set up mitigation strategies. In this dissertation we have studied the long-term Mediterranean sea level variability in the last half century paying special attention to the computation of sea level trends and the quantification of the physical processes that are responsible for the observed variability, namely: the ocean mass increase derived from the melting of ice sheets, the volume increment due to changes in temperature and salinity (steric component) and the regional atmospheric contribution. The results presented in this thesis are based on a diversity of observations: tide gauge and satellite altimetry data for total sea level, GRACE gravimetry data for the mass component and hydrographic data bases for the steric component. Model data have also been used for the estimation of the atmospheric and steric components.

In this chapter we summarize the most important conclusions outlined along this thesis and make some plans for the future work.

Linear and non-linear techniques and their application to the analysis of Mediterranean sea level variability:

- The linear and nonlinear PCA applied to satellite altimetry data in the Mediterranean Sea for the period 1993-2000 (Chapter 5) have produced very similar overall results, but with some differences: while PCA mode 1 describes only a standing oscillation of the basin as a whole, the nonlinear mode 1 shows some features from both PCA mode 1 and mode 2. This simply shows that if the physical processes driving the sea level variability are nonlinear, then the

nonlinear PCA mode 1 will be more effective in detecting it since it can detect more than just a standing oscillation. Nevertheless, the time series associated with linear and nonlinear PCA modes 1 are almost equal and the variance explained by the nonlinear mode 1 (62.3 %) is not significantly different from the variance explained by the classical PCA mode 1 (61.6 %).

- When using nonlinear PCA for the detection of sea level circulation regimes, one must be aware that sometimes the method diagnoses spurious features in Gaussian distributed data (or nearly so). Moreover, depending on the neural network architecture used for the nonlinear PCA, the class of approximation shapes could be limited, and then the parameterization of the associated time series would be arbitrary up to a homeomorphism (Christiansen, 2005).

- A reconstruction of sea level fields carried out with both linear and nonlinear PCA has shown that the results obtained from the classical PCA are more stable than those obtained from nonlinear PCA. The nonlinear reconstruction has proven to be very sensitive to the time series presented to the decoding function *g* (Eq. 5.14). Slightly different time series can produce very different results, which is a serious handicap since it implies that the nonlinear reconstruction is very sensitive to the tide gauges used in the analysis.

- All these results suggest that the use of nonlinear PCA for the analysis of Mediterranean sea level does not compensate for its much more complicated implementation in terms of both, mathematics and computer resources. Moreover, results are less robust and their interpretation is less clear than for the classical PCA.

Reconstruction of Mediterranean sea level fields for the period 1945-2000

- A reconstruction of sea level fields by using a reduced-space optimal interpolation method for the last half century has been obtained for the first time in the Mediterranean Sea (Chapter 6). This methodology combines in an optimal way spatial patterns obtained from satellite altimetry with time series obtained from tide gauges. The robustness and sensitivity of such reconstruction have been tested upon different tide gauge distributions, EOFs computed for different periods and different number of EOFs entering the analysis. The recovery of the major features has been shown to be insensitive to all these factors.

- Results for the period 1993-2000 are in very good agreement with the results obtained from satellite altimetry data. The reconstruction reproduces the distribution of sea level trends that characterizes the post-EMT years (marked negative trends in the Ionian and positive trends in the Aegean) with a high degree of accuracy. It also reproduces the observed inter-annual variability of the Mediterranean MSL and its trend (3.5±0.7 mm/yr as compared to the 3.9±0.7 mm/yr given by altimetry)

- Results for the period 1945-2000 have been validated against independent tide gauges and they have shown very high correlations (up to 0.85). The main features of the distribution of sea level trends are the maximum peak of positive trends in the Ionian Sea and the larger positive trends in the Western Mediterranean than in the Eastern Mediterranean. The rate of MSL rise has been estimated in 0.6±0.1 mm/yr for that period.

The atmospheric component:

- The atmospheric contribution has been investigated in previous works, so that here it has only been summarized for the sake of completeness (Chapter 7). It shows a clear negative inter-decadal trend of about -0.60±0.04 mm/yr (ranging from -0.5 mm/yr in the Levantine basin and in the vicinity of Gibraltar to less than -0.7 mm/yr in the Adriatic) for the period 1958-2001, mainly due to the increase of the winter atmospheric pressure over the region (Gomis et al., 2008).

Total and steric sea level from the OM8 model and comparison with the reconstruction:

- For the period 1993-2000 the OM8 model reproduces some of the main features shown by the distribution of observed and reconstructed trends (Chapter 8). However, it does not perform well in reproducing the marked negative trends found in the Ionian Sea during that period. Regional averaged time series over the Western and Eastern Mediterranean and the Aegean and Ionian Seas show that the total sea level computed from the model reflects some of the major features of the altimetric inter-annual variability, but in all regions the reconstruction shows higher correlation with observations than the model. The reconstruction also reproduces the observed regional trends closer than the model in all regions.

- The steric sea level obtained from the OM8 model is very similar to total sea level, showing the same inter-annual variability and very similar trends over all selected regions for the period 1993-2000. This is not surprising, since the model simulation does not account for remote sources of sea level variability (such as the mass contribution from the melting of continental ice). What this indicates is that the non-geostrophic changes in the circulation (the dynamical component not accounted for by the steric contribution) are rather small and local.

- For the period 1961-2000 the distribution of sea level trends obtained from the model reproduces the positive trends in the Ionian Sea shown by the reconstruction; conversely, significant differences are found in the pattern of the trends in other regions. The rate of Mediterranean MSL rise given by the model for this period is in good agreement with the reconstructed MSL rise. Regional trends are also in good agreement in the Ionian and in the Western Mediterranean, although they appear to be slightly higher in most regions.

- The distribution of steric sea level trends shows unrealistic large positive trends all over the Western basin. This is due to a warming drift in the deeper layers of the model.

More on the steric sea level: comparison of results from three baroclinic models of the Mediterranean Sea

- The MITgcm, OM8 and ORCA models have been compared for the period 1961-2000 in the Mediterranean Sea. The three models perform well in reproducing the inter-annual variability of 3D averaged temperatures over the

Western and Eastern Mediterranean in the top 500 m. For the layer 500-1000 m significant correlations between observed and modeled averaged temperature are only found for the MITgcm and OM8 models. The ORCA model shows no inter-annual variability. For the layers below 1000 m no model shows significant correlations with observations.

- No model performs well in reproducing the 3D averaged salinity shown by the observations. However, it must be taken into account that salinity observations are sparse in space and time and therefore that the gridded products obtained from observations (e.g. the MEDAR and Ishii data sets) are less reliable than for temperature. The ORCA model shows a much weaker variability than the other two models.

- All models suffer from a warming drift in the deeper layers of the Western Mediterranean, which is more pronounced in the MITgcm and OM8 models.

- The study of the EMT period (1987-1995) in terms of dense water formation and water mass properties has shown that the only model reproducing the observed deep water formation in the Aegean Sea is the MITgcm model. The OM8 model does show formation of dense water in the Aegean Sea, but most of it in the form of intermediate water. In the Adriatic Sea the MITgcm model is again the one showing higher rates of deep water formation, though the difference with respect to the OM8 model is less marked in that region. The ORCA model shows really weak rates of dense water formation in both regions.

- The MITgcm is the only model that reproduces the observed distribution of sea level trends that characterizes the post-EMT period. It is also the one giving higher correlations with observations when looking at regional sea level averages. The ORCA model shows unrealistic large total sea level trends indicating that we can barely trust total sea level from that model.

- For the total period 1961-2000 both the MITgcm and OM8 models reproduce the positive sea level trends shown by the reconstruction in the Ionian Sea. Also the inter-annual variability of regionally averaged total sea level over the Ionian and Aegean Seas given by the MITgcm and OM8 models is very similar to the reconstructed sea level. The trends shown by those two models are also in good agreement with the reconstructed trends.

- The steric sea level from the ORCA model does not show the unrealistic large trends shown by the total sea level, which suggests that the reason for the unrealistic trends must be searched for outside the Mediterranean (ORCA is a global model and therefore accounts for remote sources).

Mass contribution to Mediterranean sea level variability

- Good agreement between direct measures of the mass component of Mediterranean MSL (inferred from GRACE observations) and steric-corrected sea level (obtained from altimetry minus the steric signal derived from hydrographic data) has been found for the period August 2002 to December 2008. The agreement is found for both the inter-annual variability and the trend of the mass contribution to MSL.

- Basing on the consistency found for the gravimetric period, the mass component

for the period 1948-2000 has been estimated from the steric-corrected total sea level; for that period, the total sea level fields have been obtained from the reconstruction. The trend of the mass component has been estimated in 1.2±0.2 mm/yr, which is in good agreement with global estimates.

As a concluding remark it can be stated that, during the last five decades, Mediterranean MSL has been rising at a significantly lower rate than global MSL. The main reason is the negative contribution of the atmospheric component (due to an increase of the atmospheric pressure over the region), though the steric component has also been lower than at global scale. Both contributions are particularly negative between the sixties and the nineties. Conversely, the estimated value of the mass component is rather constant in time and similar to the global value. The trends associated with the different contributions to Mediterranean MSL and computed for different periods as they appear along this dissertation are summarized in Table 11.1.

11.1 Future work

In this thesis we have studied the long-term sea level variability of the Mediterranean Sea and answered many of the questions raised at the beginning of the work. To do this, we have based on observations and models covering a part or most of the last five decades. There are still some uncertain issues due to the absence of observations; perhaps the most important one is the estimation of the mass component. The uncertainty associated with this component is expected to reduce as the amount of gravimetric observations increases and the spatial resolution of these observations decreases. At global scale, significant efforts are devoted precisely to quantify the rate of continental ice melting and to model the distribution of the rush of freshwater over the global ocean. Therefore some additional efforts are likely to be devoted to this issue also in the Mediterranean Sea.

Basing on the acquired knowledge on the physical processes that drive Mediterranean sea level variability, it seems natural that the next step of our research is to attempt the projection of sea level variations for the 21th century under different greenhouse gases scenarios. This work will be carried out in the framework of the VANIMEDAT-2 project (CTM2009-10163-C02-01, funded by the Spanish Marine Science and Technology Program and by the E-Plan of the Spanish Government) and of a contract sponsored by the Spanish Met Office (AEMET). The geographical context of the study will be the Mediterranean Sea and a sector of the NE Atlantic Ocean, in order to cover all the Spanish shores..

The main motivation for the work is the fact that the global models used in the framework of the IPCC cannot account for regional scale variability. This is specially true for the Mediterranean Sea, where we have shown that models with low spatial resolution cannot account for relevant processes such as deep water formation.

The overall objective of the forthcoming work (the generation of oceanographic scenarios for the 21st century, with particular attention to sea level) can be split into five specific objectives and associated tasks:

1. Adapting a baroclinic model to the simulation of future scenarios. This will require a set of tests to ensure that the configuration of the model to be used (NEMO) in

terms of parameterizations, resolution, boundary conditions and other constraints, is suitable to predict the main hydrodynamical variables (temperature, salinity, currents and sea level).

2. Running the baroclinic simulations for the 21st century. The forcings will be obtained from the output of regional atmospheric models that in turn have been forced with a radiative term derived for different scenarios of greenhouse gas emissions. The product will be a set of scenarios for the main hydrographic variables.

3. Running barotropic simulations for the 21st century. The atmospheric pressure and wind fields used to force the model will be obtained from the regional atmospheric models mentioned above. The product will be the atmospheric component of sea level variability and in particular a report on eventual changes in the sea level extreme regime with respect to present.

4. Quantifying the uncertainties associated with the predictions. These uncertainties derive from multiple sources: uncertainties in the forcing fields, limitations in the resolution and physics of the models, etc.. This objective is considered to be as important as obtaining the simulation themselves.

The new projects are a real challenge, but constitute a very suitable framework to consolidate the research career of a recent PhD, as well as to trigger the career of new PhD students.

Table 11.1. Mediterran MSL trends for total sea level (a), the atmospheric contribution (b), the steric component (c) and the mass component (d). A 12-month running average was applied to all MSL time series (except to the steric sea level from MEDAR) before computing the trends. For the period 1993-2000, the 12-month running average was applied after extracting the values of that period from the whole series (with the derived consequences at the boundaries of the series) in order to obtain comparable trends with altimetry (for which data are only available for that period). P and S refer to the atmospheric and steric components, respectively.

(a) TOTAL SEA LEVEL TRENDS [mm/yr]

Period	1945-2000	1948-2000	1961-2000	1993-2000
Altimetry (with P)	-	-	-	3.9±0.7
Reconstruction	0.6±0.1	0.6±0.1	0.2±0.1	3.5±0.7
MITgcm	-	-	1.2±0.1	3.7±0.2
ORCA	-	-	8.2±0.2	23.3±2.4
OM8	-	-	1.2±0.1	5.4±0.2

(b) ATMOSPHERIC COMPONENT TRENDS [mm/yr]

Period	1948-2000	1961-2000	1993-2000
HIPOCAS	-	-0.7±0.1	0.7±0.3
NCEP	-0.4±0.1	-0.6±0.1	0.6±0.3

(c) STERIC SEA LEVEL TRENDS [mm/yr]

Period	1948-2000	1961-2000	1993-2000
MEDAR (600 m)	-0.4±0.1	-0.8±0.2	4.8±1.9
Ishii (700 m)	-0.3±0.1	-0.5±0.1	6.5±0.7
MITgcm	-	1.3±0.1	4.2±0.2
ORCA	-	1.3±0.1	3.8±0.3
OM8	-	1.3±0.1	5.9±0.2

(d) MASS COMPONENT TRENDS [mm/yr]

Period	1948-2000	1961-2000	Aug 2002-2006	Aug 2002-2008
GRACE	-	-	5.1±1.4	-0.8±0.8
Altimetry-S (Ishii)	-	-	4.9±2.7	-
Altimetry-S (EN3)			4.8±1.0	-0.6±0.9
R-S (Ishii)-P	1.2±0.2	1.2±0.2	-	-

References

Aloisi, J. C., Monaco, A., Planchais, N., Thommeret, J., Thommeret, Y., 1978. The Holocene transgression in the Gulf du Lion, southwestern France: Paleographic and Palobotanical evolution. Géographie Physique et Quaternaire, *32*, 145-162.

Álvarez-Fanjul, E., Pérez, B., Rodríguez, I., 1997. A description of the tides in the Eastern North Atlantic. Progress in Oceanography, *40*, 217–244.

Álvarez-Fanjul, E., Pérez, B., Rodríguez, I., 2001. NIVMAR: a storm-surge forecasting system for Spanish waters. Scientia Marina, *60*, 145–154.

Antonov, J.I., Levitus, S., Boyer, T.P., 2005. Steric variability of the World ocean, 1955-2003. Geophysical Research Letters, *32*(12), L12602.

Artale, V., Calmanti, S., Carillo, A., Dell'Aquila, A., Herrmann, M., Pisacane, G., Ruti, P. M., Sannino, G., Struglia, M. V., Giogi, F., Bi, X., Pal, J. S., Rauscher, S., The PROTHEUS Group, 2009. An atmosphere-ocean regional climate model for the Mediterranean area: assessment of a present climate simulation. Climate Dynamics (in press).

Barnier, B., 1998. Forcing the Ocean. In: E.P. Chassignet and J. Verron, Editors, Modeling and parameterization, Kluwer Academic Publishers, The Netherlands, 45-80.

Barnier, B., Madec, G., Penduff, T., Molines, J., Treguier, A., Le Sommer, J., Beckmann, A., Biastoch, A., Böning, C., Dengg, J., Derval, C., Durand, E., Gulev, S., Remy, E., Talandier, C., Theetten, S., Maltrud, M., McClean, J., De Cuevas, B., 2006. Impact of partial steps and momentum advection schemes in a global ocean circulation model at eddy-permitting resolution. Ocean Dynamics, *56*, 543-567, doi:10.1007/s10236-006-0082-1.

Bethoux, J.P., Gentili, B., Raunet, J., Taillez, D., 1990. Warming trend in the Western Mediterranean Deep Water. Nature, *347*, 660-662.

Bettadpur, S., 2004. Level-2 gravity field product user handbook, GRACE 327– 734, 17 pp., University of Texas at Austin, Austin.

Bettadpur, S., 2007. Level-2 Gravity Field Product User Handbook, GRACE 327-734, CSR Publ. GR-03-01, Rev 2.3. University of Texas at Austin, 19pp.

Beuvier, J., Sevault, F., Somos, S., Béranger, K., 2008. Modeling the Mediterranean Sea interannual variability over the last 40 years: impacto f the river runoff and of the Atlantic waters. 3rd ESF MedCLIVAR Workshop on understanding the mechanisms responsible for the changes in the Mediterranean Sea circulation and sea level trends. Rhodes (Greece), September 2008 (http://www.medclivar.eu/workshop_3.html).

Bindoff, N.L., Willebrand, J., Artale, V., 2007. Observations: oceanic climate change and sea level. In: Solomon, S., Qin, D., Manning, M., et al. (Eds.), Climate Change 2007: The Physical Science Basis. Contribution of Working Group I to the Fourth Assessment Report of the Intergovernmental Panel on Climate Change. Cambridge University Press, Cambridge and New York, pp. 387–429.

Carrere, L., Lyard, F., 2003. Modeling the barotropic response of the global ocean to atmospheric wind and pressure forcing - Comparison with observations. Geophysical Research Letters, *30*, 6, 1275.

Castellari, S., N. Pinardi, K. Leaman, 2000. Simulation of water mass formation processes in the Mediterranean Sea: influence of the time frequency of the atmospheric forcing. Journal of Geophysical Research, *105*, 157-181.

Cazenave, A., Cabanes, C., Dominh, K., Mangiarotti, S., 2001. Recent sea level changes in the Mediterranean Sea revealed by TOPEX/POSEIDON satellite altimetry. Geophysical Research Letters, *28*(8), 1607-1610.

Cazenave, A., Bonnefond, P., Mercier, F., Dominh, K., Tomazou, V., 2002. Sea level variations in the Mediterranean Sea and Black Sea from satellite altimetry and tide gauges. Global and Planetary Change, *34*, 59-86.

Cazenave, A., Dominh, K., Guinehut, S., Berthier, E., Llovel, W., Ramillien, G., Ablain, M., Larnicol, G., 2009. Sea level budget over 2003–2008: a re-evaluation from GRACE space gravimetry, satellite altimetry and Argo. Global and Planetary Change, *65*, 83-88, doi:10.1016/j.gloplacha.2008.10.004.

CERSAT (2002) Mean Wind Fields (MWF product) Volume 1 – ERS-1, ERS-2 & NSCAT User Manual, Ref C2-MUT-W-05-IF, Version : 1.0.

Chambers, D. P., Melhaff, C. A., Urban, T. J., Fuji, D., Nerem, R. S., 2002. Low-frequency variations in global mean sea level: 1950-2000. Journal of Geophysical Research, *107*, 3026, doi: 10.129/2001JC001089.

Chambers, D. P., 2006, Observing seasonal steric sea level variations with GRACE and satellite altimetry. Journal of Geophysical Research, *111*, C03010, doi:10.1029/2005JC002914.

Cheng, M., Tapley, B. D., 2004. Variations in the Earth's oblateness during the past 28 years. Journal of Geophysical Research, *109*, B09402, doi:10.1029/2004JB003028.

Christiansen, B., 2005. The shortcomings of nonlinear principal component analysis in identifying circulation regimes. Journal of Climate, *18*, 4814-4823.

Church, J. A., White, N.J., Coleman, R., Lambeck, K., Mitrovika, J. X., 2004. Estimates of the Regional Distribution of Sea Level Rise over the 1950-2000 Period. Journal of Climate, *17*, 2609-2625.

Church, J.A., White, N.J., 2006. A 20th century acceleration in global sea-level rise. Geophysical Research Letters, *33*, L01602. doi:10.1029/2005GL024826.

Criado-Aldeanueva, F., Del Rio Vera, J., García-Lafuente, J, 2008. Steric and mass-induced Mediterranean sea level trends from 14 years of altimetry data. Global and Planetary Change, *60* (3-4), pp. 563-575.

Déqué M., Piedelievre, J. P., 1995. High-resolution climate simulation over Europe. Clim Dynamics, *11*, 321–339.

Domingues, C.M., Church, J. A., White, N. J., Glecker, P. J., Wijffels, S. E., Barker, P. M., Dunn, J. R., 2008. Improved estimates of upper-ocean warming and multi-decadal sea level rise. Nature, *453*, 1090-1094, doi:10.1038/nature07080.

Donoho, D. L., Huber, P. J., 1983. "The Notion of Breakdown-Point," in *A Festschrift for Erich L. Lehmann*, eds. P. J. Bickel, K. A. Doksum, and J. L Hodges, Jr., Belmont, CA: Wadsworth, pp. 157–184.

Fan, Y., van den Dool, H., 2004. Climate Prediction Center global monthly soil moisture data set at 0.5_ resolution for 1948 to present. Journal of Geophysical Research, *109*, D10102, doi:10.1029/2003JD004345.

Fenoglio-Marc, L., 2001. Analysis and representation of regional sea-level variability from altimetry and atmospheric–oceanic data. Geophysical Journal International, *145*, 1–18.

Fenoglio-Marc L., 2002. Long-term sea level change in the Mediterranean Sea from multi-

satelitte altimetry and tide gauges. Physics and Chemistry of the Earth, 27, 1419-1431.

Fenoglio-Marc, L., Kusche, J., Becker, M., 2006. Mass variation in the Mediterranean Sea from GRACE and its validation by altimetry, steric and hydrologic fields. Geophysical Research Letters, *33*, L19606. doi:10.1029/2006GL026851.

Fenoglio-Marc, L., Kusche, J., Becker, M., Fukumori, I., 2007. Comment on "On the steric and mass-induced contributions to the annual sea level variations in the Mediterranean Sea" by David García et al.. Journal of Geophysical Research, *112*, C12018, doi:10.1029/2007JC004196.

Flechtner, F., 2007. AOD1B Product Description Document for product Releases 01 to 04, GRACE 327-750, CSR publ. GR-GFZ-AOD-0001 Rev. 3.1. University of Texas at Austin, 43 pp.

Freeman, J. A., Shapura, D. M., 1991. Neural Networks: Algorithms, Applications, and Programming Techniques. Addison-Wesley. USA.

Gacic, M., Kovacevic, V., Manca, B., Papageorgiou, E., Poulain, P. M., Scarazzato, P., Vetrano, A., 1996. Thermohaline properties and circulation in the Strait of Otranto. Bull. Inst. Oceanogr. Monaco, *17*, 117– 145.

García, D., Chao, B.F., Del Río, J., Vigo, I., García-Lafuente, J., 2006. On the steric and mass induced contributions to the annual sea level variations in the Mediterranean Sea. Journal of Geophysical Research, *111*, C09030. doi:10.1029/2005JC002956.

García-Lafuente, J., Del Río, J., Alvarez-Fanjul, E., Gomis, D., Delgado, J., 2004. Some aspects of the seasonal sea level variations around Spain. Journal of Geophysical Research, *109*, C09008. doi:10.1029/2003JC002070.

Giorgi, F., Marinucci, M. and Bates, G., 1993. Development of a second generation regional climate model (regcm2) i: Boundary layer and radiative transfer processes. Monthly Weather Review, *121*, 2794–2813.

Giorgi, F. and Mearns, L. O., 1999. Introduction to special section: Regional climate modelling revisited. Journal of Geophysical Research, *104*, 6335–6352.

Gomis, D., Tsimplis, M.N., Martín-Míguez, B., Ratsimandresy, A.W., García-Lafuente, J., Josey, S.A., 2006. Mediterranean Sea level and barotropic flow through the Strait of Gibraltar for the period 1958–2001 and reconstructed since 1659. Journal of Geophysical Research, *111*, C11005. doi:10.1029/2005JC003186.

Gomis, D., Ruiz, S., Sotillo, M. G., Álvarez-Fanjul, E., Terradas, J., 2008: Low frequency Mediterranean sea level variability: the contribution of atmospheric pressure and wind. Global and Planetary Change, doi:10.1016/j.gloplacha.2008.06.005.

Goosse, H., 1997. Modeling the large scale behaviour of the coupled ocean-sea ice system. Ph.D. Thesis, Université Catholique de Louvain, Louvain-la-Neuve, Belgium, 231 pp.

Greatbach, R.J., 1994. A note on the representation of steric sea level in models that conserve volume rather than mass. Journal of Geophysical Research, *99* (C6), 12767–12771.

Guedes Soares, C., Carretero Albiach, J.C.,Weisse, R., Alvarez-Fanjul, E., 2002. A 40 years hindcast of wind, sea level and waves in European waters. Proceedings of the OMAE2002: 21st International Conference of Offshore Mechanics and Arctic Engineering. Oslo, Norway. 23–28 June 2002.

Haidovel, D. B., Beckmann, A., 1999. Numerical Ocean circulation Modelin. Imperial College Press. UK.

Hampel, F. R., 1971. A General Qualitative Definition of Robustness. The Annals of Mathematical Statistics, *42*, 1887–1896.

Hays, J.D., Imbrie, J., Shackleton, N.J., 1976. Variations in the earth's orbit: pacemaker of the ice ages. Science, *194*, 1121–1132.

Heiskanen, W. A., Moritz, H., 1967. Physical Geodesy, W. H. Freeman, New York.

Herrman, M., Somot, S., 2008. Relevance of ERA40 dynamical downscaling for modelling deep convection in the Mediterranean Sea. Geophysical Research Letters, *35*, L04607. doi:10.1029/2007GL032442.

Holgate S. J., Woodworth, P. L., 2004. Evidence for enhanced coastal sea level rise during the 1990s. Geophysical Research Letters, *31*, L07305, doi:10.1029/2004GL019626.

Ingleby, B., Huddleston, M., 2007. Quality control of ocean temperature and salinity profiles-historical and real time data. Journal of Marine Systems, *65*, 158-175, doi:10.1016/j.jmarsys.2005.11.019.

IPCC AR4, 2007. Climate Change 2007. The Physical Science Basis. Summary for Policymakers. In: Contribution of Working Group I to the Fourth Assessment Report of the Intergovernmental Panel on Climate Change. Eds. R. Alley, T. Berntsen, N.L. Bindoff et al.

Ishii, M., Kimoto, M., Kachi, M., 2003. Historical ocean subsurface temperature analysis with error estimates. Monthly Weather Review, *131*, 51-73.

Ishii, M., Kimoto, M., Sakamoto, K., Iwasaki, S. I., 2006. Steric sea level changes estimated from historical ocean subsurface temperatura and salinity analyses. Journal of Oceanography, *62*, 155-170.

Ishii, M., Kimoto, M., 2009. Reevaluation of Historical Ocean Heat Content Variations with Time-Varying XBT and MBT Depth Bias Corrections. Journal of Oceanography, *65*, 287-299.

Jevrejeva S., A. Grinsted, J. C. Moore, S. Holgate, 2006. Nonlinear trends and multiyear cycles in sea level records, Journal of Geophysical Research, *111*, C09012, doi:10.1029/2005JC003229.

Jones, H., Marshall, J., 1993. Convection with rotation in a neutral ocean; a study of open ocean deep convection. Journal of Physical Oceanography, *23*, 1009-1039.

Josey, S., 2003. Changes in the heat and freshwater forcing of the eastern Mediterranean and their influence on deep water formation. Journal of Geophysical Research, *108*(C7), 1-18, doi: 10.1029/2003JC001778.

Kalnay, E., Kanamitsu, M., Kistler, R., Collins, W., Deaven, D., Gandin, L., Iredell, M., Saha, S., White, G., Woolen, J., Zhu, Y., Chelliah, M., Ebisuzaki, W., Higgins, W., Janowiak, J., Mo, K. C., Ropelewski, C., Wang, J., Leetmaa, A., Reynolds, R., Jenne, R., Joseph, D., 1996. The NCEP/NCAR 40-Year Reanalysis Project. Bulletin of the American Meterolological Society, *77* (3), 437-471.

Kantha, L. H., Clayson, C. A., 2000. Numerical models of Oceans and Oceanic Processes. Academic Press. USA.

Kaplan, A., Kushnir, Y., Cane, M. A., Blumenthal, M. B., 1997. Reduced space optimal analysis for historical data sets: 136 years of Atlantic sea surface temperatures. Journal of Geophysical Research, *102*, 27 835-27 860.

Kaplan, A., Cane, M. A., Kushnir, Y., Clement, A. C., 1998. Analyses of global sea surface temperatures 1856-1991. Journal of Geophysical Research, *103*, 18 567-18 589.

Kaplan, A., Kushnir, Y., Cane, M. A., 2000. Reduced space optimal interpolation of historical marine sea level pressure. Journal of Climate, *13*, 2987-3002.

Klein, B., Roether, W., Givitarese, G., Gacic, M., Manca, B.B., d'Alcala, M.R., 2000. Is the

Adriatic Returning to Dominate the Production of Eastern Mediterranean Deep Water?, Geophysical Research Letters, *27*(20), 3377-3380.

Kramer, M. A., 1991. Nonlinear Principal Component Analysis using autoassociative neural networks. AIChE J., *37*, 233-243.

Larnicol, G., N. Ayoub and P.Y. Le Traon, 2002. Major changes in Mediterranean Sea level variability from 7 years of TOPEX/Poseidon and ERS-1/2 data. Journal of Marine Systems*, 33–34, 63– 89.

Lascaratos, A., Williams, R., Tragou, E., 1993. A mixed layer study of the formation of Levantine Intermediate Water. Journal of Geophysical Research, *98*, 739–749.

Lascaratos, A., Nittis, K., 1998. A high-resolution 3-D numerical study of intermediate water formation in the Levantine Sea. Journal of Geophysical Research, *13*, 18,497– 18,511.

Lascaratos, A., Roether, W., Nittis, K., Klein, B., 1999. Recent changes in deep water formation and spreading in the eastern Mediterranean Sea: A review. Progress in Oceanography, *44*, 5 –36.

Le Traon, P. Y., Ogor, F., 1998. ERS -1/2 orbit improvement using Topex/Poseidon: The 2 cm challenge. Journal of Geophysical Research., *103*, C4, 8045-8057.

Le Traon, P. Y., Y. Faugère, F. Hernandez, J. Dorandeu, F. Mertz and M. Ablain, 2003. Can we merge GEOSAT Follow-on with TOPEX/POSEIDON and ERS-2 for an improved description of the ocean circulation? Journal of Atmospheric and Ocean Technology, *20*, 889-895.

Leuliette, E. W., Nerem, R. S., Mitchum, G. T., 2004. Calibration of TOPEX/POSEIDON and Jason altimeter data to construct a continuous record of mean sea level change. Marine Geodesy, *27*, 79-94, doi:10.1080/01490410490465193.

Leuliette, E. W., Miller, L., 2009. Closing the sea level rise budget with altimetry, Argo, and GRACE. Geophysical Research Letters, *36*, L04608, doi:10.1029/ 2008GL036010.

Levitus, S., Climatological Atlas of the World Ocean, NOAA/ERL GFDL Professional Paper 13, Princeton, N.J., 173 pp. (NTISPB83-184093),1982.

Levitus, S., Stephens, C., Antonov, J.I., Boyer, T.P., 2000. Yearly and Year-Season Upper Ocean Temperature Anomaly Fields, 1948-1998. U.S. Gov. Printing Office, Washington DC, pp. 23.

Levitus, S., Antonov, J.I., Boyer, T.P., 2005. Warming of the World ocean, 19552003. Geophysical Research Letters, *32*, L02604, doi: 10.1029/2004GL021592.

Madec, G., Delecluse, P., Imbard, M., Levy, C., 1998. OPA 8.1, Ocean general circulation model, reference manual. IPSL/LODYC, France, Note du Pôle de modélisation, 11.

Malanotte-Rizzoli, P., Hecht, A., 1988. Large scale properties of the Eastern Mediterranean: a review. Oceanologica Acta, *11*, 323–335.

Malanotte-Rizzoli, P., Manca, B., Ribera d'Alcala, M., Theocharis, A., Brenner, S., Budillon, G., Ozsoy, E., 1999. The eastern Mediterranean in the 80s and the 90s: The big transition in the intermediate and deep circulations. Dynamics of Atmospheres and Oceans, *29*, 365– 395.

Manca. B.B., Ibello, V., Pacciaroni, M., Scarazzato, P., Giorgetti, A., 2006. Ventilation of deep waters in the Adriatic and Ionian Seas follwing changes in the thermohaline circulation of the Eastern Mediterranean. Climate Research, *31*(2-3), 239-256.

Marcos, M., Tsimplis, M. N., 2007a. Forcing of coastal sea-level rise patterns in the North Atlantic and the Mediterranean Sea. Geophysical Research Letters, *34*, L18604, doi:10.1029/2007GL030641.

Marcos, M., Tsimplis, M. N., 2007b. Variations of the seasonal sea level cycle in Southern Europe. Journal of Geophysical Research, *112*, C12011, doi:10.1029/2006JC004049.

Marcos, M., Tsimplis, M. N., 2008. Coastal sea level trends in southern Europe. Geophysical Journal International, *175* (1), 70-82.

Marshall, J., Adcroft, A., Hill, C., Perelman, L., Heisey, C., 1997a. A finite-volume, incompressible navier stokes model for, studies of the ocean on parallel computers, Journal of Geophysical Research C: Oceans, 102 (C3), 5753–5766.

Marshall, J., Hill, C., Perelman, L., Adcroft, A., 1997b. Hydrostatic, quasi-hydrostatic, and nonhydrostatic ocean modeling, Journal of Geophysical Research C: Oceans, 102 (C3), 5733–5752.

McClean, J. L., Semtner, A. J., Zlotnicki, V., 1997. Comparisons of mesoscale variability in the Semtner-Chervin quarter-degree model, the Los Alamos POP sixth-degree model, and the TOPEX/POSEIDON data. Journal of Geophysical Research, 102 (C11), 203-226.

MEDAR Group (2002), Mediterranean and Black Sea Database of Temperature, Salinity and Biochemical Parameters and Climatological Atlas [4 CD-ROMs], Ifremer Ed., Plouzane, France. (Available at http://www.ifremer.fr/sismer/program/medar/).

MEDOC Group, 1970. Observation of formation of deep water in the Mediterranean Sea. Nature, *227*, 1037-1040.

Meehl, G. A., Stocker, T. F., Collins, W. D., 2007. Global climate projections. In: Solomon, S., Qin, D., Manning, M., et al. (Eds.), Climate Change 2007: The Physical Science Basis. Contribution of Working Group I to the Fourth Assessment Report of the Intergovernmental Panel on Climate Change. Cambridge University Press, Cambridge and New York, pp. 749–844.

Meier, M. F., 1984. Contribution of small glaciers to global sea level. Science, *226*.

Miller, A. R., 1963. Physical oceanography of the Mediterranean Sea: A discourse, Rapp. Comm. Int. Mer Mediter., *17*, 857– 871.

Monahan, A. H., 2000. Nonlinear Principal Component Analysis by neural networks: Theory and application to the Lorenz System. Journal of Climate, *13*, 821-835.

Monahan, A. H., 2001. Nonlinear Principal Component Analysis: Tropical Indo-Pacific Sea Surface Temperature and Sea Level Pressure. Journal of Climate, *14*, 219-233.

Nittis, K., Lascaratos, A., 1998. Diagnostic and prognostic numerical studies of LIW formation. Journal of Marine Systems, *18*, 179– 195.

Nittis, K., Lascaratos, A., Theocharis, A., 2003. Dense water formation in the Aegean Sea: Numerical simulations during the Eastern Mediterranean Transient. Journal of Geophysisical Research, *108*(C9), 8120, doi:10.1029/2002JC001352.

P. J. Huber, 1981. Robust Statistics. Wiley, New York.

Pal, J.S., Giorgi, F., Bi, X., Elguindi, N., Solmon, F., Gao, X., Rauscher, S. A., Francisco, R., Zakey, A., Winter, J., Ashfaq, M., Syed, F. S., Bell, J. L., Diffenbaugh, N. S., Karmacharya, J., Konaré, A., Martinez, D., da Rocha, R. P., Sloan, L. C., Steiner, A. L., 2007. Regional Climate Modeling for the Developing World: The ICTP RegCM3 and RegCNET. Bulletin of the American Meteorological Society, *88*, 1395–1409.

Pascual, A., Marcos, M., Gomis, D., 2008. Comparing the sea level response to pressure and wind forcing of two barotropic models: validation with tide gauge and altimetry data.

Journal of Geophysical Research, *113*, C07011, doi:10.1029/2007JC004459.

Paulson, A., Zhong, S., Wahr, J., 2007. Inference of mantle viscosity from GRACE and relative sea level data. Geophysical Journal International, *171*, 497–508.

Peltier, W.R., 1986. Deglaciation induced vertical motion of the North American continent and transient lower mantle rheology. Journal of Geophysical Research, *91*, 9099–9123.

Peltier, W.R., 1994. Ice-age paleotopography. Science, *265*, 195–201.

Peltier, W.R., 1996. Mantle viscosity and ice-age ice-sheet topography. Science, *273*, 1359–1364.

Peltier, W.R., 2002. Global glacial isostatic adjustment: paleo-geodetic and space geodetic tests of the ICE-4G(VM2) model. Journal of Quaternary Science, *17*, 491–510.

Peltier, W.R., 2004. Global glacial isostasy and the surface of the ice-age Earth: the ICE-5G(VM2) model and GRACE. Annual Reviews of Earth and Planetary Sciences, *32*, 111–149.

Peltier,W.R., 2007. History of Earth Rotation. In: Schubert, G. (Ed.), Volume 9 of the Treatise on Geophysics. Elsevier Press, Oxford, UK, pp. 243–293.

Pfeffer, W.T., Harper, J.T., O'Neel, S., 2008. Kinematic constraints on glaciar contributions to 21st-century sea-level rise. Science, *321*, 1340–1343.

Pirazzoli, P. A., 2004. A review of possible eustatic, isostatic and tectonic contributions in eight late-Holocene relative sea-level histories from the Mediterranean area. Quaternary Science Reviews, *24*, 1989-2001.

Preisendorfer, R. W., 1988. Principal Component Analysis in Meteorology and Oceanography, Elsevier, New York, U.S.A..

Rahmstorf, S., 2007. A semi-empirical approach to projecting future sea-level rise. Science, *315*, 368–370.

Ratsimandresy, A.W., Sotillo, M.G., Carretero, J.C., Álvarez-Fanjul, E., Hajji, H., 2008. A 44-year high-resolution ocean and atmospheric hindcast for the Mediterranean basin developed within the HIPOCAS Project. Coastal Engineering. doi:10.1016/j.coastaleng.2008.02.025.

Rixen, M., Beckers, J.-M., Brankart, J.-M., Brasseur, P., 2001. A numerically efficient data analysis method with error map generation. Ocean Modelling, *2*(1-2):45-60.

Rixen, M., Beckers, J.-M., Levitus, S., Antonov, J., Boyer, T.,Maillard, C., Fichaut, M., Balopoulos, E., Iona, S., Dooley, H., Garcia, M.-J., Manca, B., Giorgetti, A., Manzella, G., Mikhailov, N., Pinardi, N., Zavatarelli, M., and the Medar Consortium, 2005. The Western Mediterranean Deep Water: a proxy for climate change. Geophysical Research Letters, *32*, L12608. doi:10.1029/2005GL022702.

Roether, W., Manca, B.B., Klein, B., Bregant, D., Georgopoulos, D., Beitzel, V., Kovacevic, V., Luchetta, A., 1996. Recent changes in eastern Mediterranean deep waters. Science, *271*, Issue 5247, 333-335.

Roether, W., Klein, B., Manca, B. B., Theocharis, A., Kioroglou, S., 2007. Transient eastern Mediterranean deep waters in response to the massive dense-water output of the Aegean Sea in the 1990's. Progress in Oceanography, *74*(4), 540–571, doi:10.1016/j.pocean.2007.03.001.

Rousseeuw, P.J., Yohai, V.J., 1984. Robust regression by means of S-estimators. In: Franke, J., Hardle, W., Martin, D. (Eds.), Robust and Nonlinear Time Series. Lecture Notes in Statistics, vol. 26. Springer, Berlin, pp. 256–272.

Ruiz, S., Gomis, D., Sotillo, M. G., Josey, S. A., 2008. Characeization of surface heat fluxes in the Mediterranean Sea from a 44-year high-resolution atmospheric data set. Global and Planetary Change, *63* (2-3), 258-274.

Salibian-Barrera, M., Zamar, R.H., 2002. Bootstrapping robust estimates of regression. Annals of Statistics, *30*, 556–582.

Salibian-Barrera, M., 2006. Bootstrapping MM-estimators for linear regression with fixed designs. Statistics & Probability letters, *76*, 1287-1297.

Salibian-Barrera, M., Yohai, V. J., 2006. A fast algorithm for S-regression estimates. Journal of Computational and Graphical Statistics, *15*(2), 414-427.

Sannino, G., Hermann, M., Carrillo, A., Rupolo, V., Ruggiero, V., Artale, V., Heimbach, P., 2009. An eddy-permitting model of the Mediterranean Sea with a two-way grid refinement at the Strait of Gibraltar. Ocean Modelling, *30*, 56-72.

Schlitzer, R., Roether, W., Oster, H., Junghans, H., Hausmann, M., Johannsen, H., Michelato, A., 1991. Chlorofluoromenthane and oxygen in the eastern Mediterranean. Deep Sea Research, Part A, *38*, 1531–1551.

Schott, F., Visbeck, M., Send, U., 1994. Open-ocean deep convection, Mediterranean and Greenland Seas, in Ocean Processes on Climate Dynamics, edited by P.M. Rizzoli and A. Robinson, pp. 203-225, Kluwer, Norwell, Mass.

Schott, F., Visbeck, M., Send, U., Fischer, J., Stramma, L., Desaubies, Y., 1996. Observations of deep convection in the Gulf of Lions, northern Mediterranean, during the winter of 1991/92. Journal of Physical Oceanography, *6*,505-524.

Simmons A. J., Gibson, J. K., 2000. The ERA-40 Project Plan, ERA-40project report series no. 1 ECMWF, p 62.

Smith, T. M., Livezey, R. E., Chen, S. S., 1998. An improved method for analyzing sparse and irregularly distributed SST data on a regular grid: The tropical Pacific Ocean.. Journal of Climate, *11*, 1717-1729.

Somot, S., Sevault, F., Dèquè, M., 2006. Transient climate change scenario simulation of the Mediterranean Sea for the twenty-first century using a high-resolution ocean circulation model. Climate Dynamics, *27*(7-8), 851-879.

Somot S., Colin, J., 2008. First step towards a multi-decadal high-resolution Mediterranean sea reanalysis using dynamical downscaling of ERA40. Research activities in atmospheric and oceanic modelling. CAS/JSC Working group on numerical experimentation. Report No.38. (available at http://collaboration.cmc.ec.gc.ca/science/wgne/BlueBook/2008/documents/sections.html and at http://www.cnrm.meteo.fr/gmgec/publications/publications_SCL.html)

Sotillo, M.G., Ratsimandresy, A.W., Carretero, J.C., Bentamy, A., Valero, F., González-Rouco, F., 2005. A high-resolution 44-year atmospheric hindcast for the Mediterranean Basin: contribution to the regional improvement of global reanalysis. Climate Dynamics. doi:10.1007/s00382-005-0030-7.

Stratford, K., Haines, K., 2002. Modelling changes in Mediterranean thermohaline circulation 1987– 1995, Journal of Marine Systems, 33– 34, 51– 62.

Swenson, S., Wahr, J., 2002. Methods for inferring regional surface-mass anomalies from Gravity Recovery and Climate Experiment (GRACE) measurements of time-variable gravity. Journal of Geophysical Research, *107*(B9), 2193, doi:10.1029/ 2001JB000576.

Swenson, S., Chambers, D. P., Wahr, J., 2008. Estimating geocenter variations from a

combination of GRACE and ocean model output. Journal of Geophysical Research, *113*, B08410, doi:10.1029/2007JB005338.

Theocaris, A., Nittis, K., Kontoyiannis, H., Papageorgiou, E., Balopoulos, E., 1999. Climatic changes in the Aegean Sea influence the Eastern Mediterranean thermohaline circulation. Geophysical Research Letters, *26*, 11, 1617-1620.

Theocaris, A., Klein, B., Nittis, K., Roether, W., 2002. Evolution and status of the Eastern Mediterranean Transient (1997-1999). Journal of Marine Systems, 33-34, 91-116.

Tsimplis, M.N., Woodworth, P.L., 1994. The global distribution of the seasonal sea level cycle calculated from coastal tide gauge data. Journal of Geophysical Research, *99* (8), 16031–16039.

Tsimplis, M.N., Josey, S.A., 2001. Forcing of the Mediterranean Sea by atmospheric oscillations over the North Atlantic. Geophysical Research Letters, *28* (5), 803–806.

Tsimplis, M. N., Rixen, M., 2002. Sea level in the Mediterranean Sea: The contribution of temperature and salinity changes. Geophysical Research Letters, *29 (*23), 2136, doi:10.1029/2002GL015870.

Tsimplis, M. N., Álvarez-Fanjul, E., Gomis, D., Fenoglio-Marc, L., Pérez, B., 2005. Mediterranean Sea level trends: separating the meteorological and steric effects, Geophysical Research Letters, *32*, L20602, doi:10.1029/2005GL023867.

Tsimplis, M. N., Shaw, A. G. P., Pascual, A., Marcos, M., Pasaric, M., Fenoglio-Marc, L., 2008. Can we reconstruct the 20th century sea level variability in the Mediterranean Sea on the basis of recent altimetric measurements?, in: Barale, V., M. Gade (Eds.), Remote Sensing of the European Seas. Springer. ISBN:1402067712.

Tsimplis, M. N., Marcos, M., Colin, J., Somot, S., Pascual, A., Shaw, A. G. P., 2009. Sea level variability in the Mediterranean Sea during the 1990s on the basis of two 2d and one 3d model. Journal of Marine Systems, *78*, 109-123.

Vigo, I., García, D., Chao, B.F., 2005. Change of Sea Level Trend in the Mediterranean and Black Seas. Journal of Marine Research, *63*(6), 1085-1100.

Volkov, D. L., Larnicol, G., Dorandeu, J., 2007. Improving the quality of satellite altimetry data over continental shelves. Journal of Geophysical Research, *112*, C06020.

Wahr, J., Molenaar, M., Bryan, F., 1998. Time variability of the Earth's gravity field: Hydrological and oceanic effects and their possible detection using GRACE. Journal of Geophysical Research, *103*(B12), 30, 205-230, 229, doi:10.1029/98JB02844.

Wakelin, S.L., Woodworth, P.L., Flather, R.A., Williams, J.A., 2003. Sea-level dependence on the NAO over the NW European continental shelf. Geophysical Research Letters, *30* (7), 1403. doi:10.1029/2003GL017041.

Wilks, D. S., 1995. Statistical Methods in the Atmospheric Sciences. Academic Press, San Diego.

Willis, J. K., Chambers, D. P., Nerem, R. S., 2008. Assessing the globally averaged sea level budget on seasonal to interannual timescales. Journal of Geophysical Research, *113*, C06015, doi:10.1029/2007JC004517.

Woodworth, P.L., Player, R. 2003. The Permanent Service for Mean Sea Level: an update to the 21st century. Journal of Coastal Research, *19*, 287-295.

Woolf, D., Shaw, A., Tsimplis, M., 2003. The influence of the North Atlantic oscillation on sea level variability in the North Atlantic region. The Global Atmosphere and Ocean System, *9* (4), 145–167.

Woppelmann, G., Miguez, B.M., Bouin, M.N., Altamimi, Z., 2007. Geocentric sea-level trend estimates from GPS analyses at relevant tide gauges world-wide. Global and Planetary Change, *57*, 396–406.

Wüst, G., 1961. On the vertical circulation of the Mediterranean Sea. Journal of Geophysical Research, *66*, 3261–3271.

Xie, P., Arkin, P. A., 1997. Global Precipitation: A 17-Year monthly analysis based on gauge observations, satellite estimates, and numerical model outputs. Bulletin of the American Meteorological Society, *78*(11): 2539-2558.

Yan, Z., Tsimplis, M.N., Woolf, D., 2004. An analysis of relationship between the North Atlantic oscillation and sea level changes in NW Europe. International Journal of Climatology, *24*, 743–758.

Yohai, V.J., 1987. High breakdown-point and high efficiency robust estimates for regression. Annals of Statistics, *15*, 642–656.

Zervakis, V., Georgopoulos, D., Drakopoulos, P., 2000. The role of the north Aegean in triggering the recent eastern Mediterranean climatic changes. Journal of Geophysical Research, *105*, no. c11, pp. 26, 103–26, 116.

List of Figures

List of Tables

185

Curriculum Vitae

- ## **Personal Information**

Name: Mir Calafat, Francisco Jaime

Date of birth: 30/09/1979

Place of birth: Palma de Mallorca (Spain)

Nationality: Spanish

DNI: 43118075-K

Office address: C/ Miquel Marquès, 21. Esporles 07190, Illes Balears.

Office phone: +34 971610983

E-mail: kiko.mir@uib.es

- ## **Education and Fellowships**

Bachelor's degree in Physics (1997/98-2001/02) University of the Balearic Islands, SPAIN.

Master degree in Physics (September 2007) University of the Balearic Islands, SPAIN.

Fellowships

1. Fellowship of Ayuda al Estudio del Ministerio de Educación y Cultura in the years 1997/98, 1998/99, 1999/00, 2000/01 and 2001/02.

2. Seneca Fellowship, Universitat de València (2000/01)

- ## **Current Affiliation**

1. Scholarship holder of a Formación de Personal Investigador (FPI) Fellowship of the Ministerio de Educación y Cultura of Spain since October 2006 at the Institut Mediterrani d'Estudis Avançats (IMEDEA).

- ## Other Merits

1. Referee for Global and Planetary Change.
2. 124 credits of the Industrial Mechanical Engineer degree, Universidad de Educación a Distancia (UNED).

- ## Visits to other Institutions

1. National Oceanography Centre, University of Southampton and Natural Environment Research Council (Southampton, UK). 1 March – 2 May 2008.
2. Laboratoire d'Etudes en Géophysique et Océanographie Spatiales (Toulouse, France). 16 Novembre – 19 November 2009.

- ## Publications

Publications in refereed journals

1. Calafat, F. M. and D. Gomis, 2009. Reconstruction of Mediterranean sea level fields for the period 1945-2000. Global and Planetary Change, *66*, 225-234.
2. Calafat, F. M., D. Gomis, M. Marcos, 2009. Comparison of Mediterranean sea level fields for the period 1961-2000 as given by a data reconstruction and a 3D model. Global and Planetary Change, *68*, 175-184.
3. Calafat, F. M., M. Marcos, D. Gomis. Mass contribution to Mediterranean sea level variability for the period 1948-2000. Global and Planetary Change, submitted (2010).
4. Calafat, F. M., G. Jordà, D. Gomis, M. Marcos. Comparison of results from three baroclinic models of the Mediterranean Sea. Global and Planetary Change, submitted (2010).
5. Marcos, M., F. M. Calafat, W. Llovel, D. Gomis, B. Meyssignac. Regional distribution of steric and mass contributions to sea level changes. Global and Planetary Change, submitted (2010).
6. Marcos, M., M. N. Tsimplis, F. M. Calafat. Inter-annual and decadal sea level variations in the North-western Pacific marginal seas. Progress in Oceanography, submitted (2010).

- ## Conference Presentations

1. **EGU General Assembly 2008**. Vienna, Austria.

   Poster presented by F. M. Calafat: "*Recovery of sea level elds of the last decades from altimetry and tide gauge data*", F. M. Calafat, D. Gomis, A. Pascual, M. Marcos, S. Ruiz.

2. **Effects of Climate Change on The World's Oceans, International Symposyum 2008**. Gijón, Spain.

   Talk presented by F. M. Calafat: "*Recovery of sea level elds of the last decades from altimetry and tide gauge data*", F. M. Calafat, D. Gomis, A. Pascual, M. Marcos, S. Ruiz.

3. **3rd MedCLIVAR-ESF workshop 2008**. Rhodos, Greece.

   Poster presented by F. M. Calafat: "*Distribution of sea level rise in the Mediterranean Sea and the north-eastern sector of the Atlantic Ocean: 1945-2000*", F. M. Calafat and D. Gomis.

4. **Clima en España: pasado, presente y futuro 2009**. Madrid, Spain.

   Talk presented by F. M. Calafat: "*Long-term sea level variability: what observations tell us*", F. M. Calafat, M. Marcos, M. N. Tsimplis, D. Gomis, A. Pascual, S. Montserrat.

5. **Clima en España: pasado, presente y futuro 2009**. Madrid, Spain.

   Talk presented by F. M. Calafat: "*Long-term sea level variability in the Mediterranean sea: the mechanisms responsible for the observed trends*", M. Marcos, D. Gomis, M. N. Tsimplis, F. M. Calafat, S. Ruiz, E. Álvarez-Fanjul, M. García-Sotillo, S. Somot, S. Josey.

6. **Clima en España: pasado, presente y futuro 2009**. Madrid, Spain.

   Talk presented by G. Jordà: "*Estimation of sea level variability from 3D ocean circulation models*", G. Jordà, F. M. Calafat, M. Marcos, D. Gomis, S. Somot, E. Álvarez-Fanjul, I. Ferrer.

7. **EGU General Assembly 2009**. Vienna, Austria.

   Talk presented by F. M. Calafat: "*Comparison of Mediterranean sea level fields for the period 1961-2000 as given by a data reconstruction*", F. M. Calafat, D. Gomis, M. Marcos.

8. **EGU General Assembly 2010**. Vienna, Austria.

   Talk presented by M. Marcos: "*Regional distribution of steric and mass contributions to sea level changes*", M. Marcos, F. M. Calafat, W. Llovel, B. Meyssignac, D. Gomis, A. Cazenave.

9. **EGU General Assembly 2010**. Vienna, Austria.

   Talk presented by B. Meyssignac: "*Past sea level reconstruction and variability of sea level trend patterns over 1970-2001 in the Mediterranean Sea basin derived from Altimetry and 2 long OGCM runs*", B. Meyssignac, A. Cazenave, R. Morrow, M. Marcos, F. M. Calafat, W. Llovel.

10. **39th CIESM Congress 2010**. Venice, Italy.

    Talk presented by F. M. Calafat: "*Mass contribution to Mediterranean sea level variability for the period 1948-2000*", F. M. Calafat, M. Marcos, D. Gomis.

11. **39th CIESM Congress 2010**. Venice, Italy.

    Poster presented by D. Gomis: "*Storm surge variations in the Mediterranean Sea under climate change scenarios*", M. Marcos, G. Jordà, D. Gomis, F. M. Calafat, E. Àlvarez-Fanjul.

12. **39th CIESM Congress 2010**. Venice, Italy.

    Poster presented by D. Gomis: "*Western Mediterranean wave climate change scenarioos for the XXIst century*", B. Jordà, M. Marcos, D. Gomis, F. M. Calafat, M. Gòmez.

• **Computer experience and languages**

1. **Programming**: Fortran, Matlab, Java, Javascript, Html, Xml.
2. **Operative systems**: Windows, UNIX, DOS.
3. **Languages**: Catalan (native), Spanish (native), English (good), Japanese (regular).